Uncertainty in nearshore trench siltation

Including nearshore processes in trench siltation predictions, while enabling probabilistic modelling

V.R.J. Kindermann

Delft University of Technology

Boskalis

TU Delft

SVASEK HYDRAULICS

Uncertainty in nearshore trench siltation

Including nearshore processes in trench siltation predictions, while enabling probabilistic modelling

by

V.R.J. Kindermann

Student Number 4657934

In partial fulfilment of the requirements for the degree of

Master of Science

in

Civil Engineering

at Delft University of Technology

Thesis Committee:	Dr.ir. Stuart Pearson	TU Delft, Chair
	Dr.ir. Maria Nogal Macho	TU Delft
	ir. Annouk Rey	Boskalis, Daily supervisor
	ir. Ype Attema	Svašek Hydraulics, Daily supervisor

Project Duration:	February, 2024 - July, 2024
Faculty:	Faculty of Civil Engineering and Geosciences

Cover: Landfall Cable Installation Hollandse Kust West Beta by Boskalis b.v. (Modified)

An electronic version of this thesis is available at http://repository.tudelft.nl/.

TU Delft

Preface

This thesis marks the end of my Master of Science in Civil Engineering, within the specialisation of Hydraulic Engineering, at Delft University of Technology, and thus the end of my time in Delft. A time that has been wonderful in every respect. Moving from my small hometown in the south of the Netherlands to the city of Delft has opened many doors for me. I have met many great people over the past few years, and I'm proud to call the most amazing of them 'friends'. The choice to study Civil Engineering has been a 'perfect fit' with a BSS of 1. I've had the privilege to study a highly interesting study with amazing teachers, while always being surrounded by fellow students, many of whom belong to the aforementioned 'most amazing people' that I call 'friends'. I would like to use this preface to express my gratitude to some of the people who have helped and supported me over the past few years.

First of all, I would like to thank the members of my graduation committee from the faculty of Civil Engineering and Geosciences. Starting with the chair of my committee, Stuart Pearson. I still find it amazing that I met you on a study trip with the study association to Canada and the USA and now, 2 years later, you are my graduation chair. I remember our nice conversations about hydraulic engineering on that study trip, which were very valuable to me, as I was in the middle of the process of choosing a master specialisation. Over the past few months, your enthusiasm for hydraulic engineering has fascinated and helped me a lot. It was a great motivation for me. Next to that, I realised how helpful it is to have a native English-speaking chair to correct my writing. Next I want to thank Maria. Thank you for the critical view and discussions on all my work related to the probabilistic modelling. It was a great addition to have you in my committee. Not only your feedback on the things in your field of expertise, but also your thoughts on the topics that are less close to your field of work were very valuable throughout the whole process.

I had the opportunity to execute my master thesis in cooperation with two companies: Boskalis and Svašek Hydraulics. I would like to thank Annouk for always being available for questions, discussions, or just a quick chat. You taught me a lot about the practical aspects of hydraulic engineering and helped me make important decisions throughout the process, without which I would not have managed to finish all my goals on time. I would also like to thank all the other colleagues at Boskalis Hydronamic for making this a great time. I've always felt welcome and had a lot of fun with you. Next I would like to thank Ype for guiding me through the complexities of nearshore hydrodynamics and morphology. You were always available to provide extra in-depth information on anything related to my thesis I was interested in, and you brought up some very interesting topics to include in my research. I would also like to thank all the other colleagues at Svašek Hydraulic for the great time I had, including all the fun activities outside working hours. I would especially like to thank Anna Kroon for her help with the GLUE-analysis.

Last, but certainly not least, I would like to thank my family and friends for always supporting, motivating, and helping me in the last years. Without you, it would not have been as much fun as it has been.

V.R.J. Kindermann
Delft, June 2024

Abstract

As a result of growth in the offshore energy infrastructure, the connection between the offshore environment and the mainland is increasing in importance. This leads to an increased use of the seabed for cables and pipelines as part of our energy infrastructure. Cables or pipelines are placed in trenches and covered by sediment, to be protected from any damage from activity near the sea bed. During execution, the trenches will refill with sediment prior to the placement of the cable or pipeline, which is known as siltation. The siltation rates are increasing when entering the breaker zone near the shoreline. The predictability of the siltation rates are a crucial step in efficient and safe realisation of new connections between the offshore energy infrastructure and the mainland.

Inclusion of nearshore processes is missing in existing quick-assessment siltation tools. Complex process-based models, like Delft3D or XBeach, are capable of predicting siltation volumes in the nearshore environment accurately. However, these models demand large computation capacities. This makes them unsuitable for probabilistic modelling, requiring large numbers of calculations. Probabilistic modelling however is a crucial step in identifying and quantifying uncertainties and related risks in the execution. This research presents a quick-assessment tool that includes nearshore processes. Ensuring low complexity makes quick-assessment tools suitable for probabilistic modelling of siltation predictions, reducing and quantifying uncertainties within nearshore trench siltation.

This research presents an approach to include wave transformation and wave-driven currents into an existing siltation prediction tool (SedPit). The resulting SedPit Nearshore tool allows fast predictions of siltation volumes in the nearshore zone. The performance of the SedPit Nearshore tool is assessed by comparing it to data from a field case, and comparing the accuracy to the accuracy of the existing SedPit tool. The SedPit Nearshore tool gives accurate predictions on the total siltation volume, and gives good insights in the spatial distribution of siltation volumes. The potential of the SedPit Nearshore becomes most evident when comparing it to the existing SedPit tool. A great improvement compared to the existing SedPit tool is seen. For the test case, the SedPit Nearshore tool reduces the absolute error in predicting the total siltation volumes by 82% compared to the existing SedPit tool. The SedPit Nearshore tool predicts the total siltation volume with an error margin of 7%, while the existing SedPit has an error margin of 41%. The largest improvements compared to the existing Sedpit are seen in the most onshore regions, as this is the zone where most wave-driven currents are generated. The computational speed of the tool has proven its applicability for analyses on model sensitivity and uncertainty quantification. Computation times are reduced by factor 9,000 when comparing it to XBeach, a complex process-based model. Bottom roughness k_s and wave roller steepness β were identified as most influential free variables in driving nearshore siltation volumes. Calibrating the model to obtain likely values for a range of free variables has helped to reduce the 95% confidence interval of peak siltation rates by 36%.

The inclusion of wave-driven currents into existing siltation prediction tools has shown a great improvement in the accuracy of siltation predictions in the nearshore zone. Although the SedPit Nearshore tool is calibrated on one specific field case, the method and the workflow of the tool show potential to help as general prediction tool of nearshore trench siltation. The power of the SedPit Nearshore tool lays in its simplicity, making it a fast, efficient, and accurate tool, suited for probabilistic modelling.

Contents

Nomenclature

Abbreviations

Abbreviation	Definition
ANOVA	Analysis of variances
BJ78	Battjes-Janssen Model 1978
BSS	Brier Skill Score
CDF	Cumulative Density Function
CSD	Cutter Suction Dredger
GLUE	Generalised Likelihood Uncertainty Estimation
LST	Longshore Sediment Transport
MBJ	Modified Battjes Janssen
MCS	Monte Carlo Simulation
MORFAC	Morphological Acceleration Factor
NOAA	National Oceanic and Atmospheric Administration
RAE	Relative absolute error
RMSE	Root Mean Squared Error
SG	Savitzky-Golay

Symbols

Symbol	Definition	Unit
A_b	Partical excursion	[m]
A_s	Deposition surface	[m²]
A_v	Sediment coefficient SedPit	[-]
C	Chèzy coefficient	[$m^{1/2}$/s]
c	Wave velocity	[m/s]
c_{clay}	Clay concentration	[mg/L]
c_f	friction coefficient	[-]
c_g	Wave group velocity	[m/s]
c_{silt}	Silt concentration	[mg/L]
c_{vr}	Van Rijn trapping factor	[-]
d_{50}	median grain size	[m]
d_i	Hallermeier's outer limit depth	[m]
d_l	Hallermeier's littoral zone limit depth	[m]
D_f	Friction dissipation term	[J]
D_r	Roller dissipation term	[J]
D_s	Deposited sediment	[m³]
D_w	Wave breaking dissipation term	[J]
D_*	Dimensionless particle size	[-]
E	Trapping efficiency	[-]
E_r	Roller energy	[J]
E_w	Wave energy	[J]
F	Wave force	[N]
f	Wave frequency	[s^{-1}]
f_c	Current friction term	[-]
f_w	Wave friction term	[-]

Symbol	Definition	Unit
g	Gravitational acceleration	[m/s²]
H_{max}	Maximum wave height	[m]
H_s	Significant wave height	[m]
H_{rms}	Root-mean-square wave height	[m]
h	Local water depth in wave theory	[m]
k	Wave number	[-]
k_s	Bottom roughness	[m]
L	Wave length	[m]
L_i	Likelihood	[-]
CL	Combined likelihood	[-]
n	wave coefficient	[-]
q	Sediment transport rate	[kg/s/m]
Q_b	Fraction of broken waves	[-]
r	Pearson correlation coefficient	[-]
S_1	First-order Sobol' index	[-]
S_2	Second-order Sobol' index	[-]
S_m	Alongshore water level gradient	[-]
S_{yx}	alongshore component radiation stress	[N/m]
s	Siltation thickness	[m]
T	Wave period	[s]
T_p	Peak wave period	[s]
T_s	Significant wave period	[s]
U	Current velocity	[m/s]
U_{orb}	Wave orbital velocity	[m/s]
V	Longshore current	[m/s]
ΔV	Volume change	[m³]
Var	Variance	
w_s	Particle settling velocity	[m/s]
α	Wave dissipation coefficient	[-]
β	Wave roller steepness	[-]
γ	Wave breaking coefficient	[-]
θ	Wave angle	[°]
ν	Kinematic viscosity	[m²/s]
ρ_b	Bulk density	[kg/m³]
ρ_w	Density of the water	[kg/m³]
ρ_s	Density of the solids	[kg/m³]
τ_b	Bed shear stress	[N/m²]
τ_w	Wind shear stress	[N/m²]
ω	Angular wave frequency	[rad/s]

1 Introduction

1.1. Context trenches

As a result of a growing offshore energy infrastructure, the connection between the offshore environment and the mainland is increasing in importance, leading to an increased utilisation of the seabed as part of our energy infrastructure.The worldwide demand for clean energy is leading to a shift in energy production. One of the most promising clean energy sources is wind energy. Offshore environments can play a crucial role in the production of wind energy. The Dutch government has set the goal to produce 75% of the total national energy consumption by offshore wind farms by 2050. In 2021, the contribution of offshore wind energy to the total production is estimated on 15.8% (Rijksoverheid, 2022). These numbers show the rapid growth that is needed in the realisation of offshore wind farms in the upcoming years.

The offshore energy infrastructure is connected to the mainland by cables and pipelines. The cables and pipelines are placed in trenches on the seabed and are covered with enough sediment to be protected against any damage. During the design and the realisation of the trenches, the knowledge on sedimentation processes that affect the infrastructure on the seabed is of great importance.

The cables or pipelines can often not be placed simultaneously with the dredging of the trenches. The trenches will be exposed to various processes that lead to siltation (refilling due to the settlement of sediments) for a period of weeks up to months. When entering shallow waters near the coast, floatation pits and channels are needed during the construction of trenches, or during any other dredging activity near the coast. These floatation pits and channels ensure access and enough depth for waterborne equipment to operate in shallow waters. In order to reduce dredging activities, it is preferred to dredge the trenches and pits with an over-depth that ensures the design depth during the entire realisation phase. In this context, it is important to be able to predict the siltation rates in the trenches and pits during the realisation phase. For the sake of better readability, floatation pits and channels are included in the term 'trench' throughout this report.

1.2. Context uncertainty

Numerical models are a well-proven method to predict the processes that occur in coastal environments. The results of these models help understanding the processes and improving execution of interventions in coastal environments. However, these numerical models do also come with their uncertainty. This uncertainty can be the result of simplifications and assumptions within the model, or the uncertainty of natural variability of input parameters (Van Gelder, 2000). The uncertainty resulting from the model itself is often referred to as epistemic uncertainty, while natural uncertainty of input is referred to as intrinsic uncertainty (Kroon et al., 2020; Van Gelder, 2000).

One method to quantify the uncertainty in model output is to obtain a large amount of model outcomes. By randomly drawing input parameters from distributions that represent the natural variability of the input parameters, the variance in model outcome can be evaluated. This method is called Monte Carlo

Simulation (MCS) (Berends et al., 2019). MCS is relying on the possibility to create a large sample size of outcomes, which is often limited by the computational complexity of the model. However, as long as models maintain a low complexity, large sample sizes are computationally feasible to obtain (Berends et al., 2019). The large sample size of model outcomes can give insightful information on the statistics and uncertainties of the output. For example, the fact that MCS draws the input parameters from probability distributions makes it possible to quantify the intrinsic uncertainty that results from natural variability of input parameters by applying MCS (Christiaanse, 2021).

1.3. Problem description

Currently, different tools are used to estimate the siltation rates in trenches. Often, quick assessment tools are used, which have proven themselves as a fast and reliable way to estimate the siltation rates. These tools are currently based on relatively straightforward sedimentation processes that take place in offshore environments: tidal currents and wave motion. One of these tools is the SedPit tool, developed by Van Rijn. The SedPit-tool is a model that predicts siltation of trenches and pits and is based on Van Rijn's sediment formulae (Van Rijn, 2007). Given its widespread application in the field, this report will frequently make reference to the SedPit tool. Offshore environments are considered at depths where waves do not break, and therefore no wave-driven currents are generated. When trenches enter the nearshore environment, additional sedimentation processes take place. The impact of these nearshore processes is not yet included in the quick assessment tools.

Within the field of morphology, several advanced process-based models do exist, that can predict sedimentation rates accurately, also including the nearshore processes. However, due to their extensive computational time, process-based models are not used regular for the purpose of trench siltation. This has two main reasons. First of all, the project phases where prediction of siltation rates are desired often face constraints on the available time. Secondly, computationally heavy models are not suited for probabilistic modelling. When working in a highly dynamic and to some extent unpredictable environment as the offshore and nearshore environment is, uncertainty of input data is inevitable. As described in Section 1.2, a widely used way of quantifying uncertainty is the Monte Carlo approach, which relies on low model complexity that allows large sample sizes. Although process-based models can make good estimates of nearshore siltation in trenches, a quick assessment tool that does include nearshore processes is desired, as these are more suited to a probabilistic approach of uncertainties. Complex models demand larger computational power and more time, which makes them less suitable for a probabilistic approach. Currently, an extension of existing tools that includes nearshore processes, while ensuring the possibility of probabilistic modelling is missing.

1.4. Societal impact

As the main objective of solving the above-described problem originates directly from the need of the industry, the main stakeholders are parties that are active in the offshore or maritime industry. First, the main stakeholders are contractors that potentially benefit from the tool in the realisation of their work. Closely related to the contractors are the clients, that benefit from the more efficient, and therefore potentially economic more beneficial realisation of their projects. An indirect, but significant stakeholder is the end user of clean energy. Every step that increases the efficiency of the transition to renewable energies contributes positively on the environmental impact of our society. These three stakeholders will be discussed further in the next paragraphs.

Contractors strive to the most efficient way of realising their work. In the context of this research, on one hand more insights in the needed dredging activities can potentially lead to more efficient work. Besides that, the possibility of assessing the uncertainties of the projects better, gives a better understanding of potential risks and can reduce unexpected costs. All of these aspects lead in the end to a more economical business-case for the contractors, and subsequently for the clients.

The direct profiteer of the results of contractors are their clients. In this context, the focus is on energy network operators. In achieving the goal of a transition towards clean energy, every improvement that increases the efficiency of their projects related to the energy transition can lower the cost-price of renewable energy and is a step closer towards the transition to clean energy.

A more indirect, but crucial stakeholder is the end user of clean energy. This stakeholder is representing a broad spectrum of our society, including residents, industry and governments. As stated earlier, the Dutch government has set the goal to produce 75% of the total national energy production by offshore wind farms in 2050 (Rijksoverheid, 2022). To reach this goal, which is just a piece of the global transition to renewable energy, governments are depending on technological improvements that increase the pace of the energy transition. By ensuring better insights into siltation processes, a piece of this system can be improved.

1.5. Research gap

The use of tools to estimate siltation rates in trenches is a well-proven method for offshore environments. The SedPit tool, based on Van Rijn's sedimentation formulas (Van Rijn, 2007), is a widely used quick assessment tool. As introduced in Section 1.1, the effect of nearshore sedimentation processes on siltation rates in trenches is not yet included in quick assessment tools. The effect of nearshore sediment processes on trench siltation is currently only estimated using complex morphological models.

These complex models are not suited for probabilistic modelling, unlike quick assessment tools. The current quick assessment tools can be used to perform a large set of simulations to gain insights on statistics and uncertainties of the outcomes. In recent years, the use of large numbers of simulations have proven themselves valuable regarding sensitivity analysis and uncertainty analysis, resulting in the possibility to quantify model uncertainty and the contribution of different input parameters on the uncertainty.

The research gap that has been identified is the implementation of nearshore processes in quick-assessment trench siltation tool. By ensuring low complexity, the extended tools can be used to gain more insights into the importance of input parameters and their effect on model uncertainties for nearshore trench siltation predictions.

1.6. Research questions

Based on the research gap and the problem description, the following research question has been formulated:

To what extent can inclusion of nearshore processes improve existing quick assessment tools for trench siltation while ensuring low complexity for probabilistic modelling to reduce and quantify uncertainties?

This research question is subdivided in the following research sub-questions:

1. How can nearshore morphological processes be included in quick assessment tools?
2. Which variables contribute to the largest variance in the modelled outcomes of the tool?
3. How well does an improved tool perform in a field case, and what is the added value compared to existing tools?

1.7. Research objectives and scope

This research project aims to study the inclusion of nearshore processes in quick assessment trench siltation tools. By keeping the tool computationally quick, it will enable probabilistic modelling to quantify uncertainties and to gain more insights into the importance of different input parameters on the uncertainty of siltation rates in trenches.

The scope of the research is defined by the following limitations, assumptions, and simplifications:

- Fairways of harbours are not considered as a trench. Siltation rates in fairways are of interest regarding maintenance dredging to ensure accessibility. However, the timescale of continuous dredging is significantly larger then the considered timescales of previously discussed trench siltation in project execution phase.

- Only tools that are based on Van Rijn's sediment transport formula are included in this research (Van Rijn, 2007).
- Only sedimentation processes that take place below the waterline are considered. Beach development is not included. Neither are wind-induced currents included.
- The relevant timescale is defined in the order of weeks to months, as this is the typical timescale for most relevant applications (Van der Zalm, 2024).
- Morphological activities with timescales in the order of years, like sand waves and bar migration, are not considered.
- The effect of the local change in bathymetry due to the presence of a trench on wave transformation and generations of rip currents is not included.

The individual elements of the scope above are further justified in Chapter 2.

1.8. Thesis outline

The thesis is structured in the following outline. Chapter 1 has given an introduction to the topic and discussed the relevant research gap. Besides that, the research questions and the scope of the thesis are presented. Chapter 2 presents all relevant background information on the relevant subjects. Chapter 3 shows the available data that will be used further on for calibration and validation of the methods and results. In Chapter 4, the methodology is presented in detail. The results are presented in Chapter 5. Finally, Chapter 6 and Chapter 7 contain the discussion and conclusion on the findings respectively.

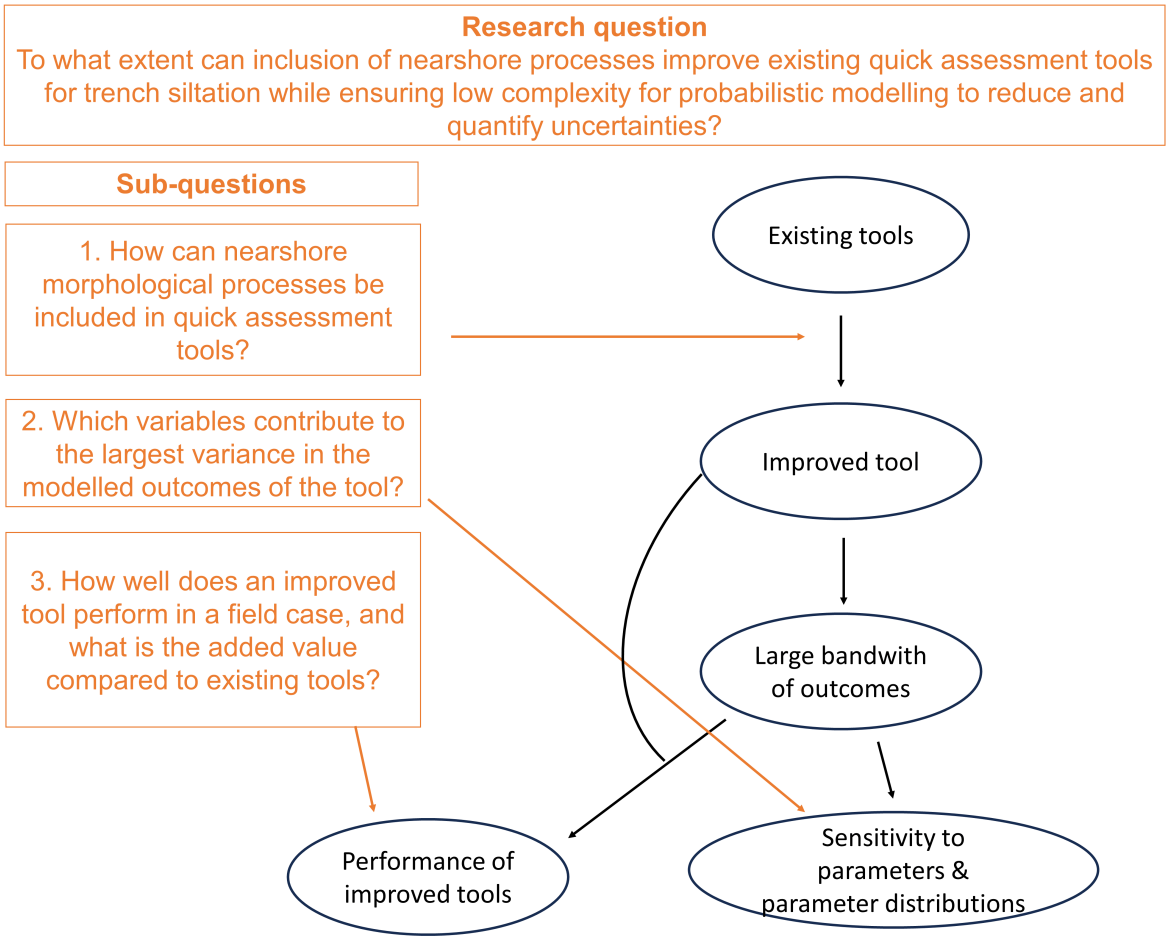

Figure 1.1: Schematic outline research: The orange boxes represent the research (sub)-question(s). The orange arrows indicate to which stage of the research the sub-questions are related.

2

Background theory

This chapter aims to provide the relevant background theory that forms the base of the methodology of this research. Besides that, this chapter will justify most of the aspects of the scope (Section 1.7). In Section 2.1, the nearshore environment will be discussed further, aiming to clarify the spatial scope of this research further. Section 2.2 explains the practical aspects of trench installation in the nearshore environment. This will further justify some application-related aspects of the scope. In Section 2.3, the hydrodynamics within the nearshore environment are addressed. This includes the tidal current, waves, and wave-driven current. Furthermore, rip currents will be discussed. In Section 2.4, the theory behind siltation processes is discussed. In Section 2.5 the theory of the sensitivity analysis is discussed, and in Section 2.6 the theory of the uncertainty analysis is discussed.

2.1. Nearshore environment

The spatial scope of this research is concentrated on the nearshore environment. As introduced in Section 1.3, the nearshore environment is not yet well represented in quick-assessment tools for trench siltation. Before diving into the processes in the nearshore environment, a clear definition of what is considered as the nearshore environment should be discussed. To start, the different zones in the shoreface are discussed, after which the beach profile will be discussed.

2.1.1. Depths

The transition between offshore water and the coastal zone (shelf) starts at the lower shoreface. The lower shoreface is dominated by tidal currents and evolves on a much longer timescale compared to the upper shoreface. The lower shoreface is only affected by waves during storm conditions (Van der Spek et al., 2022). The upper shoreface zone is dominated by wave action and extends from the shoaling zone, through the surfzone towards the shoreline. For the Dutch coastline, the lower shoreface is considered from 20 meter depths to 8 meter depths, with bed slopes ranging from 1:200 to 1:1000. The upper shoreface is reaching from 8 meter depths to the water line, and has bed slopes from 1:50 to 1:200 (Van der Spek et al., 2022).

The depths that form the border between the offshore water, the lower shoreface, and the upper shoreface can be defined by Hallermeiers's definition of closure depths. Hallermeier proposed two limit depths, d_l and d_i. These depths are based on the annual variations of a beach profile. The depth d_l represents the seaward limit to strongly wave-breaking related effects. This includes longshore sediment transport and strong onshore-offshore sediment transport (Hallermeier, 1981). The depth d_i represents a seaward limit for sediment motion during normal wave conditions. Significant onshore-offshore sediment transport is limited towards this depth. Seaward of d_i, no significant annual sediment transport is taking place (Hallermeier, 1980). In this region, sediment transport with a large timescale is dominant (Van der Spek et al., 2022). In Figure 2.1 the upper and lower shoreface, including Hallermeier limit depths are shown.

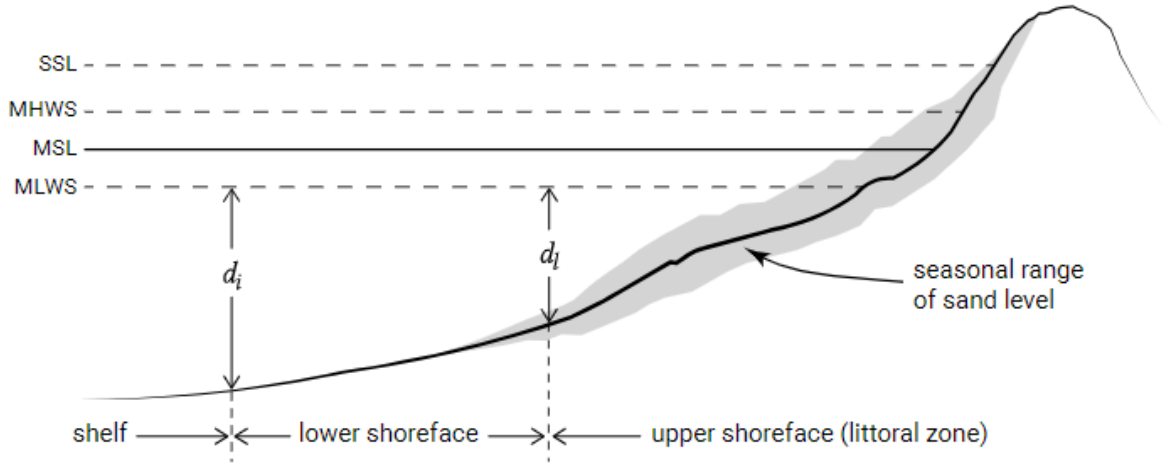

Figure 2.1: Beach profile including lower shoreface, upper shoreface, Hallermeier's outer depth limit d_i, and Hallermeier's littoral zone depth limit d_l (Bosboom & Stive, 2022)

Hallermeier's definition of the upper shoreface corresponds to the width of the surfzone during extreme conditions, which are conditions that are exceeded for twelve hours per year (0.137% occurrence probability). The depths d_i and d_l are formulated based on the relationship between the wave field and the flow velocities near the bed. This indicates that the limit depths are related to the wave climate. The flow velocities near the bed are based on linear wave theory, and the extreme wave conditions are related to the significant wave height:

$$H_{0.137\%} = \overline{H_s} + 5.6\sigma_{H_s} \tag{2.1}$$

$$d_l = 2.28H_{0.137\%} - 68.5\left(\frac{H^2_{0.137\%}}{gT^2_{0.137\%}}\right) \tag{2.2}$$

$$d_i = 0.013H_sT_s\sqrt{\frac{g}{d_{50}(s-1}} \tag{2.3}$$

where $\overline{H_s}$ is the average significant wave height, σ_{H_s} is the annual standard deviation of significant wave height, L is the local wavelength, γ' is the ratio of density difference between sand and fluid and $\overline{T_s}$ is the average significant wave period.

From Equation (2.1) and Equation (2.2) it becomes clear that the exact depth, and consequently the width of the active zone, is depending on the wave climate. This is used in the definition of the coastal zone that is considered as the region of nearshore trench siltation in Section 4.7.

2.1.2. Beach profile

The shape of the beach profile strongly affects the nearshore hydrodynamics, but it also depending on local conditions, like wave climate and sediment type. Besides that, the beach profile is seasonally varying, related to the seasonal variations in the wave climate (Van der Spek et al., 2022). All this makes it difficult to predict the beach profile without extensive bathymetry measurements. Dean (1977) has presented a variant of the theory of Bruun (Bruun, 1954), to approximate the beach profile, based on the sediment type. Bruun's theory was the first theory that stated that an empirical equation for beach profiles does exist. Different supports of Bruun's theory exist, with one of them being the the research of Dean (1977). He proposed that the depth can be described by:

$$\begin{aligned} h(x) &= A^{2/3}x^{2/3} \\ A &= \left(\frac{24\epsilon(D_{50})}{5\rho g^{2/3}\gamma^2}\right) \end{aligned} \tag{2.4}$$

where x is the distance to the shoreline, $\epsilon(D_{50})$ is the equilibrium energy dissipation rate, and γ is the wave breaking coefficient.

The theory of Dean's profile has proven itself as a reliable way to estimate the dynamic equilibrium profile for a wide range of beaches (Dean et al., 1993). However, beach profiles, and their hydrodynamics, are often characterised by the presence of bars and troughs. Bars and troughs are not included in the concept of a Dean profile, since bars and troughs are seasonal features of a profile, that can occur from a wide range of mechanisms (Thornton et al., 1996). Depending on the available knowledge on the beach profile, and the timescale of the prediction, the profile is represented differently in current estimations. Therefore, both types of profile will be included in this report.

2.2. Trench realisation

The realisation of the landfall of a cable or pipeline consists of different stages. Cables and pipelines need to be protected against various factors, such as seabed dynamics, movement due to currents, sabotage, or impact from anchors. Besides that, the ecological impact on the marine environment is minimised if a cable or pipeline is buried in a trench. Therefore, cables and pipelines are most of the time either buried in a trench or protected by an armour layer. The latter is a rather expensive solution, wherefore most cables and pipelines are placed in a trench.

The installation of the cable or pipeline can often not be executed directly after the dredging of the trench. This is due to logistic and practical limitations during the execution. As example, in most of the cases different equipment is needed for the dredging than for the cable or pipeline installation itself. This already leads to certain exposure period of an open trench. At first, the trench will be dredged. This is typically done with waterborne equipment, like backhoe dredgers or cutter suction dredgers (CSD) (Laboyrie et al., 2018). Typically, the trench is open during a period in the order of weeks, between the dredging and the installation of the cable or pipeline (Van der Zalm, 2024). The period is often scheduled based on predictions of calm wave conditions, to avoid trench exposure during extreme conditions. During this period, sedimentation processes will lead to siltation of the trench. These processes are further discussed in Section 2.4. On one hand the cables are meant to be located on a minimum design depth to ensure protection, while on the other hand a maximum depth must be considered in the case of electrical power cables, to prevent overheating. This makes prediction of siltation rates an essential step in the design of a trench.

The needed waterborne equipment can only be used if the local depth allows the draft and clearance of the equipment. As an example, a backhoe dredger can have a draft of 5.5 meter, while a typical CSD can have drafts up to 8 meter. To allow the equipment to operate as close to the shoreline as possible, floatation pits provide the nautical depth. As well as the trenches, the floatation pits and their access channels will experience siltation during the period of exposure. In some cases, it is more beneficial to dredge the trench and floatation pit with an overdepth, instead of re-deepening the trench and floatation pit after the period of siltation. This overdepth is based on the estimated siltation layer and ensures the design depth of the trench and floatation pit after the period of exposure. In designing the most economical solution, and ensuring efficient logistics in the execution, siltation estimates are crucial.

The dimensions of the trench or floatation pit vary per project. In the Netherlands, Rijkswaterstaat provides guidelines on the design of trenches. In the first 1.5 km off the coast, a minimal protection layer of 3.5 m is needed. Including the diameter of the pipeline or cable itself, this can lead up to depths of 5 meters below the seabed (Van der Zalm, 2024). When using large waterborne equipment, like a CSD, the width of the trench is determined by the size of the cutter-heads, often leading to widths of minimal 6 meter. The slopes of the trenches are mostly defined by the natural slope of the surrounding material, with a typical slope of 1:3 (Van der Zalm, 2024).

To protect trenches against siltation, cofferdams can be placed along the trench. Cofferdams are temporary groyne-like structures of steel piles and planks. This will prevent any suspended loads and bed loads from settling in the trench (Laboyrie et al., 2018). Besides cofferdams, siltation traps can be installed in the form of parallel trenches. These trenches are meant to trap all sediment that otherwise

would settle in the main trench. However, these temporary structures or trenches demand additional equipment, materials, or dredging activities.

2.3. Hydrodynamics

This section will introduce the different hydrodynamic processes in the nearshore environment. This includes the tidal current, waves, wave-driven longshore current, and rip currents.

2.3.1. Tidal current

Tidal currents are the result of gravitational interaction between the sun, moon, and the earth surface. The interaction between sun, moon, and earth lead to a movement of the water masses in seas, resulting in rising and falling water levels, which is called 'tide'. The tidal currents show periodic behaviour, with a net zero velocity over one tidal cycle (NOAA, 2024).

While the tidal current is mainly an inertia-dominated current in deep water conditions, it becomes a friction-dominated current in shallow waters. For friction-dominated currents, the following formulation results from the balance between alongshore water level gradient and bottom friction:

$$U_{tide,f} = \sqrt{\frac{hgS_m}{C_{fc}}} \tag{2.5}$$

where h is the water depth, S_m is the maximum alongshore water level gradient, and C_{fc} is the current-related bottom friction (Southgate, 1989).

If Equation (2.5) is simplified towards a situation where a constant friction coefficient is assumed, therefore neglecting the depth-dependence of C_{fc}, it follows that the tidal current is proportional to:

$$U_{tide} \propto \sqrt{hS_m} \tag{2.6}$$

In practice, the proportionality in Equation (2.6) can be used to estimate the tidal currents along cross-shore positions, based on measurements of the tidal currents at a known depth, as presented by Bosboom and Stive (2022):

$$U_{tide,2} = U_{tide,1}\sqrt{\frac{h_2}{h_1}} \tag{2.7}$$

This relation is illustrated in Figure 2.2

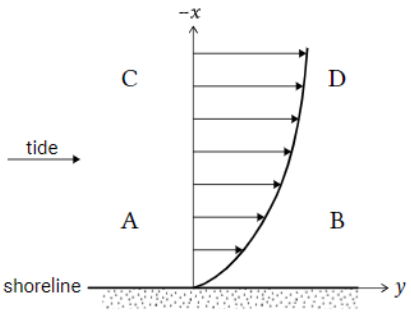

Figure 2.2: Cross-shore profile of tidal current (Bosboom & Stive, 2022)

The simplification in Equation (2.7) forms a promising quick estimation of the shore-perpendicular transformation of the tidal current. The further application and validation of the method will be described in Section 4.2.

2.3.2. Waves in shallow water

When waves leave the deep water environment and enter regions of shallow water, waves do transform. Two important processes that transform the wave propogation of waves in shallow water are shoaling

and refraction (Holthuijsen, 2007). These wave transformation processes start affecting the waves when the depth has become more or less half the wavelength. The wave energy balance in Equation (2.8) describes the balance between the energy that the waves carries, and how waves transform that energy through the different transformation processes.

$$\frac{\partial E_w}{\partial t} + \frac{\partial}{\partial x}\left(E_w c_g \cos\theta\right) + \frac{\partial}{\partial y}\left(E_w c_g \sin\theta\right) = S - D \tag{2.8}$$

In this formula, the x-axis is shore-normal, the y-axis is shore parallel, θ is the wave angle with respect to the shore-normal axis, c_g is the wave group velocity, E_w is the wave energy, S is the energy generation term, and D is the energy dissipation term (Bosboom & Stive, 2022).

As a result of the decreased depths, waves start to slow down as the waves start to feel the bottom friction. When considering the wave-energy balance in Equation (2.8), a slowing down of a wave leads to a vertical increase of the water level. This effect is called shoaling (Holthuijsen, 2007). When waves propagate towards a coast with an incident angle with respect to the shore-normal, a depth variation along the wave crest will occur (assuming parallel depth-contours). This depth variation along the wave crest leads consequently to velocity variations along the crest. The part of the waves in slightly deeper water will travel faster. This leads to the effect of refraction. The result is that waves will bend towards the coastline and the incident angle with respect to the shore-normal will decrease. This is illustrated in Figure 2.3 (Holthuijsen, 2007).

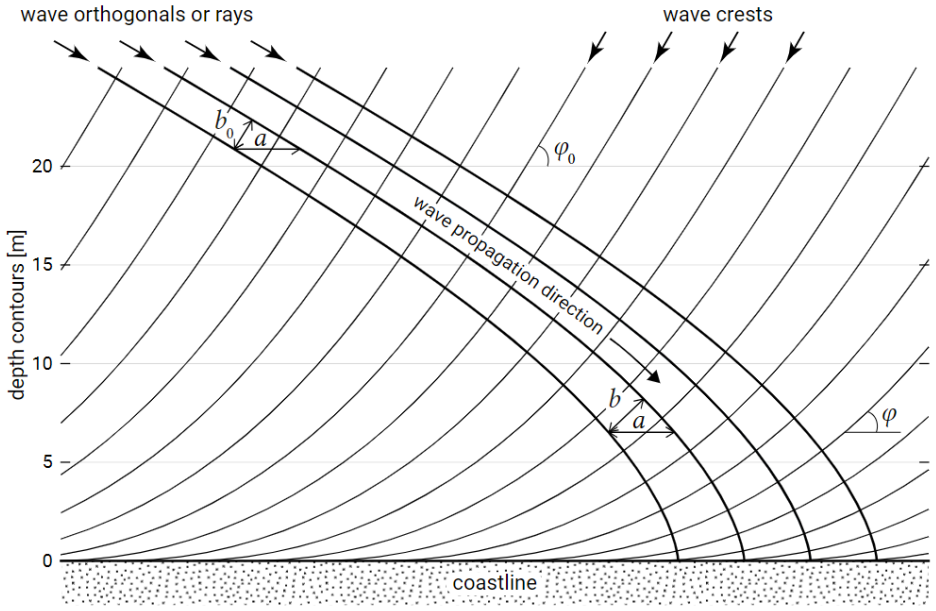

Figure 2.3: Refraction of four wave rays on a parallel depth contour according to Snell's Law. ϕ_0 is representing the deep water incident wave angle (Bosboom & Stive, 2022).

These are important processes to take into account in the context of this research. Offshore data is often used as the boundary condition for real-life projects. This data includes wave height, period, direction, and other information measured or modelled at an offshore location. In order to be able to use this data in the modelling of nearshore processes, the above-mentioned wave transformation processes form a crucial step.

A well-proven method to formulate the effect of refraction is Snell's Law. Snell's Law states that the rate of change in direction along the ray of the wave can be written as (Holthuijsen, 2007):

$$\frac{d\theta}{dn} = -\frac{1}{c}\left(-\frac{\partial c}{\partial x} sin\theta + \frac{\partial c}{\partial y} cos\theta\right) \tag{2.9}$$

where c is the wave speed, x-axis is shore-normal, and y-axis is shore-parallel. Considering a coastline with parallel depth contours will bring all derivatives in y-direction to zero ($\partial c/\partial y = 0$). This assumption makes it possible to reduce Equation (2.9) by rewriting and applying differentiation rules to :

$$\frac{d(\sin\theta/c)}{dn} = 0 \quad or \quad \frac{sin(\theta_1)}{c_1} = \frac{sin(\theta_0)}{c_0} \tag{2.10}$$

where c_1 and θ_1 are representing the wave velocity and wave angle respectively on a location on a shore-normal transect, and c_0 and θ_0 are representing the wave velocity and wave angle respectively in deep water (Holthuijsen, 2007).

2.3.3. Effect of trenches on waves

The effect of local alterations in the bathymetry on wave propagation is a known phenomenon. Harbour navigation channels or trenches affect wave refraction and wave diffraction, and consequently the wave conditions in and near the channel or trench might be subjected to change (Zwamborn & Grieve, 1974). Waves that propagate parallel to the trench will experience diffraction due to differences in wave celerity in, and adjacent to the trench, as a result of depth differences. The depth differences will also lead to a reduction of wave height in the trench, as the effect of shoaling on the wave height is dependent on the local water depth. Furthermore, waves travelling in the trench will be refracted away from the trench on its slopes (Zwamborn & Grieve, 1974). For waves that approach the trench with an incident angle, concentration of wave energy shows to have significant influence on the local wave conditions near the trench, as long as a critical angle of approach is reached. For this critical angle of approach, the waves will refract just enough to stay on the slope of the trench. Consequently, this will lead to concentration of wave energy, and increase of wave height on the slope. The critical angle of approach is reached when the resulting refracted direction is parallel to the channel axis:

$$\sin(\theta_{cr}) = \frac{c_{si}}{c_{ch}} \tag{2.11}$$

where θ_{cr} is the critical approach angle between the channel and its orthogonal, c_{si} is the wave celerity on the side of the channel, and c_{ch} is the wave celerity in the channel. Both wave celerities can be determined based on the trench dimensions and the wave characteristics.

Tests have shown that the critical angle of approach is near 25° with respect to the trench axis, for typical deep water wave conditions in a particular test case (Zwamborn & Grieve, 1974). The presence of wave concentration on slopes can lead to significant increases of wave height on the “upstream” side of the trench (Eikema et al., 2018). Consequently, the breaking of waves can show significant spatial deviations compared to the situation where the effect of a trench on wave transformation is neglected. As stated in the scope in Section 1.7, these effects are not included in the modelling. A discussion on it is presented in Section 6.2.3.

2.3.4. Wave-driven longshore current

Besides energy, waves do carry momentum. Momentum can be seen as the product between mass and wave velocity (Holthuijsen, 2007). When comparing the transfer of this momentum in a stationary flow to a flow including the presence of waves, the excess momentum transfer is known as the radiation stress (Longuet-Higgins & Stewart, 1964). When assuming waves with a perfectly normal incident angle, this radiation stress would only act in cross-shore direction. However, as waves practically always show an incident angle, an alongshore component of the radiation stress will occur as well. This alongshore component of the radiation stress forms a driving force of wave energy in alongshore direction:

$$F_y = -\frac{dS_{yx}}{dx} \tag{2.12}$$

where $S_{y,x}$ represents the alongshore component of the radiation stress. It becomes clear that a variation of the alongshore component of the radiation stress ($S_{y,x}$) in shore-normal direction (dx) drives the alongshore driving force F_y.

During the process of shoaling, the radiation stress tends to increase, as the wave height increases.

This increase in radiation stress continues until wave-breaking. As soon as the waves are broken, the radiation stress is decreasing rapidly (Bosboom & Stive, 2022). Wave-breaking can be defined as the moment where moving water particles transform from irrotational to rotational motion. This leads to a sudden disturbance of the wave and significant energy dissipation (Basco, 1985). Besides the energy dissipation due to the breaking of the waves itself, wave breaking leads to the generation of surface rollers. A surface roller represents a volume of water that is moving with the wave speed (Svendsen, 1984). Wave rollers can be seen as temporary storage of wave momentum, that is carried towards the shoreline. It leads to a delay between the expected point of peak longshore current, resulting in a shoreward shifted peak (Deigaard, 1993). The modelling of roller dissipation is explained in Section 4.2.1.

Where the hydraulic pressure gradient supplies the balancing force for the radiation stress in cross-shore direction, this counter-force is lacking in alongshore direction (assuming an infinitely long coastline). The counter-force to restore the balance will be supplied by a bed shear stress that starts developing as a result of an alongshore current (Bosboom & Stive, 2022):

$$-\frac{dS_{yx}}{dx} = \overline{\tau}_{b,y} \tag{2.13}$$

where $\overline{\tau}_{b,y}$ is the bed shear stress in y-direction, averaged over time. The bed shear stress in a current-only situation can be written as:

$$\overline{\tau}_{b,y} = \rho c_f |u| u \tag{2.14}$$

where ρ is the density, c_f is a dimensionless friction coefficient, and $|u|$ is the absolute value of the current velocity. In the presence of both waves and currents, the friction coefficient c_f should represent a combined friction by waves and currents. This will further be discussed in Section 4.2.1.

The radiation stress $S_{y,x}$ is defined as follow:

$$S_{yx} = n \cos\theta \sin\theta E_w \tag{2.15}$$

where n is the wave number, θ is the wave incident angle, and the wave energy E_w is defined as:

$$E_w = \frac{1}{8}\rho g H_{rms}^2 \tag{2.16}$$

When substituting Equation (2.14), Equation (2.15), and Equation (2.16) into Equation (2.13), an expression for the alongshore current as a result of variation in radiation stress can be obtained from the following simplified force balance:

$$-\frac{d(\frac{1}{8} n \cos\theta \sin\theta \rho g H_{rms}^2)}{dx} = \rho c_f |u| u \tag{2.17}$$

Above, some basic principles of wave transformation, energy dissipation, and the generation of a wave-driven alongshore current were presented. How these principles are used to model the hydrodynamics in the nearshore environment is explained in Section 4.2.1.

2.3.5. Rip currents

Rip currents are offshore-directed currents, with a wide variety of mechanisms at the origin of their occurrence. Rip currents create local current velocities of up to 0.5 m/s (Dalrymple et al., 2011). In most cases, rip currents are generated by alongshore variations in the water level set-up. The gradient in water level leads to a current that is directed to the alongshore position with lower waves (Bowen, 1969). In practice, these variations in water level set-up are the result of alongshore variation in bathymetry. Regions with a reduced depth will lead to local set-up, as a result of the piling up of the incoming waves in shallow water. This alongshore gradient in set-up leads to a flow directed towards the regions with higher depths where less set-up is observed (Dalrymple et al., 2011). Various other mechanism of rip current generation do exist, but this report focuses only on the mechanism as a result of alongshore variation in set-up, as this is most relevant with respect to trenches.

A trench or a floatation pit in a nearshore environment forms an alongshore variation of water depth. The trench or pit can reach depths up to 5 meter below the surrounding sea bed (Section 2.2). No experiments have been conducted on the presence of a rip current in temporary trenches, but it is plausible to assume that the local increase in depth will lead to the above described mechanism that creates offshore-directed rip current through the trench. The possible effect of rip current on sediment transport is mentioned in Section 2.3.5.

2.4. Siltation processes

In the nearshore environment, different processes take place that play a role in the transport of sediment. Sediment transport is a complicated phenomenon including a wide range of processes, and is vulnerable for any intervention that can disturbs its equilibrium. Bathymetry, sediment type, or local hydrodynamics are just a few of the elements that influence the equilibrium of sediment transport. The construction of a trench is an interventions that possibly disturbs the equilibrium sediment transport. The trench will start to fill-up with sediment which is defined as siltation. In this section, the processes that contribute to the siltation in the nearshore environment are discussed. The theory discussed in this section forms the base for the modelling of the sediment transport, discussed in Section 4.4.

2.4.1. Sediment transport

Sediment transport is defined as the movement of sediment particles through a defined plane during a certain period of time. Often, rather than sediment transport, sediment transport rates are used to characterise sediment transport. Sediment transport rates describes the rate of sediment particles that is transported per second per meter width. The quantity of sediment can be described in volumes or in immersed mass, while in more practical applications the siltation volume can be translated to a siltation thickness.

The transport rates in a moving body of water, like a current, is limited by the transport capacity of the current, also referred to as the equilibrium transport rate. If the sediment transport rate in a flow exceed the equilibrium transport rate of the flow, deposition of sediment will take place. Vice versa, if the sediment transport rate is below the equilibrium transport rate, the flow will pick-up available sediment to reach its equilibrium transport rate, known as erosion. The equilibrium transport rate of a flow is characterised by the current velocity. The precise relationship between current velocity and rates of transport remains largely unexplored. In literature, the following power-law is often used:

$$S \propto U^3 \tag{2.18}$$

The transport of sediment can be divided into two types of transport: bed load transport and suspended load transport. The bed load transport is the transport of sediment particles in a thin layer close to the bed (Van Rijn, 2007). Suspended transport is the transport of particles that are in suspension and without any contact with the bed. Both transport types can be quantified according to several formulae. Within this section, the formulae defined by Van Rijn are used (Van Rijn, 2007). These are presented in Section 4.4. While suspended transport includes sand, silt, and clay, bed load transport mainly includes sand.

2.4.2. Effect of Waves

Wave motion does play an important role in the mobilisation of sediment. By stirring up the sediment, the wave motion contributes significantly to the sediment transport rates. The mobility of sediment is characterised by the critical shear stress. This critical shear stress is exerted on a sediment particle by a flow, which can come from either a current or the motion of an orbital wave. The critical shear stress defines the ability to withstand the uplifting force of a current. If the flow exceeds the critical shear stress, initiation of motion is reached and the particle will start to move, either as suspended load in the water column, or as bed load on the bed. This is known as the Shields Criterion (Madsen & Grant, 1976). The Shields Criterion was derived initially for the shear stress on a particle in unidirectional steady flow. For oscillatory flow, like wave induced motion, several empirical relations have been derived. However, analysis on the Shields Criterion have shown that the criterion for initiation of motion in unidirectional flow serves as a reasonable criterion for initiation of motion under waves as

well (Madsen & Grant, 1976).

When considering only the oscillatory motion of symmetric waves, the time-averaged net sediment transport is theoretically zero. However, the oscillatory velocities can stir up significant amounts of sediment, and make the sediment available for transport by a current, that by itself would not be able to initiate motion (Madsen & Grant, 1976). Therefore, in a situation of combined wave-current interaction, waves have a significant contribution to the mobilisation of sediment. This is further discussed in Section 4.4.1.

2.4.3. Cross-shore sediment transport

The cross-shore transport of sediment is the result of various flow mechanism, occurring at the same time. The net cross-shore flow is build-up of a return flow, short wave motion, and long wave motion. The return flow is the near-bed flow that balances the shoreward mass flux which is located above the wave through level (Roelvink & Stive, 1989). The distinction between long and short waves is the result of considering the oscillatory motion on the time scale of short wave and on the time scale of wave groups separately. Roelvink and Stive (1989) have shown that, in the case of storm conditions, the net direction of the short waves is directed shoreward in the case of wave asymmetry, while the net direction of the long waves is directed seaward for group-bound long waves. Combining all components of the cross-shore flow during storm conditions show a net seaward directed flow. In mild conditions, the onshore flow components become relatively more important. Roelvink and Stive (1989) relate their findings on the flow directions to the resulting transport of sediment. In their considered storm condition, a seaward movement of bars is observed and measured, which indicates a net seaward directed sediment transport in storm conditions.

Besides a correlation between net direction of sediment transport and storm conditions, this correlation is in general present in the yearly seasonal cycle. In both summer and winter, a beach has a different equilibrium profile. In the transition from summer to winter, the increase in wave height leads to a net seaward transport of sediment in order to reach the winter profile (Inman et al., 1993). The exact change in wave forcing that forms the tipping point between shoreward directed transport and seaward directed transport is difficult to identify and depends on characteristics like the beach profile or the grain size (Inman et al., 1993).

In the context of sediment transport, rip currents might form a significant seaward-directed sediment sink. A rip current can strengthen the seaward directed flow locally, and consequently enhance the sediment transport on these locations. The research on sediment transport through rip currents is limited. However, Thorpe et al. (2013) have shown that the net transport of suspended sediment in a naturally formed rip current was directed seaward. This conclusion was based on in-situ measurements. Although rip currents might contribute to the nearshore sediment transport processes, the presence of rip currents will be not be included in this research analysed, as will be discussed in Section 4.2.

When nearing the shoreline, the bed slope will starts to increase significantly. This adds another transport mechanism in the cross-shore direction: gravity-driven transport. The gravity force, acting on each particle, leads to a force directed towards the deeper parts. This is either in offshore direction, or into a trough, when a trough-bar-system is shaping the bed profile (Bowen, 1980).

2.4.4. Longshore sediment transport

A large contribution to nearshore sediment transport comes from the longshore sediment transport (LST). When waves approach a coastline with an oblique angle with respect to the shore-normal, a longshore current is generated as discussed in Section 2.3.4. Other driving forces for longshore currents do exist, but the longshore current generated by the breaking of oblique incoming waves is dominant for most shorelines. This longshore current transports sediment along the shoreline, consisting of both bed load and suspended transport (Van Rijn, 2007). Two approaches in estimating LST are currently used: bulk formulae and process-based models. Bulk formulae are simplified representations of the processes taking place. The total moved mass of sediment is seen as a cross-shore constant flow of sediment, which gives insights in the total transported sediment quantities, by only needing few input variables. On the other hand, when adding more complexity by using a process-based models,

the LST transport is related to the generated current velocities, giving the opportunity to examine the cross-shore distribution of LST (Mil-Homens, 2016). The cross-shore distribution of LST is shaped by the location of the strongest wave-driven currents. These are located where the wave breaking takes place, under normal conditions near the breaker bar.

2.4.5. Sediment trapping in trenches

Local alterations in the bathymetry can form a trap for passing sediments. A trench is one of these changes of the local bathymetry that affects the shore-parallel flow of sediment. Both sediment transport types, bed load and suspended load, are affected by a trench. Bed load transport is often assumed in theory to be trapped completely by the trench. The main driver of the trapping of suspended load is the reduction in current velocity. Due to a local increase of water depth in the trench, the current velocity will decrease:

$$U_1 = U_0 \frac{h_0}{h_1} \tag{2.19}$$

where U_1 and U_0 are the current velocities above the trench and adjacent to the trench respectively, and h_1 and h_0 the water depths in the trench and adjacent to the trench respectively (Van Rijn, 2007).

The depth of the trench, with respect to the adjacent bed level, is affecting the reduction of current velocity directly. As a flow's sediment transport capacity is related to current velocity (see Equation (2.18)), the transport capacity will decrease locally in the trench. Consequently, assuming sufficient sediment supply upstream, a part of the transported sediment will be deposited in the trench (Van Rijn, 1986). The quantity of sediment trapped is closely linked to the shape and dimensions of the trench. A deeper trench results in a significant decrease in transport capacity, thus large deposition of sediment. At the same time, a wider trench allows for a longer settling distance where sediment particles can settle and be trapped in the trench. The settling distance is also affected by the angle of the incoming flow, with a large angle leading to a larger settling length and consequently more particles that are trapped by the trench.

When examining changes in the bed level within the trench, a time-dependent decrease in trapping efficiency starts to emerge. The depth of the trench, with respect to the surroundings, will decrease in time, as sediment is deposited in the trench. This affects the reduction of current velocity negatively, leading to a reduction of trapping in time. The process of trapping is further discussed in Section 4.4.1.

Besides the dimensions of the trench, the side slope of the trench affects the trapping efficiency. The steepness of the slope determines the effects occurring from separation of flow. Steep slopes lead to additional turbulence in the flow separation region. Turbulence generally leads to more resuspension of settling particle, and consequently less deposited sediment (Van Rijn et al., 2024).

2.5. Sensitivity Analysis

The goal of a sensitivity analysis is to study how uncertainty in the output of a (numerical) model can be appointed to the uncertainty of the different input parameters (Saltelli et al., 2010). The result of a sensitivity analysis can show which input parameters are most influential on the output, and on the other hand help identifying (nearly) non-influential parameters in the model. Therefore, a sensitivity analysis can function as a powerful tool to identify critical regions of the input space, identify aspects in a model that should be prioritised for research, or to justify simplifications (Saltelli et al., 2007).

A wide range of methods of sensitivity analyses do exist, that all bring their benefits and challenges. One of the key distinctions is the difference between 'Local sensitivity analysis 'versus 'Global Sensitivity Analysis'. The local sensitivity analysis is considered as the first historical approach to a sensitivity analysis (Iooss & Lemaître, 2015). In a local sensitivity analysis, the impact of an alteration on one of the input parameters on the model output is studied. This method is calculating the local partial derivatives for continuous models, or the finite differences for discrete models, at one specific point, which brings the benefit of very efficient use of computation time. As the local sensitivity analysis is a derivative-based approach, it is getting more complicated when nonlinear systems are considered

(Iooss & Lemaître, 2015; Saltelli et al., 2007), while at the same time only giving information of the change of one variable in a multi-dimensional system. However, with the rapid increase of available computational power, a computationally more intensive approach that includes the whole range of variation in the input, and is more applicable to nonlinear systems, has been established, which is known as the global sensitivity analysis. The global sensitivity analysis considers the whole range of input variance, and can therefore be used to study how the uncertainty in the output of a model can be appointed to the uncertainty in the range of input. Global sensitivity analyses are often used to define importance measures of the different input variables. A widely used global sensitivity analysis method is the method of Sobol' Indices (Iooss & Lemaître, 2015). This method is further explained in Section 2.5.2.

2.5.1. Sensitivity analysis in context of this research

The sensitivity analysis in the context of this research has several goals. First of all, the fact that the sensitivity analysis can give insights into non-influential parameters will help in the iterative cycle of optimising the aspired tool. By identifying non-influential parameters and replacing the stochastic sampling of their value by a fixed deterministic value, the computation time can be reduced. On the other hand, as soon as a well-proven tool is realised, the sensitivity analysis can evaluate the part of the total uncertainty of a model that can be attributed to certain input parameters. This can form the base of guidelines that prioritise which input parameters should be measured or determined more accurately, in order to efficiently decrease model uncertainty.

2.5.2. Variance-based sensitivity analysis (Sobol's indices)

For the purpose of this research, a global sensitivity analysis will be conducted, and more specifically a 'Variance-based method'. In these methods, the variance of the model is representing the uncertainty of the output. Variance-based methods aim to study how the variance of the model can be attributed to the variance of the input parameters. The variance of a model is defined as:

$$Var(Y) = \mathbb{E}\left[(Y - \mathbb{E}[Y])^2\right] \tag{2.20}$$

where Y denotes the actual model outcome and $\mathbb{E}[Y]$ represents the expected outcome of Y.

Different variance-based methods have developed in the time, with the most used being the method developed by Sobol (Saltelli et al., 2007). Assuming that the model Y can be described by a function $f(x)$, where $x = (x_1, ..., x_n)$ is representing the input parameters of model Y, Sobol proposes the following ANOVA-representation (Analysis of variances) of $f(x)$ (Sobol, 2001):

$$f(x) = f_0 + \sum_i f_i\left(x_i\right) + \sum_{i<j} f_{ij}\left(x_i, x_j\right) + \cdots + f_{1,2\cdots n}\left(x_1, x_2, \ldots, x_n\right) \quad \text{for} \quad 1 \leq i, j \leq n \tag{2.21}$$

This representation of $f(x)$ is based on the theory that the outcome of $f(x)$ is composed of a contribution of the expected output:

$$f_0 = \mathbb{E}[Y[x_0]] \tag{2.22}$$

a contribution made by all parameters individually:

$$\sum_i f_i\left(x_i\right) \tag{2.23}$$

and a contribution made by the interaction between parameters

$$\sum_{i<j} f_{ij}\left(x_i, x_j\right) + \cdots + f_{1,2\cdots n}\left(x_1, x_2, \ldots, x_n\right) \tag{2.24}$$

The definition of an ANOVA-representation says that all terms in Equation (2.21) are orthogonal and can be written as integrals of $f(x)$ (Sobol, 2001):

$$\int_0^1 f_{i_1\cdots i_s}\left(x_{i_1}, \ldots, x_{i_s}\right) \mathrm{d}x_k = 0 \quad \text{for} \quad k = i_1, \ldots, i_s \tag{2.25}$$

Taking the orthogonality, as stated in Equation (2.25) into account, allows us to calculate the expected value of the terms in Equation (2.22), Equation (2.23) and Equation (2.24) as follows (Shi, 2023):

$$\begin{aligned} f_0 &= \mathbb{E}[Y[x_0]] \\ f_i &= \mathbb{E}\left[Y\left[x_i\right]\right] - f_0 \\ f_{ij} &= \mathbb{E}\left[Y\left[x_i, x_j\right]\right] - f_i - f_j - f_0 \end{aligned} \tag{2.26}$$

When considering the definition of variance in Equation (2.20), the total variance of model output Y can be written as:

$$\begin{aligned} V &= Var(y) \\ &= \mathbb{E}\left[(Y - \mathbb{E}(Y))^2\right] \\ &= \mathbb{E}\left(Y^2\right) - [\mathbb{E}(Y)]^2 \\ &= \int_{i=1}^{n} Y^2 \mathsf{d}x - Y[x_0]^2 \\ &= \sum_{i=1}^{n} \sum_{1 \le i_1 < \ldots < i_n \le n}^{n} \int_0^1 \ldots \int_0^1 Y^2_{i_1,\ldots,i_n}\left(x_i, \ldots, x_n\right) \mathsf{d}x_1 \ldots \mathsf{d}x_n \\ &= \sum_{i=1}^{n} V_i + \sum_{1 \le i < j \le n}^{n} V_{ij} + \ldots + V_{1,\ldots,n}, \end{aligned} \tag{2.27}$$

where V_i=$Var(\mathbb{E}(Y[x_i])$ and $V_{i,j}$=$Var(\mathbb{E}(Y[x_i, x_j]) - V_i - V_{i,j}$, based on Equation (2.26).

Next, Sobol proposed the Sobol's Indices. These indices represent a ratio of the variance of model output $Y[x_i, x_{i,j}]$ as a result of one variable parameter or the interaction between variable parameters compared to the total variance of model output $Y[x_0]$. The first-order and second-order indices are defined below. Higher-order indices are defined in the same way, but by including the ratio of the variance as a result of the interaction between three or more variables:

$$S_i = \frac{V_i}{V} \tag{2.28}$$

$$S_{i,j} = \frac{V_{i,j}}{V} \tag{2.29}$$

The indicators in Equation (2.28) represent how much the parameter x_i from the parameter space $x = (x_1, ..., x_n)$ is contributing to the total variance of model output Y. The indicator in Equation (2.29) represent how much the interaction between parameters x_i and x_j from parameter space $x = (x_1, ..., x_n)$, is contributing to the total variance of model output Y. Equation (2.26) can be expanded for higher terms, including interaction between three or more parameters. This would consequently lead to more Sobol's indices for higher-order terms as stated in Equation (2.28) and Equation (2.29) (Shi, 2023; Sobol, 2001).

As both Sobol's indices are defined as a fraction of the total model variance, the summation of all Sobol's indices should not exceed 1. Moreover, when considering all theoretical higher-order indices (3rd order and higher), the summation of all indices should equal to the total model variance (Saltelli et al., 2010):

$$\sum S_i + \sum\sum S_{i,j} + ... + \sum S_{i,j,..,n} = 1 \tag{2.30}$$

2.6. Uncertainty Analysis

The use of numerical models makes it possible to simulate and predict complex systems, based on simplifications and approximations of complex natural processes. However, as simplifications and approximations often come with associated uncertainty, the application of simulation models require a quantitative assessment of uncertainty. Quantitative knowledge about model uncertainty can give insights into the judgement of our knowledge about processes, and might indicate systems or processes that still entail great uncertainties (Ruessink, 2005).

One of the sources of uncertainty is parameter uncertainty. Lack of knowledge about the exact occurrence of parameters lead to uncertainty in the input, which will propagate through the model and result

in contribution to model outcome uncertainty (Van Gelder, 2000). In complex models of coastal systems, parameters are often not representing directly measurable attributes (Ruessink, 2005). These parameters are consequently often estimated by calibrating the model against observed calibration data. When calibrating parameters individually against a global optimum, that is based on calibration data, the principle of "equifinality" is not considered (Beven & Binley, 1992; Ruessink, 2005). The term equifinality was introduced by Beven and Binley (1992). Equifinality refers to the characteristic of complex models where various sets of parameters can yield identical model outputs, wherefore no singular optimal parameter set exists. The obtained model outputs can reach a certain skill that is close to the optimum output. Equifinality takes the complexity of the model and the collective effect of parameter variation into account. Consider a non-influential parameter in a parameter space of a complex model. When calibrating this parameter individually, no significant variations in model output will be observed, while still having different parameter sets. On the other hand, when changing one influential parameter and obtaining a new model outcome, the initial outcome can be restored by adjusting another influential parameter. Thus obtaining the same model outcome with two different parameter sets. One of the methods within uncertainty analysis that includes equifinality is the Generalised Likelihood Uncertainty Estimation (GLUE) method, described in Section 2.6.2 (Beven & Binley, 1992).

2.6.1. Uncertainty analysis in context of this research

The goal of the uncertainty analysis in this research is to quantify uncertainty, and more specifically the "calibration uncertainty". This forms a similar approach as done by Kroon et al. (2020). In Section 2.1 to Section 2.4 it has become clear that siltation processes in the nearshore environment are complex phenomena, including a large range of input parameters, including free parameters that are difficult to measure directly. These parameters are often estimated based on earlier experience or expert judgement, as it is done by Ruessink (2005) in the context of modelling nearshore bed evolution. Similarly, in the project phase where quick-assessment tools are used, free parameters are based on experience in earlier projects. The GLUE-method will show posterior probability distributions of chosen free parameters, that are based on a comparison to observed data. While this confines the acquired knowledge to the specific validation case to some degree, the gained insights can establish a more informed foundation for future estimations of free parameters.

2.6.2. GLUE method

The GLUE-method finds its origins in modelling hydrology catchments. GLUE was first applied and presented by Beven and Binley (1992). Ruessink (2005) was the first to apply GLUE in coastal engineering. He modelled nearshore bed evolution near Egmond aan Zee. GLUE was originally used as calibration method, but its procedure includes the possibility to quantify the uncertainty bounds, making it a valuable method to quantify uncertainty (Kroon et al., 2020; Ruessink, 2005).

One of the central theories that distinguishes GLUE from other uncertainty quantification and calibration methods is the theory of equifinality. As stated in Section 2.6.1, equifinality assumes that multiple parameter sets do exist that show the same quality of modelling a certain real-world complex phenomenon. This includes that no parameter set exists that simulates the exact model output that fits perfectly to the real-world phenomenon. The outcomes of the different parameter sets are rated based on their likelihood to be a good simulator of the system (Beven & Binley, 1992). This introduces the first subjectivity of the method. A wide range of parameter sets are evaluated and the corresponding model outcomes are compared to the calibration data. Depending on how well the outcome simulates the calibration data, a likelihood weight is assigned to the parameter sets. If the parameter sets does not reach a prior defined likelihood threshold, this parameter set is rejected and considered as "non-behavioral". One of the greatest concerns associated with GLUE is reliance on subjective choices. The choices which approach is used to establish a likelihood score, and which threshold is chosen to define "non-behavioral" parameter sets, are choices up to the user of the method. In different recent works (Christiaanse, 2021; Kroon et al., 2020; Ruessink, 2005; Simmons et al., 2017) several methods are presented and discussed to control the effect of subjective choices. This will further be discussed in Section 4.8.

Besides prior defined definitions of likelihood and behavioral threshold values, prior defined distributions of the free parameters are demanded. In this step, knowledge about the system can be used to

optimise the method, by starting with distributions that are based on physical properties or experience (Beven & Binley, 1992). If no information is available in advance, uniform distributions can be used. By means of a MCS, parameter sets are drawn from the prior defined distributions. Every outcome will be evaluated based on the likelihood definition, and depending on their score with respect to the threshold considered as “non-behavioral” and rejected. The remaining (“behavioral”) parameter sets are assigned a weighted likelihood score. The remaining parameter sets and corresponding weighted likelihood scores form the base that defines a modified, posterior, parameter distribution (Beven & Binley, 1992). This posterior parameter distribution can help in future models to have more insights in the distribution of free parameters. Based on the remaining range of behavioral parameter sets, the uncertainty bounds of the model outcome can be quantified (Ruessink, 2005). Figure 2.4 is showing a schematic overview of the GLUE method.

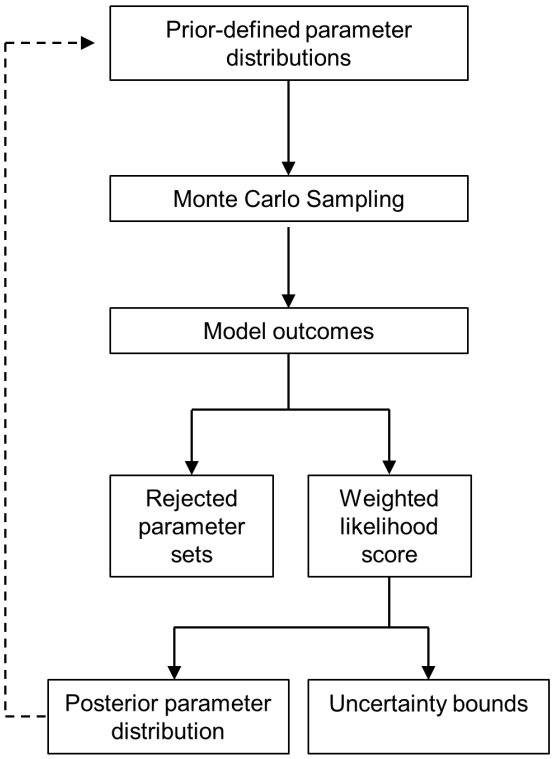

Figure 2.4: Schematised GLUE method, inspired by Simmons et al. (2017)

3

Data Analysis

This chapter aims to present the field data, which is used in the methodology to calibrate and to validate the SedPit Nearshore tool. Given that the methodology frequently references the field data, the data analysis has been positioned prior to the methodology. First, in Section 3.1 the context of the project and the available data is explained. Next, in Section 3.2 the available bathymetry is used to present the bed level change. After that, in Section 3.3 the focus is placed on the volume change of the trench, instead of on the bed level change. Finally, in Section 3.4 some artefacts of the execution which affect the data are presented.

3.1. Introduction of field case data

The field data originates from a project, executed by Boskalis. The exact location and name of the project will not be shared, due to confidentiality agreements with the client. The scope of the project consisted of the realisation of a trench for a connection to offshore energy infrastructure, and the realisation of a floatation pit to ensure nautical depth for the waterborne equipment. The trench had a design width of 8 meter at the bottom of the trench, and a design depth of 5 meter below the initial seabed. The slopes of the trench were designed with a slope of 1:3, leading to a width of around 38 meter at the level of the seabed. The trench is located at a straight stretch of coastline. In Figure 3.8, the 3 kilometers of coastline northwards and southwards of the trench are shown. This straight coastline continues in both directions for over 150 kilometers, without significant headlands or other geographical features that could disturb the hydrodynamics along the coastline significantly.

After the dredging of the trench and pit, three surveying campaigns where conducted, of which one was conducted directly after the dredging. During these surveys, the depth was measured. The cross-shore evolution of the bed level in the trench, according to the survey campaigns, is visualised in Figure 3.1. The depths are interpolated from a depth grid onto a line, located near the center axis of the trench.

3.2. Bed level change

Figure 3.1 gives a good first impression of the bed level change. It can be seen that a general upward trend of the bed level in the trench can be seen. This rise of bed level is larger for the more shallow parts, and show a peak near the shoreline. At large depths, 20 meter and deeper, the bed level change between the three surveys is an order of magnitude smaller than in the shallower regions. This shows the increased morphological activity of the nearshore environment, compared to the deeper offshore regions. When looking at the most shallow regions, visualised in the inset in Figure 3.1, some significant siltation rates of up to 7 meter can be seen at a distance of 75 meter from the shoreline. The blue line indicates that the trench is almost completely refilled with sediment after 13 days.

The depth profiles in Figure 3.1 can directly be converted to bed level changes on the center axis of the trench. By subtracting the depth profiles from the post-dredging survey, the bed level change

per period can be calculated. By adding those two, the total bed level change is obtained. This is visualised in Figure 3.2.

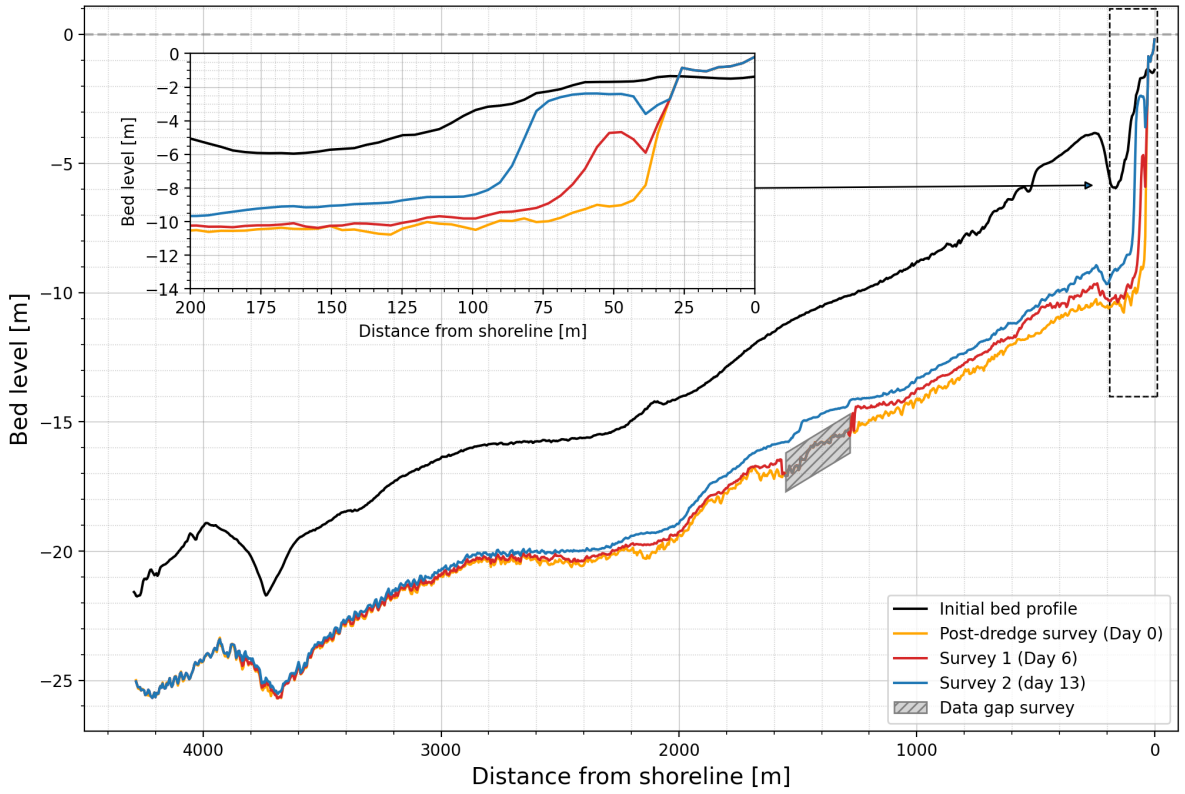

Figure 3.1: Initial bed level and the results of the three surveying campaigns. The inset is focusing on the siltation peaks at at distance of around 50 meter from the shoreline.

Besides the increased siltation rates in the nearshore environment, Figure 3.1 and Figure 3.2 show other interesting features in the data. First of all, a data gap can be seen in the first survey between 1900 meter and 1300 meter from the shoreline. This data gap in the first survey leads to a peak in the siltation thickness for the second survey.

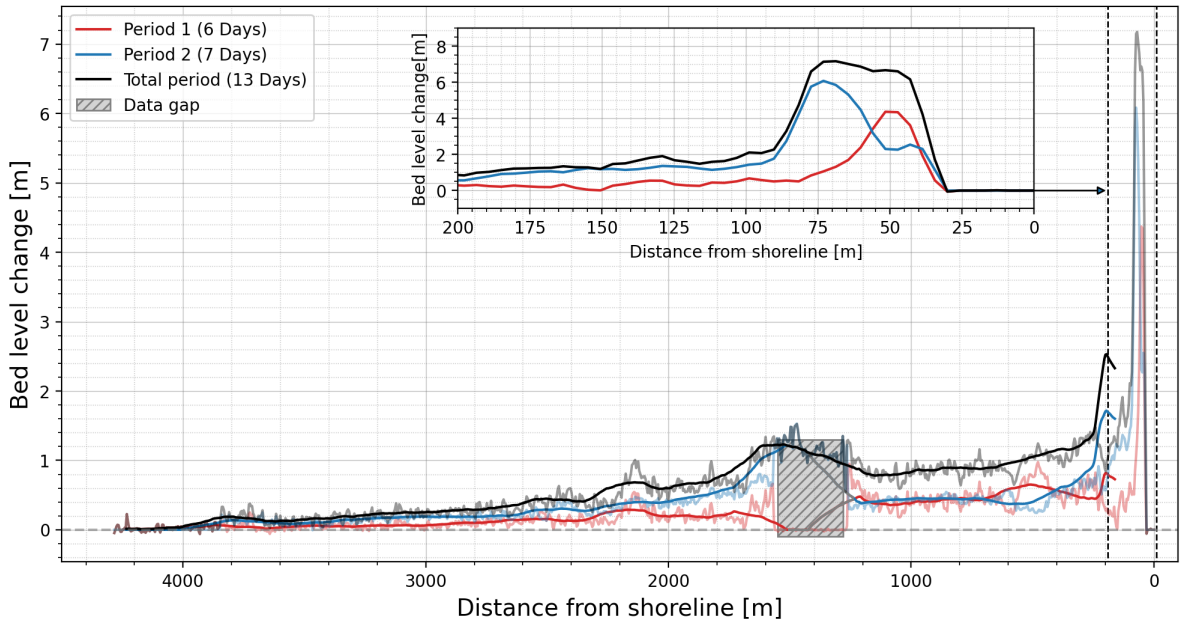

Figure 3.2: Bed level change on the center-axis of the trench per survey period. The solid lines in the foreground represent a moving average of the measurement data, to reduce the scatter in the original data. The inset is focusing on the peaks at at distance of around 50 meter from the shoreline.

3.3. Volume change

Although the representation of bed level changes on the center axis (Figure 3.2) gives some good first insights on the siltation rates, it has to be noted that these bed level changes are the result of several driving forces. On one hand, the tidal current and wave-driven current lead to siltation in the trench. However, in the first days after the dredging of a trench, instabilities of the slope and smoothing of the trench will also contribute to siltation in the center axis of the trench. This sediment transport due to instabilities and smoothing will be referred to as “internal processes”. Furthermore, cross-shore transport through the trench is likely to occur as well, as the profile of the coast has been forced out of equilibrium. To get better eyes on the combined effect of all processes leading to siltation in the trench, a two-dimensional topview of the trench (Figure 3.3) is used to indicate the bed level change in the surroundings of the trench. For better visualisation, only the last 2500 meter of the trench are shown.

When analysing the topview of the bed level change near the trench, another fraction of the data is identified which includes errors or outliers. Directly onshore of the previous mentioned data gap (x=1300 to x=1100 meter), a region of significant large sedimentation rates in survey 1, and significant large erosion rates survey 2 are visible. In this section the sedimentation rates in survey 1, and erosion rates in survey 2, do extend to significantly larger distances from the trench. The exact cause of these patterns are unknown. However, a possible explanation could be linked to the dumping of material. If material was dumped in this region, in the period between the in-survey (Day 0) and survey 1 (Day 6), that would explain the large area of bed level increase. After survey 1, the dumped material is slowly removed by the currents and waves, leading to the erosion rates in the period between survey 1 and 2. No further in-depth analysis on this fraction of the dataset is conducted. It will be taken into account during the use of the data as training data.

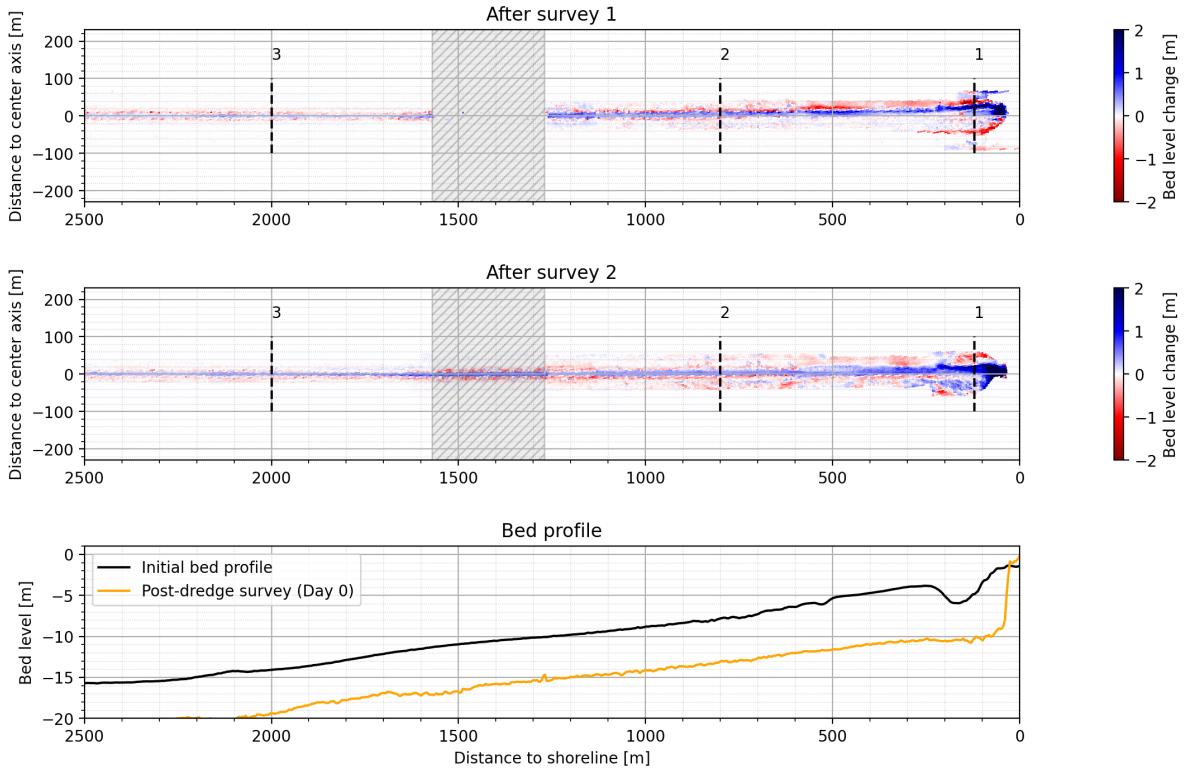

Figure 3.3: Bed level change of the trench in a horizontal perspective. The black dashed lines indicate the cross-sections that are shown in Figure 3.5

To determine the net volume changes of the trench, the trench has been divided into sections with a fixed width. This width can be chosen variable, depending on the accuracy that is desired. Within one section, the net volume change per section is calculated according to:

$$\Delta V_{net} = \sum \Delta z \times \Delta x \times \Delta y \tag{3.1}$$

where Δx = 4.2 m and Δy = 0.6 m, which are determined by the resolution of the mesh-grid that is created from the survey data. Δz is the bed level change of that grid cell according to the difference maps in Figure 3.3. The results, for both period separately, are shown in Figure 3.4.

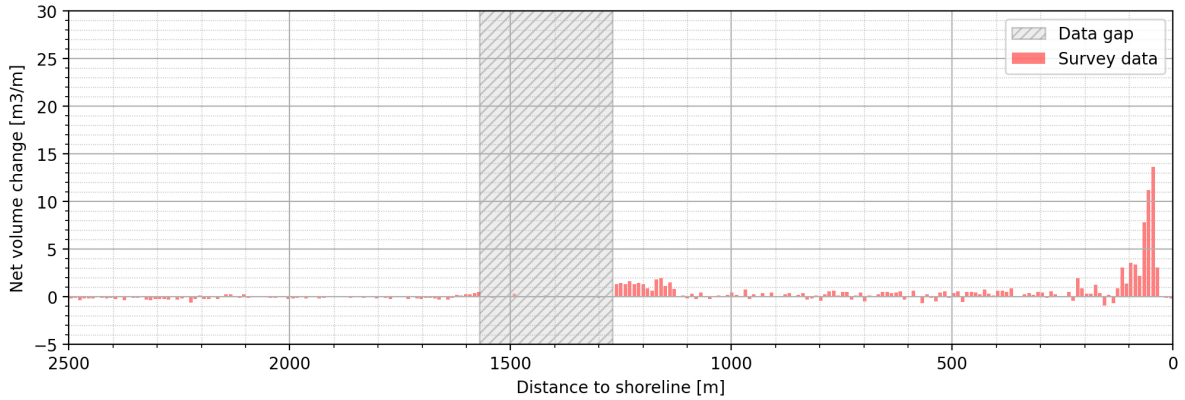

(a) Period 1 (6 Days)

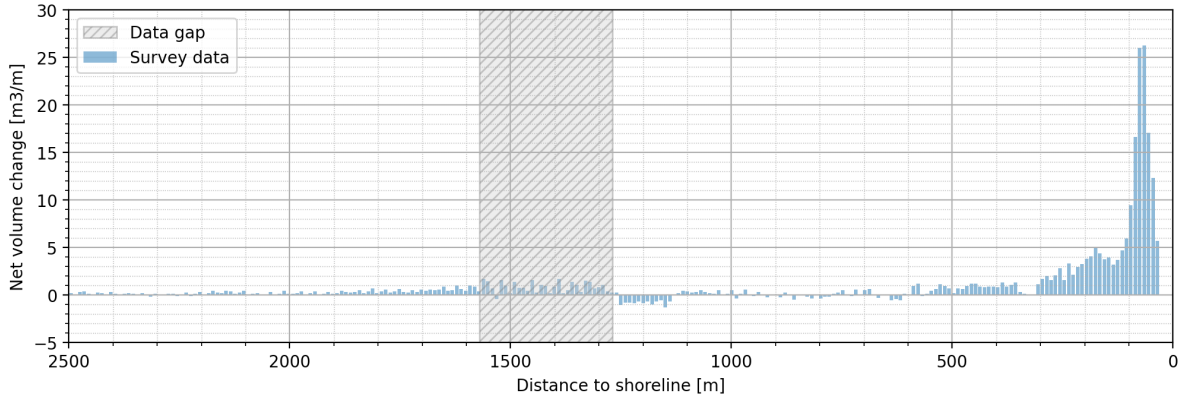

(b) Period 2 (7 Days)

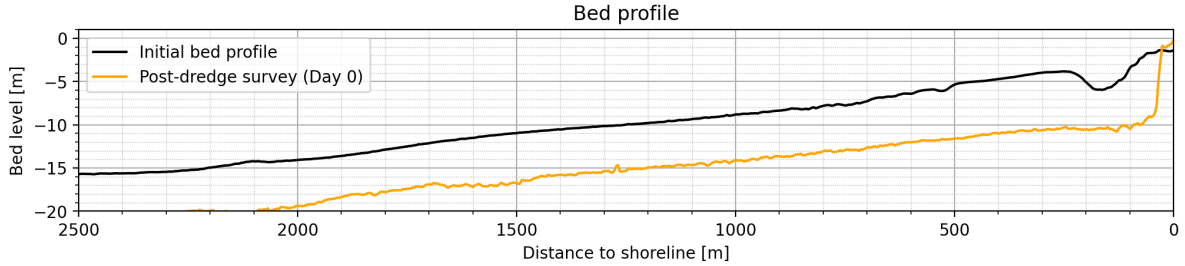

(c) Initial bed level and post-dredge bed level on the center axis of the trench.

Figure 3.4: Net volume change of the trench per section, for the two different periods. In this case a section length of 10 meters was used.

The determined volume changes per section of the trench can be used to calculate a resulting siltation thickness in that section. However, the result of this approach of determining the siltation thickness from the volume change in a section shows large differences with the bed level change that is obtained from depth measurements in the trench, as shown in Figure 3.2. The siltation thickness in Figure 3.2 is the combined siltation of internal processes, cross-shore processes, and longshore transport. The effect of internal processes can not be captured by looking at the net volume change within a section. Due to the reshaping of the trench, a net volume change of zero can have a corresponding non-zero siltation thickness. This is especially the case for the larger depths. The upper two graphs in Figure 3.5 show a negligible small ΔV, while showing a significant bed level change. This shows the large impact of internal processes on the bed level change on the center-axis of the trench. Besides that, in cross-section 3 it can be seen that the trench is behaving very dynamically in the lower depths.

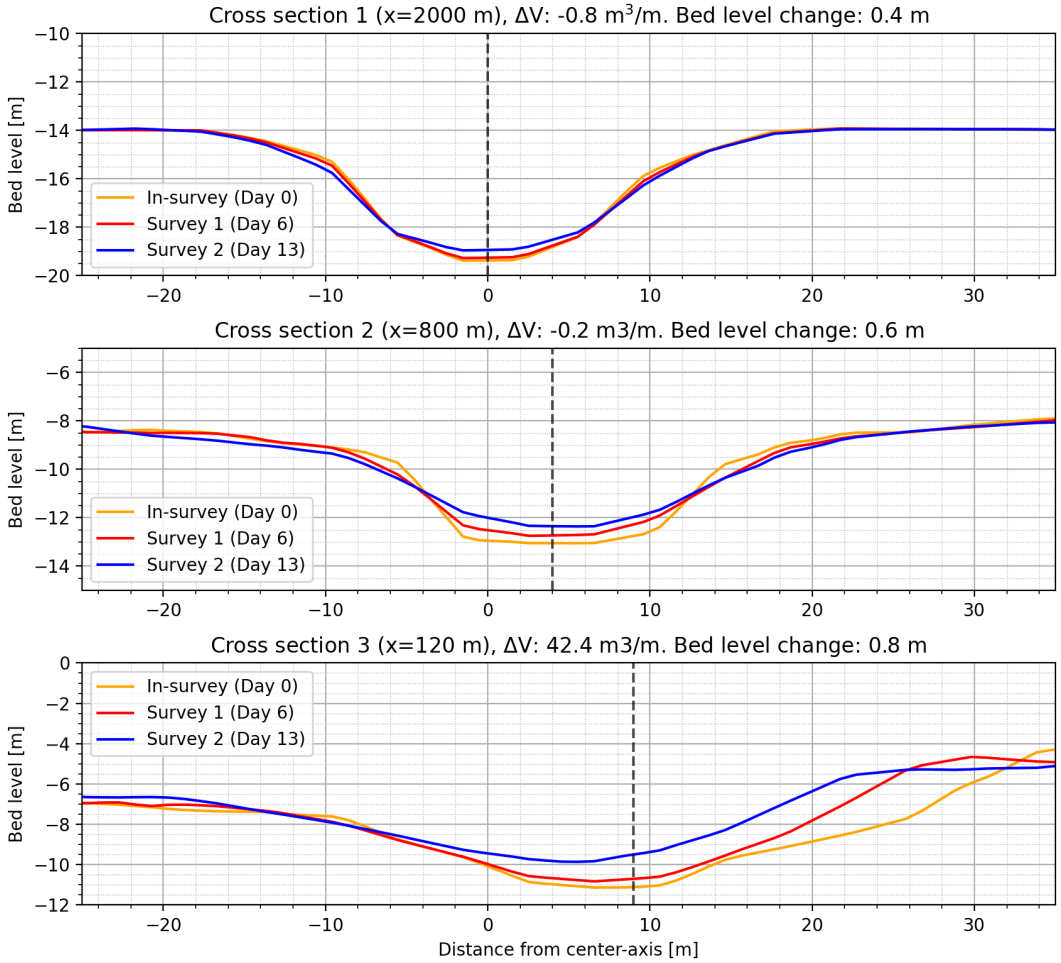

Figure 3.5: Three cross-sections of the trench at three locations. The ΔV and the observed bed level change are stated in the titles. The bed level change corresponds to the location marked by the dashed vertical lines in Figure 3.3. Note that the scale of the y-axis is different for each plot.

When assuming that no sediment is leaving the near proximity of the trench, it can be stated that all net volume change in the trench is the result of deposition of longshore transport and cross-shore transport of sediment. Taking this assumption carries a certain level of risk, as there are several locations in Figure 3.4 where a negative net volume change is calculated. This indicates that there are locations and situations where the net volume in the trench decreases. In these cases, it can be assumed that the sediment that is mobilised by the smoothing of the profile is transported out of the trench (ΔV_L). Another mechanism that is influencing the sediment balance of a trench section is the cross-shore transport of sediment (ΔV_{CS}). This transport is driven by gravitational forces, and the result of the bed profile being forced out of its equilibrium profile (see Section 2.4.3). All sources and sinks of sediment volumes that affect the sediment balance of a trench section are listed below:

$$\Delta V = -\Delta V_L + \Delta V_{LST} + \Delta V_{CS} \tag{3.2}$$

When assuming ΔV_{CS} and ΔV_L to be not affecting the volume balance of a trench section, the net volume change ΔV is a pure result of deposition of longshore transport. From ΔV, the corresponding siltation thickness can be calculated:

$$\Delta s = \frac{\Delta V}{A_s} \tag{3.3}$$

where Δs is the siltation layer in meter, and A_s is the deposition surface. The deposition surface is defined by the length of the section and the width of the bottom of the trench, over which siltation takes place. By investigating Figure 3.3 in more detail, the width of the area that shows a bed level increase, indicated by the blue color, can be estimated. On average, a siltation width of 10 meter is observed.

Dividing the net volume changes ΔV for every section by the deposition surface leads to the siltation thickness as a result of longshore transport (while excluding the effect of cross-shore transport and sediment losses), which are shown in Figure 3.6. The dotted lines represent the bed level change on the center-axis in Figure 3.2.

In Figure 3.5 it can be seen that the assumption that the deposited volume is distributed evenly on the deposition surface does not hold necessary. The deposited volume will be unevenly distributed in the trench, leading to variations in bed level change. However, as the dimensions and design of the trench will be simplified strongly in the model (see Figure 4.5), the assumption of homogeneous deposition does not add substantial over-simplification to the approach.

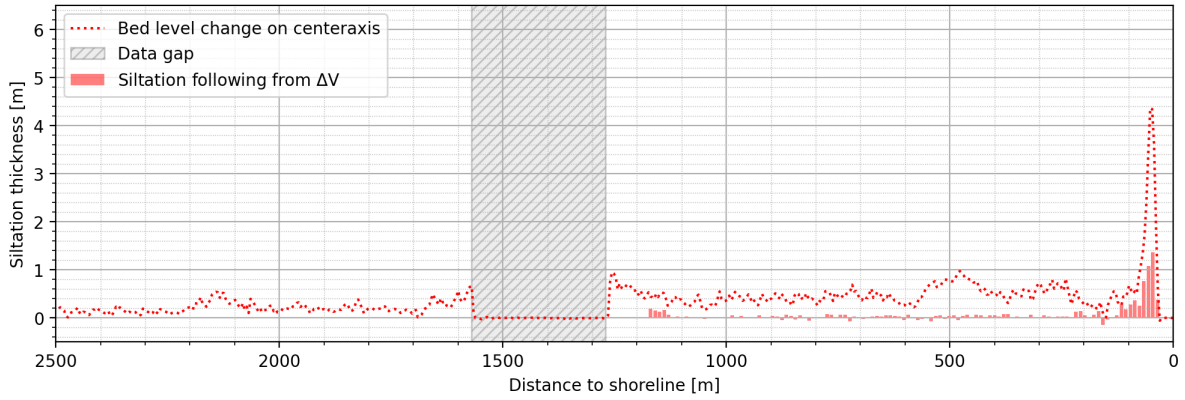

(a) Period 1 (6 Days)

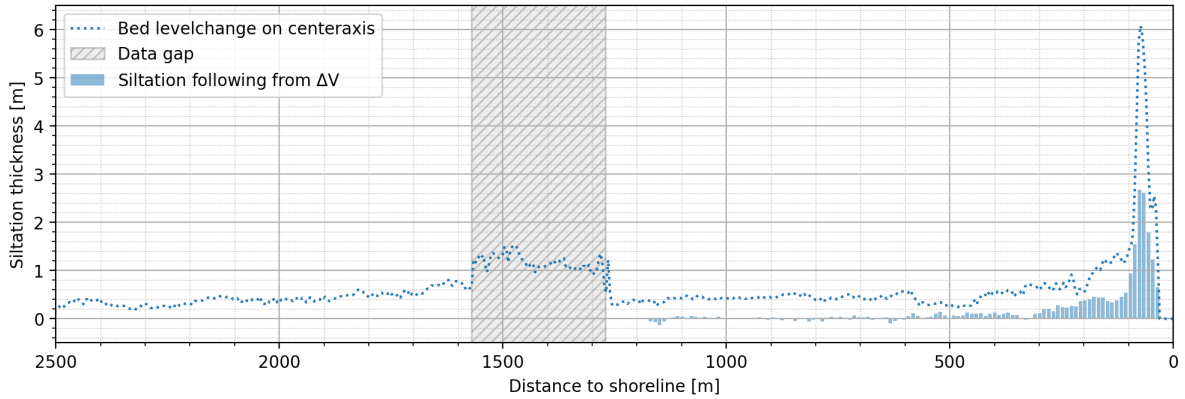

(b) Period 2 (7 Days)

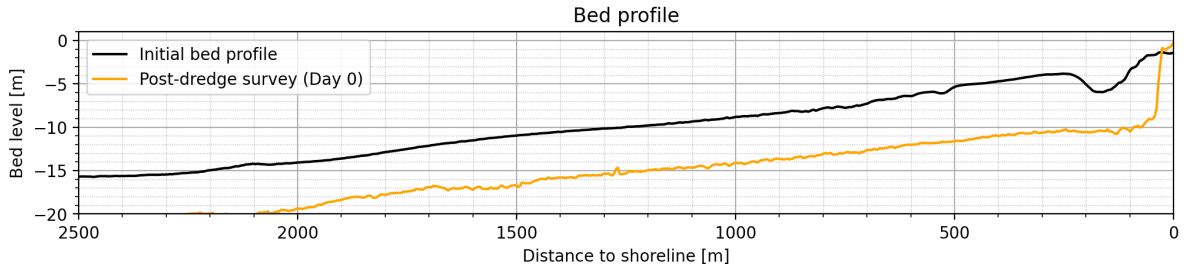

(c) Initial bedlevel and post-dredge bed level on the center axis of the trench.

Figure 3.6: Siltation thickness resulting from ΔV. The dotted lines represent the siltation thickness that results from the transect in Figure 3.2.

Figure 3.6 reveals a significant difference between the bed level change on the center-axis and the siltation thickness following from ΔV. It can be seen that the measured bed level change on the center-axis of the trench is significantly larger than the siltation layer that follows from ΔV. In the more offshore

regions, almost no net volume change is observed in Figure 3.4, while the cumulative bed level change of both periods on the center-axis of the trench reach up to 1 meter. This is expected to be the result of internal movements of sediments from the slope into the bottom of the trench, and cross-shore transport of sediment.

3.4. Execution artefacts

When looking at the more onshore regions (between x=0 m and x=300 m) in Figure 3.6, the siltation layer resulting from ΔV shows a steep increase, while still leaving behind a residual effect on the bed level change along the center-axis of the trench. In these regions, the sediment volume balance is affected by not only internal processes and cross-shore transport, but also an artefact of the execution of the project. When investigating the bed level change in Figure 3.3 in more detail, a sidecast with a length of almost 200 meter can be noted. The sidecast is indicated by the black rectangle. A sidecast is a section of sediment that is deposited parallel to the trench during the dredging process. It is placed there for practical purposes, such as using the sediment to refill the trench after cable or pipeline installation, or to reduce transportation costs of the dredged material. During the first period of surveys, the largest waves are observed with a direction that results in a southward-directed net longshore currents, which can be seen in Figure 3.9 in combination with the defined directions in Figure 3.8. The sidecast is located north of the trench, which makes it plausible that the gross of the volume of the sidecast has been transported into the trench within the first period of surveys. However, as the sidecast is included while determining the sediment balance ΔV per trench section, the erosion of the trench is not counted in the determination of the siltation thickness following from ΔV.

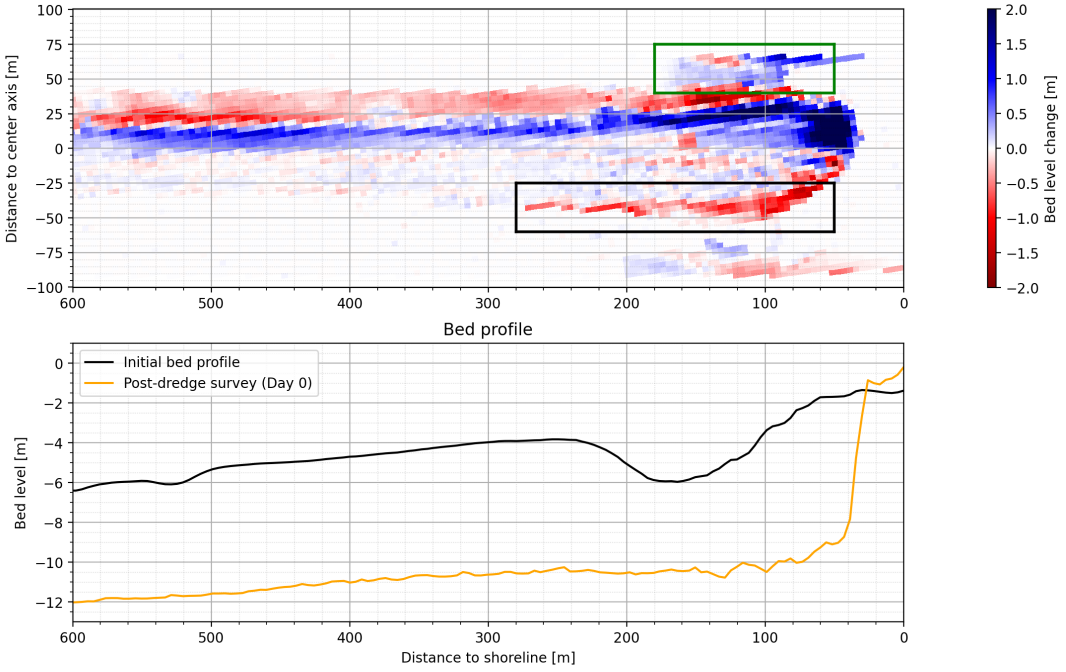

Figure 3.7: Bed level change in the first period. The black rectangle indicates the erosion of the sidecast. The green rectangle indicates the sedimentation in the floatation pit.

Another artefact of the execution can be seen in cross-section 3 in Figure 3.5. The bed levels of all three survey campaigns are up to 2 meter lower south (left) of the trench than north (right) of the trench. This is the start of the floatation pit, which is located south of the trench. As discussed in Section 2.2, a floatation pit provides the needed nautical depth of maritime equipment to operate near the shoreline. The floatation pit can also be identified in Figure 3.7 by the region of siltation just south of the trench, indicated by the green rectangle. In principle, the floatation pit behaves similar to a trench, which explains the high sedimentation rates in this region.

3.5. Metocean data

Besides the survey data of the depths, the wave conditions and local currents during the respective period were measured by an ocean buoy, located around 30 kilometers offshore, at a depth of approximately 50 meter. This data contains information on the wave height, wave period, wave direction, and local currents. The local currents are included as U_0 and U_{10}, where the subscript is indicating at which depth the current is measured. Both are shown in Figure 3.9. To exclude the effects of wind as much as possible, and remain with the value representing purely the tidal current, the value of U_{10} is used in the further analysis. Any other ocean currents are neglected in this analysis. The dataset from the buoy does not include information on the tidal elevation. As this is important information in the further analysis, data on the tidal elevation has been retrieved from Delft Dashboard (Van Ormondt et al., 2020). Delft Dashboard is an open-source program, developed by Deltares, which enables users to quickly set-up hydrodynamic models, including tidal forcing, on any location worldwide. The tidal elevation was modelled for a location at a depth of 50 meter. The data from the buoy and Delft Dashboard are shown in Figure 3.9

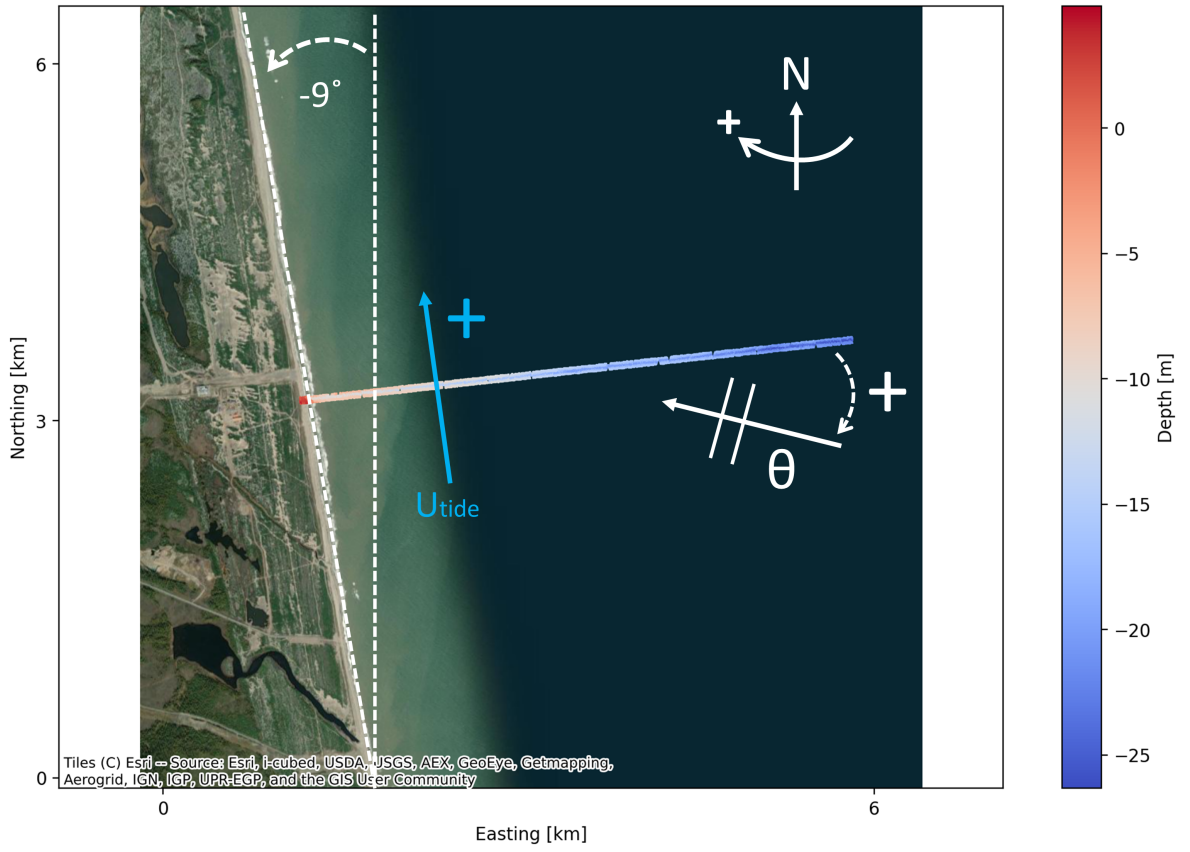

Figure 3.8: Survey data placed on satellite image of the surrounding coastline. Including the definition of the wave direction and the tidal current direction.

When looking at the wave direction θ in Figure 3.9, an outlier can be identified around day 3, where the wave angle exceeds 90°. Besides that, several other timesteps in the dataset can be seen where wave direction has an angle with respect to the shore-normal which is larger than 90°. These outliers are plotted in orange in Figure 3.9. These situations coincide with low wave heights, and relatively large wind speeds with directions that correspond with the wave directions. This could implicate that during this period, a strong offshore directed wind dominated the wave conditions, leading to no significant waves approaching the shoreline. However, wave angles that exceed 90° will lead to instabilities in the MBJ-model. To avoid these instabilities, timesteps with a wave angle θ > 90 ° are removed from the timeseries. As these are timesteps with no significant wave heights near the trench, no significant amounts of siltation are neglected.

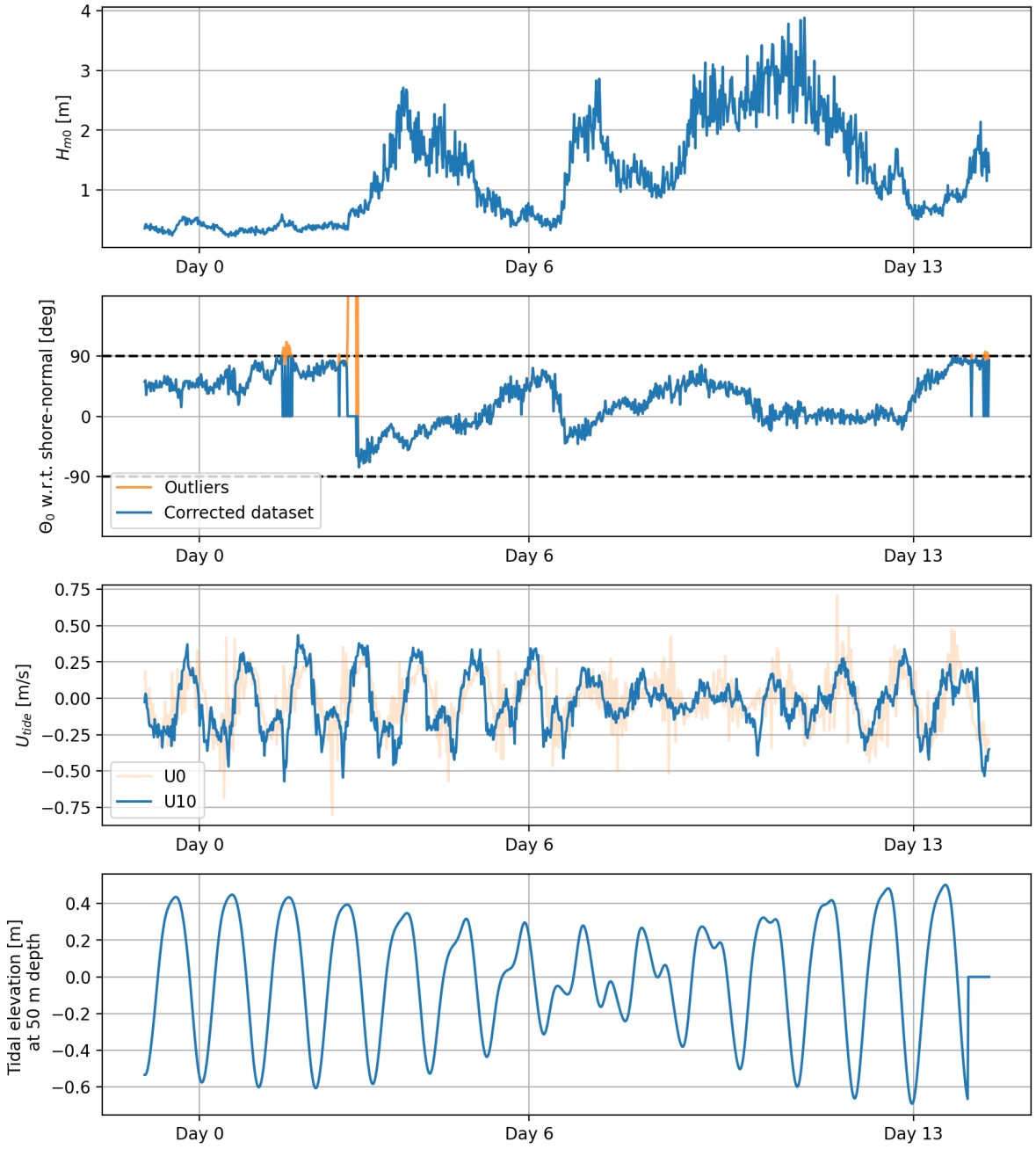

Figure 3.9: Metocean data near the location of the trench. H_{m0}, θ_0, and U_{tide} are retrieved from an offshore buoy. The tidal elevation is retrieved from Delft Dashboard. Period one starts at Day 0 and ends at Day 6, while period 2 starts at Day 6 and ends at Day 13.

4

Methodology

This section presents the methodology of this research. First, in Section 4.1, the modelling will be introduced. In Section 4.2, the modelling of the hydrodynamics is explained. In Section 4.3, the modelling of the hydrodynamics is validated. In Section 4.4, the existing formulae in SedPit are presented, and the modelling steps to combine the modelling of the hydrodynamic processes with the existing SedPit tool are presented. In Section 4.5, the method and implementation of the sensitivity analysis, is described. In Section 4.8, the method and implementation of the sensitivity analysis is described. In Figure 4.1, the relation between the research outline as presented in Figure 1.1 and the applied methods in visualised.

4.1. Introduction to modelling

The model that will be used in this report is a physics-based model. Although the recent years have shown the added value of machine learning and deep learning (neural networks) in the modelling of complex processes, the physics-based models come with some benefits that models based on neural networks do not have (Vadyala et al., 2022). Vadyala et al. (2022) stated that the use of neural networks is especially challenging in the field of civil engineering. One of the main complications identified is the "lack of generalizability to out-of-sample scenarios" (Vadyala et al., 2022). However, for the purpose of this report, the main reason that a physics-based model is used is the "interpretability". Neural networks are often considered as "black box". The relationship between input parameters and variables are often unknown to the user (Vadyala et al., 2022). By building the model around physics-based formulae, the model is more interpretable to the user, and can even easily be modified according to the needs of the user.

The whole modelling approach consists of two steps. The first step is to develop a model that simulates the generation of longshore currents on a shore-normal transect. This model is based on a 1D-transect perpendicular to the shoreline. This is shown in Figure 4.2. This transect starts just offshore of the nearshore environment. At these depths, the waves do not show nearshore transformation processes yet. The transect ends at the shoreline. The transect is located on the axis of the trench. Along this transect, the wave characteristics will be calculated on a number of grid points. The wave characteristics that are calculated on all grid points are discussed in Section 4.2. The needed input for the modelling of the hydrodynamics is a timeseries, containing the required offshore wave data. Besides that, the bed profile along the transect should be known or approximated.

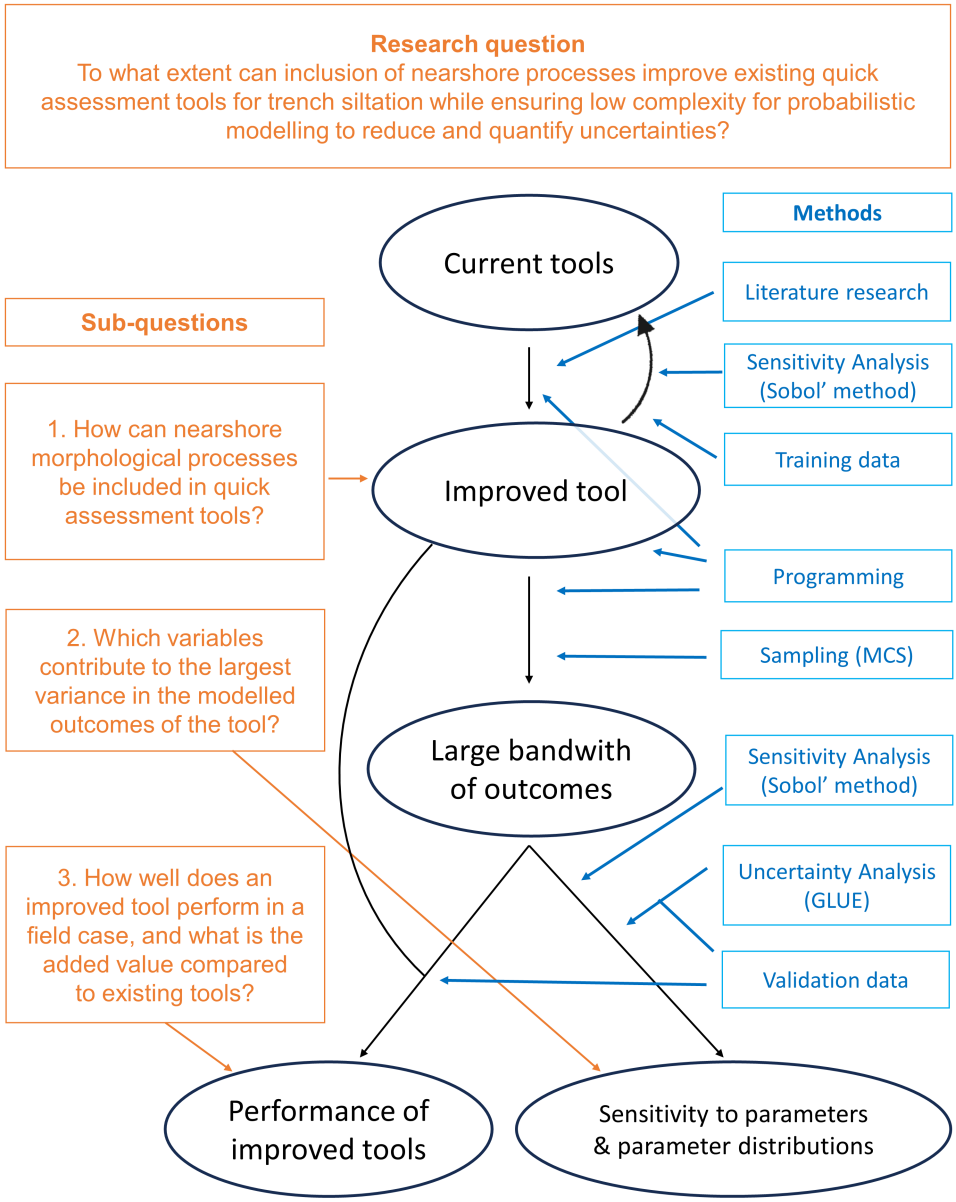

Figure 4.1: Schematic outline methodology: The orange boxes represent the research (sub)-question(s). The orange arrows indicate to which stage of the research the sub-questions are related. The blue boxes represent the methods. The blue arrows indicate where in the process the methods will be applied.

The timeseries including the wave conditions should have sufficient large timesteps to obtain reliable wave statistics, as the modelling of the hydrodynamics is based on fixed values for the significant wave height H_s, H_{rms}, θ, and T_p within a certain period. This also entails one of the simplifications of the model. A wave field is characterised by one representative value for H_s, H_{rms}, θ, and T_p each per timestep. As a result, average flow velocities during the timeframe will be calculated. The timestep can be varied, depending on the available data or the goal of the specific application of the tool. For very rough estimates, a constant wave climate can be used, while hourly data will lead to a more detailed result.

This first model is based on the work of Battjes and Janssen (1978), who developed the BJ78-model. The BJ78-model is a 1D-wave transformation model, based on relatively simple, straight-forward, and well-known formulae, which makes it a interpretable model. One of the advantages of the BJ78-model compared to alternative approaches is that it is not dependent on a monotonically decreasing depth profile, and is therefore also applicable in bar-through systems (Battjes & Stive, 1985). Also in more

recent approaches in modelling coastal morphodynamics, the BJ78-model is referred to as suitable, accurate, and widely used approach (Roelvink & Reniers, 2011). In Section 4.2 the principles of the hydrodynamic modelling of this report will be presented. The model will be referred to as modified BJ78-model (MBJ), as it is strongly based on the model by Battjes and Janssen (1978). However, some formulations are modified, the tidal current is added, and the effect of wave rollers is included.

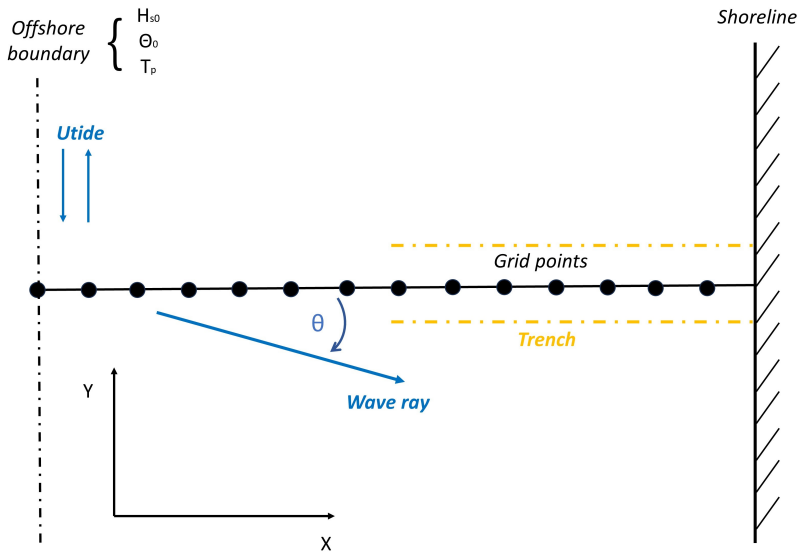

Figure 4.2: Schematisation of model geometry. Inspired by Southgate (1989)

The second step of the modelling approach is related to the siltation processes. After having computed the hydrodynamics on every grid point, the local flow velocities are used as input for the modelling of the local sediment transport. In this step, the existing SedPit-tool is integrated to model the sediment transport rates and trapping efficiency of the trench (Van Rijn, 2013). See Appendix A for information on the existing SedPit tool. The width of the trench is included in these formulae, which adds a dimension to this part of the model. The transect is divided in grid cells. For every grid cell, the input is based on the flow velocities resulting from the modelling of the hydrodynamics. The formulae in SedPit will return a siltation volume and siltation layer for every grid cell. In this way, the cross-sectional variation of flow velocities are incorporated into a cross-sectional variation of siltation rates.

4.2. Modelling of hydrodynamics

In this section the steps taken in formulating the MBJ-model are presented. First, in Section 4.2.1 the formulae to calculate the wave-driven longshore current will be presented, followed by the modelling of the tidal current in Section 4.2.2.

The effect of rip currents is not included in this report. As described in Section 4.1, the model is based on a 1D shore-normal transect. On all grid cells on this transect, the relevant wave characteristics will be modelled, in order to estimate the alongshore current on these location. The presence of rip currents leads to seaward directed currents (Dalrymple et al., 2011). The directions of the rip currents and alongshore current are therefore perpendicular. An accurate inclusion of rip currents would demand a 2D-approach, which would add complexity to the model and contradict the aim of a quick-assessment approach. Nevertheless, this report does take into consideration the potential impact of rip currents on the cross-shore transport of sediment.

4.2.1. Formulae and simplifications wave-driven current

The modelling of the longshore current is based on the following momentum balance, that also forms the base of the work by Ruessink et al. (2001):

$$-\frac{dS_{yx}}{dx} + \tau_w - gh\rho\frac{d\zeta}{dy} = c_f\rho\overline{|\vec{u}V|} - \frac{d}{dx}\left(\nu h\frac{dV}{dx}\right) \tag{4.1}$$

However, within the scope of this project the wind friction τ_w and mixing $\frac{d}{dx}\left(\nu h\frac{dV}{dx}\right)$ are not considered, due to simplification needs. Besides that, the tidal forcing is not included by means of its driving force, which is the alongshore water gradient $gh\rho\frac{d\zeta}{dy}$, but is included in the model in a later step through offshore tidal current velocities. However, this approach of not including tidal forcing within the momentum balance brings some additional modelling steps in a later phase, where wave-driven currents and tidal currents are combined. This is discussed in Section 4.2.3. The choice of including the tidal forcing as offshore currents, instead of alongshore water gradient is the result of the available data in common applications of siltation tools. Together with data on the wave climate, the tidal currents are retrieved from a offshore buoy or simulated based on the tidal amplitude at the specific project location. The above-mentioned simplification steps and modelling choices reduce the momentum balance in Equation (4.1) to:

$$-\frac{dS_{yx}}{dx} = c_f\rho\overline{|\vec{u}V|} \tag{4.2}$$

The first step in the modelling methodology of the MBJ-model is to model the wave transformation, which consequently leads to the gradient in radiation stress that forms the driving force for the longshore current in Equation (4.2).

The MBJ-model includes several formulae related to to wave transformation of waves in deep water to waves in shallow water. One of the formulae describes the dispersion relation. The dispersion relation is used to find the wave number k as a function of the angular frequency ω and the water depth h:

$$\omega^2 = \left(\frac{2\pi}{T}\right)^2 = gk\,\mathsf{tanh}(kh) \tag{4.3}$$

where T is the wave period, k is the wave number, h is the local water depth, and ω is the angular wave frequency. Since Equation (4.3) is a nonlinear function in terms of k, it is not possible to find an analytical solution (Guo, 2002). Hunt (1979) proposed an approximation that makes it possible to analytically approximate the dispersion relation, which is based on a Taylor expansion of the function $y = x\,\mathsf{tanh}(x)$:

$$(kh)^2 = x^4 + \frac{x^2}{1 + \sum_{\beta=1}^{6} d_\beta (x^2)^\beta} \tag{4.4}$$

where $x = \omega h/\sqrt{gh}$, $d_1 \approx 0.67$, $d_2 \approx 0.35$, $d_3 \approx 0.16$, $d_4 \approx 0.47$, $d_5 \approx 0.021$, $d_6 \approx 0.0065$. This approximation shows an error of 0.01% (Hunt, 1979). By using the approximation in Equation (4.4), the wave number k can be found by:

$$k = \frac{kh}{h} \tag{4.5}$$

When knowing the wave number k, the local depth h and the wave period T, next the wave coefficient n, wave velocity c, group velocity c_g, and wave length L can be found with Equation (4.6), Equation (4.7), Equation (4.8), and Equation (4.9) respectively:

$$n = \frac{1}{2}(1 + \frac{2kh}{\mathsf{sinh}(2kh)}) \tag{4.6}$$

$$c = \frac{L}{T} \tag{4.7}$$

$$c_g = cn \tag{4.8}$$

$$L = \frac{2\pi}{k} \tag{4.9}$$

The effects of refraction are included in the BJ78-model according to Snell's Law as described in Equation (2.10):

$$\frac{\sin(\theta_1)}{c_1} = \frac{\sin(\theta_0)}{c_0} \tag{4.10}$$

where c_1 and θ_1 are representing the wave velocity and wave angle respectively on a location on a shore-normal transect, and c_0 and θ_0 are representing the wave velocity and wave angle respectively in deep water.

The MBJ-model includes depth-induced breaking. The maximum wave height H_{max} is defined according to Battjes and Janssen (1978):

$$H_{max} = \frac{0.88}{k} \tanh\left(\gamma \frac{kh}{0.88}\right) \tag{4.11}$$

where γ is the wave breaking coefficient, k is the wave number, and h is the local water depth.

As the MBJ-model is considering one representative wave height for a distribution of wave heights, a probability distribution is used to describe the effect that the fraction of waves that are larger than the chosen representative wave height might reach the maximum wave height H_{max} earlier than the representative wave. This is a common simplification to describe the breaking behaviour in a random wave field. The probability that a wave in the field breaks on a certain location is known as the fraction of broken waves Q_b. A variety of probability descriptions do exist (e.g. Baldock et al. (1998)). The distribution as defined by Battjes and Janssen is:

$$\frac{1 - Q_b}{\ln(Q_b)} = -\frac{{H_{rms}}^2}{H_{max}} \tag{4.12}$$

Equation (4.12) is a implicit relation which can not be solved analytically. An accurate approximation is given by Grasmeijer (2006):

$$Q_b = \exp\left(\frac{0.97(\frac{H_{rms}}{H_{max}})^2}{0.657(\frac{H_{rms}}{H_{max}})^2}\right) \tag{4.13}$$

In the MBJ-model, the wave energy balance is used to include dissipation sinks. Dissipation by wave breaking and dissipation by bottom friction are included in the wave energy balance.

$$\frac{\partial E_w c_g \cos\theta}{\partial x} = -D_w - D_f \tag{4.14}$$

where c_g is the wave group velocity, θ is the incident wave angle, and E_w is wave energy, formulated by (Equation (2.16)).

The energy of the wave rollers is included according to the approach of Ruessink et al. (2001). Ruessink et al. introduces an energy balance for rollers, which defines the roller energy as a function of wave breaking dissipation:

$$\frac{\partial}{\partial x}(2E_r c \cos(\theta)) = -D_r + D_w \tag{4.15}$$

where E_r is the roller energy, D_r the roller dissipation, and D_w the dissipation by wave breaking.

The wave energy dissipation due to wave breaking is formulated by Battjes and Janssen (1978):

$$D_w = \frac{1}{4}\alpha Q_b f \rho g H_{max}^2 \tag{4.16}$$

in which Q_b is the fraction of broken waves, f is the mean frequency ($1/T$), and α is a wave dissipation coefficient, in the order of 1 (Battjes & Janssen, 1978). According to Roelvink and Reniers (2011) the value of α is generally kept at $\alpha = 1$.

The roller dissipation is defined according to (Deigaard, 1993):

$$D_r = \frac{2gE_r \sin(\beta)}{c} \tag{4.17}$$

where E_r is the roller energy (according to Equation (4.18)), β is the wave-front slope, which is usually estimated at a value of 0.1 or less (Walstra et al., 1997).

As Equation (4.15) and Equation (4.17) mutually influence one another, the inclusion in the model needs a schematic forward-stepping approach. The roller energy is calculated, based on the roller energy, roller dissipation, and breaker dissipation in the previous step. At the offshore boundary, the roller energy is set to zero, given that no rollers are generated at the offshore boundary.

$$E_{r,x+\Delta x} = E_{r,x}\frac{c_x \cos(\theta_x)}{c_{x+\Delta x}\cos(\theta_{x+\Delta x})} + \frac{(-D_r + D_{br})\,\Delta x}{2c_{x+\Delta x}\cos(\theta_{x+\Delta x})} \tag{4.18}$$

The third dissipation term is dissipation due to bottom friction. Bottom friction is not part of the original BJ78-model, as the original BJ78-model was developed to model the wave transformation of waves in the breaking zone, in which the dissipation due to wave breaking is dominating the dissipation of bottom friction. The same conclusion is drawn by Ruessink et al. (2001), who did not include bottom friction in their model to predict hydrodynamics in the nearshore environment. However, the principle of bottom friction is presented below.

$$D_f = \rho f_w |u|^3 \tag{4.19}$$

where u is the near-bed orbital wave motion, according to (Roelvink & Reniers, 2011) (2011) defined as:

$$u_{orb} = \frac{\omega H_{rms}}{2T\sinh(kh)} = \frac{\pi H_{rms}}{T_{rep}\sinh(kh)} \tag{4.20}$$

where T_{rep} is a representative wave period that is related to the peak period T_p. According to (Holthuijsen, 2007), for wind-waves $T_{rep} \approx 0.95 \times T_p$, while $T_{rep} \approx 1 \times T_p$ for swell waves (Goda, 1988). In Equation (4.20), f_w is the wave-related friction coefficient described according to the reformulation by Swart (1974), of the formula derived by Jonsson (1963):

$$f_w = \exp\left(-6 + 5.2\left(\frac{A_b}{k_s}\right)\right) \tag{4.21}$$

where k_s is the bottom roughness, A_b is the particle excursion amplitude near the bed, defined as:

$$A_b = \frac{uT}{2\pi} = \frac{H}{2\sinh(kh)} \tag{4.22}$$

The wave height transformation in MBJ-model follows from the wave energy balance in Equation (2.16). By substituting Equation (2.16), and Equation (4.8) into Equation (4.14), the following expression for the gradient of H_{rms} in x-direction is obtained:

$$\frac{\partial H_{rms}}{\partial x} = \frac{8(-D_f - D_w)}{\rho g n c \cos\theta} \tag{4.23}$$

The transformation of wave height leads to a gradient in radiation stress S_{yx} in x-direction, as discussed in Section 2.3.4, with a resulting wave force in y-direction:

$$F_y = -\frac{dS_{yx}}{dx} \tag{4.24}$$

The addition of roller dissipation leads to an addition of a roller energy related term in the formulation of the radiation stress S_{yx} in Equation (2.15):

$$S_{yx} = n\cos\theta\sin\theta E_w + 2E_r\cos\theta\sin\theta \tag{4.25}$$

where E_w is the wave energy according to Equation (2.16).

The gradient of the alongshore component of the radiation stress $S_{y,x}$ in shore-normal direction (dx) can be approximated by linearisation between two cross-sectional points. By calculating the definition

of the radiation stress S_{yx} as defined in Equation (2.15) for two consecutive points on the shore-normal x-axis, the following approximation for the gradient in radiation stress is obtained:

$$\frac{dS_{yx}}{dx} = \frac{n_{x+\Delta x} \cos\theta_{x+\Delta x} \sin\theta_{x+\Delta x} E_{x+\Delta x} - n_x \cos\theta_x \sin\theta_x E_x}{\Delta x} \tag{4.26}$$

As stated in Section 2.3.4, the force that is generated by the gradient in radiation stress is balanced by the bed shear stress. The formulation for the bed shear stress as presented in Equation (2.14) is representative for a current-only situation. However, the nearshore environment is a situation where current and waves occur simultaneously (Grant & Madsen, 1979). Therefore, the dimensionless friction coefficient c_f in Equation (2.17) should represent both current-related as well as wave-related friction. Besides that, the term of $|u|u$ for current velocity in Equation (2.14) should be replaced by a combination of wave motion and longshore current. In a wave-only situation, the water particles would be expected to move up-and-down a straight line, as a result of the wave orbital velocity. The combination of the wave orbital velocity and the longshore current leads to a sinusoidal path of the water particle, as is illustrated in Figure 4.3.

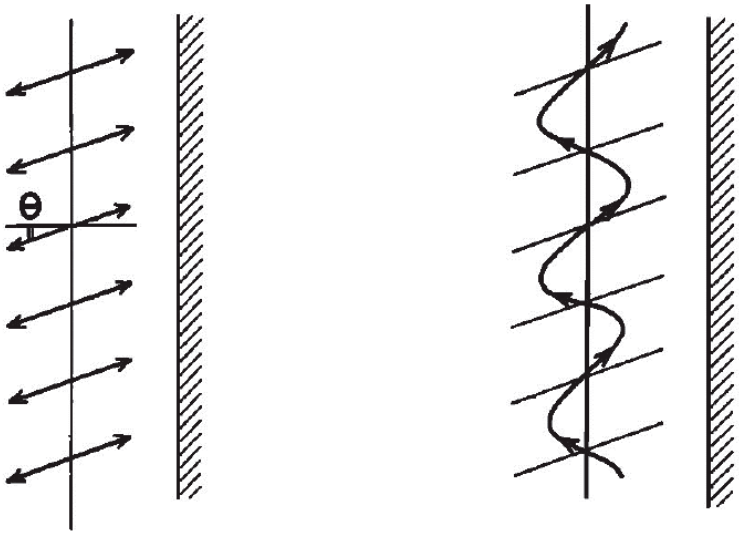

Figure 4.3: Schematic representation of (left) water particle motion with only wave orbital velocity, and (right) water particle motion with wave orbital velocity and longshore current. θ is representing the nearshore wave angle (Longuet-Higgins, 1970)

According to Longuet-Higgins (1970), the term $|u|u$ in Equation (2.14) can be replaced by $\overline{|\vec{u}V|}$, in which $\vec{u}$ is the orbital velocity vector, V is the alongshore current, and the overbar is representing a time-average over multiple wave periods:

$$\overline{\tau}_{b,y} = \overline{\rho c_f |\vec{u}| V} \tag{4.27}$$

Ruessink et al. (2001) proposed an approach on the bed shear stress associated with currents and waves. He proposes the following definition of $\overline{|\vec{u}V|}$:

$$\overline{|\vec{u}V|} = \sigma_T V \sqrt{1.16^2 + (V/\sigma_T)^2)} \tag{4.28}$$

where σ_T is the wave-orbital velocity variance, which is given by $\sigma_T = u_{rms}/\sqrt{2}$ (Feddersen et al., 2000). In this formula u_{rms} represents the root-mean squared orbital wave velocity amplitude, which is, according to Holthuijsen (2007) formulated as:

$$u_{rms} = \frac{u_{orb}}{\sqrt{2}} = \frac{\pi H_{rms}}{T_{rep} \sinh(kh)} \tag{4.29}$$

where u_{orb} is defined according to Equation (4.20). This approach is also incorporated in recent modelling packages, including XBeach (Deltares, 2023).

Different approaches are presented throughout literature for the definition of the friction coefficient c_f in Equation (4.27). One of the most simplified methods is presented in the original BJ78-model (Battjes & Janssen, 1978). Battjes and Janssen propose to use a wave-current combined friction coefficient, defined as:

$$f_{cw} = \sqrt{f_w f_c} \tag{4.30}$$

where f_w is defined according to Equation (4.21) (Swart, 1974), and f_c is defined according to the Chézy-law:

$$f_c = \frac{g}{C^2} = \frac{g}{(18\log(12h/k_s))^2} \tag{4.31}$$

Substituting Equation (4.30) in Equation (4.27) yields a formulation for the bed shear stress. Substituting this definition of bed shear stress in Equation (2.13) yields the following expression for the longshore current V:

$$V = \frac{dS_{yx}}{dx}\frac{1}{\rho\sqrt{f_w f_c}\overline{|\vec{u}V|}} \tag{4.32}$$

Besides the definition of bed friction according to Battjes and Janssen (1978) in Equation (4.30), different approach to formulate the bed friction do exist. One of them being the empirical equation by Bijker (1967), which is used in the work of Ruessink et al. (2001):

$$c_f = 0.015\left(\frac{k_s}{h}\right)^{1/3} \tag{4.33}$$

From the varying formulations above, it becomes clear that parameters can be described in different ways. During the validation of the MBJ-model, it is important to take into account what definitions are used in the origin of the validation data.

4.2.2. Modelling tidal current

The tidal current velocities in the nearshore environment are depending on the offshore current velocities and the local water depth, as discussed in Section 2.3.1. The tidal current velocity can be related to the offshore tidal current velocity according to Equation (2.7):

$$U_{tide,2} = U_{tide,1}\sqrt{\frac{h_2}{h_1}} \tag{4.34}$$

where $U_{tide,1}$ and h_1 are the tidal current velocity and water depth at a known location respectively, and $U_{tide,2}$ and h_2 are the tidal current velocity and water depth at a more onshore location. The resulting nearshore current velocities on a shore-normal transect are shown in Figure 4.4. Figure 4.4 illustrates the transformation of the tidal current velocity for a Dean profile (Figure 4.4a) and for a bar profile (Figure 4.4b).

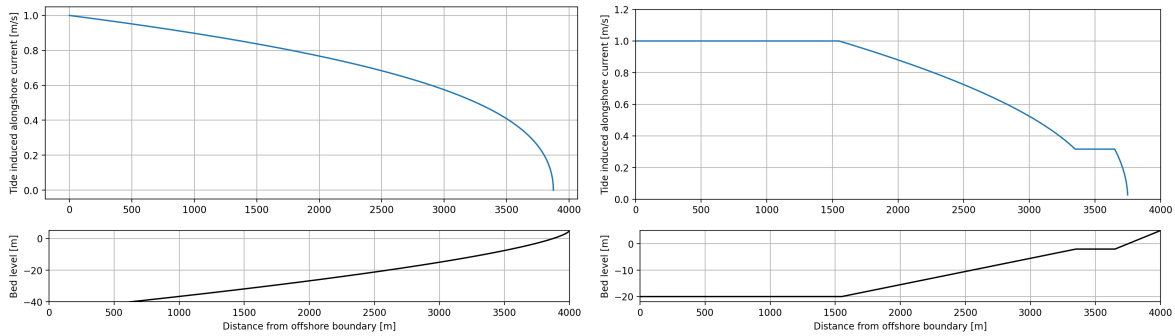

(a) Run 01: Dean profile, U_1 = 1.0 m/s

(b) Run 07: Bar profile, U_1 = 1.0 m/s

Figure 4.4: Nearshore tidal current velocities for two different types of profile. In both cases, the tidal current at the offshore boundary is set to 1.0 m/s

4.2.3. Modelling the combination of tidal and wave-driven currents

The resulting current is a combination of the tidal current and the wave-driven current. However, the combined current can not be calculated by a simple summation of both currents. This is the result of including the tidal forcing in the form of current velocities, instead of waterlevel gradient in Equation (4.1).

The momentum balance in Equation (4.1) is implying that any generated current is counter-forced by the bed friction. The relation between current and bed shear stress is a quadratic relation, as can be seen in Equation (2.14). To account for this quadratic relation in the summation of tidal current and wave-driven current, the following simplified approach will be implemented in the MBJ-model:

$$|U_{tot}| = \sqrt{|U_{tide}^2 + V^2|} \tag{4.35}$$

Although Equation (4.35) takes the absolute value, the resulting direction of the combination of tidal current and wave-driven current is taken into account.

4.3. Validation modelling of hydrodynamics

Different approaches are used to validate the accuracy of the MBJ-model. First, the modelling of the tidal current is validated by a comparison to the results of a study by De Wit (2016). Next, the wave-driven longshore current, including the wave transformation is validated by comparison to results from XBeach runs, and field data from the Coast3D campaign. The different validations are presented extensively in Appendix B. This section points out the most important conclusions from the validation.

The modelling of the tidal current, according to Equation (4.34) is a good and efficient method. It does not demand much input data, besides a bed profile and an offshore tidal current. The validation is done by a comparison to the work of De Wit (2016).

The validation of modelling of the wave-driven alongshore current in the MBJ-model is conducted in several steps. First, the wave transformation in the MBJ-model is compared to the wave transformation in XBeach. In Appendix B, one test case is used to illustrate the wave transformation. Next, the modelling of the wave-driven alongshore current is validated by the outcomes of 8 different XBeach runs. XBeach is an open-source numerical model to simulate hydrodynamic and morphodynamic processes. Amongst others, it includes short-wave transformation, long wave (infragravity waves) transformation, and currents. XBeach has three modes regarding the wave transformation and hydrodynamics: the stationary mode, the surf-beat mode, and the non-hydrostatic mode. In the stationary mode, all wave-group variations and the resulting long waves are neglected. In the surf beat mode, these long waves are included, as well as their effect on currents (Deltares, 2023). The non-stationary mode is wave-resolving mode, allowing the modelling of individual waves. In this validation, all XBeach runs are done in the stationary mode, since the MBJ-model does not include long waves. XBeach is chosen as validation method for the wave-driven current, since it is possible to enable all effects of the tide. This makes it possible to isolate the currents occurring from waves. Besides that, XBeach is considered to be a well-tested model, is applied throughout the academia and industry, and has been validated for different cases (Bolle et al., 2011).

The next and final step of the validation of the modelling of the hydrodynamics is a comparison to the work of Ruessink et al. (2001). This contains the comparison to the model that is presented in the work, and measurements that resulted from the Coast3D campaign (Klein et al., 2001). The model of Ruessink et al. and the measurements from the Coast3D campaign do include tidal currents, which ensures that the combination of tidal current and wave-driven current as presented in Section 4.2.3 is also included in the validation.

To conclude the validation: when comparing the RMSE of the modelled outcomes to the magnitude of the peak values, an error of 15% to 20% can be observed for all three comparisons, which is considered as an acceptable accuracy, considering the large amounts of variables and the type of comparison material. The amount of measurement data is very limited, while it is the most valuable way of comparison. XBeach and the model of Ruessink et al. are considered well-established; however, it is important to note that these models do not perfectly represent reality and bring their own errors. When looking at

the shapes of the curves in Figure B.5, the MBJ-model is modelling the longshore currents accurately. A process that has not been included in the MBJ-model, but is part of the model by (Ruessink et al., 2001), is mixing due to turbulence and viscosity. The exclusion of mixing explains the somewhat too steep gradients of longshore current in the MBJ-model. This is most pronounced in Figure B.5c, where the model by (Ruessink et al., 2001) (black dotted line) shows less fluctuation compared to the MBJ-model.

Overall, an acceptable representation of nearshore hydrodynamics can be modelled by the MBJ-model. Although a certain error is inevitable, the performance is considered to be well enough in the context of a quick-assessment tool. In Section 4.6, the behaviour of the MBJ-model will be analysed by means of a sensitivity analysis. This can be seen as verification, and as an addition on the validation of the MBJ-model. Although the sensitivity analysis does not validate the magnitude of the model's outcome, the sensitivity analysis can verify whether the model reacts appropriately to a broad range of input variables in accordance with physical laws.

4.4. Modelling sediment transport

In this section, the second step of the modelling approach is presented: the sediment transport, and the resulting siltation processes. As stated in Section 4.1, this step in the modelling approach is centered around the existing SedPit tool. Therefore, in Section 4.4.1, first all formulae and assumptions within the existing SedPit-tool are presented. Next, in Section 4.4.2 the integration of the MBJ-model in SedPit is presented. Additional information on SedPit is given in Appendix A.

4.4.1. SedPit formulae and assumptions

In this section, all relevant formulae and approaches of the existing SedPit-tool are stated. All formulae, assumptions, variables, and approaches in Section 4.4.1 are retrieved from Van Rijn (2007) and Van Rijn (2013).

The input of SedPit consists of a wide range of boundary conditions and parameters. The boundary conditions consist of the hydrodynamic conditions and the geometrical dimensions of the trench. The hydrodynamics conditions that are considered in SedPit are the tidal current, tidal water level fluctuation, and the orbital wave motion. The relevant dimensions are the width (B) and the length (L) of the trench, as well as the local initial depth (h_0), and the depth in the trench (h_1). All relevant dimensions are visualised in Figure 4.5.

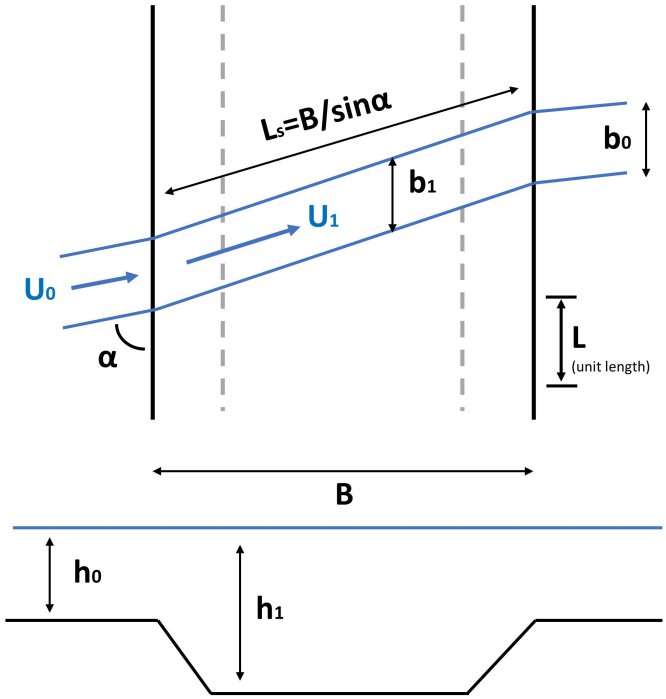

Figure 4.5: Schematic outline of trench dimensions in SedPit. Visualisation inspired by Van Rijn (2013)

A wide range of input parameters is included in SedPit. Not all parameters are explained in this section. For a more complete overview, please refer to Appendix A. SedPit includes sand, silt and clay. Clay and silt are handled differently than sand. While the transport of sand is calculated extensively, the transport of clay and silt is based on a background concentration and more simplifed transport processes. As a result of that, only the grain size of the sand is included as parameter, including d_{50} and the d_{90}, while silt and clay are included according to their average fall velocity. All three sediment types have a fixed fall velocity. Besides that, the different relevant densities, bottom roughness, and a range of calibration factors are included as parameters. The first step in the calculation of the sediment transport is the determination of the initiation of motion. Only the transport of sand is considered in this case. Transport of clay and silt is included according to Equation (4.48) and Equation (4.49). A particle will show movement as soon as the force of the moving fluid is larger than the resisting force of the particle. Before diving into the formulae that describe the fluid force and the resisting force of particles, a dimensionless particle size is introduced:

$$D_* = d_{50} \left(\frac{(s-1)g}{\nu^2} \right)^{1/3} \tag{4.36}$$

where s is the relative density, defined as ρ_s/ρ_w, and ν is the kinematic viscosity.

Based on an approximation off the dispersion relation, the wave number k is determined, in which the tidal water level fluctuations are taking into account. The wave number k and wave height H are used to determine the wave orbital velocity:

$$U_{orb} = \frac{\pi H}{T \sinh(kh)} \tag{4.37}$$

This wave orbital velocity is one of the two components of the effective velocity that exerts a force on the particles. SedPit defines the effective velocity on a particle as a combination of the depth averaged flow velocity U (tidal current in this case) and the wave orbital velocity U_{orb}:

$$U_{eff} = U + (\gamma U_{orb}) \tag{4.38}$$

where γ is a wave-dependent calibration factor, which was determined based on detailed numerical wave modelling, and U is the current-related velocity. A value of γ = 0.4 for irregular waves, and γ = 0.8 for regular waves is used.

The next step is to determine the critical velocities, at which the resistance force of the particles is reached. The formulation of this is dependent on the grain size of the sand. Furthermore, the critical velocities consists, just like the effective velocity, of a current-related ($U_{cr,f}$) and a wave-related ($U_{cr,w}$) component. The wave-related critical velocity is based on the work of Komar and Miller (1975). These are defined as follow:

$$\begin{aligned} U_{cr,f} &= 0.19(d_{50})^{0.1} \log\left(\frac{12h}{3d_{90}}\right) \quad \text{for} \quad d_{50} < 0.0005 \\ U_{cr,f} &= 8.5(d_{50})^{0.6} \log\left(\frac{12h}{3d_{90}}\right) \quad \text{for} \quad d_{50} > 0.0005 \end{aligned} \tag{4.39}$$

$$\begin{aligned} U_{cr,w} &= 0.24((s-1)g)^{0.66}\, d_{50}^{0.33}\, T_p^{0.33} \quad \text{for} \quad d_{50} < 0.0005 \\ U_{cr,w} &= 0.95((s-1)g)^{0.57}\, d_{50}^{0.43}\, T_p^{0.14} \quad \text{for} \quad d_{50} < 0.0005 \end{aligned} \tag{4.40}$$

where h is the local water depth, s is the relative density, T_p is the peak period, and d_{50} and d_{90} are the sediment characteristics.

These two components of the critical velocity are combined into a weighted critical velocity according to:

$$U_{cr} = \beta U_{cr,f} + (1-\beta)U_{cr,w} \tag{4.41}$$

$$\beta = \frac{U}{U + U_{orb}} \tag{4.42}$$

The β-coefficient in Equation (4.42) describes the weighted contribution of the flow related critical velocity, and the wave related critical velocity. Looking at Equation (4.42) shows that for a larger orbital velocity U_{orb}, the contribution of the wave related critical velocity is increasing.

In situations where the combined effective velocity U_{eff} has exceeded the weighted critical velocity U_{cr}, initiation of motion is reached. The extent of initiation of motion is often described by the mobility parameter M_e. A larger exceedance of the critical velocity leads to a larger mobility parameter η:

$$M_e = \frac{U_{eff} - U_{cr}}{\sqrt{(s-1)g d_{50}}} \tag{4.43}$$

When initiation of motion is reached, sediment transport will occur in two ways: bed load transport and suspended transport. First, the transport rates outside of the trench are determined, described by the subscript zero in Equation (4.44) and Equation (4.45).

The bed load transport is the transport of sediment particles in a thin layer close to the bed. The bed load transport is defined as a transport rate q_b, expressed in mass sediment per second per meter width (kg/s/m):

$$q_{b0} = \gamma_{sand}\, \alpha_b \rho_s U h \left(\frac{d_{50}}{h}\right)^{1.2} (M_e)^{\eta_b} \tag{4.44}$$

where γ_{sand} is a calibration factor related to sand, α_b is a calibration factor related to bed load, ρ_s is the particle density, U is the current-related velocity, M_e is the mobility parameter (see Equation (4.43)), and η_b is a coefficient related to bed load. Calibration with numerical model result has led to the optimal values of α_b = 0.015 and η_b = 1.5.

Suspended transport is the transport of particles that are in suspension. In the presence of a current, particles are assumed to move with the same velocity as the water particles, leading to a transport capacity of a current. The suspended transport is defined as a transport rate q_s, expressed in mass sediment per second per meter width (kg/s/m):

$$q_{s0} = \gamma_{sand}\, \alpha_s \rho_s U h \left(\frac{d_{50}}{h}\right) (M_e)^{\eta_s}\, D_*^{-0.6} \tag{4.45}$$

where γ_{sand} is a calibration factor related to sand, α_s is a calibration factor related to suspended transport, ρ_s is the particle density, U is the current-related velocity, M_e is the mobility parameter (see Equation (4.43)), and η_s is a coefficient related to bed load. Calibration with numerical model result has led to the optimal values of α_s = 0.012 and η_s = 2.4.

After determining the sediment transport rates, the total flow of sediment that crosses the trench can be determined. By multiplying the transport rates with the length and the timestep, the total mass of sediment can be determined:

$$Q_{b0} = q_{b0}\Delta t L \tag{4.46}$$

$$Q_{s0} = q_{s0}\Delta t L \tag{4.47}$$

In this step, clay and silt transport is included in the calculations. By means of a background transport rate, the total inflow of silt and clay is determined:

$$Q_{silt0} = q_{silt0}\Delta t L \tag{4.48}$$

$$Q_{clay0} = q_{clay0}\Delta t L \tag{4.49}$$

As soon as the current, and the corresponding transport rates, cross the trench, the flow is disturbed. Due to an increase of the local depth, the current will decrease:

$$U_1 = U_0 \frac{h_0 \sin(\phi)}{h_1 \sin(\phi)} \tag{4.50}$$

where U_0 is the depth-averaged current outside of the trench, h_0 is the depth outside of the trench, h_1 is the depth in the trench, and ϕ is the angle of the flow with respect to the orientation of the trench.

As the ratio h_0/h_1 will always be smaller than one, the current in the trench will decrease. A decrease of current leads to a decrease of equilibrium transport rate q_1 in the trench:

$$q_1 = \left(\frac{U_1}{U_0}\right)^3 q_0 \tag{4.51}$$

Equation (4.51) holds for all sediment types.

A decrease in transport rate will consequently lead to deposition of sediment. The difference between the incoming transport rate, and the equilibrium transport rate in the trench is driving the deposition D_s [kg] in the trench:

$$D_s = E\left(\frac{b_0}{b_1} q_{b0} - q_{b1}\right)\Delta t L \sin(\phi) \tag{4.52}$$

The ratio b_0/b_1 is related to the streamtube width. When considering a certain width of the approach current b_0, this width will change as soon as the current crosses the trench and slows down. The streamtube width in the channel b_1 is related to the change in current and depth:

$$b_1 = b_0 \frac{h_0 U_0}{h_1 U_1} \tag{4.53}$$

The variable E in Equation (4.52) is representing the trapping efficiency. The concept of trapping efficiency was introduced by Van Rijn (1986). It describes the fraction of the theoretically deposited sediment which is actually deposited in the trench, referred to as “trapped” by the trench. It is determined by the trench dimensions, the current, and the sediment type.

$$E = 1 - \exp\left(\frac{-A_v L_s (h_1 - h_0)}{h_1^2}\right) \tag{4.54}$$

where A_v is a coefficient that is related to the sediment type according to Equation (4.56), and L_s is the settling length, formulated as:

$$L_s = \frac{B}{\sin(\phi)} \tag{4.55}$$

where B is the width of the trench. L_s is describing the distance that a particle moves across the trench.

The sediment coefficient A_v is dependent on the sediment type and its fall velocity w_s :

$$A_v = c_{vr} \frac{w_s}{U_*} \left(1 + \frac{2w_s}{U_*}\right) \tag{4.56}$$

where c_{vr} is the Van Rijn trapping factor, and U_* is representing the bed shear velocity:

$$U_* = \frac{\sqrt{g}}{C} U_1 = \frac{\sqrt{g}}{18 \log(12h_1/k_s)} U_1 \tag{4.57}$$

where C is the Chézy coefficient, and k_s is the bottom roughness.

With increasing time, the deposition will lead to an upward bed level change in the trench. This consequently affects the trapping efficiency, leading to a lower trapping efficiency for reduced channel depth. Besides this bed level update, the water level can be updated according to the tidal regime, as well as the tidal current. The output is given in the form of a timeseries of deposited volume, deposited mass, or siltation thickness on a fixed location.

A variety of output values can be obtained with SedPit. The most common used output are the deposited volume, deposited mass, and the siltation thickness. See Appendix A for more information on the SedPit output.

4.4.2. Integration of nearshore hydrodynamics in SedPit: SedPit Nearshore

To adapt the existing SedPit tool for nearshore environments, the tool has been extended with nearshore hydrodynamics. This addition was achieved by integrating the MBJ-model with the SedPit tool. This combined model will be referred to as the SedPit Nearshore tool.

SedPit operates as a one-dimensional model with respect to time, while the MBJ-model functions as a one-dimensional model in terms of space. By combing these two models, a two-dimensional model is created, with both space and time as dimensions. The boundaries of this model are formed by the input timeseries of the offshore wave climate, and a fixed bed profile. When combining two one-dimensional models into one two-dimensional model, it is important to understand the processes and is propagation through the dimensions thoroughly. In the case of the SedPit Nearshore tool, the dimensions are not interconnected directly. For every timestep, a new sequence of the input timeseries is used, without needing any information from the previous timestep. This stepwise scheme of modelling the hydrodynamics on the transect creates a timeseries of local hydrodynamics for every spatial grid point, which forms the input for all spatial grid points where the SedPit model is executed. This includes the wave height, tidal current, wave-driven current, and water level (including tidal fluctuations) for each spatial grid point. The integration is schematised in Figure 4.6.

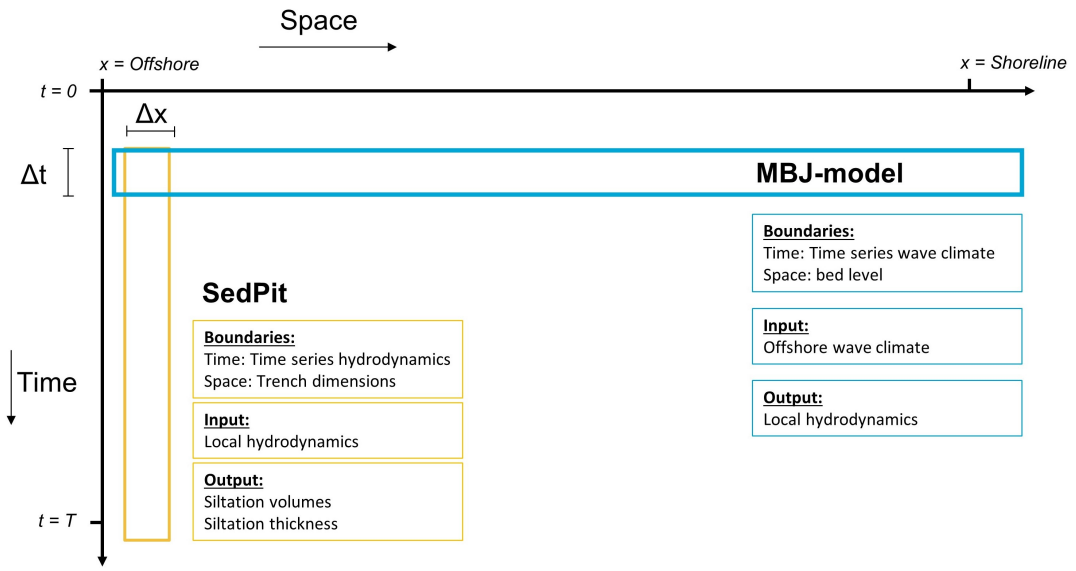

Figure 4.6: Schematisation of the inclusion of the MBJ-model in SedPit to obtain the combined SedPit Nearshore-model

The following list presents all changes that have been made to the existing SedPit-tool, in order to combine it with the MBJ-model.

- Spatial dimensions: As visualised in Figure 4.6, the existing SedPit-tool operates on one fixed point in space. By looping through a matrix with space and time as dimension, the SedPit-functions run at different spatial locations within one simulation.
- This addition of space as dimension makes it possible to easily change the depth according to a bed profile, which is used as input in the SedPit Nearshore tool.
- The wave height transformation, tidal current velocity reduction (see Section 4.2.2), and generation of a wave-driven current (see Section 4.2.1) are used as output from the MBJ-model. For every grid cell, the wave height, and total current are used as local hydrodynamic input for the existing SedPit-tool. This enables the inclusion of wave-driven currents, which is not possible in the existing SedPit-tool, and an fast and accurate way to include wave transformation.

4.5. Sensitivity Analysis - General

In two phases of this research, a sensitivity analysis has been conducted. In both cases, the Sobol's method, as presented in Section 2.5, is used. The first sensitivity analysis is conducted on the hydrodynamic part of the model, which is earlier referred to as the MBJ-model. The second sensitivity analysis is conducted on the combined SedPit Nearshore-model.

Considering the large amount of variables in both models, and the fact that the models outcomes are a combination of multiple formula, it is plausible to assume that interaction between variables has significant influence on the models outcomes (Owen et al., 2014), which leads to the introduction of higher-order Sobol's indices. Higher-order Sobol's indices capture the effect of variable interaction on the model outcomes variance. As stated in the work of Saltelli et al. (2010), the relations and formula for second and higher order terms within the Sobol's method hold if the variables are statistically independent, which is the case in the sampling method within this sensitivity analysis. According to the theory of Sobol (2001), the summation of all first-order and higher-order indices should sum up to 1 (Equation (2.30)). If the summation of all first order indices is close to 1, it can be concluded that the higher-order indices do not play an important role. However, if the summation of all first order indices is not close to 1, it can be concluded that higher-order indices do play a significant role (Saltelli et al., 2010). In that case, an analysis including the second-order indices is valuable. However, an analysis that includes second-order indices requires more than twice the sample size as compared to an analysis that only uses first-order indices. This trade-off has to be made, depending on the outcomes from the first-order indices, and the computation time that is available.

The Sobol' method has been conducted by using the SALib Python package. This method includes the sampling, normalisation, and Sobol' method analysis. The package is used in literature regularly (Herman & Usher, 2017; Iwanaga et al., 2022).

The sampling in this method is done by a quasi-Monte Carlo sampling, in combination with the Sobol' sequence. Quasi-Monte Carlo sampling entails low discrepancy sampling, which implies that the deviation of the sampled points to their distribution is relatively low. This is also where the term "quasi" comes from in this context. The samples are distributed more evenly in the parameter space, leading to significant improvements in computational demands. The Sobol' sequence has proven itself as superior to other low-discrepancy sampling methods (Kucherenko et al., 2015). For more background on the Sobol' sequence and quasi-Monte Carlo sampling, the reader is referred to Kucherenko et al. (2015).

4.6. Sensitivity Analysis - Hydrodynamics (MBJ)

The first sensitivity analysis is conducted on the hydrodynamic part of the model, which is earlier referred to as the MBJ-model. The goal of this sensitivity analysis is to analyse the behaviour of the model on a wide variety of input values of variables. This can verify if the model responses according to physical laws. An additional sensitivity analysis on the independent variables only (k_s, β, γ, α) is presented in Appendix C. Appendix C gives some more attention to the independent variables, by excluding the variance added by the wave climate related variables and tidal current.

The MBJ-model is including a range of 8 variables, which can be subdivided in two categories: measurable variables and non-measurable variables. The measurable variables are related to the wave climate and tidal regime and consist of wave height H_{s0}, wave period T_p, wave angle θ_0, and tidal current U_{tide}. The non-measurable variables include the wave breaker coefficient γ, the bottom roughness k_s, the roller steepness β, and the wave dissipation coefficient α. All variables are listed in Table 4.1, including the bounds of the uniform distributions that are considered in the sampling procedure. The goal of the upcoming sensitivity analyses is to analyse the behaviour of the model on a wide variety of input values of variables from a mathematical perspective, and compare to the expected response according to physical laws. By conducting the sensitivity analysis from a mathematical perspective, all theoretically possible combinations of input variability are taken into account. This gives the opportunity to assess the behaviour of the model on the whole input range. As this is related to the theoretical output space of all possible input combinations, the probability distribution where the variables are drawn from do not have to represent a realistic distribution of occurrence, like a Rayleigh distribution for wave height, yet. It is meant to analyse the model's response to changes in input variables, wherefore the whole range of occurrence distribution is evenly important to include. This makes uniform distributions the most straight-forward approach. However, it has to be noted that these choices regarding the probability distributions in Table 4.1 has its consequences. On one hand, the choice of a uniform distribution, instead of one that more accurately reflects physical reality, ensures that values near the edges are represented just as frequently as those in the middle of the distribution. From a physical point of view, this implies that large waves are evenly much represented as normal waves. Besides that, the chosen width of the probability distribution of a variable affects the potential importance of that variable. A wider distribution leads to relatively larger input variance, which potentially translates itself into a larger influence on the model's output variance.

The measurable variables represent the wave climate and the tidal regime, having corresponding wide distribution bounds to represent the large natural variability. In the context of modelling, these variables are considered as the forcing. On the other hand, the non-measurable variables are variables that are in most models represented by a fixed value that is determined based on prior research, or obtained by calibration against available data (Ruessink, 2005). The distribution bounds of the non-measurable variables are based on values from literature. When comparing the bounds of the measurable variables to the bounds of the non-measurable variables, significantly wider bounds are used for the measurable

variables, to capture the large natural variability. However, wider bounds of variables can potentially lead to a larger contribution of these variables to the model variance. This has to be taken into account when drawing conclusion from the results of the sensitivity analysis.

Table 4.1: Variables in the MBJ-model, including the lower and upper bound during the sampling. All variables are assumed to follow an uniform distribution.

	Lower bound	**Upper bound**	**Unit**
Measurable Variables			
H_{s0}	0.5	6	m
θ	-75	75	$^{\circ}$
T_p	3	14	s
U_{tide}	-1	1	m/s
Non-measurable Variables			
γ	0.5	0.9	-
k_s	0.01	0.1	m
β	0.01	0.1	-
α	0.5	1.5	-

The Sobol's method creates a large sample size of the input variables through Monte Carlo sampling, and translates this, into a large model outcome space. For all variables, a Sobol' index is calculated, that represents the influence of that variable's variance on the variance of the model outcome. In order to create this outcome space, a specific target value that represents the model outcome is defined. The outcome of the MBJ-model is the generation of a longshore current. This includes several relevant characteristics, including the peak value, location of the peak, and the shape of the curves. In the context of this research, the generated longshore current is used as the variable that is driving sediment transport. The current velocity is incorporated into the sediment transport rates equation to the power of three, as shown in Equation (2.18) (Van Rijn, 2007). Consequently, the integral of the longshore current raised to the third power is utilized as the target value in the sensitivity analysis:

$$Y = \int_{x=X1}^{x=X2} |(U_{total})^3| dx \tag{4.58}$$

The model outcome Y is the summation of the absolute values of U_{total}^3, where U_{total} is representing the combination of tidal current and wave driven current, as explained in Section 4.2.3. Due to the fact that the tidal current and the wave-driven current can occur in opposite directions simultaneously, a resulting model outcome of zero can be obtained while actually the model outcome consists of a series of non-zero values. This can be avoided by summing the absolute value.

However, taking the absolute value also brings it downsides. The variables θ and U_{tide} are the variables that are leading to changes in direction, which is corresponding to changes in sign. Only considering absolute values is equivalent to assuming a constant direction of the flow. This consequently leads to a smaller variance, which especially affects the sensitivity indices of θ and U_{tide}. This shortcoming is acceptable when looking a step ahead in this report. The MBJ-model is only the first step of a combined model, which will ultimately model the siltation rates in a trench. For these siltation rates, the source direction of the sediment is not relevant.

In the definition of this model outcome Y, the boundaries X_1 and X_2 of the integral in Equation (4.58) have a large influence on the outcome Y. As this research is focusing on the nearshore environment, the boundary X_1 should represent a depth at which this nearshore environment is considered. During this sensitivity analysis, the bound X_1 is based on the depth of closure at the Dutch coastline, as stated in Section 2.1.1, resulting in a starting depth of 10 m. The upper bound X_2 is defined by the shoreline.

As stated above, the input values of the above-mentioned 8 variables will be drawn from a distribu-

tion by means of a quasi-MCS. The distributions that are used in this sampling are shown in Table 4.1. Any correlation in the occurrence of variables is not included in the sampling strategy. The most prominent correlation that physically occurs, is the positive correlation between wave height H_{s0} and peak period T_p. Large wave heights can physically only maintain its energy with a sufficiently large period. As a result of ignoring this correlation in the sampling strategy, unrealistic combinations of wave height H_{s0} and peak period T_p are included, which would lead to instabilities in the MBJ-model. To avoid these unrealistic combinations, the samples are filtered. In the purpose of this filtering, the Pierson-Moskowitz criterion, that relates wave height to peak period , could be used (Holthuijsen, 2007). However, as this criteria does not work well in the case of high waves, it has been chosen to use a more simplified, but effective criterion. By removing samples where the criterion $T_p > H_{s0}$ is not met, most of the unrealistic samples are removed.

The results of this sensitivity analysis are presented in Section 5.2.2.

4.7. Sensitivity Analysis - Siltation (SedPit Nearshore)

The second phase of this research where a sensitivity analysis is conducted is the phase after combining the MBJ-model with the existing SedPit tool. This results in SedPit Nearshore tool. This sensitivity analysis has two objectives. On one hand, to analyse the behaviour of the model on a wide variety of input values of variables, comparable to the goal described in Section 4.6 above. At the same time, the most influential variables are identified, which is information that will be used in the approach of the GLUE-method (Section 4.8). In the GLUE-method, the probability distribution of a selection of non-measurable variables will approximated, based on the training data from the field case. By identifying the most influential variables in this sensitivity analysis, the GLUE-method can be approached more efficiently. Therefore, this sensitivity analysis focusses on the non-measurable variables. The same mathematical approach of the Sobol' method is used in this case, although certain choices in this sensitivity analysis differ from the previous one.

First of all, the target value to represent the model outcome Y is redefined. While the model outcome of the MBJ-model was used as an approximation to represent sediment transport, the outcome of the SedPit Nearshore tool is the siltation volume along the trench. As the scope of this research focuses on the effect of nearshore processes on trench siltation, the target value of the model outcome should also focus on the effect of nearshore processes. In Figure 4.7, the cross-shore evolution of the wave-driven current for all timesteps in period 1 and period 2 of the field data, presented in Chapter 3, are plotted. The depth that is considered as the start of the nearshore zone is defined as follow: the depth where the 90%-percentile of the wave-driven currents start to show a significant gradient. This gradient indicates that waves start to break and start to generate longshore currents. This method of defining the nearshore zone allows to base this choice on the wave conditions during the period of interest, while focusing on the depths where nearshore processes start to increase. It is in line with the theory of Hallermeier's inner closure depth, as presented in Section 2.1.1. However, as the available wave data does not represent one whole year, it is difficult to define the extreme conditions with a occurrence probability of 0.137 %. Besides that, the definition of the nearshore zone should be a representative value for the period of exposure of the trench. The execution of trenches are generally planned during calm conditions (see Section 1.1), wherefore an extreme value of a year would be a too conservative condition. Therefore, a more graphical method, which is based on the start of sediment transport due to wave action as proposed by Hallermeier (1980), is used in the definition of the nearshore zone in this context. Visual inspection of Figure 4.7 gives a start of the nearshore zone at a depth of 12.9 m. However, Equation (2.2) is used as a validation method. Using the maximum wave height H_s of 3.8 meter from Figure 3.9, and a corresponding peak period of T_s of 8 seconds, results in a inner closure depth of 11.5 meter. This confirms that the definition of 12.9 meter as start of the nearshore zone is in line with the theory of Hallermeier (1980).

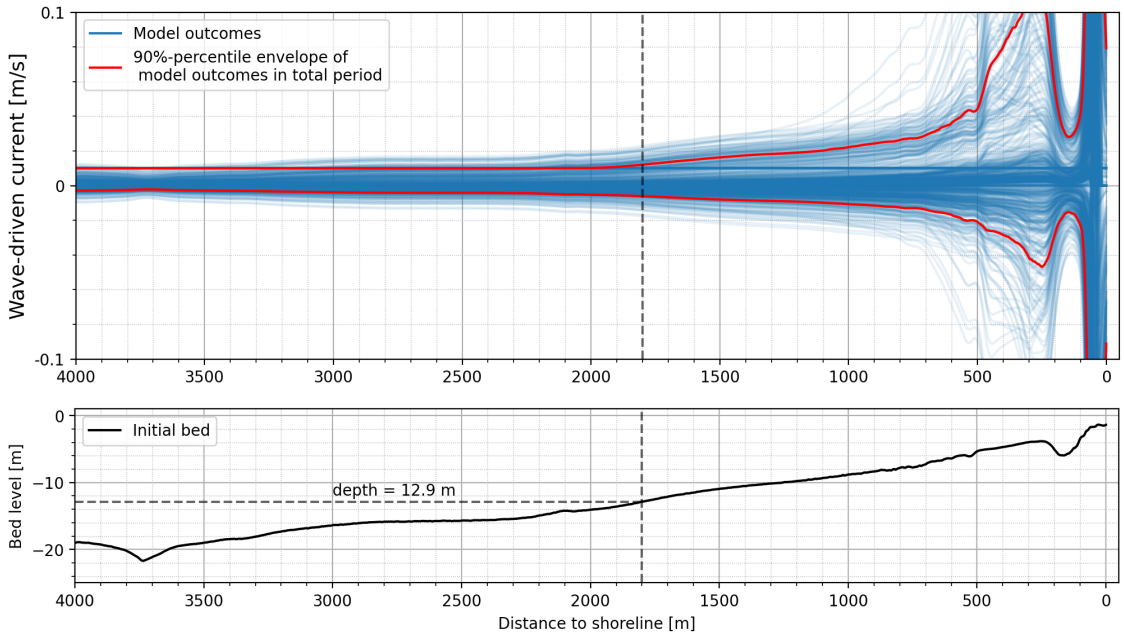

Figure 4.7: Upper graph: the wave-driven current on all timesteps in period 1 and period 2. The red lines indicate the envelop of the 90% percentile of all timesteps. Lower graph: the bed profile, including the depth that is considered as the start of the nearshore zone indicated by the dashed line.

The next step in setting up the sensitivity analysis, is to choose which variables are included in the sampling, and which remaining variables are included as constants. In this sensitivity analysis, a distinction between the forcing (all variables related to the wave climate and the tidal regime) and non-measurable variables is made. As one of the goal of this sensitivity analysis is to find the most influential non-measurable variables that are later on included in the GLUE-method, only non-measurable variables are included. This means that no forcing variables are included in the sampling, and neither are the sensitivity indices calculated for the forcing variables. However, as the available metocean data of the field case is used as input for the model, natural variability of wave conditions and tidal regime are included.

The variables that are included in this sensitivity analysis originate from both the MBJ-model, as well as the existing SedPit-tool. As the upcoming sensitivity analysis is focusing on the non-measurable variables, as preparation for the GLUE-method, all four non-measurable variables from the MBJ-model, which are listed in Table 4.1, are included. Besides that, three variables from the SedPit-tool are included: sand grain size d_{50}, dry bulk density ρ_b, and the Van Rijn trapping factor c_{vr}. This selection is based on an sensitivity analysis on the existing SedPit-tool (Appendix D). The results of this sensitivity analysis on the existing SedPit-tool have shown that the sand grain size d_{50} and the Van Rijn trapping factor c_{vr} (Equation (4.56)), are among the most influential variables in the existing SedPit-tool. Besides that, the dry bulk density ρ_b is known to be a variable which is very difficult to estimate in early stages of execution. Due to the interest from a practical point of view, this variable is included in the sensitivity analysis as well. An overview of all included variables is given in Table 4.2.

Other variables with potentially large influence on the siltation volumes are the background concentration of silt and clay, referred to as fines. The deposition of fines is included in the existing SedPit-, as well as in the SedPit Nearshore tool. By means of a background concentration of fines, the deposition is calculated in a simplified way (Equation (4.49) and Equation (4.48)). The concentration of fines is a highly location-specific variable, that can have a large impact on the siltation volumes, depending on the local hydrodynamics and the dimensions of the trench. The small particle size of fines makes them highly sensitive to hydrodynamic conditions. The settling of fines largely depends on the presence of calm conditions. Particularly in areas with breaking waves, the hydrodynamic conditions are too turbulent to allow for the settling of fines. In the more deeper regions, the wave action near the bed will have reduced to conditions where fines can settle and contribute to trench siltation. The extent

of contribution to trench siltation is strongly dependent on the background concentration of fines. The sensitivity analysis does not account for the variability in background concentration, as the large influence of the background concentration of silt is known. The influence of fines in the specific field case is analysed in Appendix E. From this analysis, it follows that, for this specific field case, the influence of clay concentration is negligible, while the silt concentration is a highly influential variable. Both silt and clay concentration will be excluded in the sensitivity analysis by using a constant value of zero. Excluding these variables from the sampling procedure avoids that the effect of the remaining variables is overwhelmed by the effect of the concentration of silt. Furthermore, excluding these variables saves computation time, as the needed sample size is dependent on the amount of independent variables. Nonetheless, the concentration of fines will be included in the GLUE-method in Section 4.8.1. A more detailed analysis on the effect of fines is presented in Appendix E.

Similar to the sensitivity analysis on the MBJ-model, the goal of this analysis is to explore the behaviour of the model and to identify the mathematical response of the model. As is has been shown in the sensitivity analysis on the MBJ-model (see Section 4.6), the bounds of the input variables play a large role on their contribution to the model variance. When considering the variables in Table 4.2, the theoretical range of the sand grain size d_{50} would range from 63 μm, to 2000 μm (ISO, 2017). This range represents the finest sand particles to the most coarse sand types. However, as this range is a few magnitudes larger than the ranges of the remaining variables in Table 4.2, the results of the Sobol' method would be completely determined by the effect of d_{50}. Bearing that in mind, a more narrow range for d_{50} has been chosen, to obtain a more balanced analysis. However, when drawing conclusions from the analysis, this modification of the range of d_{50} has to be taken into account. The range of d_{50} that is stated in Table 4.2 is representing the range for "medium fine sand" (ISO, 2017). The choice to base the range on one particular type of sand makes sense from a practical point of view as well. In many cases involving siltation prediction, there is usually some basic understanding of the local sand grain size. This information is typically enough to determine the most likely category of sand present in the area, narrowing down the theoretical distribution. The ranges of k_s and β are based on the same literature values as presented in Section 4.6. A typical value for the dry bulk density ρ_b of sand is 1700 kg/m³. This value changes depending on how densely the sand is packed. To account for the range of very loosely packed sands to densely packed sands, a range from 1100 to 1900 kg/m³ is used. The Van Rijn trapping coefficient c_{vr} is a coefficient that was derived by Van Rijn (1987). In applications of Van Rijn's trapping theory, a value of 0.25 is used. For this analysis, a range from 0.01 to 1 is chosen to explore.

Table 4.2: Variables in the SedPitNearshore-model, including the lower and upper bound during the sampling. All variables are assumed to follow an uniform distribution

Variable	Lower bound	Upper bound	Unit
d_{50}	200	630	μm
k_s	0.01	0.05	m
β	0.01	0.1	–
ρ_{bulk}	1100	1900	kg/m^3
c_{vr}	0.01	1	–
γ	0.5	0.95	[-]
α	0.5	1.5	[-]

The choice of the bounds has a large influence on the outcomes of the model. The reduced range of the possible grain sizes d_{50} underestimates the influence of d_{50} when considering all possible grain sizes of sand. On the other hand, the variability of the dry bulk density ρ_b is in relative sense much narrower than the variability of the other variables.

As the Sobol' method is depending on increasing sample sizes with increasing degrees of freedom, certain steps were taken to reduce the computation time. First of all, only a fraction of the available timeseries of metocean data is used. This entails the assumption that the influence of the variables is not time-dependent. The only process that affects future timesteps in the model is the bed level change

in the trench. The bed level change in the trench influences the trapping efficiency of the trench. However, when considering the significant reduction in computation time by taking only a subset of the timeseries, the exclusion of time-dependence is an acceptable loss of accuracy. In Appendix F, the effect of the bed level change on the trench siltation is presented in more detail. In Figure 4.8 the reduced timeseries is shown. More information on the origin and the background of this data is given in Section 3.1. First, a part of the timeseries including a relatively large variety of wave height H_{m0} and wave angle θ is selected, in order to simulate the natural variability of the wave conditions as good as possible. Next, this selected period is reduced in dimensions, by increasing the timestep by a factor of five. This results in new timesteps of 100 minutes, instead of initially 20 minutes. The resulting schematisation of the timeseries is visualised by the orange line in Figure 4.8. The same reduction in dimensions is done for all other variables that are included in the available metocean data. As this sensitivity analysis does not include any comparison or validation to the field data, the exact accuracy of the reduced timeseries compared to the measured data is not relevant. In the approach of the GLUE-method (see Section 4.8), a more accurate method to reduce the dimension of the timeseries is used, as GLUE includes a comparison between observed data and modelled data.

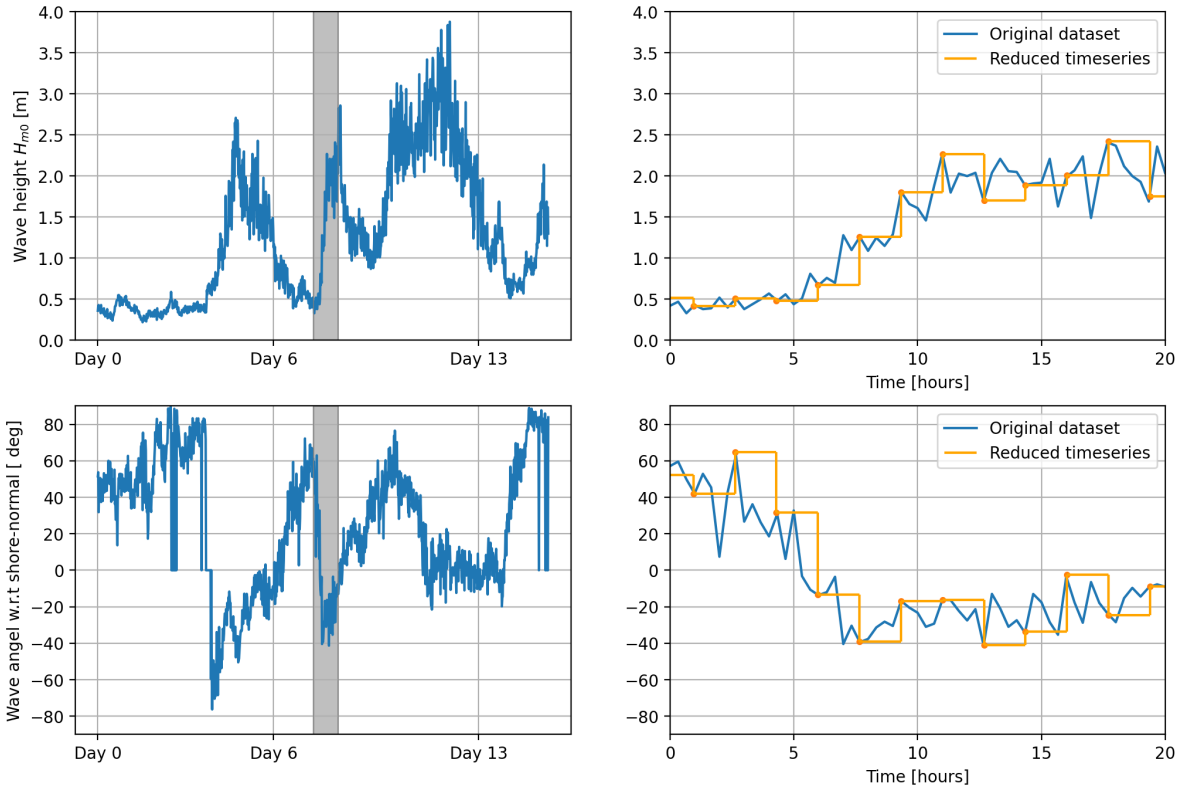

Figure 4.8: Reduction of input timeseries. The grey marked section is the part of the timeseries that is used in the sensitivity analysis, and zoomed-in on in the right graphs. The orange lines indicate the reduced timeseries, where the timestep is 5 times larger.

To conclude, the total siltation volume during the period that is shown in Figure 4.8 in the nearshore zone that is defined by a depth of 12.9 m (see Figure 4.7) is used as model outcome Y in the Sobol' method. The included variables are stated in Table 4.2. The results of the sensitivity analysis are presented in Section 5.2.3.

4.8. Uncertainty Analysis - GLUE

This section presents the methodology and steps that were taken to perform the GLUE-method. The goal of the GLUE-method is to obtain probability distributions of a variety of variables, which represents the most likely distribution of these variables for the field case. This gives insights in the probability distributions of variables which are unknown and generally chosen based on experience or estimations,

and can help in reducing the uncertainty of the model. Additionally, the GLUE-method gives insights in the uncertainty width of a model's outcome, after calibration to training data.

For the purpose of this GLUE-method, the available dataset is split in two: period 1 and period 2, which is based on the measurement campaigns presented in Chapter 3. Period 2 will be used as training set, while period 1 will be used as validation set. The validation is discussed separately in Section 4.9. This choice is based on the characteristics of the two periods. As it is presented in Figure 3.9, period 2 is a more energetic wave climate than period 1, which leads to a generally more "active" period. This activity tends to reduce the relative impact of potential errors. Besides that, as explained in Section 3.4, certain artefacts from the execution might influence the results. As the effect of these artefacts is expected to be more pronounced in period 1, it is beneficial to perform the GLUE-method on period 2. The resulting probability distributions of the independent variables are tested on period 1, while taking the possible effects of the execution artefacts into account. The comparison to the validation data of period 1 is presented in Section 5.3.

A larger sample size N of variable sets gives a more accurate representation of the probability distribution of the independent variables. As the available computation power is a limiting factor, certain methods to reduce the needed computation time were explored. The most promising way to reduce the computation time is to use an increased timestep. In order to be able to work with a sufficient large sample size, the computation time per run has been reduced significantly. To do so, the dimension of the input timeseries was reduced by using a larger timestep, while minimising the associated data loss. This procedure is explained in Appendix G.

In this section, the different steps of the GLUE-method will be presented, including the selection and sampling of variables, the performance measures, rejection threshold and likelihood measure, the optimisation of the independent variables, and the use of the optimised parameter distributions to reduce the uncertainty in the model's outcome. The results will be presented in Section 5.3. As the GLUE-method includes several subjective choices, which do affect the outcomes, Appendix H is added to discuss and showcase the effect of some of these choices.

4.8.1. Included variables

In the context of the GLUE-method, a distinction between two types of variables will be made. First, the variables that are included in the sampling, and whose probability distribution will be approximated by the GLUE-method, are referred to as the "independent variables". All other variables that are part of the SedPit Nearshore tool, which are defined by a constant value or the metocean conditions, are referred to as background variables or metocean variables respectively.

The choice which variables are amongst the independent variables is based on the outcomes of the sensitivity analysis on the MBJ-model (Section 5.2.2) and the sensitivity analysis on the SedPit Nearshore tool (Section 5.2.3). These results show the fraction of the model's variance that can be attributed to variability of a selection of input variables; the Sobol' indices. Based on the Sobol' indices in Figure 5.5, the most influential, and therefore most interesting independent variables are the bottom roughness k_s, roller steepness β, and sand grain size d_{50}. Furthermore, the background concentrations for silt and clay will be included. These were not included in the sensitivity analysis in Section 4.7, as their impact on the model outcome is expected to be large and strongly dependent on the local background concentration. Their relevance for the GLUE-method comes mainly from a practical point of view. In situations where siltation predictions are desired, the information on the concentration of fines is often scarce, wherefore they are often considered as free calibration variables. This makes it interesting to see how both background concentrations affect the model outcome, and if they show some clear patterns related to the model performance.

All five independent variables will be drawn from a prior (uniform) distribution, which are characterised by a lower and an upper range as stated in Table 4.3. The bounds of the bottom roughness k_s and the roller steepness β are based on the earlier mentioned values in literature. The bounds of the sand grain size are based on information on the grain size that was available in the field case. This information gives that the sand grain size d_{50} lays within the range of 140 μm - 200 μm, while the d_{90} is

approximately 1.5$\times$ d_{50} (Boskalis, 2024). The same sources provides estimations on the background concentration of the fines. For silt and clay, a background concentration between 20 - 80 mg/L and 5 - 20 mg/L respectively is expected. As the exact source of this information is not available due to confidentiality of the project, the bounds for the silt concentration in Table 4.3 are extended beyond the given information. This ensures that potential values of the silt concentration that would lead to a good fit, are not excluded by a too narrow definition of the lower and upper bound. This is only done for silt, as the large influence of silt concentration is known, while clay seemed to be less influential (see Appendix E). To give some level of reference: these values are comparable to typical concentrations of fines near the Dutch coast (Van Alphen, 1990).

Table 4.3: Independent variables for the GLUE-method. All independent variables are drawn from an uniform distribution.

Variable	Lower bound	Upper bound	Unit
k_s	0.01	0.10	[m]
β	0.005	0.100	[-]
d_{50}	90	350	[μm]
c_{silt}	10	100	[mg/L]
c_{clay}	5	20	[mg/L]

The sampling is done according to Monte-Carlo sampling (MCS), by drawing random values from uniform distributions. The number of runs is determined by the desired sampling resolution and the number of independent variables (Ruessink, 2005). No clear guideline exist on how to decide the desired sampling resolution, and corresponding needed sample size. Simmons et al. (2017) uses a sample size of 15,000 for a GLUE-method with six independent variables, which corresponds with a sampling resolution of approximately 5 ($5^6 \approx$ 15,000). As this GLUE-method includes five independent variables, a sample size of 14,000 was considered as sufficient, as it exceeds the sampling resolution proposed by Simmons et al. (2017).

4.8.2. Performance measures

Based on the comparison to the training data, every sampled set of variables will obtain a performance score. The performance of the SedPit Nearshore tool will be based on two performance measures. Both performance measures will be quantified by means of a Brier Skill Score (BSS). The BSS compares the mean squared error to the baseline “no-change” situation. Perfect agreement between the modelled and observed values would lead to a score of 1, while a model outcome where the error is larger than the observed value will lead to a negative skill score. The BSS is a common used method to evaluate model performance of morphological models (Simmons et al., 2017; Van Rijn et al., 2003).

First, the total siltation volume in the nearshore zone is used as performance measure. The total siltation volume is crucial knowledge in efficient scheduling of dredging equipment, and the reservation of sufficient time in the case of additional re-deepening. The total siltation volume is very similar to the target value in the sensitivity analysis in Section 4.6, with the difference that a different start of the considered nearshore zone is used. As presented in Section 3.3, the volume changes in the region between x=1300 m and x=1100 m show a behaviour that indicates that the data is not too trustworthy. Although it would be most consistent to use again the depth of 12.9 meter that was based on the relevant wave climate, it is more important to exclude the volume changes that result form the outliers between x=1300 m and x=1100 m. Consequently, the total siltation volume is determined starting at x=1100 m, with a corresponding depth of 9.5 m.

The BSS for the total siltation volume is defined according to Equation (4.59).

$$BSS_{tot} = 1 - RAE = 1 - \frac{|\Delta V_{T,obs} - \Delta V_{T,mod}|}{\Delta V_{T,mod}} \tag{4.59}$$

where RAE represent the relative absolute error, $\Delta V_{T,obs}$ represents the observed total siltation volume in the nearshore zone, and $\Delta V_{T,mod}$ represents the modelled total siltation volume in the nearshore

zone.

The definition for BSS_{tot} is slightly different from the traditional definition of the BSS, which is used for the second performance measure and shown in Equation (4.60). First of all, as there is only one observed and one modelled value for the total siltation volume, the commonly used “mean” error is not applicable in this case. Secondly, as the absolute error can reach relatively large values, compared to the observed value, the use of a squared error would make the method very sensitive to outliers that would result in negative skill scores (Van Rijn et al., 2003). As an example: A model has an absolute error of 50 m³, compared to an observed value of 2000 m³. In this case, using the squared error would lead to an relative error of 125% and a negative skill score. However, comparing the (non-squared) absolute error to the observed value, it is only an relative error of 2.5% and a high skill score.

The second performance measure (BSS_s) is related to the spatial distribution of the modelled siltation volumes. Accurate predictions of the spatial distribution of siltation volumes can potentially help in an efficient design of over-depth to avoid the need of re-deepening. This performance measure is inspired by the work of Simmons et al. (2017). To quantify the performance of the model, the modelled siltation volumes is compared to the observed siltation volumes on a series of locations. The error between the observed and modelled values is compared to the ’no-change’ situation, corresponding to the situation immediately after dredging with zero siltation. This definition compares the magnitude of error to the observed siltation volume. As it follows from the data analysis on the siltation volume in Section 3.3, the spatial distribution of siltation volumes shows large variability, with most siltation taking place in the last ca. 400 meter in front of the coast. Therefore, when evaluating the performance measure BSS_s, it is important to ensure that the in absolute sense small offsets in the deeper parts (“flat zone” in Figure 4.9), do not compensate for the in absolute sense larger offsets in the shallower zone (“peak zone” in Figure 4.9). However, when obtaining a poor fit on the long “flat zone”, this can contribute significantly to errors in the prediction of the total siltation volume, and corresponding needed maintenance dredging. This trade-off is important in the choice of the test locations. By adjusting the interval distance between the evaluation points, the user can steer manually at the region that deserves more “weight” in the calculation of the MSE in Equation (4.60). For this analysis, twice as much test locations are introduced in the “peak zone” (every 10 meter) as in the “flat zone” (every 20 meter).

Equation (4.60) is used to calculate the BSS of the spatial distribution.

$$BSS_s = 1 - \frac{MSE}{MSE} = 1 - \frac{\sum_{X1}^{X2}(|\Delta V_{x,obs} - \Delta V_{x,mod}|)^2}{\sum_{X1}^{X2}(|\Delta V_{x,obs} - \Delta V_{x,0}|)^2} \tag{4.60}$$

where $X1$ and $X2$ represent the bounds of the nearshore zone, $\Delta V_{x,obs}$ is the observed siltation volume per meter width at x, $\Delta V_{x,mod}$ is the modelled siltation volume per meter width at x, and $\Delta V_{x,0}$ is the baseline “no-change” siltation volume per meter width at x, which is zero for all x.

When considering the “peak zone”, as depicted in Figure 4.9, it can be seen that the shape of the siltation volume curve is prone to the problem of “double penalty”. This concept is extensively discussed by Bosboom (2020). The “double penalty” occurs in a situation where the performance of a model is determined based on comparison to observation data. When a certain spatial feature of the observed data, like the peak in Figure 4.9, is included in the modelled data albeit on a wrong location, the performance of the model is considered twice as worse as a modelled dataset where the feature is not included at all. This can lead to false conclusions. More specific in the context of the GLUE-method; a parameter set that leads to a model outcome with low variability and average performance on most evaluation locations can score better than a model outcome that includes a well shaped peak, located a few meters next to the observed peak.

To deal with the effect of a “double penalty” in the GLUE-method, a simple but effective method was used. Although Bosboom (2020) presents more advanced methods, it was chosen to use a method which does not increase the computation time significantly. The implemented method focuses on the location of the largest peak in the “peak zone”. The displacement distance d is determined by compar-

ing the location of the local maxima of the observed and modelled data. Based on all 14,000 model runs, the displacement distance d is generally in the order of 30 meter. By shifting the peak of the modelled dataset seaward with a distance of d, the locations of the modelled and observed peaks do align better, which allows a fair evaluation of the BSS with exclusion of a "double penalty". The shifting is only performed on the first 150 meter of the domain, which is the most outer bound of the peaks based on the 14,000 model runs. The more seaward part is not affected by the shift. It has to be noted that this shifting of the peak is only done to enable the evaluation of the BSS_s. The shifting is not included in the model itself as the displacement distance d is not based on any physical processes, but solely on graphical estimations. The procedure is visualised in Figure 4.9.

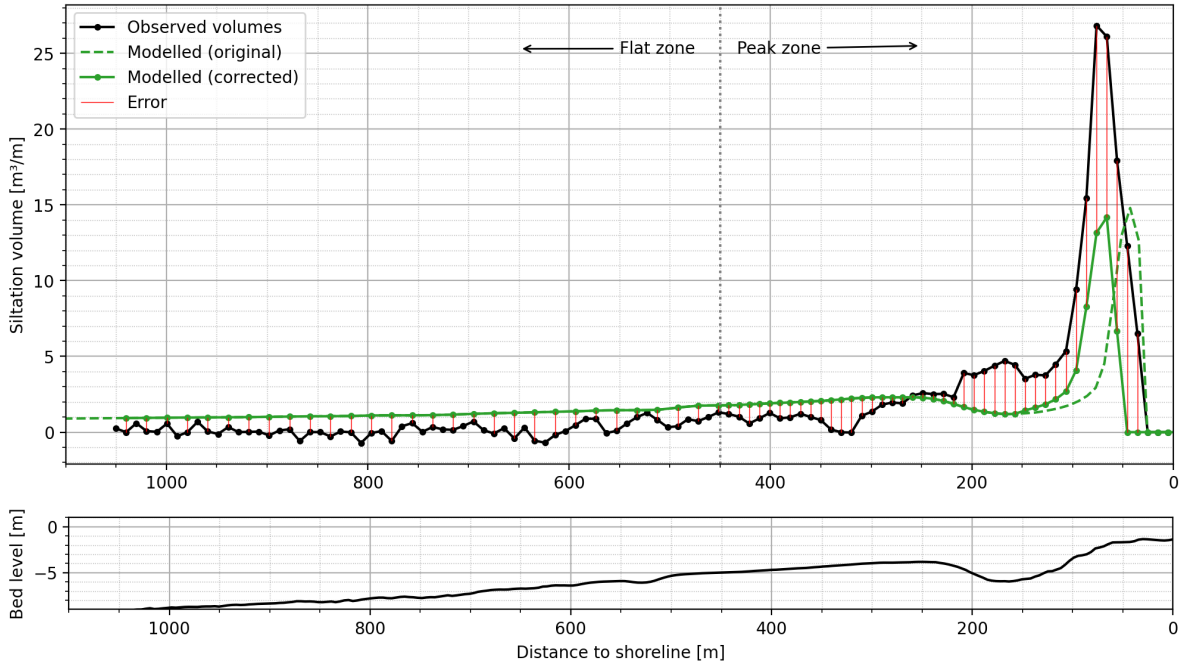

Figure 4.9: Example on the evaluation of the BSS_s for an arbitrary run. The red lines indicate the error on the test locations, where twice as much test locations are evaluated in the "peak zone", compared to the "flat zone". Besides that, the correction for the peak is indicated: the green dashed line represents the original location of the peak, while the green solid line shows the corrected position of the peak which avoids the "double penalty". The black solid line represents the observed siltation volumes.

To conclude, in the definition of the two performance measures BSS_{tot} and BSS_s, subjective choices have been made. First of all, BSS_{tot} does not include a squared error to avoid that errors of outliers are overvalued. Secondly, in the definition of BSS_s, the test location interval and shifting the modelled data according to the peak location gives the possibility to focus on the shape in the most nearshore zone. Eventually, by having twice as much evaluation locations in the peak zone, and applying the correction to better align the peak, some manipulation of the data is included that allows a evaluation with a slight focus on the peak. An even further reduction of evaluation locations in the flat zone would lead to undervaluation of the effect of the flat zone on the total siltation volumes at these depths.

4.8.3. Rejection and likelihood

The next step in the GLUE-method is to define how well a set of variables has to perform to be considered as a "behavioural"(well-performing) set. For this step, for every performance measure a threshold has to be defined. This is another choice in the procedure of a GLUE-method that includes subjectivity and should be considered with care. Van Rijn et al. (2003) proposed a classification related to the BSS.

Table 4.4: Classification of BSS by Van Rijn et al. (2003)

Classification	BSS
Excellent	0.8 - 1.0
Good	0.6 - 0.8
Reasonable/fair	0.3 - 0.6
Poor	0 - 0.3
Bad	<0

When choosing the threshold, there is always the trade-off between a sufficient number of remaining behavioural sets, and quality of remaining behavioural sets. With a low threshold, more behavioural sets are remained. However, the average performance of the behavioural sets is lower than in case of a more strict threshold. The choice of threshold directly affects the width of the posterior probability distribution of the independent variables. The thresholds that are used in the GLUE-method are the result of this trade-off, and are based on the insights from an iterative procedure. When seeing the results in Section 5.3, summarised in Table 4.5 below, it is evident that the SedPit Nearshore tool performs significantly better in estimating the total siltation volume than predicting the spatial distribution of the siltation volumes. For that reason, two different threshold values for the two performance measures are chosen. This allows to steer the number of behavioural sets, and to ensure that only sets that are among the best outcomes for both performance measures are considered as behavioural. The effect of the choice in threshold is shown in Appendix H.

As indicated in Table 4.5, eventually a threshold of 0.8 was used for the performance measure BSS_{tot}, and a threshold of 0.6 for BSS_s. According to the classification of Van Rijn et al. (2003) these threshold correspond to 'excellent' and 'good' performances respectively. This variation is related to the mean performance of the samples for both measures. As stated in Table 4.5, the average score of BSS_{tot} is significantly higher than the mean score of BSS_s. Consequently, a higher threshold for the BSS_{tot} still leaves enough behavioural samples for the remaining parameter optimisation.

Table 4.5: Rejection threshold of the BSS. Depicted are the maximum and mean score of all sets for both performance measures. Next the used threshold is shown, and the amount of runs that are accepted according to that threshold. The lower row indicates how many sets are accepted according to both thresholds and therefore considered as behavioural set.

N=14,000	Max BSS	Mean BSS		Threshold	# Accepted sets
BSS_{tot}	0.999...	0.6237		0.8	4928
BSS_s	0.8405	0.4888		0.6	5527
			# Behavioural sets		2412

After rejecting all sets of variables that are not considered as behavioural, a selection of behavioural variables sets remains. These variables are now rated, depending on how well they score according to both performance measures. This leads to the likelihood measure of each variables set, which is an indication on how well this particular set performs, compared to the other behavioural sets. A method to define the likelihood in such a way that the sum of all likelihood measures is scaled to one was proposed by Simmons et al. (2017):

$$L_i^Y = \frac{BSS_i^Y}{\sum_{i=1}^{n} BSS_i^Y} \tag{4.61}$$

where L_i^Y and BSS_i^Y are the likelihood measure for performance measure Y (total siltation volume or spatial distribution of siltation volume) for behavioural set i, and n is the total amount of behavioural variable sets.

When using multiple performance measures, it is useful to combine the different likelihood measures into one combined likelihood. This allows to find the most likely set of variables, based on all performance measures. A definition for the combined likelihood, that ensures that the sum of the combined

likelihood measures scales to one is given by Simmons et al. (2017):

$$CL_i = \left(\prod_{Y=1}^{N} L_i^Y \right)^{1/N} \tag{4.62}$$

where L_i^Y is the likelihood measure of set i for the performance of BSS_Y, where Y represents BSS_{tot} and BSS_s. Equation (4.62) represent the situation where the likelihood of both performance measures in included equally in the determination of the combined likelihood CL. However, depending on the application, it can be useful to work with a weight for one of the performance measures. As example; in a situation where the total siltation volume is considered to be more important, a weight W can be assigned to L_i^{tot}, giving it a larger contribution in the calculation of the combined likelihood CL. This is showcased in Figure 5.8.

4.8.4. Parameter optimisation

The final step in the GLUE-procedure is to optimise the probability distribution of the independent variables. Equation (4.62) assumes that both likelihood measures are weighted evenly in the determination of the combined likelihood. However, due to the significant difference in average score between the two performance measures, it is also interesting to look at the individual likelihood measures of both performance measures. In that sense, four optimal sets of variables, with a different objective, can be defined: based on total siltation volume, based on the spatial distribution of siltation volumes, based on the evenly combined likelihood measure, and based on the weighted combined likelihood measures.

The probability distribution of the independent variables are determined by using the corresponding likelihood measure of each variable set as weight. This adds more weight to variable sets with a higher BSS. Introducing these weights leads to an alteration with respect to the prior defined uniform distribution. The obtained posterior distribution represent a probability distribution for each variable that is the optimal distribution for each independent variable. Besides the probability distribution, the GLUE-method also gives the optimal set of parameters from the sampled sets, which is considered as the best performing set of variables. In this case, four optimal sets of variables are obtained, which are presented in Section 5.3.

4.8.5. Uncertainty quantification

One of the goals of the GLUE-method is to reduce the uncertainty of the model. From the obtained set of behavioural variables, the corresponding posterior optimised probability distribution for each variable is approximated. One of the approaches to determine the posterior confidence intervals would be to draw samples of variables from the posterior optimised distributions. However, when using this approach, the possible correlation between a pair of variables and the corresponding model performance should be included. This avoids that unrealistic combinations of variables are selected that lead to unrealistic, unbehavioural combinations. As an example: imagine two sets of behavioural independent variables. Exchanging the values of one of the independent variables could result in two unbehavioural sets, as the effect of variable correlation on the likelihood is not considered. This is shown in Figure 5.10 and further discussed in Section 5.3.1. A possible solution to ensure this would be to incorporate copula's into the approach. By using a copula, the correlation between two stochastic variables from independent distributions can be taken into account. This is a complex approach which is increasingly complex for increasing numbers of variables. Although it would be a good addition to the method, in this research a different approach is followed. See Section 6.3 for a further discussion on the use of copula.

To ensure that only behavioural combinations of variables are considered, the uncertainty width is quantified by using the 2412 behavioural sets of variables. This has the consequence that the choice of the rejection threshold is directly affecting the resulting confidence bound. When deciding on a stricter rejection threshold, one would obtain a more narrow uncertainty bound, and vice versa. This is another consequence of the subjective choices in the GLUE-method. This particular consequence can be avoided by implementing a method that draws new samples, while considering the correlation between behavioural variables by using copula.

The bandwidth of uncertainty is defined as the 95% confidence interval of all behavioural outcomes. First this is done for the calibration period (Period 2) (see Section 5.3). In the determination of the 95% percentile, the likelihood weights of each set are included, to give more weight to the most likely sets of parameters.

4.9. Validation

As outlined in Section 4.8, the data of period 2 is used to calibrate the different model variables. The data of period 1 is used to validate the calibrated SedPit Nearshore tool. When splitting the data in a training and validation set, it is important to compare the two sets and identify striking differences between both. Figure 3.9 shows the metocean conditions in both conditions. The most striking differences are shown in Table 4.6. Most notable is the significant increase in average wave height H_{m0} in period 2. The differing metocean conditions will be discussed, along with the findings of the validation in Section 6.2. Next to the differences in wave conditions, it can be expected that the 'internal processes' of smoothing are more pronounced in the first period. The excavation of the trench will not only bring the profile out of equilibrium, but will also lead to erosion at the borders of the excavation. Additionally, it has been seen in Figure 3.3 that the sidecast has been eroded during the first period. The sidecast is within the range of the sections that are used to define the net sediment balance. However, transport in cross-sectional direction of the volume of the sidecast can still affect the siltation data in period 1.

Table 4.6: Comparison of the most diverging metocean conditions and total siltation volume of both periods. The mean over the total period is presented.

	Period 1 (Validation)	**Period 2 (Calibration)**
$\overline{H_{m0}}$ [m]	0.80	1.73
$\overline{T_p}$ [s]	4.4	5.6
$\overline{\Theta_0}$ w.r.t. shore-normal [deg]	24.6	18.7
Total observed siltation volume [m³]	723.3	2034.2

The SedPit Nearshore tool has been calibrated by means of the GLUE-method. For five different variables, an optimised posterior probability distribution has been approximated, based on 2412 behavioural sets of variables. These are based on the training dataset (period 2). As mentioned in Section 4.8.5, the uncertainty bounds will not be based on new sampled sets, as the correlation between the variables would not be included in a regular sampling approach. Instead, the 2412 behavioural sets of variables, including their likelihood weights, will be used as input for the SedPit Nearshore tool, to model the siltation volumes of the validation period; period 1. The resulting 2412 model outcomes for siltation volumes in period 1, will be based on the calibration on the siltation volumes in period 2. The SedPit Nearshore tool can be considered as validated for this scope, if the sets of variables give a 95% confidence interval that is a good representation of the observed siltation volumes. The validation considers both the total siltation volume, as well as the spatial distribution of the siltation volumes. The results are presented in Section 5.4

5
Results

This chapter presents the results that were obtained within this research. First of all, the general principle of the developed SedPit Nearshore tool is presented in Section 5.1. Next, the results of the sensitivity analyses are presented in Section 5.2. In Section 5.3, the results of the GLUE-method are presented. The validation of the calibrated SedPit Nearshore tool is presented in Section 5.4. Finally, the performance of the SedPit Nearshore tool, compared to the existing SedPit tool is discussed in Section 5.5.

Section 5.2, Section 5.3, Section 5.4 and Section 5.5 end with a concluding summary on the sensitivity analysis, GLUE-method, validation, and performance respectively. Discussions on how these conclusion relate to each other are presented in Chapter 7 and Chapter 6.

5.1. SedPit Nearshore-model

In this section, the SedPit Nearshore tool will be presented. The SedPit Nearshore tool is the result of combining the MBJ-model with the existing SedPit tool, as explained in Section 4.4.2. First, the needed input to use the SedPit nearshore tool is presented. Next, the output of the model is presented. Finally, some remarks on the computation time of the model are made. More detailed information on the existing SedPit tool is given in Appendix A, while more information on the modelling approach of the SedPit Nearshore tool is given in Section 4.4.2.

5.1.1. Input SedPit Nearshore tool

The input for the SedPit Nearshore tool can be divided in two categories: case-specific input and modelling input. The modelling input includes variables that are related to physical processes in the MBJ-model or the existing SedPit tool, but also includes numerical settings.

A crucial part of the case-specific data is the local bathymetry. This does not only include the bed profile of the coast, but also includes the dimensions of the trench which are indicated in Figure 4.5. The direct inclusion of a complete bed profile is one of the additions of the SedPit Nearshore tool, compared to the existing SedPit tool. In the existing SedPit tool, a variation in depth is possible by changing the depth in the input, which could be done manually or more efficiently through a loop, but this was not linked directly to wave transformation processes. The bed profile is converted to a grid that includes information on the horizontal and vertical position of each grid cell. To ensure accurate modelling of the wave transformation, the grid should start at a depth of deep water conditions ($kh >> 1$, see Section 4.2.1). Depending on the available information on the bed profile, the grid will need a (simplified) extended grid to ensure deep water conditions at the offshore boundary.

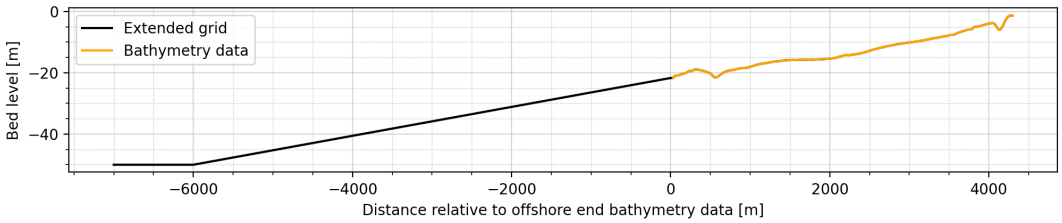

Figure 5.1: Example of an extended grid. The orange part is the available bathymetry data, while the black part is a simplified representation of an extended bed profile towards a depth that is sufficient to assume deep water conditions

The bed profile, including the extension to deep water conditions, is used with the same grid size for all timesteps. A possibility to increase the computational speed further would be to vary the spatial grid size based on the wave number k. However, this is not included in this research.

The offshore wave conditions are the next essential part of the case-specific input input data. Information on the following offshore wave characteristics are needed: significant wave height H_{s0}, peak period T_p, and wave direction θ_0. Besides the wave climate, the tidal regime plays an important role. This includes the tidal current and the tidal amplitude. An important note is that the tidal current should be given at a known depth, in order to be able to account for a reduction of tidal current due to decrease in depth in the nearshore environment. An example of the needed data on wave conditions and the tidal regime can be seen in Figure 3.9.

Other input variables that are related to the wave climate are the roller steepness β, wave breaker coefficient γ, and the breaker coefficient α. Although these variables are related to the wave climate, they are hard to predict based on wave climate data.

Lastly, information on the local sediment characteristics is needed. First of all, an approximation of the sand grain size is needed. Related to this is the bottom roughness k_s, which is hard to estimate accurately but can be defined based on the sand grain size. Besides the data on sand, information on the background concentration of silt and clay is crucial, if the location is exposed to fine sediments. Besides the background condition, the settling velocity of silt and clay are used as input data.

Most of the numerical settings in the SedPit Nearshore tool are also required in the existing SedPit tool, which are discussed in Appendix A. Two numerical input variables are added, which represent choices of the user. First of all, the variable d_{NS} is included. d_{NS} defines the seaward boundary of the nearshore zone where the model predicts the siltation. On the other hand, the cut-off depth d_{cu} defines the onshore boundary. This depth is either defined by the onshore end of the available bathymetry data, or it should represent a depth until which the model is expected to produce realistic outcomes.

5.1.2. Output SedPit Nearshore tool

The SedPit Nearshore tool gives information on siltation predictions. In Figure 5.2 the output is shown for a test case. The main objective of the model is to predict the siltation volumes along a transect perpendicular on the shoreline. The domain at which the siltation volumes are predicted can be defined by the user by appropriate choices for the nearshore depth d_{NS} and cut-off depth d_{cu}. The output is a graph that plots the siltation volume in volume per meter width (m³/m) along the transect. Consequently, the surface below the line represent the total siltation volume in the nearshore environment. The test case in Figure 5.2 is based on a constant wave climate without tidal fluctuations. A range of possible values of k_s is shown, to illustrate the corresponding outcome space. For this example, a varying value for k_s was used, as this is the most influential variable, according to Figure 5.5. Adding a varying wave climate, and including water level fluctuations would lead to more spatial variation of the peaks, as a result of varying breaking depths.

Related to the siltation volume, the model can predict the corresponding siltation thickness. This thickness is based on a simplified approach of estimating the deposition surface of the trench (see Equation (3.3)).

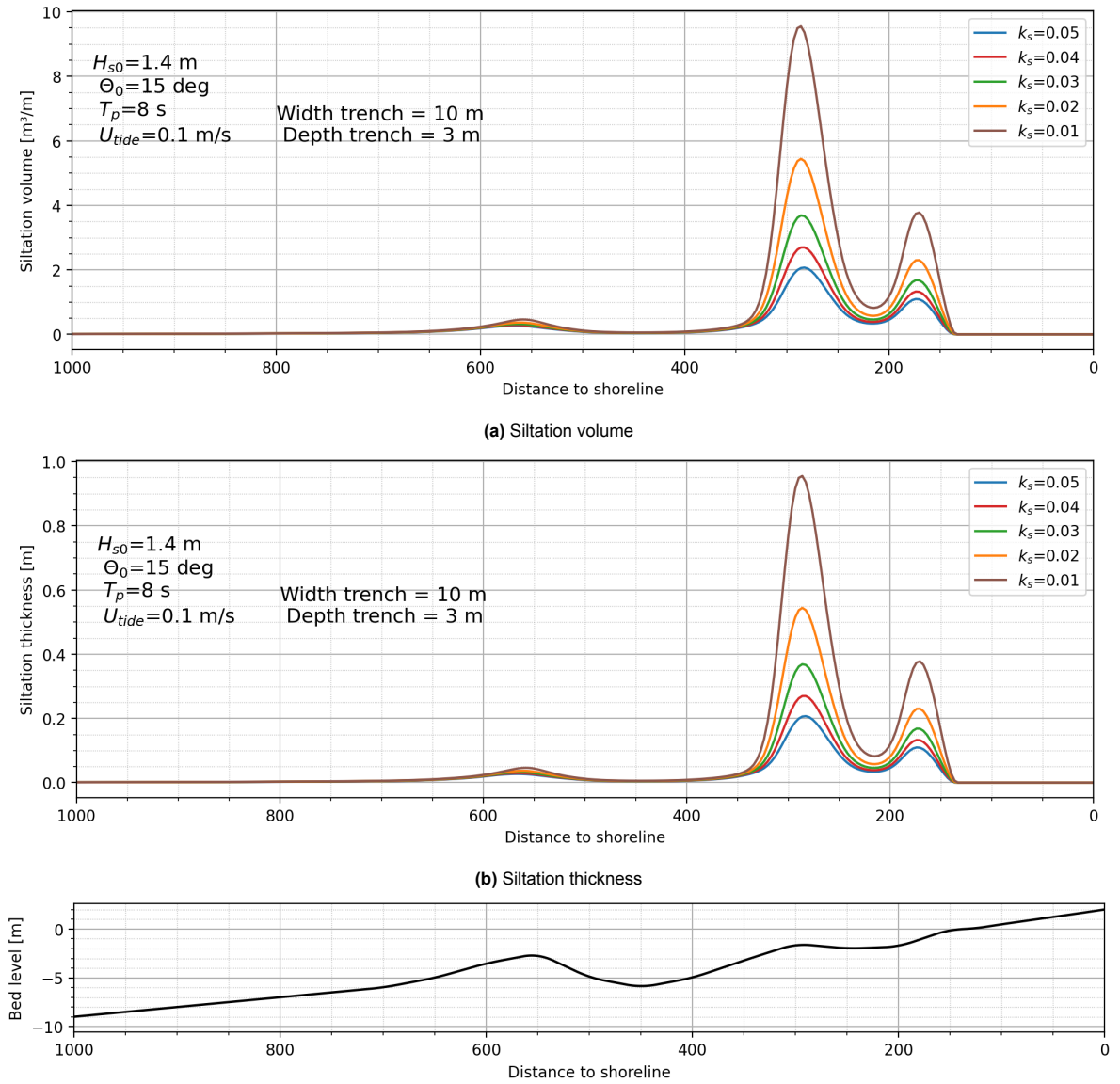

(a) Siltation volume

(b) Siltation thickness

Figure 5.2: Output of the SedPit Nearshore tool for a constant wave climate, with a varying bottom roughness k_s. The used bed profile originates from the bed profile at Egmond aan Zee, retrieved via the Coast3D dataset (Klein et al., 2001).

5.1.3. Computation time

Considering the context of a quick-assessment tool, the computation time is an important aspect of the model. The SedPit Nearshore tool includes two time-consuming steps in its calculations. First of all, the hydrodynamic conditions along the transect for all timesteps. The total needed computation time for this step is determined by the grid size of the transect, and the length of the timeseries. The second step contains all morphological calculations from the SedPit tool. The needed computation time is also dependent on the length of the timeseries, and on the length of the grid. However, this part of the calculation is only done for the nearshore domain that is defined by the user, as explained in Section 5.1.1.

The modelled situation in Figure 5.2 is used as an example. The used timespan consisted of 144 timesteps, with a timestep of 20 minutes. The grid, including the extended offshore grid, consists of 538 grid cells, where the finest grid has a resolution of 3.4 m. The needed time to compute the hydrodynamics for all timesteps on the whole transect was 10 seconds. On average, 13 timesteps were computed per second. The nearshore depth was defined at a depth of 10 m, which lead to 283 ”nearshore grid cells”. Calculating the siltation of all timesteps on all 283 cells took 4 seconds. On average, 72 cells were calculated per second. Combined, this leads to a computation time of 14 seconds.

5.2. Sensitivity Analysis

In this section, the results of the different sensitivity analysis that were performed in this research are presented. First, an elaboration on how to interpret the results of the Sobol' method is given. Than the results of the sensitivity analysis on the MBJ-model, and on the combined model are presented.

5.2.1. Interpretation results Sobol method

The Sobol' method is a variance-based global sensitivity analysis. It defines the contribution of the uncertainty of an input value on the model's output variance. Two types of sensitivity indices are considered in this research: first order indices S_1 and second order indices S_2. The exact mathematical notation of these indices can be found in Equation (2.28) and Equation (2.29) respectively. However, to clarify the interpretation of the upcoming results, these indices will be explained in a slightly more plain language below.

The indices are always related to the total variance of a model outcome, which approximately indicates the bandwidth of possible model outcomes due to the variance of the input values. The bandwidth of the model outcomes is strongly depending on the sampling, as earlier explained in Section 4.6, while the contribution of each variable to the model's variance is depends on the probability distributions where the variables are sampled from.

For every input variable, one first order index S_1 is calculated. The first order indices compare the fraction of the model variance that can be attributed to changes in their corresponding variable. In a situation, where the interaction between variables does not contribute to the total model variance, all first order indices would sum up to 1 (Saltelli et al., 2010). However, in a model with a wide variety of input variables, and interaction between formulae within the model, it is safe to assume that variables show interactions that affect the model variance. For every set of two variables, a second order index S_2 is determined. This second order index indicates the fraction of the total model variance that can be attributed to interaction between these two variables. When assuming that higher order interactions (interactions between three or more variables) do not contribute significantly to the model outcome, the summation of all first order indices and second order indices should appropriately be 1 (Saltelli et al., 2010).

5.2.2. Results Sensitivity Analysis hydrodynamics model (MBJ)

As introduced in Section 4.6, the sensitivity analyses on the MBJ-model has the objective to analyse the behaviour of the model on variety of input. In this section, the results of the sensitivity analysis including all 8 variables are presented. The results are presented in the form of the Sobol' indices in Figure 5.4, and boxplots in Figure 5.3.

A first conclusion that can be drawn from Figure 5.4 is the importance of interaction effects within the MBJ-model. The sum of all first-order indices is 0.55, which means that a large fraction of the model variance can be attributed to higher order interactions. As the wave climate entails many correlated processes, like wave height and peak period, this is not a surprising finding. Judging only on the first-order variance, U_{tide} stands out as most influential variable. Considering the summed amount of second-order effects, the wave climate variables H_s, θ, and T_p show the strongest interaction effects. However, when looking at the summation of first- and second-order indices, U_{tide} is still the most influential variable. When looking at the definition of model outcome Y in Equation (4.58), this not a surprising finding. Although only the nearshore stretch is considered in Y, the contribution of the tide is overwhelming the effects of the wave climate as the wave-driven current is generated only in the final meters of the nearshore zone.

Figure 5.3 shows how the model outcomes are distributed within the bounds of the input variables. The bounds are combined in bins with a certain width. The data is presented through a boxplot, which reveals some interesting insights.

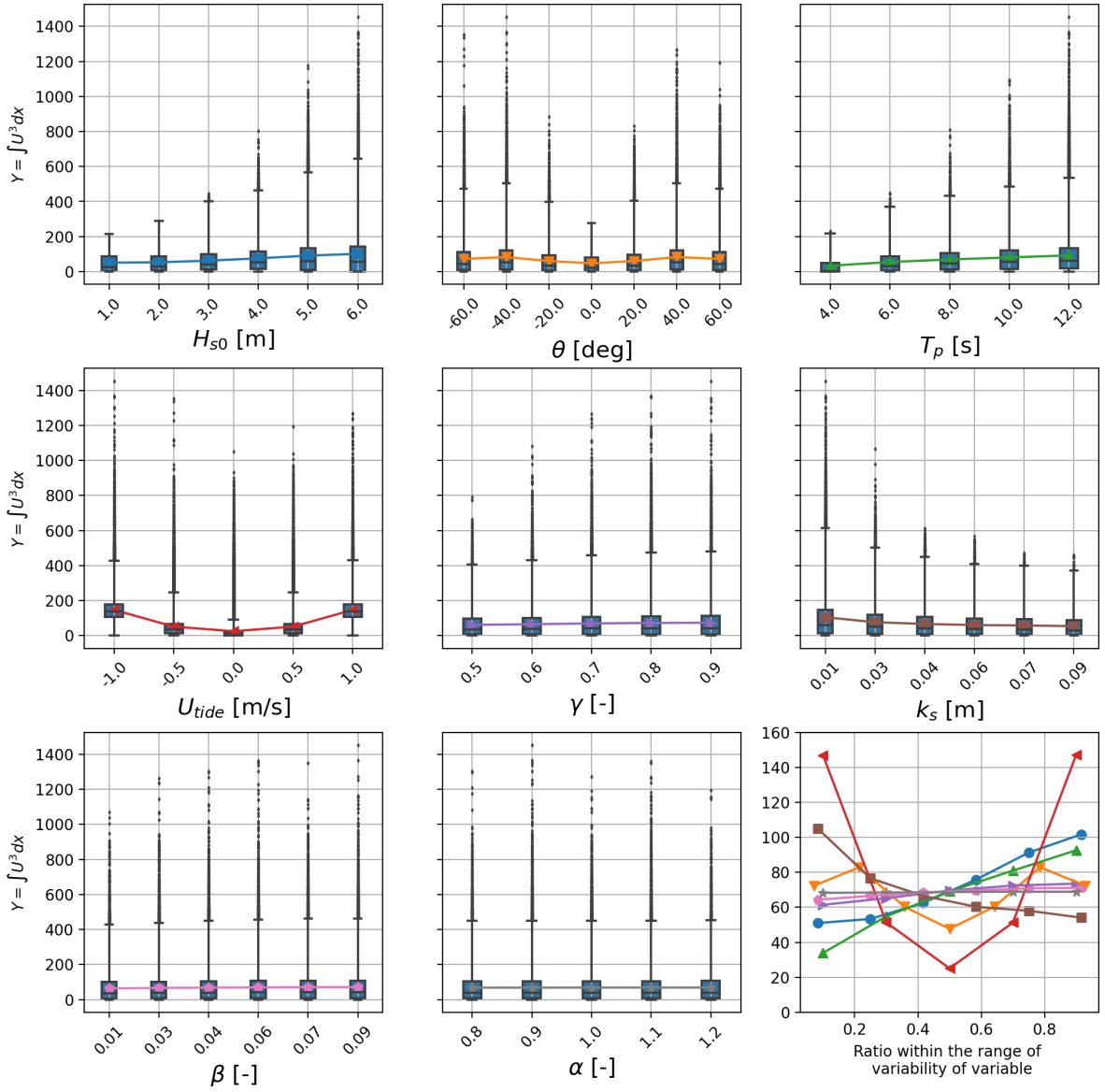

Figure 5.3: Model response on 8 varying input values. The colored markers are representing the mean. The horizontal whisker extend to the furthest data point within 2.5 times the interquartile range (IQR) from the first and third quartiles, while any data points beyond this range are considered outliers and are individually plotted. The bottom right figure is plotting the mean model outcomes on a normalised range of the variability.

The first insight given by the boxplot is the mean model outcome within a bin of the input variability. The mean model outcome of each bin is indicated by the colored marker in Figure 5.3. The bottom right graph in Figure 5.3 is zooming-in on these mean values. It can be stated that the effect of input variability on the mean model outcome is different per variable. The variables U_{tide}, H_{s0}, T_p, θ, and k_s seem to have visible influence on the mean model outcome, where U_{tide} is by far most influencing the mean model outcome. This is in line with the values of the first-order indices that are presented in Figure 5.4. The effect on the mean model outcomes is also in line what is expected based on the physical processes. Increasing absolute values for H_s, T_p, U_{tide}, and θ lead to more generated currents. Similar, a decrease in bottom roughness k_s is leading to more generated currents.

The second important insight from Figure 5.3 is the correlation between extreme values and input variability. When looking at the trend of the most extreme outliers in the different subplots, the effect of

a variable on extreme events can be described. This method of graphically describing the effect of input variability on extreme values is based on the work of Nogal and Nogal (2021). The variables H_{s0} and T_p show the strongest influence on achieving an extreme values. In other words, from a mathematical point of view, acting upon these variables is the most effective manner to avoid extreme values of Y. The variables U_{tide} and γ show a smaller role in creating extreme values. The variables β and α play the smallest role in achieving extreme values, as the outliers are distributed very similar throughout the input variability. These findings are in line what would be expected from physical laws. Generation of strong wave-driven currents are strongly dependent on a wave climate with large wave heights, which again is correlated with larger wave periods. Especially considering the large input variability for the wave height, compared to the smaller input variability of non-measurable variables, the strong influence of wave height and peak period on extreme values is intuitive.

Furthermore, the variability of the length of the vertical whiskers indicate how much a variable is dominating the model outcome. As an example to illustrate this, the boxplot of the wave height H_{s0} is used. When considering a small value for H_{s0}, the other variables do not have the capacity to obtain a large model outcome. While on the other hand, when considering a large value of H_{s0}, the remaining variables have the capacity to result in a large variety of small and large model outcomes. A similar pattern can be seen for the peak period T_p, while this pattern is less pronounced for the remaining variables.

Finally, the boxplots do give a clear impression of the direction of the influence of variables on the model outcome. This is especially visible for the variables U_{tide} and θ. It becomes clear that the model outcome is influenced by the absolute value of both variables in a positive manner; larger absolute values, lead to large model outcomes. On the other hand, the variable bottom roughness k_s shows a negative direction in its influence on the model outcome; smaller values lead to larger model outcomes.

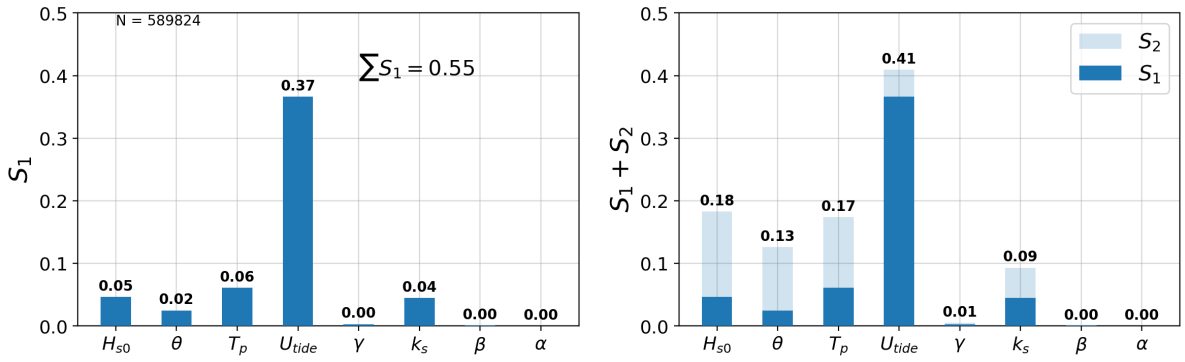

Figure 5.4: Sobol' indices of all 8 variables. Left: first-order indices. Right: summation of first- and all second-order indices where a variable is represented. The effect of second order indices in the right graph, consists of the summation of all second-order indices where a variable is represented. For each pair of variables, one second-order index is calculated. These are stated in Table 5.1.

Table 5.1: Second order Sobol' indices. The second order Sobol' indices for each pair of variables is stated, along with the summation of all second order Sobol' indices where a variable is represented in the bottom row. Due to rounding errors, the values do not exactly coincide with the contribution of S_2 in Figure 5.4.

	H_{s0}	θ_0	T_p	U_{tide}	γ	k_s	β	α
H_{s0}	/	0.022	0.084	0.002	0.000	0.037	0.003	0.004
θ_0	0.022	/	0.016	0.033	0.005	0.017	0.005	0.004
T_p	0.084	0.016	/	0.007	0.002	0.012	0.002	0.001
U_{tide}	0.002	0.033	0.007	/	0.000	0.001	0.001	0.001
γ	0.000	0.005	0.002	0.000	/	0.000	0.000	0.001
k_s	0.037	0.017	0.012	0.001	0.000	/	0.008	0.008
β	0.004	0.005	0.002	0.001	0.000	0.008	/	0.000
α	0.004	0.004	0.001	0.001	0.001	0.008	0.000	/
$\sum S_{2,i}$	**0.153**	**0.102**	**0.124**	**0.045**	**0.008**	**0.083**	**0.019**	**0.018**

The following conclusions can be drawn from the results presented above:

- When assessing all 8 variables, it becomes clear that the variables related to the wave climate and tidal current are by far the most influential variables. This is partly the result of the wide distributions for these variables, but is also in line with the the expected physical effect of the forcing on the model outcome.
- The variables wave height H_{s0} and T_p play the largest role in achieving extreme values.
- The model variance is strongly affected by interaction between variables.
- The tidal current U_{tide} is the most influential variable when considering first-order effects only. When considering the higher-order interaction effects, the tidal current U_{tide} is still the most influential variable, although the wave climate variables (H_{s0}, T_p, and θ_0) are becoming more influential.
- Overall, the MBJ-model responses to varying input as expected according to physical laws. Besides that, the fact that the tidal current U_{tide} and the wave climate variables H_{s0}, T_p, and θ_0 are the most influential variables is in line with the expectations.

5.2.3. Results Sensitivity Analysis combined model

As introduced in Section 4.7, the sensitivity analyses on the combined SedPit Nearshore-model has two objectives: analyse the behaviour of the model on variety of input, and identify the most influential variables. Based on the insights on the most influential variables, a choice can be made which variables will be included in the GLUE-procedure.

A first conclusion that can be drawn from Figure 5.5 is the effect of higher-order terms, indicating interaction effects between variables. The sum of all first-order indices is 0.83, which means that only a small fraction of the model variance can be attributed to higher order interactions. Therefore, the Sobol' method has been conducted with exclusion of second-order indices. This saves significant computation time, and makes the sample size of $N = 36,864$ large enough to obtain a stable outcome. It can be concluded that the variables k_s and β are the most-influential variables, with d_{50} also having a significant contribution to the model's variance. The contribution of the variables ρ_b and c_{vr} is sigificantly lower compared to the other variables.

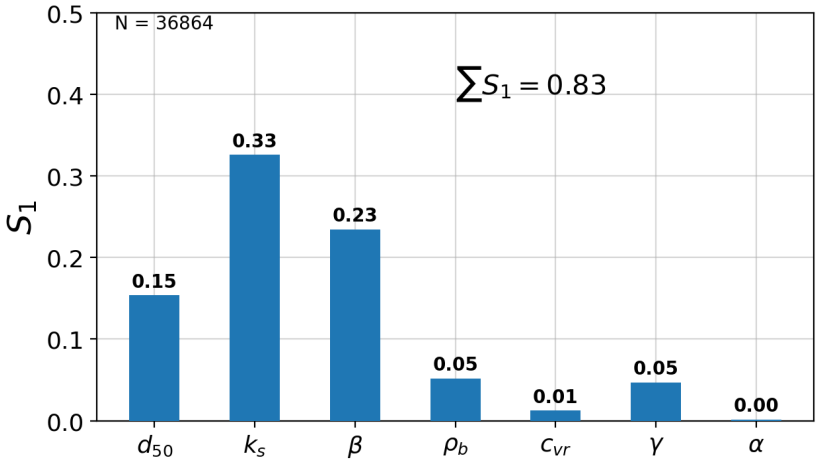

Figure 5.5: First order Sobol' indices of the independent variables in the SedPit Nearshore-model.

Figure 5.6 show how the model outcomes are distributed within the bounds of the input variables. The bounds are combined in bins with a certain width. The data is presented through a boxplot, which reveals some interesting insights.

The first insight given by the boxplot is the mean model outcome within a bin of the input variability, and the direction of its effect. The mean model outcome of each bin is indicated by the colored marker in Figure 5.6. The bottom right graph in Figure 5.6 is zooming-in on these mean values. The findings that were based on the first-order indices in Figure 5.5 are in line with what can be seen in the effect on the mean model outcomes. The influence on the mean model outcomes is most for the variables k_s, β, and d_{50}. The effect on the mean model outcomes, and the its direction, is also in line what is expected based on the physical processes. A larger roller steepness β leads to shorter length of roller dissipation, meaning that the generation of the wave-driven current is more concentrated, thus being larger in magnitude and consequently transporting more sediment. A larger sand grain size d_{50} leads to a larger critical flow, which negatively affects the transport rates. A lower bottom roughness k_s allows currents to reach a larger magnitude, with a corresponding larger sediment transport rate.

While drawing conclusions regarding the most influential variables, the chosen bounds have to be taken into account. During the sampling for this sensitivity analysis, only a part of the natural variability of grain size of sand was included.

In Section 5.2.2, the boxplot graphs were also used to indicate the possibility to achieve extreme values. Extreme values are less pronounced visible in Figure 5.3. This is related to the fact that the variables that were most likely to cause an extreme value (H_{s0} and T_p) are defined by the metocean data depicted in Figure 4.8. Within the assessed period, the wave height H_{s0} and peak period T_p reach significantly lower values than the values that are associated with extreme values in Figure 5.3. It can be concluded that most of the included non-measurable variables, are not capable of causing extreme values. However, the variables k_s and β show the strongest effect on extreme values.

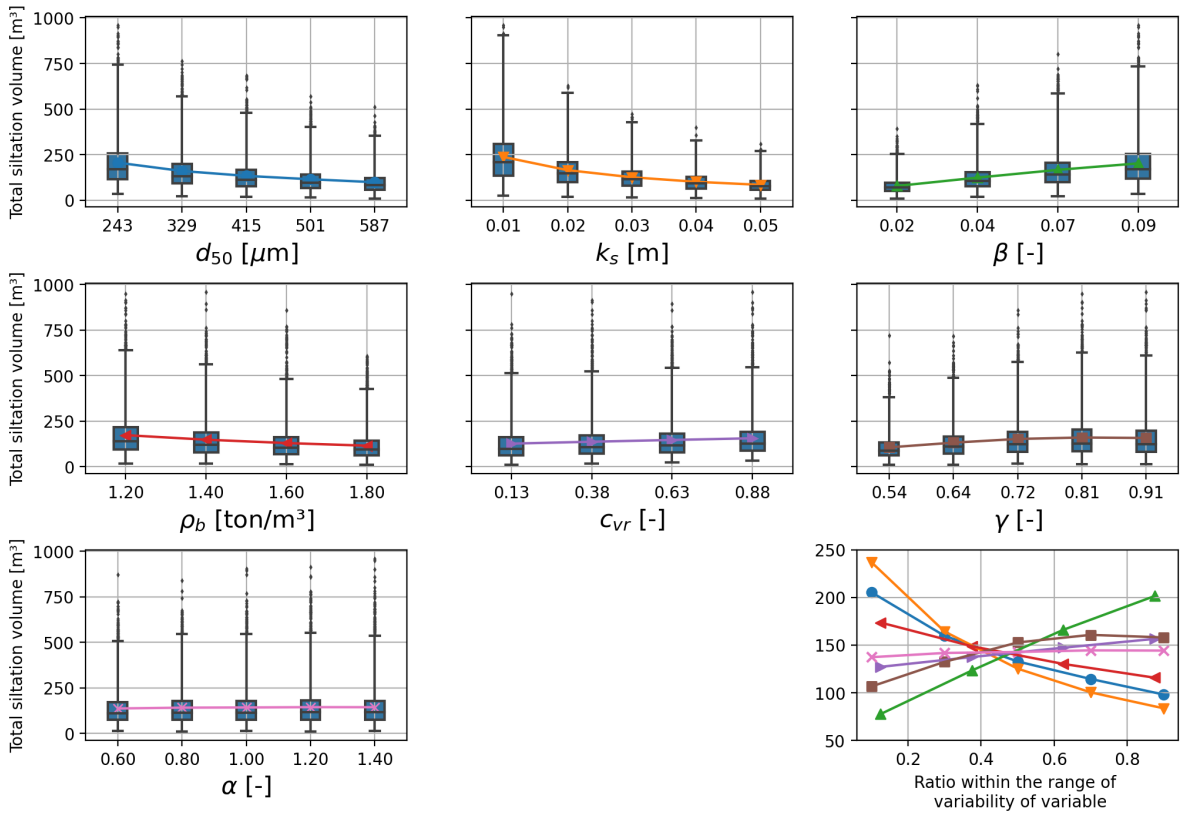

Figure 5.6: Model response on the independent variables in the SedPit Nearshore-model. The colored markers are representing the mean. The horizontal whisker extend to the furthest data point within 2.5 times the interquartile range (IQR) from the first and third quartiles, while any data points beyond this range are considered outliers and are individually plotted. The bottom right figure is plotting the mean model outcomes on a normalised range of the variability.

An interesting finding is the negative effect of sand grain size d_{50} on the total siltation volume. On one hand, according to Equation (4.56) and Equation (4.54), a larger d_{50} has a larger settling velocity, leading to a larger trapping efficiency. In that case a positive relation between d_{50} and siltation volume would be expected. However, on the other hand, a larger d_{50} leads to a larger critical velocity, meaning that less sediment is in suspension at a certain current velocity for a larger d_{50}. For the used range of d_{50}, the negative relation due to the increase in critical velocity seems to be dominant in this situation.

Another interesting finding from Figure 5.5 and Figure 5.6 is the minor influence of the Van Rijn trapping coefficient c_{vr}, when comparing it to the results of the sensitivity analysis on the existing SedPit tool in Appendix D. In the existing SedPit tool, the effect of c_{vr} on the mean model outcome is significantly more pronounced. The Van Rijn trapping coefficient is included in the formulation of the trapping efficiency via Equation (4.56). A clear explanation for this differing sensitivity is hard to find. In the SedPit Nearshore tool, significantly larger currents are included in the breaker zone, compared to the tidal currents in the existing SedPit tool. As A_v is negatively correlated to the bed shear velocity U_*, the large wave-driven currents result in a lower A_v. This has its implications on the exponent of e in the formula for the trapping efficiency E in Equation (4.54). A smaller A_v leads to smaller trapping efficiency. Having a lower trapping efficiency, makes the total siltation volume in the trench less sensitive to increments in the driving forces of the trapping efficiency. This would explain that the siltation volume in the nearshore zone is more sensitive to variables that affect the magnitude of the generated current (k_s and β) than variables that affect the trapping efficiency of the trench.

The following conclusions can be drawn from the results presented above:

- The most influential non-measurable variables in the SedPit Nearshore tool are the bottom roughness k_s, the wave roller steepness β, and the sand grain size d_{50}. These are the variables that will be included in the GLUE-method in Section 4.8.

- When excluding the forcing variables (tidal current U_{tide} and the wave climate variables), interaction terms play a significantly smaller role, compared to when these variables are included.

5.3. GLUE

This section presents the results of the GLUE-method, according to the methodology that is described in Section 4.8. The section is structured according to the different steps in the GLUE-method, in order to show some of the intermediate results. First, the steps towards the optimised parameter distribution are presented in Section 5.3.1. Next, the results are used to quantify the uncertainty of the SedPit Nearshore tool in Section 5.3.2.

5.3.1. Performance, rejection, and parameter optimisation

First of all, Figure 5.7 shows three graphs with respect to the performance of the samples. From these graphs, it can be stated that a positive correlation is present between the performance regarding both performance measures. A sample set that performs well on BSS_s is likely to perform well on BSS_{tot}. The fact that the model performs better in predicting total siltation than in predicting the spatial distribution can be seen from the fact that the upper limit of $BSS_{tot} = 1$ is reached by several sets, while no set is close to the upper limit of $BSS_s = 1$.

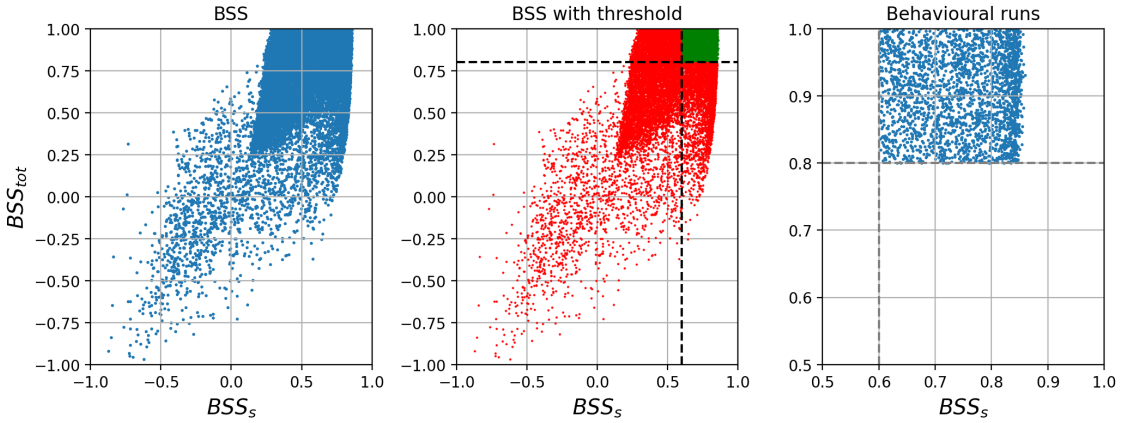

Figure 5.7: The performance measures BSS_s and BSS_{tot} of all sets of samples. The middle graph shows the thresholds and the resulting rejection of sample sets. The right graph zooms in on the behavioural sets.

Next, the likelihood of each behavioural set is plotted in Figure 5.8. In both graphs in Figure 5.8, the x- and y-axis are representing the performance score for BSS_s and BSS_{tot} respectively. Consequently, a point that is located in the upper right corner is performing better in both measures than a point located in the bottom left corner. The color of the dot is representing the combined likelihood, according to Equation (4.62). The difference between the left and plot in Figure 5.8 visualises the effect of the weight factor W which was introduced in Section 4.8.3. It can be seen that a high combined likelihood in the right graph is more dependent on a high likelihood of BSS_{tot}, as a result of a weight factor W of 3.

As discussed in Section 4.8.4, the likelihoods are used as weights to approximate an optimised distribution of the independent variables. Figure 5.9 shows the obtained optimised probability distributions, for both the equally weighted combined likelihood, and the weighted combined likelihood. Besides that, the prior uniform distributions are plotted, to visualise how the GLUE-method changes the probability distribution. It becomes evident that the variables k_s, β, and c_{silt} are not well represent by the prior uniform distribution. The variables d_{50} and c_{clay} do not show significant variation to the prior-distribution, which indicates that the chosen value of these variables does not affect the performance of the model as much as the other three variables do. The fact that the weighted density of β does not decrease towards its upper bound might indicate that even better values of β lay outside of the chosen bounds. Although the bounds are based on the theoretical meaning of β (Walstra et al., 1997), it is possible that the model favours values that are numerically optimal, while not aligning with the theory. Further-

more, it can be seen that the weighted average likelihood does not lead to significant changes in the parameter probability distributions.

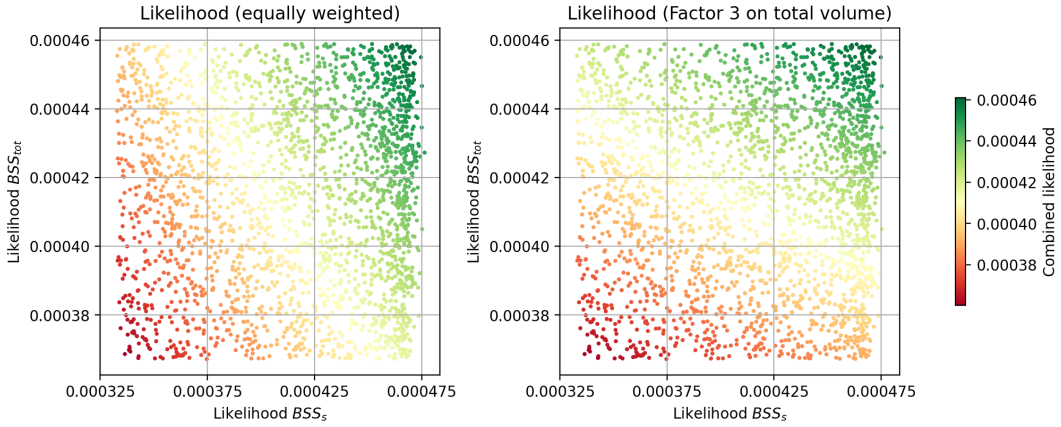

Figure 5.8: The likelihood for each set of both performance measures BSS_s and BSS_{tot}, with the combined likelihood represented by the color. On the right graph, a weight factor of 3 was assigned to the performance measure BSS_{tot}, which leads to a rearrangement of the combined likelihood.

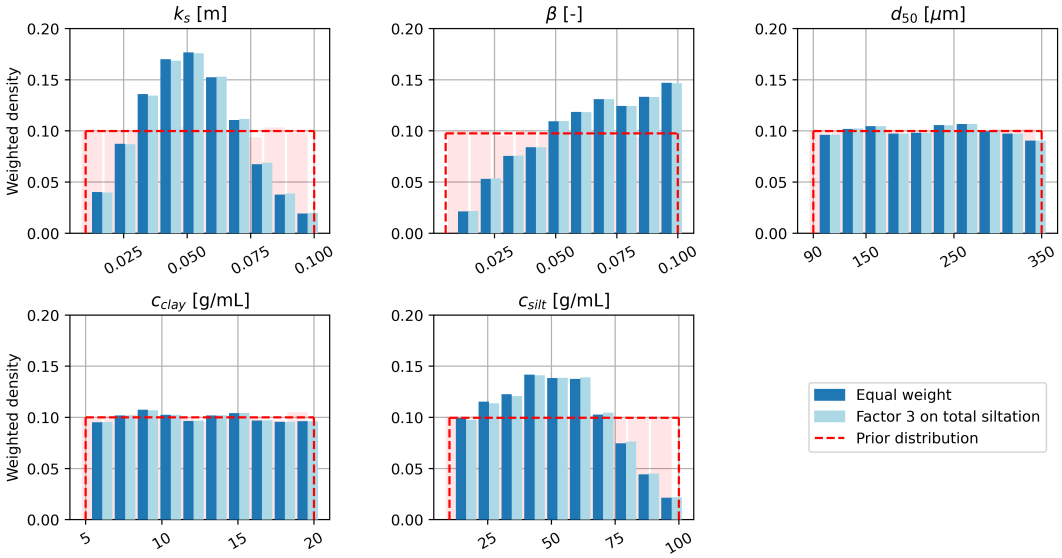

Figure 5.9: Posterior optimised parameter distributions. All histograms consist of a total of 2412 sets of variables.

Finding an optimal parameter set purely based on the information in Figure 5.9 is difficult, due to the interdependence between variables. Picking the value for all five variable with the highest weighted density does not give you the optimal set of variables, as this is not taking correlation between variables into account. Each pair of two variables of all behavioural sets is plotted in Figure 5.10. It becomes clear that the variables that show the strongest deviation from the prior assumed distribution have the largest correlations. To indicate this, the Pearson correlation coefficient is calculated. Although the Pearson correlation coefficient only takes linear correlation into account, it is a good indicator for correlations.

Correlation coefficient values of up to 0.57 for k_s/β, or -0.52 for k_s/d_{50} indicate the presence of significant correlations among the values of behavioral variables. The correlation do not have a straightforward physical meaning. Instead, the most pronounced correlation seems to exist to compensate for an extreme value of one of the variables of that pair. As an example, bottom roughness k_s and roller steepness β are the two most influential variables, according to the sensitivity analysis in Section 5.2.

Figure 5.6 show that k_s is inversely correlated to siltation volumes, while β has a positive correlation with siltation volumes. In Figure 5.10 it can be seen that this leads to a positive correlation between k_s and β. In other words: if a large value of k_s is sampled, which is related to low siltation volumes, a large value of β is needed to reach the aimed value of the calibration dataset. Similarly, a large k_s is compensated by large concentration of silt c_{silt}. The correlation between between k_s and the sand grain size d_{50} is more complicated to interpret, but has been explained in the interpretation of the results of the sensitivity analysis in Section 5.2.3. The negative correlation between d_{50} and siltation volume leads to a combination of large values for k_s and small values for d_{50}.

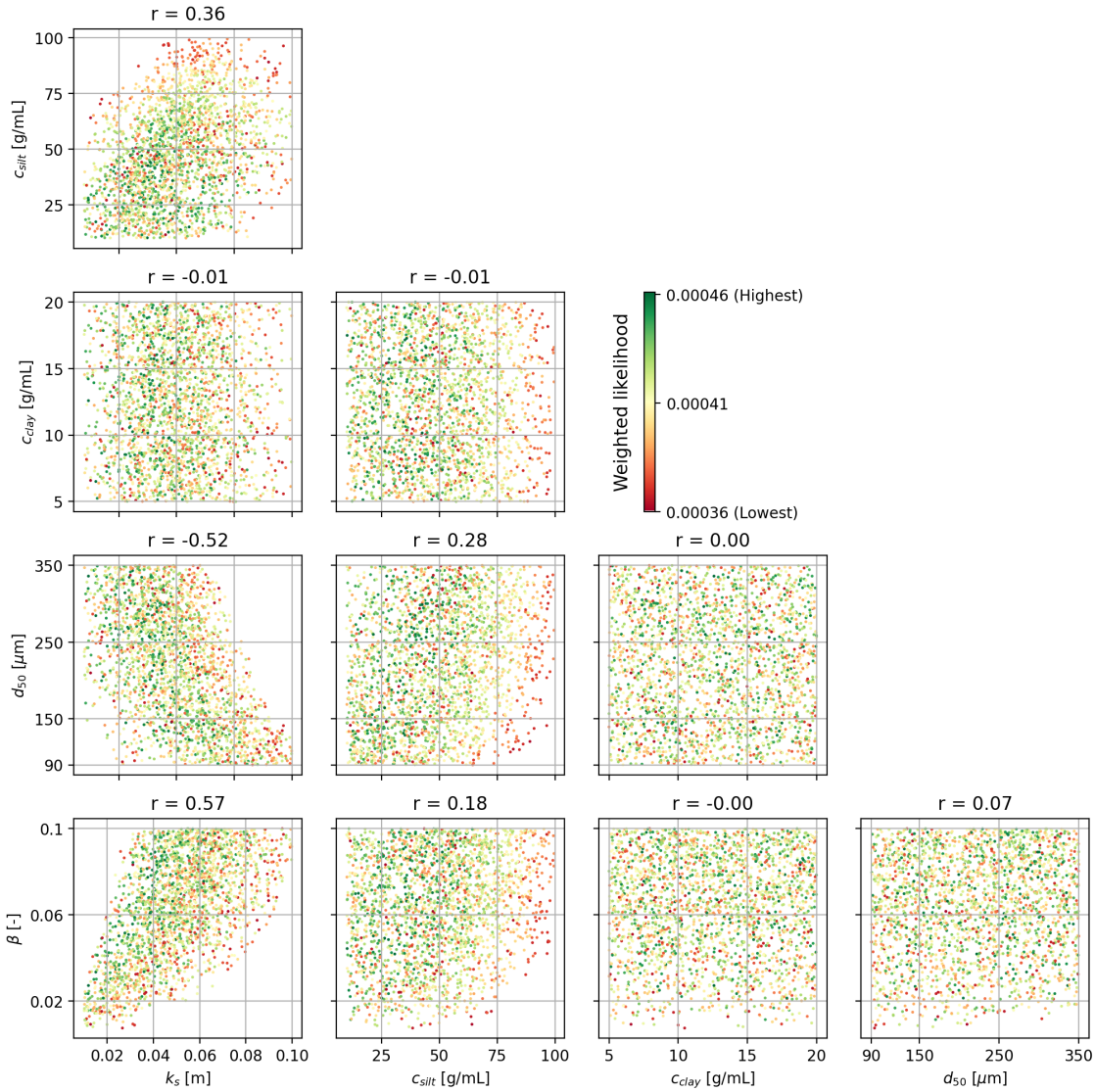

Figure 5.10: Correlations between all behavioural variables for each set of variables. The color indicates the likelihood based on weighted average. The number above each plot indicates the Pearson correlation coefficient, to indicate the level of linear correlation between the behavioural variables.

The optimal set of parameters should be determined based on the likelihoods depicted in Figure 5.8. In this analysis, optimal parameter sets for four different objectives were identified: based on total siltation volume, based on the spatial distribution of siltation volumes, based on the evenly combined likelihood measure, and based on the weighted combined likelihood measures. These are shown in Table 5.2. These sets are also helpful to verify if the method is conducted correctly and to visually evaluate the performance of the optimal sets, which is done in Figure 5.11. To place the siltation volume in reference: the total excavated volume of the trench is estimated on 75 m³/m, giving a total volume of approximately 75,000 m³ when considering the first 1000 meter length of the trench. Consequently,

2.7% of the excavated volume is siltated during period 2.

Table 5.2: Optimal parameter set for four different objectives. The most right column shows the modelled total siltation volume during period 2.

Objective	k_s [m]	β [-]	d_{50} [μm]	c_{clay} [mg/L]	c_{silt} [mg/L]	Total siltation volume [m³]
Total siltation volume	0.061	0.080	219	13.5	61.8	2034.2
Spatial distribution	0.013	0.021	218	16.3	17.0	2174.6
Evenly combined	0.012	0.027	336	12.6	27.3	2051.6
Weighted combined	0.041	0.049	164	8.8	26.4	2037.7
					Observed total siltation volume	2033.9

The model outcomes corresponding to the four sets of variables in Table 5.2 are plotted in Figure 5.11. An interesting finding is that the model is generally overestimating the total siltation volume if the performance on modelling the spatial distribution is included. When comparing Figure 5.11c and Figure 5.11d, the small differences between the posterior optimised probability distributions in Figure 5.9 can be explained. It can be seen that the weighted combination outcome has a lower, but more accurate total siltation volume than the evenly combined outcome, as a result of the increases weight of BSS_{tot}. When looking at the distribution of k_s in Figure 5.9, it can be seen that the weighted combination tends to slightly larger values, which do correspond with a decrease in siltation volumes.

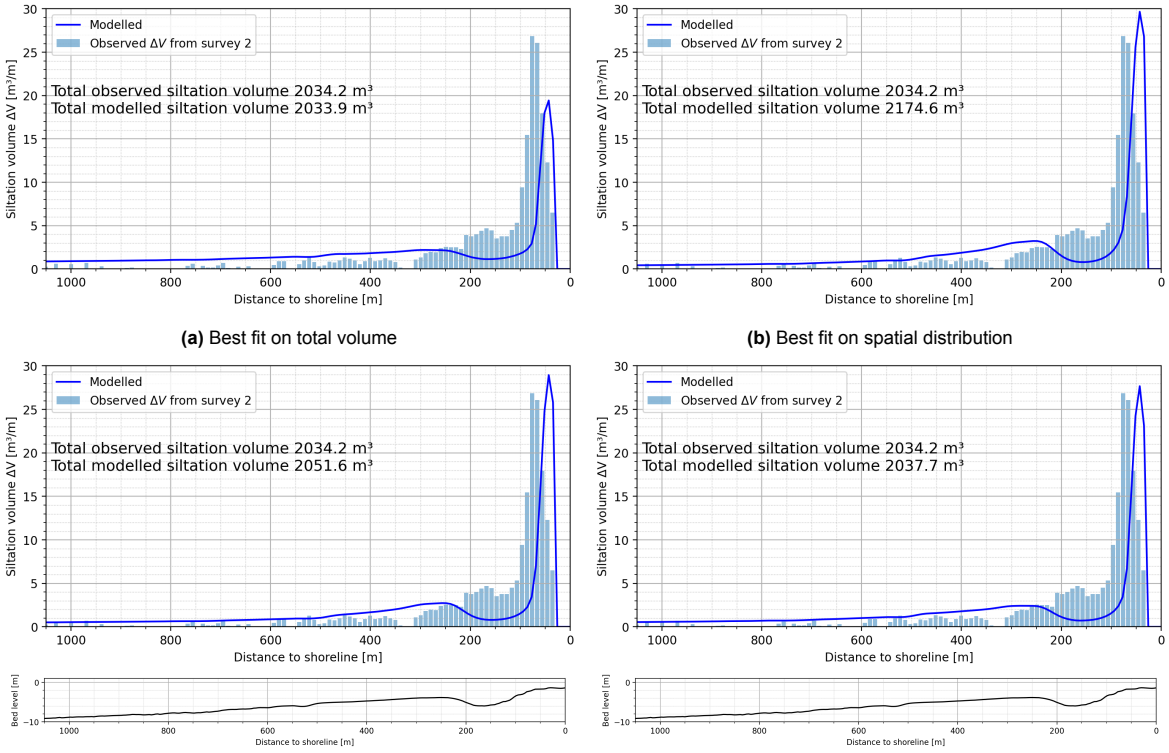

(a) Best fit on total volume

(b) Best fit on spatial distribution

(c) Best fit on evenly combined averaged

(d) Best fit on weighted average

Figure 5.11: The result of the best parameter sets for all four objectives. Note that the performance on modelling the spatial distribution is evaluated while correcting for the location of the peak to avoid the “double penalty”(See Section 4.8.2).

5.3.2. Uncertainty quantification

As explained in Section 4.8.5, the uncertainty of the SedPit Nearshore tool will be quantified based on the behavioural runs. In Figure 5.12 the resulting 95% confidence interval is shown, and compared to the 95% confidence interval of all priori-sampled sets of parameters. It can be seen that imposing a performance threshold and corresponding selection of behavioural sets leads to a significant reduction of the uncertainty width. At the peak, the width of the 95% confidence interval is reduced by 36%. Although this is a significant improvement compared to the prior-sampling, the remaining uncertainty width is still $\pm$ 42% of the observed siltation at the peak. Besides that, Figure 5.12 shows once again that the location of the peak is not modelled correctly. A significant part of the curve representing the observed siltation volumes is not within the 95% confidence interval, which is for a large part the result of the offset of the modelled peak. This is a striking short-coming of the SedPit Nearshore tool, which will be further discussed in Section 5.5. Furthermore, the inset between x=900 and x=1000 shows that the model is generally overestimating the siltation volumes in the deeper regions. Lastly, an underestimation on siltation volumes is seen between x=120 and x=200. Physical explanations for all mentioned short-comings will be discussed in Section 5.5.

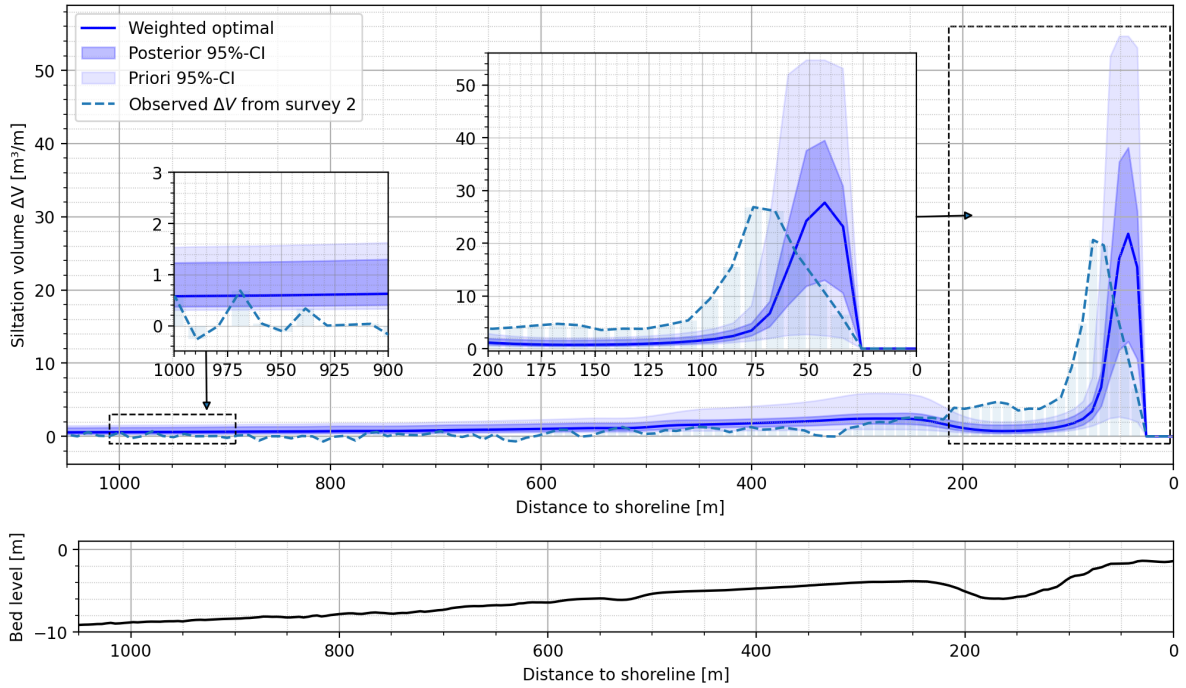

Figure 5.12: The obtained 95% confidence interval (dark blue area), compared to the prior 95% confidence interval. The solid line represents the model outcome of the optimal set of variables based on the objective of a weighted average (see Table 5.2). The dashed line represent the observed siltation volumes. The (physical) explanation of some of the offsets are discussed in Section 5.5 and Chapter 6.

Besides the uncertainty width of the spatial distribution, the uncertainty in predicting the total siltation volume is an important aspect in the application of the SedPit Nearshore tool. However, as the bandwidth of all behavioural model outcomes is directly related to the choice of performance threshold for BSS_{tot}, the outcomes are somewhat biased due to the subjectivity of the choice in threshold. Figure 5.13 shows the distribution of the 2412 behavioural outcomes for the total siltation volume. The main finding from Figure 5.13 is that the 95% confidence interval has a width of 800 m³, leading to an uncertainty of $\pm$ 20% compared to the observed siltation volume. The shape of the histogram and the curve of the cumulative density function (CDF) do show that a slight trend towards a normal distribution is visible, although the sharp edges are not in line with that. The sharp edges are a direct result of the choice in performance threshold.

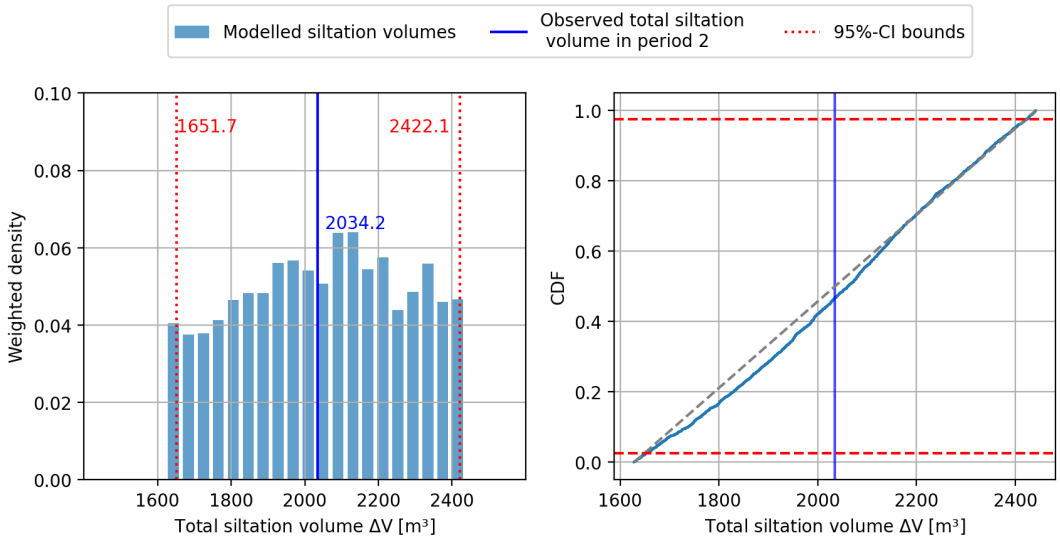

Figure 5.13: Probability distribution of total siltation volumes in period 2. The solid blue line indicates the observed total siltation volume. The red dashed lines indicate the bounds of the 95% confidence interval.

5.3.3. Conclusions GLUE

The main findings from the GLUE-method are:

- After calibration, the SedPit Nearshore tool fits the calibration data excellent on the prediction of total siltation volumes. The spatial distribution shows a less accurate fit to the calibration data, especially in predicting the location of the peak.
- The optimisation of the independent variables do show that the choice of the variables k_s, β, and c_{clay} strongly affect the model outcome, resulting in clear patterns for the posterior optimised probability distributions.
- The posterior optimised probability distributions of the variables d_{50} and c_{silt} do not change compared to the prior assumed uniform distribution. This shows that these variables do not affect the performance of the model in the calibration significantly.
- Correlation coefficient values of up to 0.57 for k_s/β, or -0.52 for k_s/d_{50} indicate the presence of significant correlations among some of the pairs of independent variables.
- Imposing a performance threshold and corresponding selection of behavioural sets leads to a significant reduction of the uncertainty width when predicting the spatial distribution of siltation. At the peak, the width of the 95% confidence interval is reduced by 36%. Although this is a significant improvement compared to the prior-sampling, the remaining uncertainty width is still $\pm$ 42% of the observed siltation at the peak.
- The 95% confidence interval of the spatial distribution of siltation does not capture the observed siltation patterns at all locations. This is further discussed in Section 5.5.
- The 95% confidence interval of the total siltation volume is strongly affected by the choices in performance threshold.
- The chosen performance thresholds lead to an uncertainty of $\pm$ 20% compared to the observed total siltation volume.

5.4. Validation

This section presents the validation of the calibrated SedPit Nearshore tool. The procedure has been explained in Section 4.9. Figure B.4 shows the 95% confidence interval of the spatial distribution of the siltation volume, based on the 2412 sets of behavioural variables. The solid line represents the model outcome of the optimal set of variables, based on the weighted combination (see Table 5.2). The first thing to note is the fact that the 95% confidence interval does give the right order of magnitude on most of all considered locations. However, the observed values do not fall within the 95% confidence interval at all locations. Again, the largest offsets are visible around the peak. The location of the

peak is modelled better compared to what was seen for period 1 in Figure 5.12, while this case the peak value exceeds the 95% confidence interval. However, in general the model performs well in terms of identifying the location of the peak. While it captures the locations accurately, there is some underestimation in the magnitude of these peaks. In the deeper regions, the observed values show larger variability than the model, which is typical for measurement values compared to modelled values. In these deeper regions, the model tends to overestimate the siltation volumes, which could lead to a significant mismatch in the prediction of the total siltation volume. In the regions between x=200 and x=400, the model is overestimating the siltation volumes quite significantly.

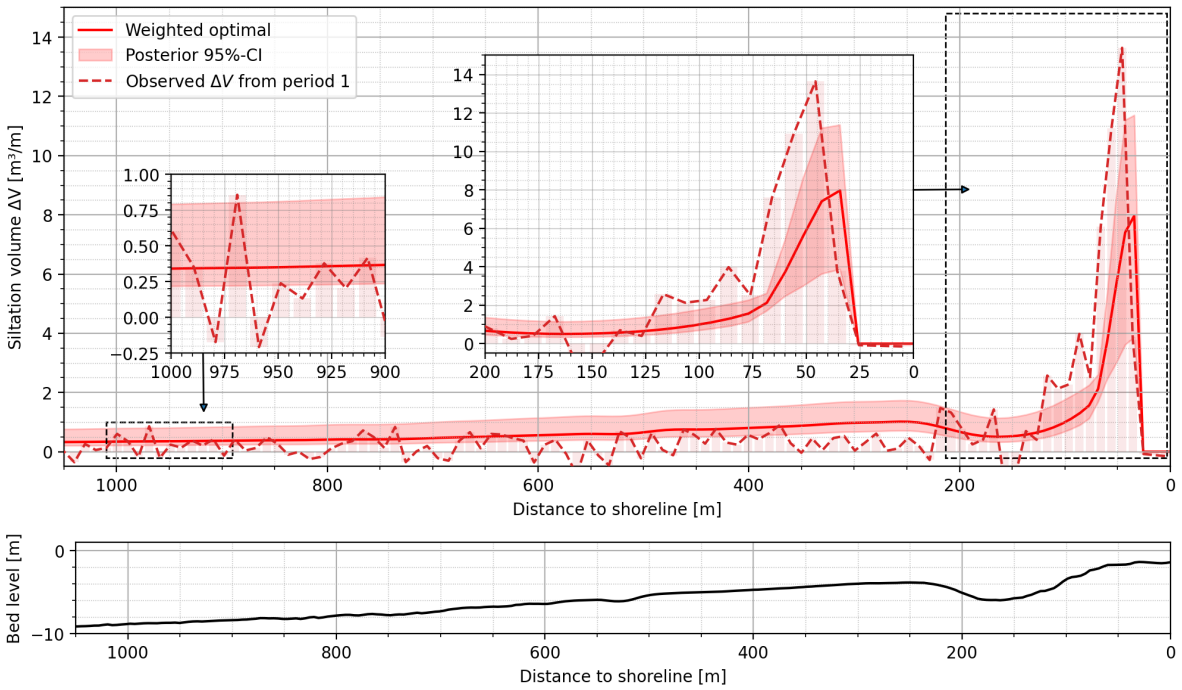

Figure 5.14: The obtained 95% confidence interval, based on all 2412 behavioural sets of variables. The solid line represents the model outcome of the optimal set of variables based on the objective of a weighted average (see Table 5.2). The dashed line represent the observed siltation volumes.

Next, the prediction of the total siltation volume is validated. Figure 5.15 shows the total bandwith of predicted total siltation volumes based on the 2412 behavioural sets of variables. The red solid line represent the observed siltation volume. It can be seen that the observed value of 723 m³ is barely within the 95% confidence interval. Besides that, the width of the uncertainty interval is approximately as large as the observed value itself, resulting in an uncertainty of $\pm$ 50%. It can be stated that the calibrated SedPit Nearshore tool overestimates the total siltation volumes for the validation case, while modelling the spatial distribution on an acceptable level. In Figure 5.15 it can be seen clearly that the CDF of the predicted total siltation follows the shapes of normal distribution.

To conclude, the validation shows that the SedPit Nearshore tool, after being calibrated on the data from period 2, predicts the spatial distribution of the siltation with an acceptable accuracy. The total siltation is overestimated structurally, although the observed siltation volume is within the 95% confidence interval. The overestimation of the siltation is also noted in the spatial distribution, where the model overestimates especially the siltation in the deeper regions.

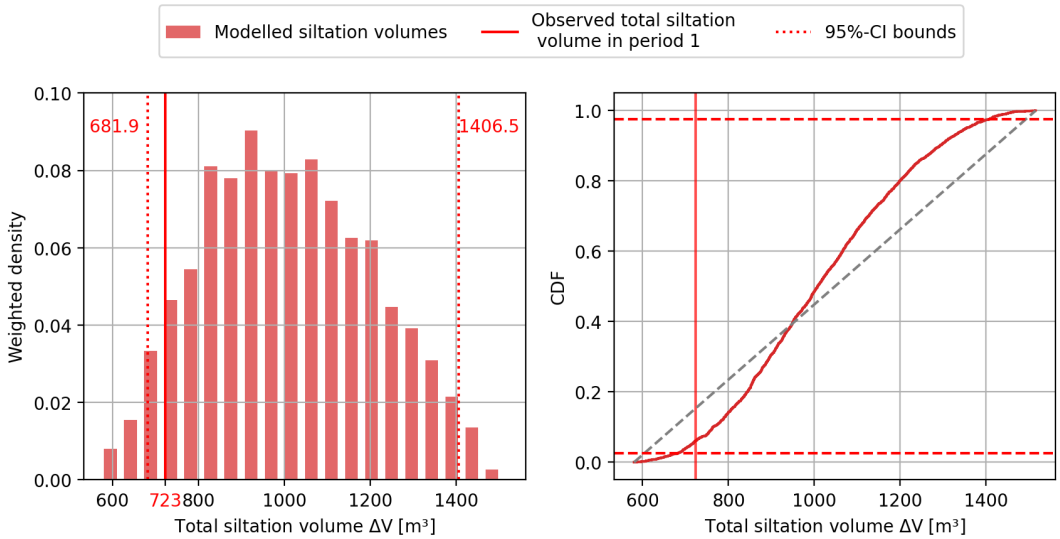

Figure 5.15: Probability distribution of total siltation volumes in period 1. The solid red line indicates the observed total siltation volume. The red dashed lines indicate the bounds of the 95% confidence interval.

5.5. Performance SedPit Nearshore tool

The performance of the SedPit Nearshore tool is discussed in three ways. First of all, the performance of the SedPit Nearshore tool compared to the data from the field case is analysed. For this comparison, the optimal set of variables based on weighted combination is used, see Table 5.2, and applied on the combined period of period 1 and 2. Next, the yield in prediction capability is presented by comparing the SedPit Nearshore tool to the existing SedPit tool. This is done in two ways: once by using one of the optimal sets of independent variables according to the GLUE-method, and once by using default values that are often used as initial guesses in the practical application of the existing SedPit tool. In these comparisons, the practical application of the existing SedPit tool is used as base case. This includes practical approaches to include reducing water depths and decreasing tidal currents in the existing SedPit tool. Although the existing SedPit tool calculates the siltation volumes on a fixed location, it is possible to simulate decreasing water depths by using the tool for different depths. Similarly, by using a rule of thumb, like Equation (4.34), a decreasing tidal current towards the shoreline can be simulated. Besides that, the wave height transformation, which is calculated within the MBJ-tool, is also applied for the existing SedPit tool. Eventually, the only difference between the existing SedPit-tool and the SedPit Nearshore tool in this comparison is the inclusion of the wave-driven currents.

Both comparisons look into the spatial distribution of the siltation and the total siltation volume. The results of the existing SedPit tool and the results of the SedPit Nearshore tool, as well as the observed siltation of the total period, are plotted in Figure 5.16. The inset shows the outcomes for the total siltation volumes.

5.5.1. Performance based on field data

The results that are obtained with the optimal set of variables gives a good prediction of the siltation volumes. The peak value is modelled very accurate, while the location of the peak is accurately predicted as well with an offset of approximately 30 meter. When taking the correction for the location of the peak into account, the offset is minimised. In the deeper regions, the SedPit Nearshore tool tends to overestimate the siltation volumes. The observed data shows a spiky character, but it can be seen that the modelled values are always near the values of the peaks, thus overestimating it in general. In the transition zone (x=150 to x=400) a mismatch can be seen. The modelled as well as the observed data show a local maxima. For the model, this maximum is near x=300, while it is observed near x=200 m. This spatial mismatch is in the opposite direction as the offset of the peaks.

As already mentioned in Section 5.3.2 and Section 5.4, all above-mentioned shortcomings of the model were earlier observed in the calibration to the data of period 2, and in the validation to the data of period 1 as well. First the location of the peak. It seems that the offset is most pronounced in period 2. One of the possible explanations is related to the increased cross-shore transport during more energetic wave conditions, which is explained in Section 2.4.3. As stated in Table 4.6, period 2 shows a larger average wave height H_{m0}. For increasing wave heights, it is known that the net cross-shore transport, which is not included in the SedPit Nearshore tool, tends to be more seaward directed. This could be an explanation of the more pronounced error in predicting the location of the peak.

Next the overestimation of the siltation volumes in the deeper regions. The siltation volumes in the deeper regions are more sensitive to the concentration of silt (see Appendix E), as the more quite conditions in deeper water allow silt particles to settle in the trench. When considering the optimal parameter set, based on spatial distribution only, it can be seen that a lower value of silt concentration leads to an improved fit in the deeper regions in Figure 5.11b, since the silt particles are strongly contributing to the deposition of sediment in the deeper zones. This shows that the model is capable of modelling the right siltation volumes in the deeper part, but that this leads to larger offsets is the shallower parts. However, the resulting optimal set of variables is steered by the fact that the deeper zone has twice as less evaluation points for the performance measure. Choosing the same evaluation point interval for the whole domain could lead to a better fit of the deeper zone, but with possible consequences for the peak zone.

Finally the mismatch in local maxima in the intermediate zone. All modelled siltation curves show a local maximum near x=300, which is correlated to the top of the breaker bar at that location. In all periods, the observed siltation curves do show a local maximum slightly more onshore, approximately above the through that is located between the breaker bar and the waterline. A possible explanation could be the gravity-induced transport of sediment towards this trough. Gravity-induced transport is not included in the SedPit tool, neither in the SedPit NS tool. Another explanation could be related to the effect of the trench on the local wave height, and consequently the location of breaking. This is discussed in Section 6.2.3.

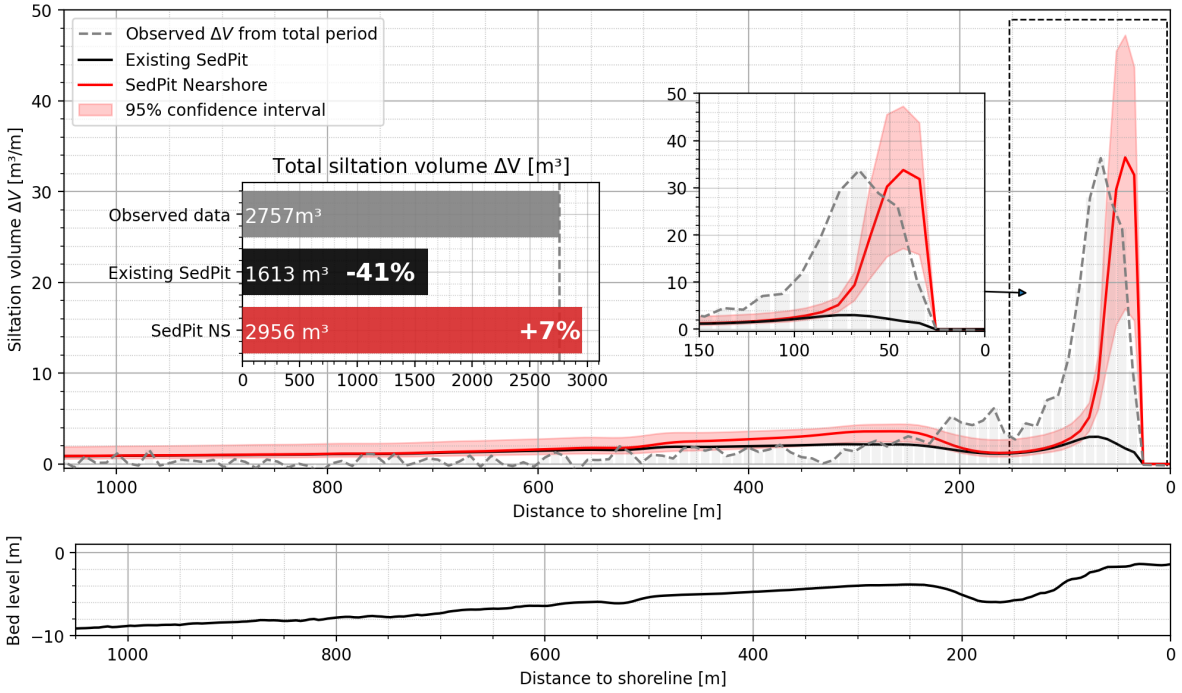

Figure 5.16: Comparison of the existing SedPit and the SedPit Nearshore tool to the observed siltation volumes. The barchart focuses on the total siltation volume, in which the percentages indicate the difference of both model to the observed values.

5.5.2. Performance compared to the existing SedPit tool

Next, the performance of the SedPit Nearshore tool is compared to the existing tool. As introduced in Section 5.5, the performance of the existing SedPit will be based on the inclusion of a bed level change, reduction of tidal current, and wave transformation. The inclusion of wave-driven currents is the only difference between the SedPit Nearshore tool and the existing SedPit. The used independent variables are based on the results of the GLUE-method. For the solid line, the variables of the optimal set of variables for a weighted average of performance measures is used. The confidence interval is based on the outcomes of 100 of the 2412 behavioural sets of independent variables.

Figure 5.16 shows the results of both tools, and the observed data of the total period (13 days). When looking at the spatial distribution of siltation, it can be seen that both models perform equally until x= 500. Until there, the effect of the wave-driven currents on siltation is minimal, wherefore both models perform equally compared to the observed data. In the intermediate zone, both tools show a local maximum between x=200 and x=400. These maxima are not seen on that location in the observed data. Considering the peak at x=200 of the observed data, it can be stated that the SedPit Nearshore tool is predicting the magnitude of that peak better than the existing SedPit. However, both tools capture this peak poorly, regarding location as well as magnitude. Looking at the onshore peak, it is clear that the SedPit nearshore tool outperforms the existing tool. This is not a surprising finding, as this is the region where most of the wave breaking takes place, and consequently significant rates of wave-driven currents are generated. The extend to which the SedPit Nearshore tool improves the existing SedPit tool is showing the relevance of this addition to the existing siltation prediction tools.

When looking at the total siltation volume, depicted in the barchart inset in Figure 5.16, it can be seen that the SedPit Nearshore tool shows an error of 7% compared to the observed data, which is significantly better than the error of the existing SedPit tool of 41%. The SedPit Nearshore tools reduces the absolute error by 82%.

5.5.3. Performance when using default values

In the comparison to the existing SedPit tool above, it has to be noted that the used independent variables are corresponding to the optimal fit based on the weighted average. The same variables are included in the existing SedPit. The fact that the selected variables are optimal according to a calibration of the SedPit Nearshore tool, does not necessary say that this set of variables is also resulting in the optimal input for the existing SedPit tool. Besides that, the use of the SedPit Nearshore tool is mainly in the preliminary phase of a project, where no information is available to calibrate the tool. Therefore, default values are often used to run the prediction models. The default value for the bottom roughness k_s is often set at 0.05 meter and is not varied for different locations. The bottom roughness k_s remains a value which has to be “guessed”. The values for d_{50}, c_{silt}, and c_{clay} are generally based on preliminary field investigations, including particle size distributions and estimations on the background concentrations of fines. For this comparison, the values from the preliminary confidential investigations from the field case were used (Boskalis, 2024). As mentioned earlier, is the exact source not known. The used value for the roller steepness β is based on the posterior distribution for β in Figure 5.9.

As it can be seen in Figure 5.17, the SedPit Nearshore tool performs significantly better when using default values. While there is a minor reduction in accuracy compared to the run with the optimised set of variables (Figure 5.16), the yield with respect to the existing SedPit tool is still considerable. This is a further implication that the SedPit Nearshore tool shows considerable potential to improve nearshore siltation predictions.

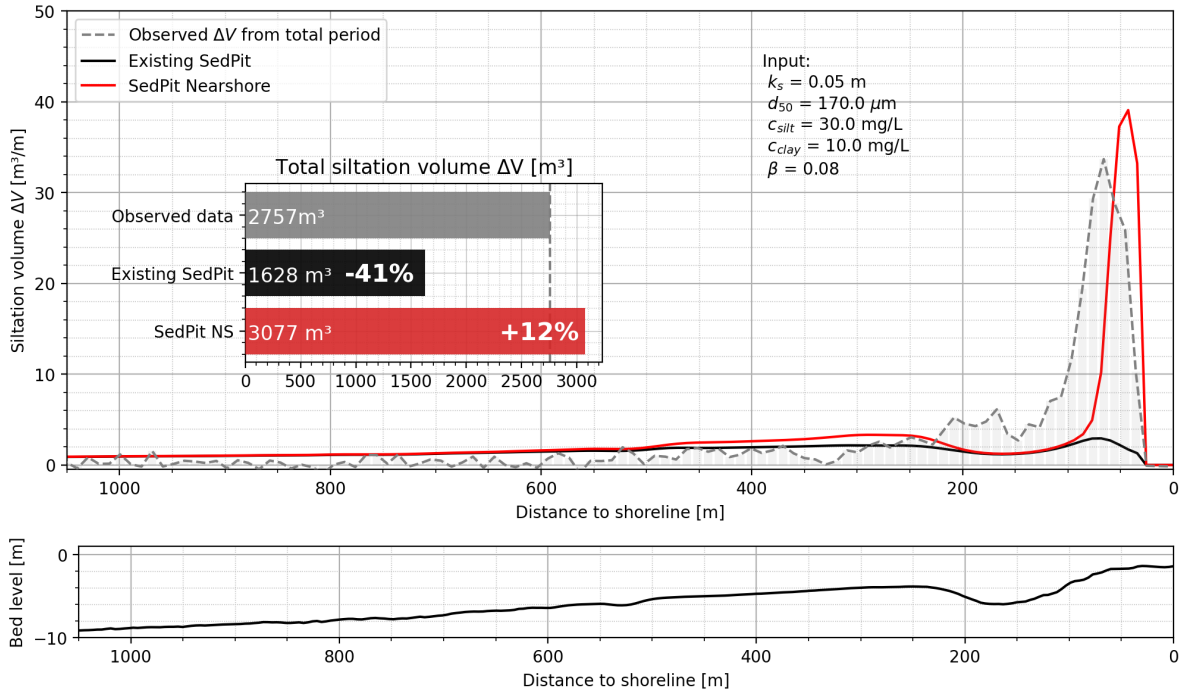

Figure 5.17: Comparison of the existing SedPit and the SedPit Nearshore tool to the observed siltation volumes, where a set of default input values was used. The barchart inset focuses on the total siltation volume, in which the percentages indicate the difference of both models to the observed values.

5.5.4. Performance computation time

The goal of this section is to compare the computation time of the SedPit Nearshore tool to the computation time needed when using XBeach. XBeach is a process-based model that includes hydrodynamics processes, as well as morphological processes (Deltares, 2023).

Section 5.1.3 discusses the computation time of the SedPit Nearshore tool. In the presented example, a timeseries consisting of 144 timesteps of 20 minutes each, and therefore 144 different wave conditions, took 14 seconds. In short, 0.1 seconds is needed to calculate the siltation rates for one wave condition with a duration of 20 minutes. As the SedPit Nearshore tool calculates the siltation rates per unit of time, and simply multiplies this with the desired period, the computation speed is not dependent on the duration of the wave condition. The SedPit Nearshore tool was used in single-core mode on a normal laptop.

Determining the computation time of XBeach is less straight-forward. As the model is computationally heavy, different methods are commonly used to reduce the computation time. First of all the morphological acceleration factor (MORFAC). The MORFAC multiplies the simulated effects of the hydrodynamics on the bed level change with a factor to reduce the needed computation time for changes of the bed level. This enables faster modelling of cases where the timescale of interest for the bed level change exceeds the average timescale of the hydrodynamic forcing (Ranasinghe et al., 2011). Next to using a MORFAC, Appendix F shows that there is potential to reduce the computation time by simulating only periods of peak wave heights, as these contribute to the majority of the siltation. By selecting only influential timesteps, the number of timesteps simulated can be further reduced. This would reduce the required computation time for the SedPit Nearshore tool, as well as for XBeach. Therefore, this option is not included in the comparison, leaving the computation time required for a wave condition as the comparison value.

Throughout this research, a selection of XBeach models were run to analyse different processes. In this comparison, the XBeach runs that are used to discuss the effect of concentration of wave energy (presented in Section 6.2.3) are included. In XBeach, the duration time to compute the hydrodynamics

during a period of 20 minutes took 600 seconds. Including the morphological processes comes with an increase of the computation time by factor 1.5, consequently 900 seconds for siltation rates for one wave condition during 20 minutes. This is not taking the MORFAC into account. This sums up to a computation time in the SedPit Nearshore tool which is factor 9,000 faster than iusing XBeach. Lastly, it is important to state that the XBeach computations were done on a 16-core computation cluster, while the SedPit Nearshore tool has only been used in single-core mode on a laptop.

In summary, the SedPit Nearshore tool is 9,000 times faster than the XBeach model for modelling siltation rates during a 20 minute wave condition. This number can be used as an order of magnitude. However, as several factors in this comparison depend on the choice and capacity of the user, the yield in computational time from the SedPit Nearshore tool may vary in practice.

6 Discussion

6.1. Interpretation of results

The research gap this research anticipated to fill is related to the availability of a quick-assessment tool to predict nearshore trench siltation, in order to be able to conduct extensive sensitivity and uncertainty analyses. The objective to create a tool that includes nearshore processes that affect trench siltation has been reached. The resulting tool has an acceptable accuracy in predicting the siltation in the used field case. The total siltation volumes, as well as the spatial distribution of the siltation does not predict the exact siltation behaviour precisely, but considering the yield with respect to the existing tools that are used in this context, a structural improvement has been reached. The largest offsets are seen in the intermediate depths near a trough in the bed profile, and at the location of the peak (see Figure 6.1). The latter is especially pronounced during energetic wave conditions, as discussed in Section 5.5.1. In order to state that this tool is a general useful tool, it has to be validated on additional field cases. Although the available field data was split into training and validation data, it must be validated that the tool performs comparable on a completely different set of input. This includes a different bed profile, timescale, spatial scale, sediment composition, and wave conditions. Comparing the SedPit Nearshore tool to such an independent additional validation case would add the needed credibility.

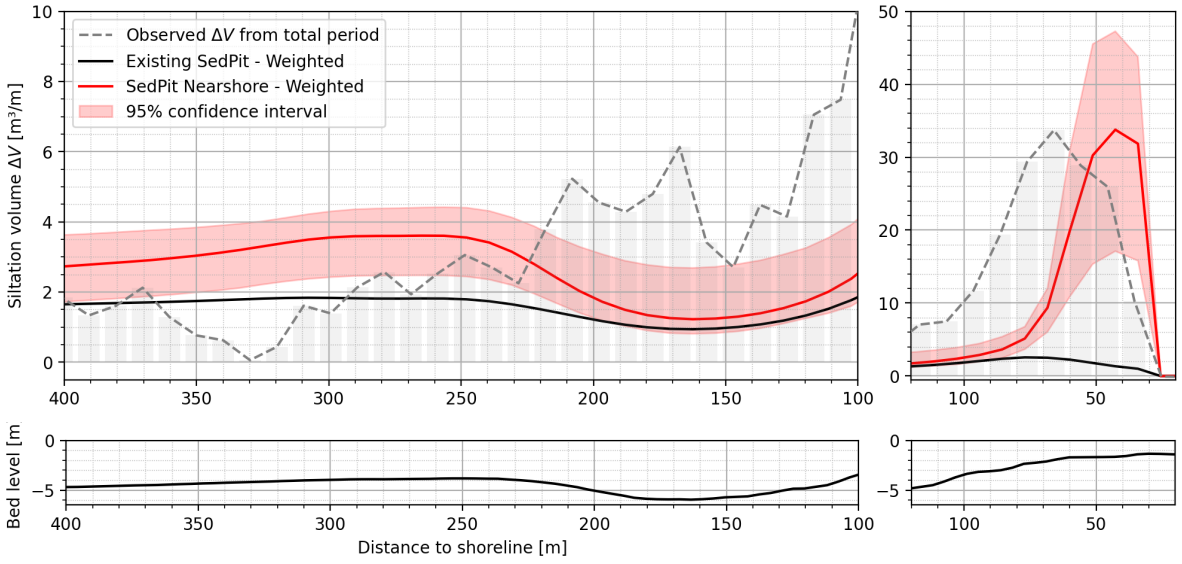

Figure 6.1: The two above-mentioned offsets. Left: the offset between SedPitNearshore and the data near the trough. Right: the offset in the location of the peak. Note that both plots have a different scale on the vertical axis.

The goal to maintain a computationally light tool, in order to make it useful for quick assessments, as well as for sensitivity and uncertainty analyses, is reached. Although the SedPit Nearshore tool is slightly more complex compared to the existing SedPit tool, the results are still achievable within the order of seconds. This made it possible to use the SedPit Nearshore tool for a sensitivity analysis and an uncertainty analysis, relying on a sample size in the order of N = 14,000, to find the most influential variables and to quantify and reduce the uncertainty.

The sensitivity analysis, by means of a global Sobol's sensitivity analysis, has shown that the tool is sensitive to a range of variables. The most influential variables originate from the wave transformation model, as well as from the morphological modelling. Regarding the wave conditions, the roller steepness β shows a strong influence on the magnitude of wave-driven currents in the breaker zone. A variable that is influencing both the hydrodynamics as well as the morphological processes is the bottom roughness k_s. The bottom roughness is not only the most influential independent variable for the wave transformation, but also for the siltation predictions. Besides these independent variables, the effect of concentration of silt c_{silt} and the sand grain size d_{50} has proven to influence the model outcome. Identifying the most influential variables has helped to construct the GLUE-analysis, and is useful for future users of the tool to decide on which variables will be included and which need a certain accuracy to ensure reliable outcomes.

The quantification and reduction of uncertainty has been achieved through the application of the GLUE-analysis, including a total of 14,000 randomly sampled sets of independent variables. This analysis has shown that correlations in the likelihood of input variable are strongly present in the case of the field data. This means that it is important to consider the interdependence of input variables, when conducting a MCS-like approach to quantify the model's variance. Imposing a performance threshold made it possible to identify unlikely combinations of independent variables, leading to a reduction of the 95% confidence interval width of 36%. Besides that, the distribution of the behavioural (well-performing) independent variables has shown that some of the independent variables are likely to not follow uniform distributions, since the performance of the model varied strongly dependent on the sampled input value.

Although the insights on independent variables and uncertainty ranges are valuable insights, it is important to critically discuss the concept of overfitting in this research. The available field data was split into training and validation data. However, as these datasets still show strong similarities, overfitting and applicability for different datasets are topics that deserve some additional attention. Overfitting occurs when a model is trained and calibrated to data, and tends to fit the training too accurate, with as a result that the model variables are only suited for the specific training data (Burnham & Anderson, 1998). Overfitting becomes more likely as the number of independent variables to be calibrated increases. For the field case, three independent variables were found to significantly affect the performance of the model (k_s, β, c_{silt}). Regarding the specific value of these independent variables in this field case, in Figure 5.17 in Section 5.5.3 it has been shown that when using default values, that differ from the calibrated optimal values, gives a result with an error margin of 12% for the total siltation volume, compared to the error margin of 7% with the calibrated input values. This shows that the accuracy does indeed decrease when the fitted values are replaced. However, when using a set of default input values, the absolute error in predicting the total siltation volume is still reduced by 71%, compared to the existing SedPit tool. To some extent, this proves that the tool is not overfitted, as it shows some robustness regarding variation from the calibrated values. However, its applicability to a different dataset has yet to be demonstrated. Adding to that, it is likely that for a case with different site conditions and trench dimensions, the influence of the sand grain size d_{50} or clay concentration C_{clay} might increase. As a final note on the potential use of the tool, it has to clarified that this tool only predicts the siltation volume due to longshore currents. Any volumes that move from the slope into the center of the trench are not captured by the tool. Consequently, the total volume to be dredged when redeepening a trench is likely to be greater due to internal movement of sediments.

6.2. Limitations of this research

This section presents some limitations of the research, related to recommendations for future research. First, a selection of theoretical concepts that have affected the research and could form steps towards further research are discussed. Next, some remarks on the use of the field case are discussed in Section 6.2.5 and Section 6.2.6.

6.2.1. Modelling of hydrodynamics

The first step made towards the SedPit Nearshore tool was the modelling of wave transformation, and related local hydrodynamics, in an efficient but accurate way. This ensures that offshore wave conditions are transformed correctly along an 1D transect towards the shoreline. The modelling of the wave transformation is the most time-demanding part of the model. Therefore, simplifications were used to keep the wave modelling suitable for a quick-assessment tool. This section presents some of the simplifications in the wave modelling, and the implications of them.

First of all, the simplification of the wave spectrum. Within a wave field, a variety of wave heights, period, and wave angles are observed. However, in the available metocean data, these variations are combined into one average value for wave height, period, and wave angle each during a period of 20 minutes. Using average values to describe the wave spectrum characteristics as input implies that swell waves, long waves, and short wind waves are all combined into one representative wave condition. Depending on the local wave climate, and the presence of swell or long waves, this averaged wave condition can lead to exclusion of potential significant effects of swell or long waves.

Next, the metocean data is retrieved from a buoy, located around 30 kilometers offshore at a depth of approximately 50 meter. Consequently, the generation of wind waves, with a possible fetch of 30 kilometers depending on the wind direction, is not included in the averaged wave field. Especially in periods with low waves measured by the buoy, the nearshore generated wind waves could have added significantly to the wave conditions near the shoreline.

Next, not all relevant processes are covered in the modelling of the wave transformation. The processes included in the wave modelling are refraction, shoaling, wave set-up, dissipation by bottom friction, dissipation by wave breaking, and dissipation by roller dissipation. One relevant process that is excluded is the lateral mixing of energy. Especially in the breaker zone, the eddy viscosity leads to lateral mixing and diffusion of energy, resulting in lower peaks and less pronounced troughs in the generation of alongshore current, and consequently in the sediment transport (Ruessink et al., 2001). However, as the inclusion of mixing entails an iterative step in the modelling, it was excluded to remain low in complexity.

Besides that, the generated wave-driven current is determined based on the wave force balance in alongshore direction. In the next modelling step, wave-driven current is combined with the tidal current. In essence, the wave-driven current and the tidal current do originate from the same momentum balance, Equation (4.1). However, the tidal current is often only available as measured current in a set of metocean data, which makes it difficult to calculate the tidal current based on the water level gradient as described in Equation (2.5). Therefore, it is a more practical approach to combine the modelled wave-driven current and the measured tidal current, while taking the quadratic relation into account in the summation. An implication of this is that the wave-driven current is overestimated slightly at large depths where the tidal current would have added significantly to the momentum balance in Equation (4.1). However, as this research focuses on the nearshore zone, where a continuous decrease of tidal current takes place, this shortcoming of the approach is accepted.

6.2.2. Cross-shore processes

The SedPit Nearshore tool adds wave-driven longshore currents to the processes in the existing SedPit tool. Although this addition is one step closer to the reality, crucial processes are still missing. The generation of wave-driven currents is not the only process that increases in importance when shifting towards the shoreline. As discussed Section 2.4.3, the effect of cross-shore transport starts to play

an important role in the nearshore zone as well. An inclusion of the cross-shore processes would add additional important nearshore processes, and most likely improve the accuracy of siltation predictions in the nearshore zone. The fact that one of the shortcomings of the SedPit Nearshore tool is related to the location of the peaks in cross-shore directions (see Figure 6.1), might suggest that inclusion of cross-shore processes can improve the performance of the model.

The addition of cross-shore processes might lead to the necessity to add another dimension to the model, as the direction of cross-shore processes is perpendicular to the direction of longshore processes. Adding a dimension should be considered with care in the context of a quick-assessment tool. In literature, different approaches exist to relate cross-shore currents to the wave conditions (Deigaard et al., 1991; Kennedy et al., 1999). These approaches could be used to indicate the magnitude of cross-shore sediment transport. The way in which these processes are incorporated into the tool will determine how much accuracy is added, but also how much the complexity of the tool is increased.

6.2.3. Effect of trenches on nearshore hydrodynamics

In this research, it is assumed that the hydrodynamics are not affected by the presence of a trench. This assumption makes it possible to model the nearshore hydrodynamics based on a given bed profile which is assumed to be homogeneous in the proximity of the trench. However, depending on the size of the trench, significant increases in depth will be associated with the presence of a trench. This will affect the local hydrodynamics in different ways. First of all, the presence of a trench affects the local wave height, as described in Section 2.3.3. This effect is visualised in Figure 6.2, where the case of a fictive trench with large dimension is used to emphasise the effect. The second effect is related to rip currents. The trench might enhance seaward directed rip currents, as discussed in Section 2.3.5. Thorpe et al. (2013) have shown that rip currents can contribute significantly to seaward directed sediment transport. The results of both processes are not included in the modelling of the hydrodynamics, and are consequently not considered in the siltation processes. The exact effect of the exclusion on the results is hard to explain, but some hypotheses are discussed below.

Firstly, if a rip current is generated through the trench, more seaward directed sediment transport is expected within the breaker zone, while no effect on the total siltation volume is expected. The assumption that the offset in the predicted location of peak siltation is the result of a rip current is too unfounded to be considered as an explanation. Alterations in the bathymetry are common causes of rip currents (Dalrymple et al., 2011). However, it is not proven that trenches lead to significant generation of rip currents. Further research into the generation of rip currents in trenches could be a valuable step towards a more comprehensive approach to modelling coastal siltation processes.

Next, to interpret the effect of wave concentration due to refraction along the slope of the trench accurately, it is important to know whether the critical angle of approach is likely to occur. The principle of critical angle of approach was introduced by Zwamborn and Grieve (1974). The critical angle of approach can be determined with Equation (2.11) and local metocean data. The process of concentration of wave energy is presented in Section 2.3.3. The possible effects of the concentration of wave energy on the siltation volumes is two-sided. On one hand, it affects the spatial distribution of siltation volumes. As a result of the increased wave heights on the slope of the trench, the wave breaking will show different peak locations than for the same wave climate with a homogeneous bathymetry. This effects were also presented by Eikema et al. (2018). The effect of concentration of wave energy on the total siltation volume is hard to estimate. On one hand, the amplification of wave heights could lead to larger sediment transport rates locally. At the same time, the reduced wave height in the trench leads to less turbulence in the trench, leading to reduced resuspension of sediment and enhanced deposition. However, the refraction of waves on the slopes of the trench do affect the direction of the flow. The refraction on the slopes will lead to a direction component that is directed away of the trench. This component will decrease the magnitude of the wave-driven currents generated more upstream and of the tidal current. Lastly, the timescale of the concentration of energy is dependent on the duration of certain wave angle conditions. In general, it can be stated that the effects of concentration of wave energy are to complicated to draw any conclusion from. Including the effect of wave refraction on the slopes, and the associated concentration of wave energy, into the modelling requires 2D wave modelling, which

may have a negative impact on the computational speed of the model. However, checking the presence of the effect of concentration of wave energy during the design phase of a trench excavation might add valuable information to improve the prediction accuracy.

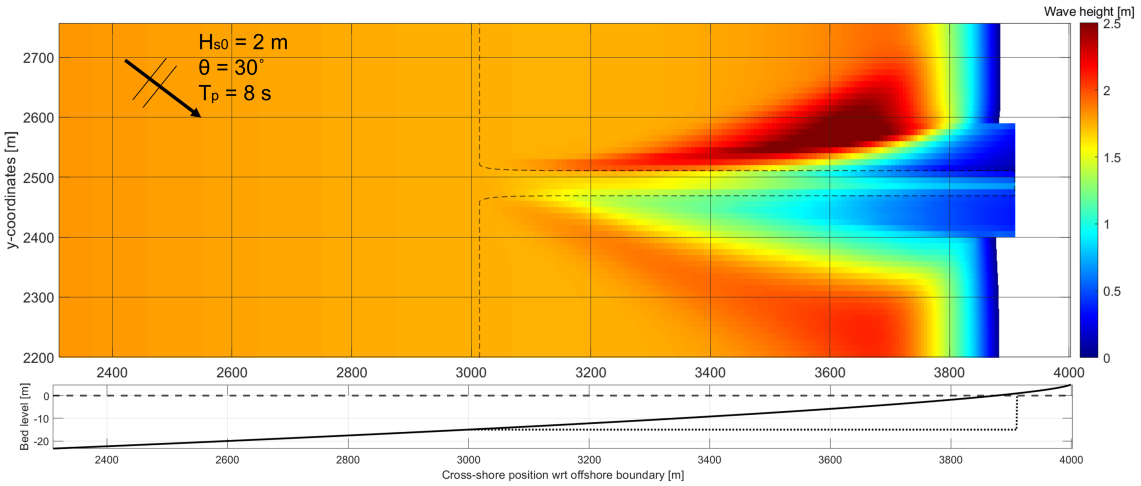

Figure 6.2: Visualisation of the concentration of wave energy. It can be seen that the offshore wave height of 2 m is amplified near the trench towards a wave height of 2.5 m. The black dashed line in the upper graph indicates the contours of the trench. These results are obtained by 2D-modelling in XBeach (Deltares, 2023). The included trench is an example of an extreme case, with a large trench depth.

6.2.4. Subjective choices within GLUE analysis

The GLUE-analysis is known as a powerful calibration method, and method to approximate independent variables and quantify model uncertainty (Beven & Binley, 1992). However, the GLUE-analysis is known as a method that strongly relies on some subjective choices throughout the process. This section aims to discuss the implication of some of the subjective choices in the GLUE-analysis in this research. A more extensive discussion, including visualisations of the effects, is presented in Appendix H.

The first choice in the GLUE procedure is the definition of the performance measures. In this research, the total siltation volume and the spatial distribution of siltation volume are selected as performance measures. This choice defines the output of the model to which the model will be calibrated. Both the total siltation volume, and the spatial distribution of siltation volumes are valuable information in the execution of trenches, as discussed in Section 4.8.2. However, by choosing only one of the performance measures, or adding a third measure, the overall outcome of the GLUE-analysis will change. The possibility to focus on one of the two performance measures was added in the analysis, and has shown that the optimal set of variables shows some significant changes (Table 5.2). Within the definition of the performance measure BSS_s, additional decisions were made on how to evaluate the spatial distribution. This entails the evaluation locations and the correction of the peak location. Eventually, the choice to have twice as many evaluation points in the peak zone compared to the deeper zone did not change the result compared to having a constant amount of evaluation locations. The choice to correct for the location of the peak in the evaluation of the BSS did lead to a significant improvement of the BSS_s, and a visually better fit with the observed data.

Regarding the calibration procedure, the performance threshold defines which set of variables are rejected and which are considered as “behavioural” and are used to calibrate the model. The choice which value is used as threshold is completely up to the user of the method. The threshold defines on one hand the number of behavioural sets. Although the threshold value should not be chosen solely based on the resulting amount of behavioural sets, a threshold that is too high, and thus a small remaining sample size, can negatively affect the quality of the posterior parameter distribution. At the same time, a high threshold ensures that only good model outcomes are considered in the calibration process. To some extent, this could be seen as a bias, neglecting possible outcomes that do not perform too good but could still be interpreted as behavioural outcomes. The presence of a strict threshold leads to a selection of outcomes with a relatively high likelihood, without taking outcomes into consider-

ation with slightly lower likelihoods. This results in a sharp, quasi-uniform, probability distribution of the model outcome, as is shown in Figure H.5. Choosing a low threshold value will lead to a larger number of behavioural sets. The posterior distribution will not necessary become wider, as due to equifinality, for every value (within the defined bounds) of each independent variable, a certain combination of the remaining independent variables does exist that performs well enough to be considered behavioural. However, as the number of these combinations and their likelihood is lower, the posterior distribution will be shaped with a focus on more likely values. A larger size of behavioural sets will however decrease the individual effect of the more likely sets. This reduces the variation of the posterior distribution to the prior uniform distribution.

Lastly, the choice of bounds in the sampling of the independent variables determines the width of the model outcomes. In determining the bounds, the challenge is to narrow the bounds sufficiently down to focus on realistic and potential values without wasting computation time on unrealistic extremes. However, taking too narrow bounds in the sampling procedure might exclude potential well-fitting values of independent variables. Hypothetically, the optimal approach would be an iterative approach that starts with sufficiently wide bounds, and corresponding large sample size, to include all potential values, and start narrowing down based on the results of the whole parameter space. Due to the limited (computational) time, a limited sample size was used in the first iterations, which ultimately did not predict the possible exclusion of potential values for the wave roller steepness β.

6.2.5. Calibration and validation on same field case

A large part of this research is related to the calibration and the validation of the SedPit Nearshore tool. For that purpose, the available data from the field case was divided into one calibration dataset, and one validation dataset. Despite this division, there is considerable overlap between the two datasets. What distinguishes one dataset from the other is the large difference in wave climate conditions. Both datasets are siltation data in the same trench, with the same surrounding beach profile. This does not give the desired independence of the validation dataset. Nonetheless, as this is the only available dataset, suitable for this research, no other option was possible that could have lead to a more independent validation.

Consequently, the first step in future research should include the validation of the tool to a completely independent test case, including variations in trench dimensions, a different bed profile, and an even larger variation in wave conditions. The performance in this additional validation case would give a more independent assessment of the accuracy of the SedPit Nearshore tool.

6.2.6. Quality of available data

Throughout the research, the comparison of modelled values with observed values is a frequently applied method to assess the models' performances. As well as being critical of the output of the models, it is important to be critical of the data available. The data in this research are the result of bathymetry measurement on 3 moments. The resolution of the data was extremely high, giving a good spatial coverage of the data. However, in order to make the data usable, the measurements had to be interpolated onto a sparser grid. This comes with a loss of accuracy. Adding to the uncertainty was the fact that the measurements were taken immediately, 6 days and 13 days after dredging. After dredging, the bed profile tends to be very dynamic as it smooths out all the roughness caused by the dredging. Furthermore, it is not known how the dredged sediment was handled. The presence of the sidecast, as described in Section 3.4, implies that the handling of dredged material possibly has affected the trench siltation. These are both processes that intervene with the processes that this research aims to identify.

Besides that, the accuracy of the available input is a concern in itself. Little is known about the accuracy of the available metocean data, while the exact depth at which these conditions were measured is unknown as well. The potential measurement errors propagate throughout the wave transformation processes and affect the model's outcome.

6.3. Potential and guidelines for application

The inclusion of wave-driven longshore currents into the existing siltation prediction tool SedPit has shown a great improvement in the accuracy of siltation predictions in the nearshore zone. Although the obtained optimal parameter sets are calibrated on one specific field case, the method and the workflow of the tool show great potential to help as a general prediction tool for a wide range of input. The computational speed of the tool has also proven its applicability for analysis on model sensitivity or uncertainty, to better understand and estimate uncertainties in the prediction of siltation. Wihtin 0.1 seconds, the siltation rates for a specific wave condition can be computed. In the design phase of projects located in or near the nearshore zone, the tool has potential to be a valuable prediction tool. However, before widely applying the tool, some recommendations for future research are presented in Chapter 7.

Although the tool has proven its potential, some important remarks on the use of the tool should be made. Firstly the needed metocean data. As discussed in Section 6.2.1, the type of available metocean data is determining the accuracy of the input of the tool. When using metocean data for the tool, it is important to know the approximated depth at the measurement location, and the distance to the shoreline. This is needed to ensure deep water conditions at the offshore boundary of the wave transformation, and to be able to reflect on possible wind-generated waves that are not covered in the metocean conditions. Besides that, the validity of the tool for trenches exposed to swell waves is not proven yet.

Another aspect to consider in the use of the SedPit Nearshore tool is the effect of project execution features. First of all the handling of the dredged sediment. The tool assumes that the adjacent bed profile is not affected by any interventions, and that the adjacent bed profile does not change during the period of interest. This includes that the effects of sidecasts (dumping of dredged material in near proximity) or floatation pits are not included in the tool. If the dredged sediment is dumped in near proximity, the tool might underestimate the siltation volumes in the trench. The effect of a floatation pit on the siltation predictions is more complicated and demands additional care during the use of the tool. Lastly, the location of the project might affect the hydrodynamics. The field case was located on a long straight stretch of coast, allowing the assumption that the propagation of the tidal current and waves from deep water to the shoreline follow simplified rules. However, if the project is located near headlands, in a bay, or close to other coastal features that might affect the propagation of currents and waves, additional analysis can add important information on the hydrodynamics.

To continue on the importance of hydrodynamics: prior 2D-modelling can help to further understand wave-driven currents in general, and gain more insights into the effect of wave refraction on the slopes, and the associated concentration of wave energy. This does not entail that 2D-modelling should be used to predict siltation volumes. However, the results of 2D-modelling can give important information on the relevance of the above-mentioned processes for a specific case.

Another interesting step in the preparation phase is a sensitivity analysis on the influence of the concentration of fines and the sand grain size. For the field case in this research, it has been concluded that the clay concentration and sand grain size do not influence the siltation volume significantly, while the silt concentration was a largely influential variable. These results are site-specific, meaning that it is likely that different conclusions would be drawn for different trench dimensions and wave conditions. When knowing the trench dimensions and the relevant wave conditions, an initial sensitivity analysis on the effect of the concentration of fines and the sand grain size can help in assigning resources to measurements on the most relevant site-specific variables.

While the conclusions on site-specific variables in this research should not be used as general values for future use of the tool, the findings on the independent variables roller steepness β and bottom roughness k_s can be used as general guidelines. Although the values obtained from the calibration in the GLUE-analysis are based on the available field data, it is a safe first assume to use for β a value of 0.08 - 0.10 and for k_s a value 0.05 meter. This value for k_s corresponds to the value that is often used as default in existing tools. The roller steepness β does not come back in existing tools, but the above-mentioned values are within often referred ranges (Ruessink et al., 2001; Walstra et al., 1997). The use of these values is only partly validated in Section 5.5.3. A further validation on this is recommended.

7

Conclusion & Recommendations

7.1. Conclusion

The objective of this research was to study the inclusion of nearshore processes in quick assessment trench siltation tools. By keeping the tool computationally quick, the aim was to quantify uncertainties and to gain more insights into the importance of different input parameters on the uncertainty of siltation rates in trenches.

To reach this objective, the research has been divided into three sub-research questions:

1. How can nearshore morphological processes be included in quick assessment tools?

This research has presented an approach to include wave transformation and wave-driven currents into an existing siltation prediction tool; SedPit (Van Rijn, 2007)). The resulting SedPit Nearshore tool allows fast predictions of siltation volumes in the nearshore zone, based on a local bed profile, time-series of wave conditions, and a selection of input variables.

By using a 1D-model that models the wave transformation from deep water to the shoreline, the local wave conditions in the nearshore zone can be estimated. This is done for a 1D-line perpendicular to the shoreline. The used formulae are based on the Battjes-Janssen 1978 model (Battjes & Janssen, 1978). This includes wave refraction, shoaling, wave set-up, dissipation by bottom friction, dissipation by wave breaking, and dissipation by roller dissipation, of which the latter was not part of the earlier work by Battjes and Janssen (1978). The generated wave-driven current (alongshore current) is obtained from the wave force balance. Along the transect, the locally generated wave-driven current is used as additional input for the modelling of the siltation. Existing tools (SedPit) include the effects of tidal currents and wave action only, while predicting the siltation volumes. The exclusion of wave-driven currents is a significant shortcoming in the nearshore zone.

The morphological modelling is included based on Van Rijn's sediment formulae, adopted from the SedPit tool (Van Rijn, 2013). An increase in water depth within a trench results in a decrease in current velocity. This reduction in velocity leads to a reduced sediment transport capacity, causing deposition of sediment. By adding the magnitude of the wave-driven current, a better representation of the hydrodynamics in the nearshore zone is used as driving force for the siltation. The existing SedPit tool was a suitable tool to include new processes in. It is an interpretable tool that is based on well-known physical formulae.

By including the wave transformation on a 1D-transect, and adopting the computationally quick morphological modelling from the existing SedPit tool, the inclusion of nearshore processes in quick assessment tools is effective in prediction performance, and remains low computation costs. The computation speed of the SedPit Nearshore tool is in the order of 0.1 seconds per wave condition, This is strongly dependent on the used grid resolution, but is independent from the duration of the wave condition. A

high-level comparison of computation time between the SedPit Nearshore tool and XBeach has shown a reduction of factor 9,000 in computation time when using the SedPit Nearshore tool (Section 5.5.4).

2. Which variables contribute to the largest variance in the modelled outcomes of the tool?

The Sobol' method is a global sensitivity analysis that decomposes a model's variance into the contribution of each variable, and interaction between variables (Sobol, 2001). This gives valuable insight into the influence of the different variables on a model's uncertainty. In this research, the Sobol' method has been applied to the wave transformation model separately, as well as to the SedPit Nearshore tool.

Regarding the wave transformation model, the sensitivity of variables on the generation of wave-driven currents to the power of three, as proxy for sediment transport, was assessed. It followed that, when including all variables into the sensitivity analysis, the wave climate and tidal regime-related variables are the most influential. This includes the wave angle θ, wave height H_s, peak period T_p, and tidal current U_{tide}. However, for practical implications it is more interesting to investigate the sensitivity of non-measurable, independent variables. It resulted that the bottom roughness k_s is by far the most influential variable within the wave transformation model. An interesting finding is that the roller steepness β does not show strong effects on the wave transformation model.

Next, the sensitivity on the siltation volume following from the SedPit Nearshore tool was analysed. With respect to siltation volumes, the bottom roughness k_s is the most influential variable, followed by the roller steepness β, silt concentration c_{silt}, and sand grain size d_{50}. The fact that the effect of the roller steepness β is more pronounced in the SedPit Nearshore tool than in the wave transformation is related to the definition of the considered model output. For the wave transformation model, the currents along a relatively long transect were used as model output. Considering this whole transect, the effect of β plays a role in just a relatively short zone where the wave rollers are generated, giving it a low contribution to the model's outcome. However, as this short zone of wave breaking is the zone where significant amounts of the siltation volumes are predicted in the SedPit Nearshore tool, β has a considerably larger effect on the total siltation volume. The influence of the silt concentration c_{silt} and grain size d_{50} is largely location specific. The grain size d_{50} followed to be influential based on a specific piece of the input timeseries, while not showing large influence on the model performance regarding the field case in the GLUE-analysis. This is partly due to the combination of the present hydrodynamics and trench dimensions. Secondly, a change in d_{50} is in most of the cases compensated by changes in other variables, and mainly in k_s. As a result, variations in d_{50} do not lead to significant changes in model performance. The effect of the silt concentration is strongly dependent on the specific field case. It has to be noted that any conclusion on grain size, silt concentration, and clay concentration is based on this specific location and field case, and different conclusion could be valid for different locations or cases.

3. How well does an improved tool perform in a field case, and what is the added value compared to existing tools?

The performance of the SedPit Nearshore tool is assessed by comparing it to data from a field case, while the added value is based on the yield in accuracy compared to the existing SedPit tool. The available data consists of depth measurements along the complete trench on two different moments after dredging, dividing the total period of siltation into two. One of these periods is used to calibrate the tool, according to the GLUE-analysis, while the other period is used as validation.

It can be stated that the SedPit Nearshore tool gives accurate predictions on the total siltation volume, and gives good insights in the spatial distribution of siltation volumes. An accuracy of 12% in predicting total siltation volumes has been reached by using a selection of default values in the field case. In predicting the spatial distribution, the accuracy is varying per cross-shore position. The prediction of the location of the most onshore peak includes an offset of up to 30 meter in cross-shore direction, while the magnitude of the peak is modelled accurately with a relative error of 14% when using a selection of default values in the field case (Figure 5.17). An error of less than 1% can be reached when using calibrated input values.

However, the potential of the SedPit Nearshore becomes most evident when comparing it to the existing SedPit tool. Using the calibration procedure of the GLUE-analysis gives insights into the optimal sets of independent variables. Using these variables in the SedPit Nearshore tool reduces the error in predicting the total siltation volumes by 82% compared to the existing SedPit tool. The SedPit Nearshore tool predicts the total siltation volume with an error margin of 7%, while the existing SedPit has an error margin of 41%. Especially in the breaker zone, the accuracy of the SedPit Nearshore tool is outperforming the existing SedPit tool.

For the practical application of the SedPit tool, it is interesting to see how well the tool performs when using a set of default values. A set of default values is more representative for a practical application of the tool, where no calibration procedure is possible, than a set of optimal variables determined during the calibration. When using a set of default values, that where defined based on the field case, the SedPit Nearshore tool has an accuracy of 12% , while the existing SedPit tool has an accuracy of 41%.

With the sub-research question above being answered, the main research question can be addressed.

To what extent can inclusion of nearshore processes improve existing quick assessment tools for trench siltation, while ensuring low complexity for probabilistic modelling to reduce and quantify uncertainties?

The inclusion of wave-driven currents into siltation prediction tools shows great potential to increase predictions' accuracy in the nearshore zone. This research did not address other nearshore processes than the wave transformation and the resulting wave-driven currents. The inclusion of other nearshore processes, like cross-shore directed processes and the effect of trenches on the wave transformation, can potentially improve the predictability further.

By remaining a low complexity in the wave transformation model and the inclusion of wave-driven currents in the morphological modelling, the computational time was reduced by a factor of 9,000 compared to existing process-based models. This makes the tool valuable for probabilistic modelling. The low computational demands allowed extensive sensitivity and uncertainty analysis that have given great insights in the statistical behaviour of siltation predictions. The most influential variables, bottom roughness k_s and roller steepness β, are identified. By imposing a performance threshold in the calibration procedure of the GLUE-analysis, the correlation between input values and the corresponding model's performance is determined. The performance of each set of variables is used to describe the likelihood of a variable being a good fit. This has shown that the probability of occurrence of the most influential variables k_s and β show some significant deviation from often used uniform sampling distributions. By taking the posterior optimised parameter distributions into account, the 95% confidence interval of a model can be reduced by 36%. However, strong interdependence between best performing input values have shown that the posterior distributions only lead to more efficient MCS-approaches when considering the interdependence.

Based on the results and the performance assessment of the SedPit Nearshore tool, it can be concluded that it is a simple and effective way to increase the accuracy of siltation predictions in the nearshore zone. Inclusion of wave-driven longshore currents show great potential, reducing the absolute error by 81% in predicting total siltation volume in the used field case. The accuracy of the spatial distributions includes peak offsets of up to 30 meter. The low complexity of the SedPit Nearshore tool ensures its ability as a quick-assessment tool to be useful in probabilistic modelling. Compared to XBeach, the computation time has been reduced by factor 9,000 and is in the order of 0.1 seconds per wave condition.

7.2. Recommendations

This section presents some recommendations for future research. The recommendations are partly based on the topics that are discussed in the discussion (Chapter 6).

First of all, as mentioned in Chapter 6, the first step to improve the SedPit Nearshore tool should include an additional validation. The presented calibration and validation was done by two separate timeseries. Nonetheless, the same bed profile and trench dimensions were used for calibration and validation. Validating the accuracy of the tool in a case with a different bed profile, and a trench with a different order of magnitude in dimension would add the needed credibility to the tool. However, the validation demands sufficient bathymetry measurements and available metocean data to be a valuable addition to the validation process.

Next, the inclusion of cross-shore processes and the effect of the trench on the wave propagation, as described in Section 6.2.2 and Section 6.2.3 might improve the accuracy of the tool further. However, while adding more processes and complexity to the tool, the effect on the computation time must always be a central concern. When demanding too much complexity of the model, more complex process-based models might be more suited for the task. The power of the SedPit Nearshore tool lays in its simplicity, making it an efficient and interpretable tool, suited for probabilistic modelling. A first step would be to conduct an independent investigation study on the presence and magnitude of cross-shore processes in trenches and the effect of trenches on the wave propagation. This study should include 2D-modelling of a range of varying trenches with varying wave conditions. Potentially this study can give valuable insights that can indicate whether additional processes are relevant to add in the SedPit Nearshore tool. The balance between added accuracy and added complexity should play a central role in this study.

Finally, two recommendations on the use and interpretation of the GLUE-analysis. Firstly, a note on the accuracy of site specific variables. In this research, the grain size d_{50} and the concentration of fines (c_{silt} and c_{clay}) were included with relative wide bounds in the GLUE-analysis. This was the consequence of having scarce information on the field case, and the lack of access to the source of the information due to the confidential nature of the project. When having more accurate information on these site characteristics, more narrow, or even constant values could have been used. Consequently, the available computation capacity could have spent on more accurate results for the remaining independent variables.

The second note is on the interpretation of the posterior probability distributions of the independent variables. During the interpretation of the results of the GLUE-analysis, the importance and the implications of the principle of equifinality became clear. The GLUE-analysis gives approximations of the probability distributions for the independent variables. Nonetheless, this alone does not exploit all potential for more efficient Monte-Carlo sampling. Although the shift from a prior uniform distribution towards a distribution that gives more weight to more likely values will increase the sampling efficiency to some extent, there is potential for greater efficiency yield. Equifinality says that two unique combinations of independent variables can lead to the same outcome. This also entails that a set of variables that individually are all considered as an accurate estimate according to the their posterior distribution (Figure 5.9), is not necessary the most accurate set of variables. This introduces the need to take the interdependence between variables into account. Including copula into the sampling procedure could be one possible solution to address the correlation between individual variables that are distributed according to unique and independent probability distributions (Jaworski et al., 2010). Taking this correlations into account increases the efficiency in Monte-Carlo sampling.

References

Baldock, T., Holmes, P., Bunker, S., & Van Weert, P. (1998). Cross-shore hydrodynamics within an unsaturated surf zone. *Coastal Engineering*, *34*(3-4), 173–196. https://doi.org/10.1016/S0378-3839(98)00017-9

Basco, D. R. (1985). A Qualitative Description of Wave Breaking. *Journal of Waterway, Port, Coastal, and Ocean Engineering*, *111*(2), 171–188. https://doi.org/10.1061/(ASCE)0733-950X(1985)111:2(171)

Battjes, J. A., & Janssen, J. P. F. M. (1978). Energy loss and set-up due to breaking random waves. *Proceedings of 16th Conference on Coastal Engineering, Hamburg, Germany, 1978*.

Battjes, J. A., & Stive, M. J. F. (1985). Calibration and verification of a dissipation model for random breaking waves. *Journal of Geophysical Research: Oceans*, *90*(C5), 9159–9167. https://doi.org/10.1029/JC090iC05p09159

Berends, K., Scheel, F., Warmink, J., de Boer, W., Ranasinghe, R., & Hulscher, S. (2019). Towards efficient uncertainty quantification with high-resolution morphodynamic models: A multifidelity approach applied to channel sedimentation. *Coastal Engineering*, *152*, 103520. https://doi.org/10.1016/j.coastaleng.2019.103520

Beven, K., & Binley, A. (1992). The future of distributed models: Model calibration and uncertainty prediction. *Hydrological Processes*, *6*(3), 279–298. https://doi.org/10.1002/hyp.3360060305

Bijker, E. W. (1967). The Increase of Bed Shear in a Current Due to Wave Action. *Coastal Engineering 1966*, 746–765. https://doi.org/10.1061/9780872620087.043

Bolle, A., Mercelis, P., Roelvink, D., Haerens, P., & Trouw, K. (2011). APPLICATION AND VALIDATION OF XBEACH FOR THREE DIFFERENT FIELD SITES. *Coastal Engineering Proceedings*, (32), 40. https://doi.org/10.9753/icce.v32.sediment.40

Bosboom, J., & Stive, M. (2022). *Coastal Dynamics* (1.1). Delft University of Technology.

Bosboom, J. (2020). *Quantifying the quality of coastal morphological predictions* [Doctoral dissertation, Delft University of Technology].

Boskalis. (2024). *Siltation study - [project]* (tech. rep.).

Bowen, A. J. (1969). Rip currents: 1. Theoretical investigations. *Journal of Geophysical Research*, *74*(23), 5467–5478. https://doi.org/10.1029/JC074i023p05467

Bowen, A. J. (1980). Simple models of nearshore sedimentation; beach profiles and longshore bars. In S. McCann (Ed.), *The coastline of canada* (pp. 1–11).

Bruun, P. (1954). *Coast Erosion and the Development of Beach Profiles*. Corps of Engineers.

Burnham, K., & Anderson, D. (1998). *Model Selection and Multimodel Interference* (2nd). Springer.

Christiaanse, J. (2021). *Quantifying parameter uncertainty in predictions of coastal mega-nourishments* [Doctoral dissertation, Delft University of Technology].

Dalrymple, R. A., MacMahan, J. H., Reniers, A. J., & Nelko, V. (2011). Rip Currents. *Annual Review of Fluid Mechanics*, *43*(1), 551–581. https://doi.org/10.1146/annurev-fluid-122109-160733

De Wit, F. (2016, January). *Tide-induced Currents in a Phase-Resolving Wave Model* [Doctoral dissertation, Delft University of Technology].

Dean, R. (1977, January). *Equilibrium Beach Profiles: U.S. Atlantic and Gulf Coast* (tech. rep.). Department of Civil Engineering, University of Delaware. Newark.

Dean, R., Healy, T., & Dommerholt, A. (1993). A “blind-folded” test of equilibrium beach profile concepts with New Zealand data. *Marine Geology*, *109*(3-4), 253–266. https://doi.org/10.1016/0025-3227(93)90064-3

Deigaard, R. (1993). A note on the three-dimensional shear stress distribution in a surf zone. *Coastal Engineering*, *20*(1-2), 157–171. https://doi.org/10.1016/0378-3839(93)90059-H

Deigaard, R., Justesen, P., & Fredsoe, J. (1991). Modelling of undertow by a one-equation turbulence model. *Coastal Engineering*, *15*(5-6), 431–458.

Deltares. (2023, November). XBeach manual documentation.

de Rooi, J. J., van der Pers, N. M., Hendrikx, R. W. A., Delhez, R., Böttger, A. J., & Eilers, P. H. C. (2014). Smoothing of X-ray diffraction data and K α ₂ elimination using penalized likelihood and the composite link model. *Journal of Applied Crystallography*, *47*(3), 852–860. https://doi.org/10.1107/S1600576714005809

Eikema, B., Attema, Y., Talstra, H., Bliek, A., de Wit, L., & Dusseljee, D. (2018). SPECTRAL MODELING OF WAVE PROPAGATION IN COASTAL AREAS WITH A HARBOR NAVIGATION CHANNEL. *PIANC-World Congress*.

Feddersen, F., Guza, R. T., Elgar, S., & Herbers, T. H. C. (2000). Velocity moments in alongshore bottom stress parameterizations. *Journal of Geophysical Research: Oceans*, *105*(C4), 8673–8686. https://doi.org/10.1029/2000JC900022

Goda, Y. (1988). Statistical Variability of Sea State Parameters as a Function of Wave Spectrum. *Coastal Engineering in Japan*, *31*(1), 39–52. https://doi.org/10.1080/05785634.1988.11924482

Grant, W. D., & Madsen, O. S. (1979). Combined wave and current interaction with a rough bottom. *Journal of Geophysical Research: Oceans*, *84*(C4), 1797–1808. https://doi.org/10.1029/JC084iC04p01797

Grasmeijer, B. (2006, March). *CROSS-SHORE TRANSFORMATION OF WAVE HEIGHT, ORBITAL MOTION, CROSS-SHORE AND ALONGSHORE CURRENT* (tech. rep.). University of utrecht. Utrecht.

Guo, J. (2002). Simple and explicit solution of wave dispersion equation. *Coastal Engineering*, *45*(2), 71–74. https://doi.org/10.1016/S0378-3839(02)00039-X

Hallermeier, R. J. (1980). A profile zonation for seasonal sand beaches from wave climate. *Coastal Engineering*, *4*, 253–277. https://doi.org/10.1016/0378-3839(80)90022-8

Hallermeier, R. (1981). Seaward Limit of Significant Sand Transport by Waves: An Annual Zonation for Seasonal Profiles. *Coastal Engineering Technical Aid*, *81*(2).

Hendriks, A. (2020). Monte Carlo Sampling SedPit.

Herman, J., & Usher, W. (2017). SALib: An open-source Python library for Sensitivity Analysis. *The Journal of Open Source Software*, *2*(9), 97. https://doi.org/10.21105/joss.00097

Holthuijsen, L. (2007). *Waves in Oceanic and Coastal Waters* (1st ed.). Cambridge University Press.

Hunt, J. N. (1979). Direct Solution of Wave Dispersion Equation. *Journal of the Waterway, Port, Coastal and Ocean Division*, *105*(4), 457–459. https://doi.org/10.1061/JWPCDX.0000168

Inman, D. L., Elwany, M. H. S., & Jenkins, S. A. (1993). Shorerise and bar□berm profiles on ocean beaches. *Journal of Geophysical Research: Oceans*, *98*(C10), 18181–18199. https://doi.org/10.1029/93JC00996

Iooss, B., & Lemaître, P. (2015). A Review on Global Sensitivity Analysis Methods. https://doi.org/10.1007/978-1-4899-7547-8{_}5

ISO. (2017, December). ISO 14688: Geotechnical investigation and testing - Identification and classification of soil.

Iwanaga, T., Usher, W., & Herman, J. (2022). Toward SALib 2.0: Advancing the accessibility and interpretability of global sensitivity analyses. *Socio-Environmental Systems Modelling*, *4*, 18155. https://doi.org/10.18174/sesmo.18155

Jaworski, P., Durante, F., Härdle, W., & Rychlik, T. (2010). *Copula Theory and Its Applications* (P. Jaworski, F. Durante, W. K. Härdle, & T. Rychlik, Eds.; Vol. 198). Springer Berlin Heidelberg. https://doi.org/10.1007/978-3-642-12465-5

Jonsson, I. (1963). Measurements in the Turbulent Wave Boundary Layer. *10th I.A.H.R. Congress*, 85–92.

Kennedy, D. L., Cox, D. T., & Kobayashi, N. (1999). Application of an Undertow Model to Irregular Waves on Barred Beaches. *Coastal Engineering 1998*, 311–324. https://doi.org/10.1061/9780784404119.022

Klein, M., Elias, E., Walstra, D., & Van Rijn, L. (2001, March). *The Egmond model: Hydrodynamics validation of Delft3D with field measurements of Egmond-Main experiment, October-November 1998* (tech. rep.). Delft University of Technology, WL | Delft Hydraulics (Deltares). Delft.

Komar, P., & Miller, M. (1975). On the Comparison Between the Threshold of Sediment Motion Under Waves and Unidirectional Currents with a Discussion of the Practical Evaluation of the Threshold. *Journal of Sedimentary Petrology*, *45*(1).

Kroon, A., de Schipper, M. A., van Gelder, P. H., & Aarninkhof, S. G. (2020). Ranking uncertainty: Wave climate variability versus model uncertainty in probabilistic assessment of coastline change. *Coastal Engineering*, *158*. https://doi.org/10.1016/j.coastaleng.2020.103673

Kucherenko, S., Albrecht, D., & Saltelli, A. (2015, May). *Exploring multi-dimensional spaces: a Comparison of Latin Hypercube and Quasi Monte Carlo Sampling Techniques* (tech. rep.).

Laboyrie, H., Van Koningsveld, M., Aarninkhof, S., Van Parys, M., Lee, M., Jensen, A., Csiti, A., & Kolman, R. (2018, November). *Dredging for Sustainable Infrastructure* (tech. rep.). CEDA / IADC. The Hague.

Longuet-Higgins, M. (1970). Longshore Currents Generated by Obliquely Incident Sea Waves, 1. *Journal of Geophysical Research*, *75*(33).

Longuet-Higgins, M., & Stewart, R. (1964). Radiation Stress in Water Waves: a Physical Discussion with Applications. *Deep-Sea Research*, *11*, 529–562.

Madsen, O. S., & Grant, W. (1976, January). *Sediment Transport in the Coastal Environment* (tech. rep.). Massachusetts Institute of Technology.

Mil-Homens, J. (2016). *Longshore Sediment Transport* [Doctoral dissertation, Delft University of Technology].

NOAA. (2024). Tides & Currents Products.

Nogal, M., & Nogal, A. (2021). Sensitivity method for extreme-based engineering problems. *Reliability Engineering & System Safety*, *216*, 107997. https://doi.org/10.1016/j.ress.2021.107997

Owen, A. B., Dick, J., & Chen, S. (2014). Higher order Sobol' indices. *Information and Inference*, *3*(1), 59–81. https://doi.org/10.1093/imaiai/iau001

Ranasinghe, R., Swinkels, C., Luijendijk, A., Roelvink, D., Bosboom, J., Stive, M., & Walstra, D. (2011). Morphodynamic upscaling with the MORFAC approach: Dependencies and sensitivities. *Coastal Engineering*, *58*(8), 806–811. https://doi.org/10.1016/j.coastaleng.2011.03.010

Rijksoverheid. (2022). Nederland maakt ambitie wind op zee bekend: 70 gigawatt in 2050.

Roelvink, J. A., & Stive, M. J. F. (1989). Bar□generating cross□shore flow mechanisms on a beach. *Journal of Geophysical Research: Oceans*, *94*(C4), 4785–4800. https://doi.org/10.1029/JC094iC04p04785

Roelvink, J., & Reniers, A. (2011, October). *A Guide to Modeling Coastal Morphology* (Vol. 12). World Scientific Publishing Company. https://doi.org/10.1142/7712

Ruessink, B. G., Miles, J. R., Feddersen, F., Guza, R. T., & Elgar, S. (2001). Modeling the alongshore current on barred beaches. *Journal of Geophysical Research: Oceans*, *106*(C10), 22451–22463. https://doi.org/10.1029/2000JC000766

Ruessink, B. (2005). Predictive uncertainty of a nearshore bed evolution model. *Continental Shelf Research*, *25*(9), 1053–1069. https://doi.org/10.1016/j.csr.2004.12.007

Saltelli, A., Annoni, P., Azzini, I., Campolongo, F., Ratto, M., & Tarantola, S. (2010). Variance based sensitivity analysis of model output. Design and estimator for the total sensitivity index. *Computer Physics Communications*, *181*(2), 259–270. https://doi.org/10.1016/j.cpc.2009.09.018

Saltelli, A., Ratto, M., Andres, T., Campolongo, F., Cariboni, J., Gatelli, D., Saisana, M., & Tarantola, S. (2007, December). *Global Sensitivity Analysis. The Primer*. Wiley. https://doi.org/10.1002/9780470725184

Savitzky, A., & Golay, M. J. E. (1964). Smoothing and Differentiation of Data by Simplified Least Squares Procedures. *Analytical Chemistry*, *36*(8), 1627–1639.

Shi, D. (2023, June). *Uncertainty Quantification of a Wind Farm Control Mode: FLORIDyn* [Doctoral dissertation, Delft University of Technology].

Simmons, J. A., Harley, M. D., Marshall, L. A., Turner, I. L., Splinter, K. D., & Cox, R. J. (2017). Calibrating and assessing uncertainty in coastal numerical models. *Coastal Engineering*, *125*, 28–41. https://doi.org/10.1016/j.coastaleng.2017.04.005

Sobol, I. (2001). Global sensitivity indices for nonlinear mathematical models and their Monte Carlo estimates. *Mathematics and Computers in Simulation*, *55*(1-3), 271–280. https://doi.org/10.1016/S0378-4754(00)00270-6

Southgate, H. (1989). A Nearshore Profile Model of Wave and Tidal Current Interaction. *Coastal Engineering*, *13*(3), 219–245. https://doi.org/10.1016/0378-3839(89)90050-1

Svendsen, I. (1984). Wave heights and set-up in a surf zone. *Coastal Engineering*, *8*(4), 303–329. https://doi.org/10.1016/0378-3839(84)90028-0

Swart, D. (1974, December). *Offshore Sediment Transport and Equilibrium Beach Profiles* [Doctoral dissertation, Delft University of Technology].

Thornton, E. B., Humiston, R. T., & Birkemeier, W. (1996). Bar/trough generation on a natural beach. *Journal of Geophysical Research: Oceans*, *101*(C5), 12097–12110. https://doi.org/10.1029/96JC00209

Thorpe, A., Miles, J., Masselink, G., Russell, P., Scott, T., & Austin, M. (2013). Suspended Sediment Transport in Rip Currents on a Macrotidal Beach. *Journal of Coastal Research*, *165*, 1880–1885. https://doi.org/10.2112/SI65-318.1

Vadyala, S. R., Betgeri, S. N., Matthews, J. C., & Matthews, E. (2022). A review of physics-based machine learning in civil engineering. *Results in Engineering*, *13*, 100316. https://doi.org/10.1016/j.rineng.2021.100316

Van Alphen, J. (1990). A mud balance for Belgian-Dutch coastal waters between 1969 and 1986. *Netherlands Journal of Sea Research*, *25*(1-2), 19–30. https://doi.org/10.1016/0077-7579(90)90005-2

Van der Spek, A., van der Werf, J., Oost, A., Vermaas, T., Grasmeijer, B., & Schrijvershof, R. (2022). The lower shoreface of the Dutch coast – An overview. *Ocean & Coastal Management*, *230*, 106367. https://doi.org/10.1016/j.ocecoaman.2022.106367

Van der Zalm, G. (2024). Practicalities on trenches.

Van Gelder, P. (2000). *Statistical Methods for the Risk-Based Design of Civil Structures* [Doctoral dissertation, Delft University of Technology].

Van Ormondt, M., Nederhoff, K., & van Dongeren, A. (2020). Delft Dashboard: a quick set-up tool for hydrodynamic models. *Journal of Hydroinformatics*, *22*(3), 510–527. https://doi.org/10.2166/hydro.2020.092

Van Rijn, L. C. (2007). Unified View of Sediment Transport by Currents and Waves. I: Initiation of Motion, Bed Roughness, and Bed-Load Transport. *Journal of Hydraulic Engineering*, *133*(6), 649–667. https://doi.org/10.1061/(ASCE)0733-9429(2007)133:6(649)

Van Rijn, L. C., Meyer, K., Dumont, K., & Fordeyn, J. (2024). Practical 2DV Modeling of Deposition and Erosion of Sand and Mud in Dredged Channels due to Currents and Waves. *Journal of Waterway, Port, Coastal, and Ocean Engineering*, *150*(2). https://doi.org/10.1061/JWPED5.WWENG-2065

Van Rijn, L. (1986). Sedimentation of Dredged Channels by Currents and Waves. *Journal of Waterway, Port, Coastal and Ocean Engineering*, *112*(5).

Van Rijn, L. (1987, June). *Mathematical Modelling of Morphological Processes in the case of Suspended Sediment Transport* [Doctoral dissertation, Delft University of Technology].

Van Rijn, L. (2013). *Basics of Channel Deposition/Siltation* (tech. rep.).

Van Rijn, L. (2016). *Harbour siltation and control measures* (tech. rep.).

Van Rijn, L., Walstra, D., Grasmeijer, B., Sutherland, J., Pan, S., & Sierra, J. (2003). The predictability of cross-shore bed evolution of sandy beaches at the time scale of storms and seasons using process-based Profile models. *Coastal Engineering*, *47*(3), 295–327. https://doi.org/10.1016/S0378-3839(02)00120-5

Vivó-Truyols, G., & Schoenmakers, P. J. (2006). Automatic Selection of Optimal Savitzky−Golay Smoothing. *Analytical Chemistry*, *78*(13), 4598–4608. https://doi.org/10.1021/ac0600196

Walstra, D. J. R., Mocke, G. P., & Smit, F. (1997). Roller Contributions as Inferred from Inverse Modelling Techniques. *Coastal Engineering 1996*, 1205–1218. https://doi.org/10.1061/9780784402429.094

Zwamborn, J., & Grieve, G. (1974). Wave Attenuation and Concentration Associated with Harbour Approach Channels. *Coastal Engineering 1974*, 2068–2085. https://doi.org/10.1061/9780872621138.123

A

SedPit description

This appendix presents the existing SedPit tool in more detail. First, all input variables are explained. Most of the included formulae are present already in Section 4.4, which will therefore be excluded in this appendix. Some additional processes that are not mentioned in Section 4.4 are presented here. Next the different available outputs are presented.

An important disclaimer to start this appendix with is the wide variety in which the SedPit tool is available. The original tool was developed by Van Rijn 2013, and written as an Excel-tool. Different parties have modified the tool and made them suitable for their purposes. This holds as well for the two companies that were involved in this research; Svašek Hydraulics and Boskalis. The modelling in this research is based on the Python-version of SedPit, developed by Boskalis. Therefore, this appendix is based on that version. Possible deviations from the here presented SedPit tool are therefore possible, depending on the modification made to the original version by another party.

A.1. Input

The following input is included in the existing SedPit tool:

- Dimensions
  - Length l. The length is defined in the direction of the trench, i.e. for a shore-perpendicular trench, the length is defined in shore-perpendicular direction. If the existing SedPit is used in nearshore environments, the total length is divided in pieces, of which each is assigned a different depth.
  - Width b. The width of the trench in cross-direction. The width defines the settling length, and is defined at the bed level. The width is not the same as the deposition width, as the slopes will lead to a decrease width in the bottom of the trench.
  - Depth outside of the channel h_0. The water depth adjacent to the trench. By varying this depth, a bed profile can be simulated.
  - Depth in channel h_1. The water depth in the channel. This is the summation of h_0 and the depth of the trench.
- Sediment and water properties
  - Sand grain size d_{50} [m]. The median grain size of the sand particles.
  - Sand grain size d_{90} [m]. The 90% percentile of the grain size of the sand particles.
  - Sand fraction ps [-]. The fraction of sand in the sediment composition.
  - Fluid density ρ_w [kg/m³]. The density of the fluid. Default of 1025 kg/m³ in the case of seawater.
  - Sediment density ρ_s [kg/m³]. The density of the sediment. Default of 2650 kg/m³ for most sediment types.
  - Viscosity ν [m²/s]. The kinematic viscosity. Default value of 1e^{-6} m²/s.

  - Specific density s [-]. The relative density difference between sediment and fluid. Defined as:
$$s = \frac{\rho_s - \rho_w}{\rho_w} \tag{A.1}$$
  - Fall velocity clay ws_{clay} [m/s]. The fall velocity of clay, with a default value of 0.0001 m/s.
  - Fall velocity silt ws_{silt} [m/s]. The fall velocity of silt, with a default value of 0.001 m/s.
  - Fall velocity sand ws_{sand} [m/s] is calculated based on the grain size:
$$ws_{sand} = \frac{g d_{50}^2 (\rho_s - \rho_2)}{18\nu} \tag{A.2}$$
  - Bed roughness outside channel k_{r0} [m]
  - Bed roughness inside the channel k_{r1} [m]. In most situations, the same roughness is used for k_{r0} and k_{r1}.

- Hydraulics
  - Tidal period [h]. The duration of one tidal period in hours.
  - Duration [-]. The number of tidal periods that are considered as exposure period.
  - Timestep dt [s]. The timestep used to calculate the deposition.
  - Flow approach angle ϕ [°]. The approach angle of the flow with respect to the orientation of the trench.
  - Streamtube width b_0 [m]. The streamtube width is used to calculate the extend of the flow contraction or expansion when the flow enters the trench.
  - Water level to MSL WL [m]. The tidal water level fluctuation with respect to MSL, which is subtracted or added on the local water depths h_0 and h_1.
  - Depth-averaged flow velocity U [m/s]. The depth-averaged flow velocity, based on the tidal current.
  - Significant wave height H_s [m]. The local significant wave height.
  - Peak period T [s]. The peak period of the local wave conditions.
  - Background concentration clay c_{clay}. Used to determine the contribution of clay to the siltation.
  - Background concentration silt c_{silt}. Used to determine the contribution of silt to the siltation.

- Deposition
  - α_b. Constant related to the bed load transport, with a default value of 0.015. Comes back in Equation (4.44).
  - α_s. Constant related to the suspended load transport, with a default value of 0.012. Comes back in Equation (4.45).
  - η_b. Constant related to the bed load transport, with a default value of 1.5. Comes back in Equation (4.44).
  - η_s. Constant related to the suspended load transport, with a default value of 2.4. Comes back in Equation (4.45).
  - Bulk density ρ_b [kg/m³]. The density of the deposited sediment. The default value is 1600 kg/m³. This changes per location and sediment composition.
  - Van Rijn trapping coefficient c_{vr}. Coefficient describing the trapping efficiency, according to Van Rijn 1986. A value of 0.25 is considered to be the best fit.

- Calibration parameters
  - Calibration on wave types. The contribution of the wave orbital velocity to the effective velocity is dependent on the wave type. For regular waves, a factor of 0.8 is used, for irregular waves a factor 0.4 is used.

A.2. Additional processes

Two processes, that were not addressed in detail yet, are presented in this section: bed level update and consolidation.

The bed level update is enabled in default settings. The bed level update ensures that the deposition of sediment leads to a reduction of the water depth in the trench. In this way, the trapping efficiency experiences a time-dependence, with a decrease in trapping efficiency as a result.

The consolidation of the deposited sediment is a process which is strongly affected by its timescale. In the model, the consolidation process is included as soon as the total duration of exposure exceeds 1 year. This is barely the case for cable trenches, but is interesting for siltation predictions in harbour navigation channels.

A.3. Output

The SedPit tool returns different types of output:

- Total inflow of sediment [m³].
  The total inflow of sediment is the volume of all sediment that flows into the trench, which is calculated for the desired length l of the trench. Important to note that only a fraction of the inflow is actually deposited, depending on the trapping efficiency. It is the summation of the inflow volumes of sand, silt, and clay, which are also returned as separate output.
- Total inflow of sediment [ton].
  The total inflow can also be calculated in tons. To obtain the total inflow of mass from the inflow volume, the bulk density ρ_b is used for conversion.
- Total sedimentation volume [m³]
  The total deposited volume. This is the summation of the deposited volumes of sand, silt, and clay, which are also returned as separate output.
- Total sedimentation mass [ton]
  The total deposition can also be calculated in tons. To obtain the total deposition of mass from the deposited volume, the bulk density ρ_b is used for conversion.
- The trapping efficiency [-]
  The trapping efficiency is returned as timeseries of the fraction deposited volume from the total inflow volume. Here, the time-dependence becomes interesting.
- Siltation thickness [m]
  The siltation thickness is based on the deposition volume and the dimensions of the trench. It is assumed to be a constant value throughout the trench section.

B

Validation modelling of hydrodynamics

Different approaches are used to validate the accuracy of the MBJ-model described in Section 4.2.1 and Section 4.2.2. First, the modelling of the tidal current is validated by a comparison to the results of a study by De Wit (2016) in Appendix B.1. Next, the wave-driven longshore current, including the wave transformation is validated by comparison to model outcomes and field data. This is further explained in Appendix B.2.

B.1. Validation tidal current

Equation (4.34) is a simplification of Equation (2.5), in which the parameter S_m is included to represent the alongshore water level gradient as a result of tidal forcing. However, as parameter S_m needs more detailed information on the tidal elevation levels, while tidal currents are often available from historic data, Equation (4.34) is a promising way to model the tidal current with the available measurement data. To validate the accuracy of Equation (4.34), the work of De Wit (2016) is used. In his work, the alongshore tidal current at Egmond is modelled for different tidal gradients S_m according to Equation (2.5), using SWASH. In Figure B.1, the tidal current as a function of the depth is plotted for four different offshore current velocities. The dotted lines are the results from De Wit (2016), the solid lines are the current velocities that follow from Equation (4.34). It can be concluded that Equation (4.34) is a good approximation compared to the model results of De Wit.

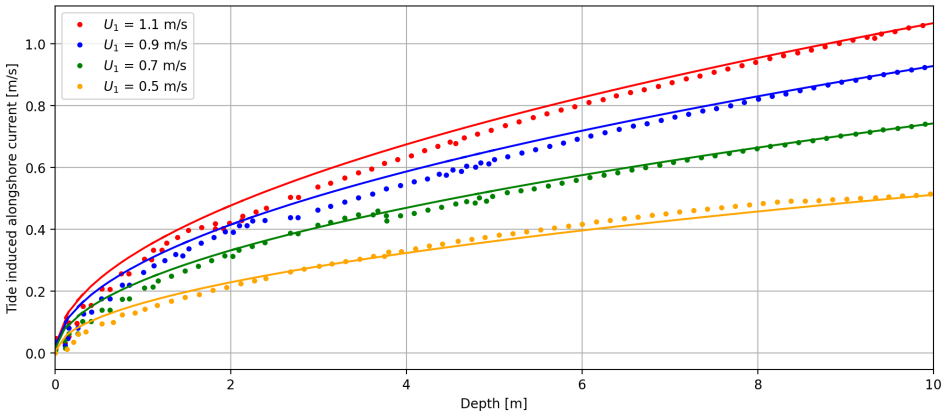

Figure B.1: Comparison between SWASH data and the approximation according to Equation (4.34). The dots are the data from the work of De Wit (2016), the solid line is Equation (4.34)

Figure B.1 shows that the relation between depth and tidal current is accurately approximated by the simplified formula Equation (4.34). To check the results of the approximation in Equation (4.34) for a

specific bed profile, the formula is tested on the same bed profile as modelled by De Wit (2016) in his paper. A tidal current velocity of 0.8 m/s is used at the offshore boundary. In Figure B.2, it becomes clear that the approximated tidal current is in good agreement with the results from the model by De Wit.

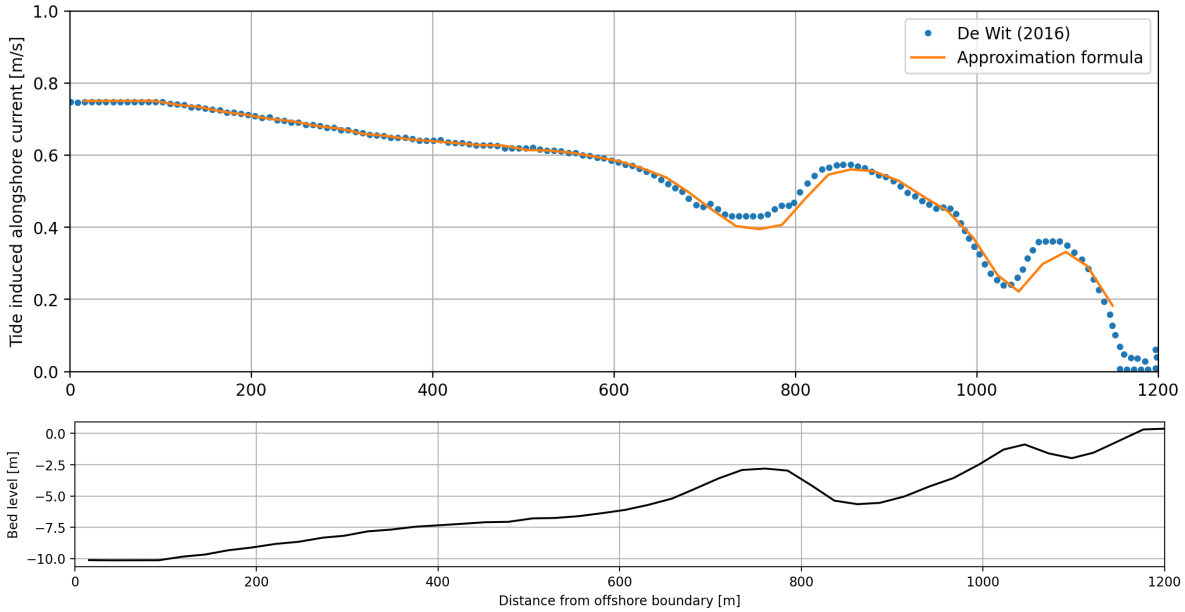

Figure B.2: Cross-shore transformation of tidal currents at Egmond. Bed profile retrieved from De Wit (2016)

The above presented validation of the approach in modelling the tidal current shows that the simplified formula Equation (4.34) is accurately modelling the cross-shore transformation of the tidal current velocities. The inclusion of the tidal current in the MBJ-model is further validated in Appendix B.2.

B.2. Validation wave-driven current

The validation of modelling of the wave-driven alongshore current in the MBJ-model will be presented in several steps. First, the wave transformation in the MBJ-model is compared to the wave transformation in XBeach. One test case is used to illustrate the wave transformation (Figure B.3). Next, the modelling of the wave-driven alongshore current is validated by means of 8 different cases. These case are compared to results from XBeach simulations. XBeach is an open-source numerical model to simulate hydrodynamic and morphodynamic processes. Amongst others, it includes short-wave transformation, long wave (infragravity waves) transformation, and currents. XBeach has three modes regarding the wave transformation and hydrodynamics: the stationary mode, the surf-beat mode, and the non-hydrostatic mode. In the stationary mode, all wave-group variations and the resulting long waves are neglected. In the surf beat mode, these long waves are included, as well as their effect on currents (Deltares, 2023). The non-stationary mode is wave-resolving mode, allowing the modelling of individual waves. In the coming sections, only XBeach runs in stationary mode are used, since the MBJ-model does not include long waves. XBeach is chosen as validation method for the wave-driven current, since it is possible to enable all effects of the tide. This makes it possible to isolate the currents occurring from waves. Besides that, XBeach is considered to be a well-tested model, is applied throughout the academia and industry, and has been validated for different cases (Bolle et al., 2011). The next and final step of the validation of the modelling of the hydrodynamics is a comparison to the work of Ruessink et al. (2001). This contains the comparison to the model that is presented in the work, and measurements that resulted from the Coast3D campaign (Klein et al., 2001). The model of Ruessink et al. and the measurements from the Coast3D campaign do include tidal currents.

In Figure B.3 the transformation of the significant wave height H_s and the wave angle θ is showed. The base case which is plotted simulates a wave climate, characterised by an offshore significant

wave height H_{s0} of 2 meter, a wave incident angle of 30°, and a peak period T_p of 8 seconds. In the MBJ-model, as well as in the XBeach model, a bottom roughness k_s of 0.01 m is used, and a breaker coefficient γ = 0.78 is used.

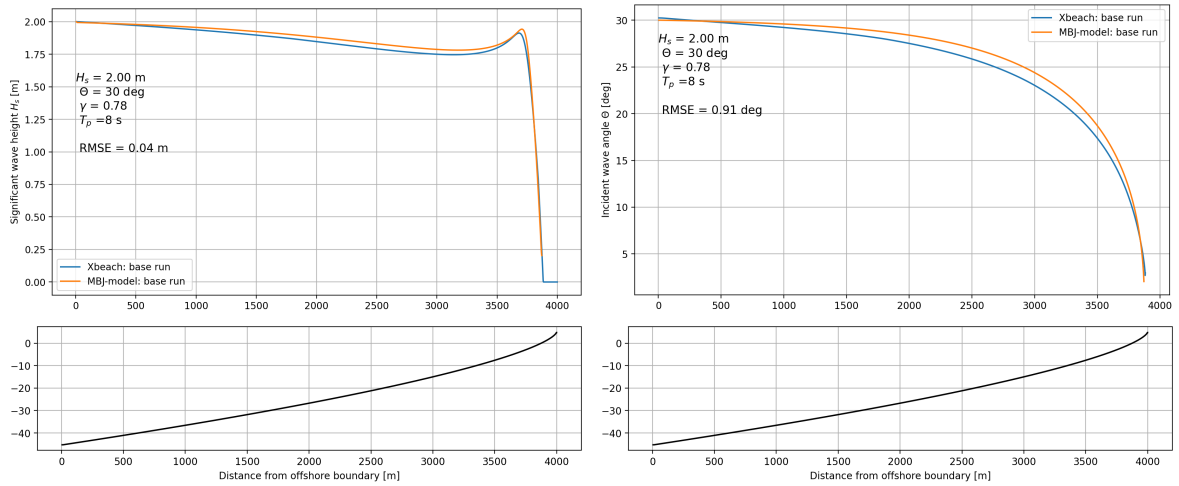

(a) Significant wave height H_s test case

(b) Wave angle θ base run

Figure B.3: Wave transformation of MBJ-model, compared to the base case in XBeach.

The wave height is modelled accurately, with a RMSE of 0.04 meter, while the wave angle is modelled accurate as well with a RMSE of 0.91°.

In order to validate the wave-driven alongshore current modelled in the MBJ-model, 8 runs in XBeach are performed. A variation of input parameters is chosen, to explore a range of possible shortcomings. These runs are presented in Table B.1. Four different bed profiles are used, including three Dean's profiles with different slopes. The profile "Dean (3)" has the steepest slope, while the profile "Dean (2)" has the most gentle slope. As fourth profile a bar profile is modelled in Run07 and Run08. The sensitivity to an increase in bottom roughness k_s is investigated in Run02, while Run03 is focusing on a variation in breaker coefficient γ. In Run04 and Run05 high and low waves on a gentle slope are modelled, with a decreased incident wave angle. Run06 and Run07 are including different wave height and incident wave angles on the bar profile. Run08 is including waves with a larger period, representing swell waves. In all XBeach runs, the roller dissipation is enabled, with a β-coefficient (related to Equation (4.17)) of 0.08. The bottom friction is disabled in the default settings of XBeach. This is related to the fact that bottom friction is often neglected in the breaking zone due to its limited contribution compared to dissipation by breaking and rollers. Bottom friction is also disabled in the MBJ-model for these runs. Although most of the formulae in the MBJ-model correspond to the formulae incorporated in XBeach, some differences are present. First of all, XBeach is modelling in a 2D-grid, leading to x- and y-constituents, while the MBJ-model is considering a 1D-grid in x-direction. Besides that is the combination of wave and current friction as presented in Equation (4.30) a different approach than what is applied in XBeach. XBeach is furthermore including lateral mixing, which is not part of the MBJ-model. It is to be expected that these differences in XBeach and the MBJ-model will consequently lead to slight variations in the outcomes.

Table B.1: Input validation runs

Run ID	Bed profile	H_{s0} [m]	θ_0 [°]	T_p [s]	γ	k_s [m]	Goal
Run01	Dean (1)	2	30	8	0.78	0.01	Base case
Run02	Dean (1)	2	30	8	0.78	0.03	Sensitivity to bottom roughness
Run03	Dean (1)	2	30	8	0.5	0.01	Sensitivity to breaker coefficient gamma
Run04	Dean (2)	4	15	12	0.78	0.01	High wave energy, small angle, & gentle slope
Run05	Dean (2)	0.8	15	7	0.78	0.01	Low wave energy, small angle, & gentle slope
Run06	Bar	2	30	8	0.78	0.01	Bar profile, moderate waves
Run07	Bar	3	60	8	0.78	0.01	Bar profile, high waves, large angle
Run08	Dean (1)	2	30	14	0.78	0.01	Swell waves

In the section below, the different simulations in Figure B.4 are discussed.

- When comparing Run02 (Figure B.4b) to Run01 (Figure B.4a), it can be seen that the MBJ-model is more sensitive to an increase in bottom roughness k_s. An increase to a bottom roughness of 0.03 meter leads to a larger decrease in wave-driven longshore current in the MBJ-model, compared to the XBeach results. This is also seen in the increase of the RMSE from 0.10 m/s to 0.13 m/s. This difference can be attributed to a different approach of the friction coefficients. In the MBJ-model, the approach of Battjes and Janssen (1978) in Equation (4.30) is used, as this has proven to return the best correspondence with the XBeach results. A consequence of this approach is a higher sensibility to bottom roughness.
- Run03 (Figure B.4c) and Run04 (Figure B.4d) show that the shape of the curve is simulated less accurate than in the other runs. The skewness is more pronounced in the XBeach results for a lower gamma and at higher wave heights. In the case of a lower gamma or higher waves, the breaking of the waves starts earlier and extend through a wider breaking zone, consequently leading to a larger contribution of roller dissipation and dissipation by breaking. The dissipation by breaking is modelled in the MBJ-model similar to the approach in XBeach. The dissipation by rollers however, is modelled 1D (x-direction only) in the MBJ-model, while XBeach is in 2D (x, y-directions). The dissipation in y-direction could explain the lower peaks in XBeach compared to the MBJ-model.
- Run05 (Figure B.4e) is a situation with very low waves (H_{s0} = 0.8 m). It is observed that the MBJ-model is not modelling the wave-driven longshore current very accurate in this situation. Although the absolute value of the RMSE is not significantly high, it is high when comparing it relative to the peak value of the curve.
- Run06 (Figure B.4f) and Run07 (Figure B.4g) are simulations of a bar-profile. It can be seen that the MBJ-model in both cases overestimates the first, and underestimates the second peak slightly. This could be related to the wave breaking theory applied in the MBJ-model, according to Equation (4.12).
- In Run08 (Figure B.4h) swell waves with a period T_p of 14 seconds are modelled. The observed differences are very comparable to what is seen in the base run (Figure B.4a). The longer swell waves carry more momentum, leading to the increase of the peak in wave-driven longshore current.

The following conclusions can be drawn from this validation of the wave-driven longshore current:

- The MBJ-model generally aligns well with XBeach in terms of peak locations, displaying a high degree of overlap. The peak values also typically show good correspondence, although there are some notable discrepancies at lower values of γ or under conditions of high waves.
- In conditions of low waves, the alignment between the MBJ-model and XBeach is not particularly strong.
- The MBJ-model is more sensitive to bottom roughness k_s than XBeach.

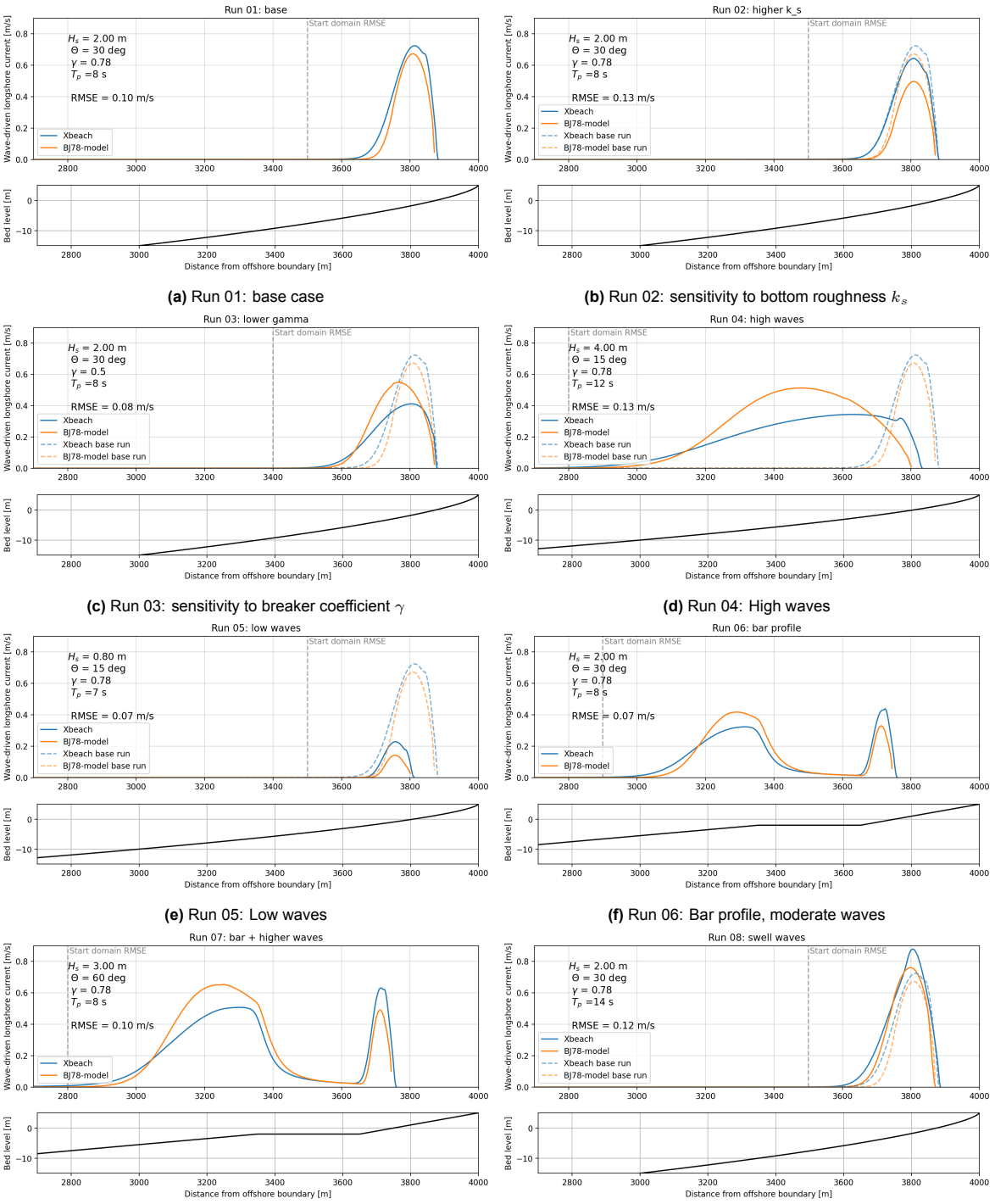

(a) Run 01: base case

(b) Run 02: sensitivity to bottom roughness k_s

(c) Run 03: sensitivity to breaker coefficient γ

(d) Run 04: High waves

(e) Run 05: Low waves

(f) Run 06: Bar profile, moderate waves

(g) Run 07: Bar profile with higher waves

(h) Run 08: Swell waves

Figure B.4: Validation runs XBeach vs Modified MBJ-model. The dashed curves represent the base case, and the dashed vertical line indicates in which domain the RMSE is calculated.

Besides a validation with XBeach data, the results are compared to the work of Ruessink et al. (2001), including measurements from the Coast3D campaign. Although XBeach is a well-proven model, it is not necessary modelling the truth. Therefore, it has been decided to compare it to measurements of the Coast3D campaign, and the work by Ruessink et al. The purpose of the Coast3D campaign was to obtain a data set to validate and calibrate numerical models. During a period of 32 days, measurements of different nearshore wave characteristics were obtained in a stretch of 600 meter wide coastline. Besides that, offshore wave conditions were measured. Ruessink et al. (2001) developed

a method that models the alongshore wave-driven current, including dissipation by wave breaking and wave rollers. Dissipation by bottom friction is not included. The method is very similar to the concepts of the MBJ-model, although some differences do exist. First of all, the method of Ruessink et al. does include lateral mixing. Secondly, the friction coefficient is determined by the Manning-Strickler equation (Equation (4.33)). The use of the Manning-Strickler equation is included in the MBJ-model as an option, to make the comparison to the results of Ruessink et al. possible. Besides that, all parameter choices that are documented by Ruessink et al. are included in the settings of the MBJ-model. These values were chosen based on the best fit with the available measurement data. This includes a roller steepness β = 0.05, and a bottom roughness k_s = 0.022 m.

Ruessink et al. present the wave height H_{rms} and longshore current in three different conditions: low tide, mid tide, and high tide. A complication in this validation is related to the offshore wave conditions. The exact used values for H_{s0}, θ, T_p, and γ are unknown, based on the paper of Ruessink et al. In order to determine representative wave conditions, the information provided by Ruessink et al. has been complemented by data from the original Coast3D report (Klein et al., 2001). The offshore significant wave height H_{s0} has been calibrated to fit with the most offshore measurement of H_{rms}. The offshore wave angle θ_0 and the peak period T_p has been determined based on the Coast3D data from that specific time step. The wave breaker coefficient γ is determined based on the wave height difference between the first and second bar (bottom profile is shown in Figure B.5). Ruessink et al. mention a relation between offshore wave steepness and breaker coefficient γ in their work. However, this approach demands offshore wave conditions, which had to be estimated from the Coast3D data. The resulting values for γ showed a less accurate fit to the wave heights than the values determined by visual calibration. The water levels corresponding to low, mid, and high tide were retrieved from the Coast3D data. Neither the Coast3D data, nor the paper of Ruessink et al. give information on the offshore or nearshore tidal current. The offshore tidal current in the MBJ-model is calibrated based on the most offshore modelled current in Figure B.5a, Figure B.5b, and Figure B.5c.

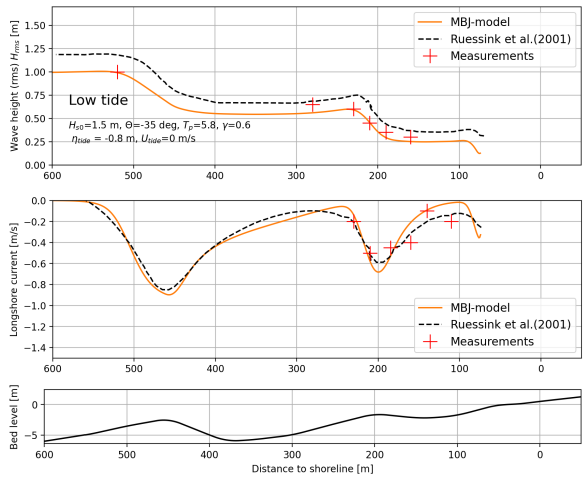

(a) Wave height H_{rms} and longshore current for low tide conditions.

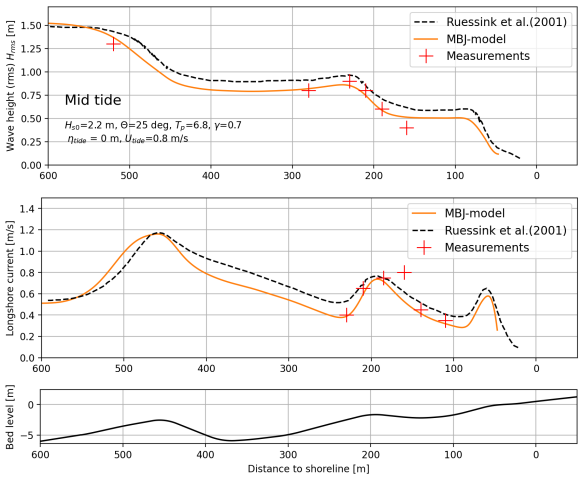

(b) Wave height H_{rms} and longshore current for mid tide conditions.

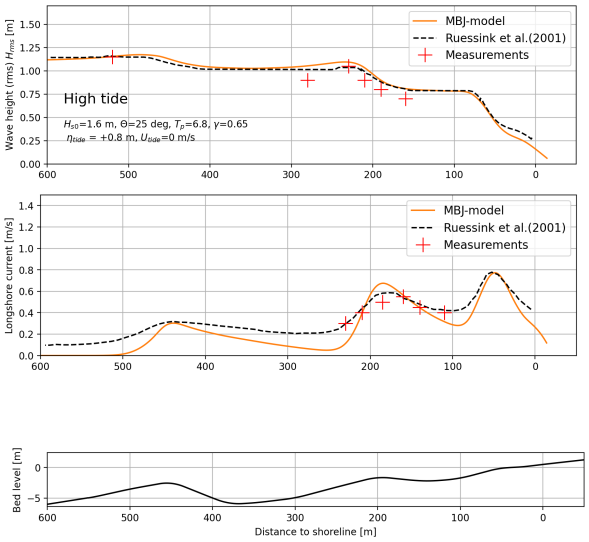

(c) Wave height H_{rms} and longshore current for high tide conditions.

Condition	RMSE Ruessink	RMSE obs.
Low Tide	0.23 m/s	0.12 m/s
Mid Tid	0.12 m/s	0.12 m/s
High Tide	0.15 m/s	0.10 m/s

(d) RMSE of longshore current in three conditions, compared to the model results of Ruessink et al., and to the measurements from Coast3D (Klein et al., 2001)

Figure B.5: Comparions between MBJ-model and the work of Ruessink et al., including measurements from the Coast3D campaign (Klein et al., 2001). Figure B.5d states the RMSE values.

B.3. Conclusion on validation of hydrodynamics

In the sections above, the MBJ-model has been compared to model data from XBeach, to the model in the paper of Ruessink et al. (2001), and the measurements included in that paper, originating from the Coast3D campaign (Klein et al., 2001).

When comparing a pair of models, it can be helpful to quantify the comparison. This is done by means of the root-mean squared error (RMSE), presented in Figure B.4 and Figure B.5. This is a simple and well interpretable way of quantifying the performance of a model. However, in this context it brings it complications. First of all, a specific range of the domain has to be selected. The model performance would be largely overestimated if the whole domain, from the offshore boundary to the shoreline, would be considered. Generation of longshore currents starts in the nearshore environment, wherefore the differences between the two models are only visible in that range. Secondly, the RMSE focuses purely on an absolute error, without relating it to the magnitude of the outcome itself. As a result, the RMSE may not adequately capture the significance or impact of errors in the context of the specific problem.

When comparing the RMSE to the magnitude of the peak values, an error of 15% to 20% can be observed, for all three comparisons, which is considered as an acceptable accuracy, considering the

large amounts of variables and the type of comparison material. The amount of measurement data is very limited, while it is the most valuable way of comparison. XBeach and the model of Ruessink et al. are considered well-established; however, it is important to note that these models do not perfectly represent reality and bring their own errors.

When looking at the shapes of the curves in Figure B.5, the MBJ-model is modelling the longshore currents accurately. A process that has not been included in the MBJ-model, but is part of the model by Ruessink et al., is mixing due to turbulence and viscosity. The exclusion of mixing explains the somewhat too steep gradients of longshore current in the MBJ-model. This is best visible in Figure B.5c, where the model by (Ruessink et al., 2001) (black dotted line) shows less fluctuation compared to the MBJ-model.

Overall, an acceptable representation of nearshore hydrodynamics can be modelled by the MBJ-model. Although a certain error is inevitable, the performance is considered to be well enough in the context of a quick-assessment tool. The combined SedPit Nearshore tool is validated, and evaluated in Section 5.4 and Section 5.5.

In Section 4.6, the behaviour of the MBJ-model will be analysed by means of a sensitivity analysis. This can be seen as verification, and as an addition on the validation of the MBJ-model. Although the sensitivity analysis does not validate the magnitude of the model's outcome, the sensitivity analysis can verify whether the model reacts appropriately to a broad range of input variables in accordance with physical laws.

C

Sensitivity analysis on non-measurable variables in MBJ-model

As introduced in Section 4.6, a separate sensitivity analysis is performed including only the four non-measurable variables (Table 4.1). The results of this sensitivity analysis will form a first step for future calibration procedures. By identifying the most-influential among these non-measurable variables, the calibration procedures can be optimised.

The four variables that are excluded from this sensitivity analysis are still part of the model, and therefore need to be defined as deterministic value. The simplest choice could be to define one wave climate with a corresponding value for wave height H_s, wave angle θ, peak period T_p, and tidal current U_{tide} each. However, to take possible correlation between wave climate and variable influence into account, three different sets of wave climate variables are defined, representing mild, medium, and heavy conditions. The tidal current is excluded. This choice is based on the results from the first sensitivity analysis, which are presented in Section 5.2.2. The tidal current is affecting the model outcome strongly, while showing little interaction effects when comparing it to the interaction effects of the wave conditions. The results of the sensitivity analysis on the 8 variables (see Section 5.2.2) have shown that U_{tide} is heavily affecting the model outcome. To exclude the effects of U_{tide} and focus on the effect of the non-measurable variables, U_{tide} has been excluded.

Table C.1: Wave conditions for sensitivity analysis on the non-measurable variables

Condition	H_s [m]	θ [$^\circ$]	T_p [s]	U_{tide} [m/s]
Mild	1	5	5	0
Medium	2.5	10	8	0
Heavy	5	30	14	0

Next, the results of the sensitivity analysis on the four non-measurable variables are presented. The analysis is conducted with three different combinations of wave climate input values, representing mild, medium, and heavy wave conditions (see Table C.1). The conclusions that can be drawn from these results are structured in the same way as in Section 5.2.2. First of all, from Figure C.1 it can be concluded that interaction affects are way smaller when isolating the four non-measurable variables from the forcing, as the sum of all first order indices is close to 1 in all three wave conditions. Among the four non-measurable variables, the bottom roughness k_s is by far the most influential variable. While the second-order indices do not show substantial differences, the first-order indices clearly indicate that k_s is the most influential variable.

When looking at the model response in the boxplots in Figure C.2 it becomes evident that k_s is most influencing the mean of the model outcome, which is in line with the sensitivity indices in Figure C.1. The other three variables do not show notable influence on the mean model outcome.

When looking at the three different wave conditions, no clear trends can be identified. Nonetheless, during heavy wave conditions, there is a reduction in the sum of the second-order indices (Figure C.1c). This might suggest that the minor interaction effects between the variables are overshadowed by the effects of the more energetic waves during the heavy wave conditions. However, in general a changing wave climate does not have a significant effect on the influence of the non-measurable variables.

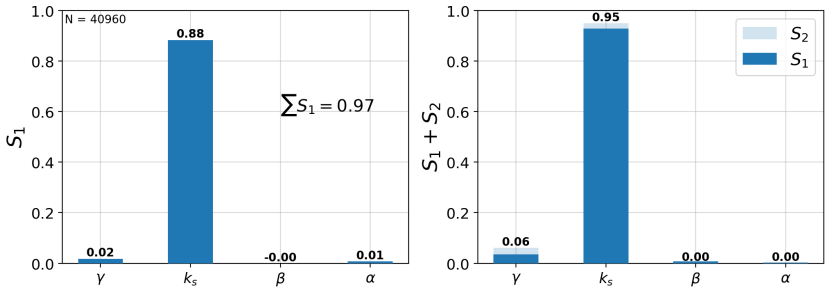

(a) Mild conditions: H_{s0}= 1 m, θ_0 = 5 °, T_p = 5 s

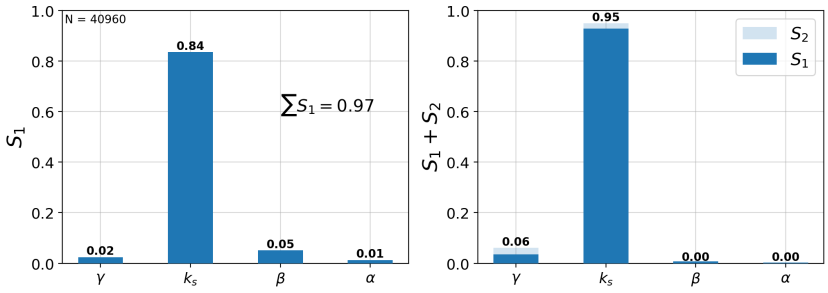

(b) Medium conditions: H_{s0}= 2.5 m, θ_0 = 10 °, T_p = 8 s

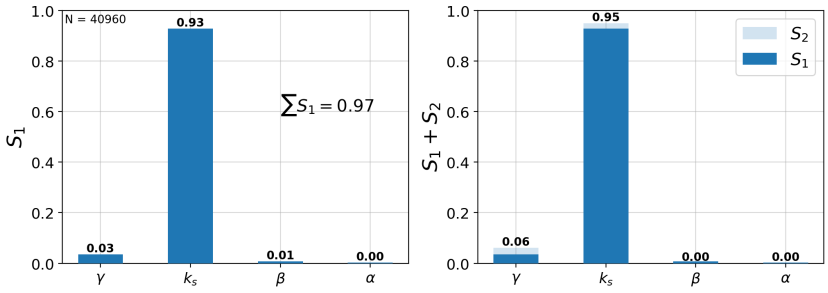

(c) Heavy conditions: H_{s0}= 5 m, θ_0 = 30 °, T_p = 14 s

Figure C.1: Sensitivity indices of non-measurable variables α, β, k_s, and γ. Left: first-order indices. Right: summation of first- and all second-order indices where a variable is represented.

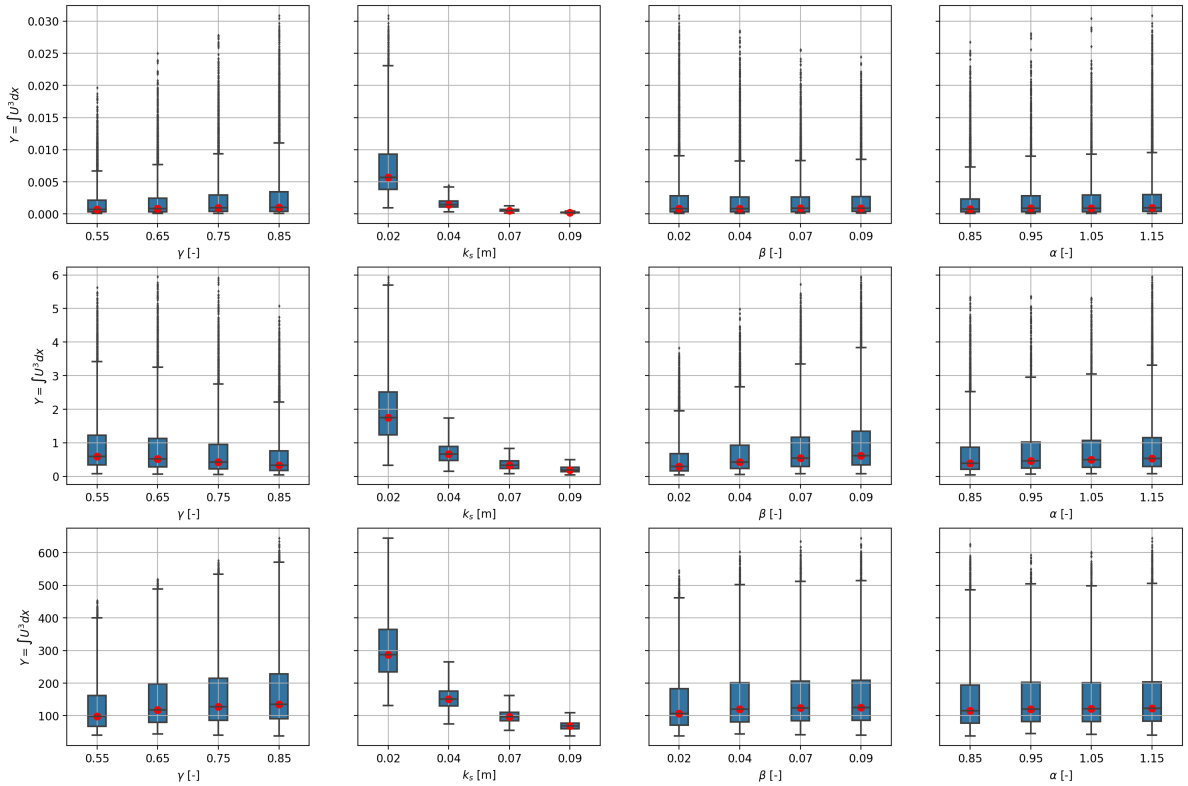

Figure C.2: Model response on 4 varying input values, for 3 different wave conditions. The red dots are representing the mean. The horizontal whisker extend to the furthest data point within 2.5 times the interquartile range (IQR) from the first and third quartiles, while any data points beyond this range are considered outliers and are individually plotted.

D

Sensitivity analysis on existing SedPit-tool

As introduced in Section 4.7, the results of a sensitivity analysis on the existing SedPit tool are used to select the variables to include in the sensitivity analysis on the SedPit Nearshore model. The aim of this appendix is to clarify this step further.

The sensitivity analysis on the existing SedPit tool is done by using the MatLab environment, provided by Hendriks (2020). This environment is a ready-to-use environment that performs a sensitivity analysis. A MCS is included that defines the distributions of the sampled variables. The model calculates the siltation layer thickness in one month, in an arbitrary trench. The results for the Van Rijn trapping coefficient c_{vr}, sand grain size d_{50}, bulk density ρ_b, clay concentration c_{clay}, and silt concentration c_{silt} are shown in Figure D.1.

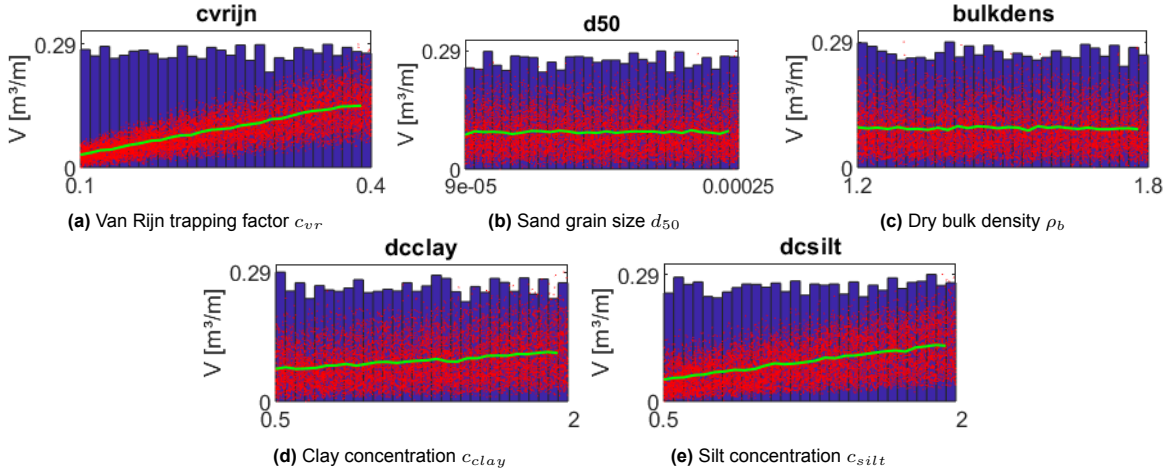

(a) Van Rijn trapping factor c_{vr} **(b)** Sand grain size d_{50} **(c)** Dry bulk density ρ_b

(d) Clay concentration c_{clay} **(e)** Silt concentration c_{silt}

Figure D.1: Results of preliminary sensitivity analysis on the existing SedPit-tool. The used modelling environment was developed by Hendriks (2020). The y-axis is representing the modelled siltation volume per meter width after one day, for a different project than the field case used in this report. The red dots represent the individual model outcomes. The green line is the average model outcome.

Among all included variables, especially the concentration of clay c_{clay}, concentration of silt c_{clay}, and the Van Rijn trapping coefficient c_{vr} show a significant effect on the mean model outcome. The effect of the concentration of fines is in line with the predicted large effect, as discussed in Section 4.7 and shown in Appendix E. The effect of the sand grain size d_{50} is not too clear in Figure D.1, but considering the wide possible range of the grain size, it can be seen as a variable with large effect on the model outcome. As mentioned in Section 4.8.1, the dry bulk density ρ_b will be included in the GLUE-analysis

as well. ρ_b is known to be a variable which is very difficult to estimate in early stages of execution. Due to the interest from a practical point of view, this variable is included in the sensitivity analysis as well.

E

Sediment types in nearshore siltation

As stated in Section 4.7, the variability of the background concentration of fines is not included in the sensitivity analysis. The goal of this appendix is to illustrate the effect of varying background concentrations on the siltation in a trench. Besides that, this appendix presents the contribution of each of the three sediment types to the total deposition of sediment. This is part of the discussion on the effect of the concentrations of silt and clay in Section 5.4.

Coastal sediments are often considered to consist of three types of sediments: sand, clay, and silt, of which clay and silt are often referred to as 'fines'. Silt particles are defined as particles smaller than 63 μm, while clay particles are the smallest sediment type with sizes below 3.9 μm (ISO, 2017). The difference in particle size leads to differences in settling velocity, which gives silt and clay both an unique settling behaviour. As described in Section 4.4.1 and Appendix A, the existing SedPit-tool includes all three types of sediment. The transport of fines is calculated in a simplified manner, which relates a background concentration and a current velocity to the corresponding transport rates of clay and silt.

E.1. Effect of extreme background concentrations

Two extreme values of background concentrations are considered in this comparison. As a base case, the siltation during period 2 with a clay concentration of 50 mg/L is used. This background concentration is based on a rough estimate of the clay concentration near the location of the field case. The effect of clay and silt is investigated separately by comparing the runs as stated in Table E.1. The chosen upper values (400 mg/L) for silt and clay concentration are determined by extreme cases of concentration of fines in estuaries or harbours (Van Rijn, 2016). All runs are simulated for the hydrodynamic boundary conditions and bed level of the field case, as presented in Section 3.1.

Table E.1: Comparison runs for fine sediments

Run	c_{silt} [mg/L]	c_{clay} [mg/L]
Base case	50	50
Clay	0	400
Silt	400	50

The results of the three runs are shown in Figure E.1. It can be clearly seen that the large increase in concentration of clay particles does not significantly affects the siltation volume. However, the large increase in concentration of silt particles does lead to significant increases in siltation volume. It can be concluded that in the wave conditions of the test case, the hydrodynamics conditions are not calm enough to let the finest particles of clay settle. However, especially at the larger depths, the contribution of silt to the siltation is significantly in case of large background concentrations.

When focusing on the most onshore peak, it can be seen that the contribution of silt to the siltation is decreasing. This is the result of the larger wave action within the breaker zone, which does not allow fines to settle.

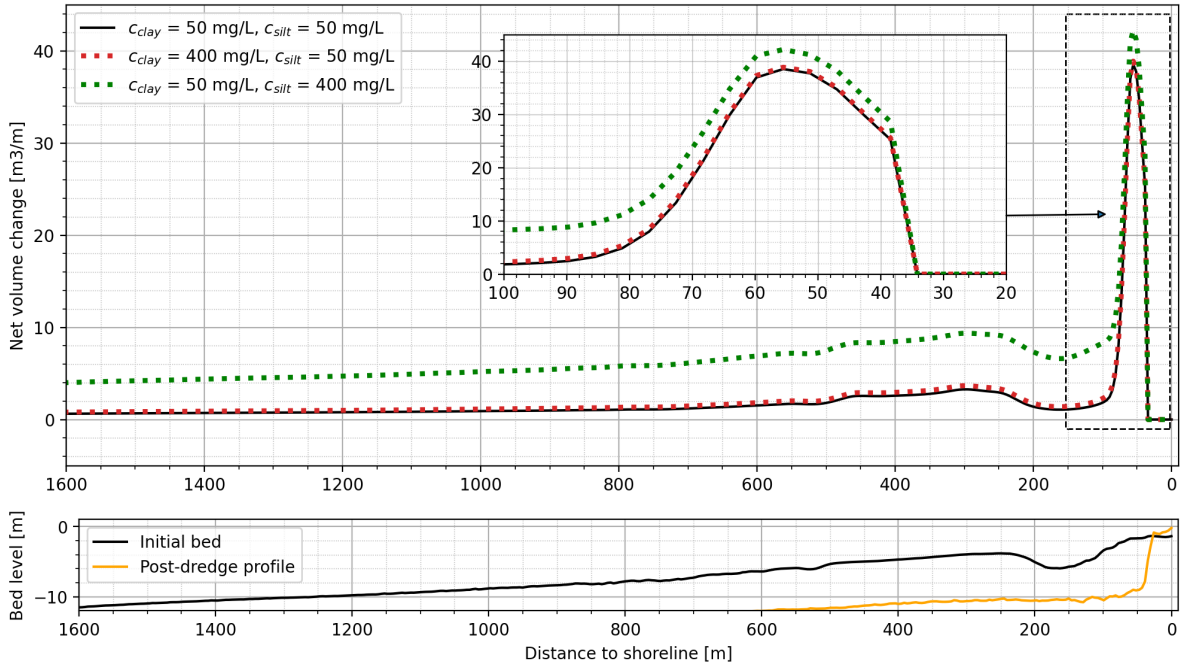

Figure E.1: Comparison between different concentrations of fines.

E.2. Contribution of sediment types

In Figure E.2 the contributions of silt and clay to the total deposition of sediment is shown. On the left graphs, it can be seen that the total deposition of sediment, as expected, is increasing towards the shoreline. Besides that, it becomes clear that the concentration of silt has significantly more influence on the deposition in the deeper zone. The upper graph (Figure E.2a) corresponds to the situation of a factor 2 lower concentration of clay, and a factor 1.5 higher concentration of silt, compared to the lower graph (Figure E.2b). Still, the absolute combined contribution of the fines (red dotted line) is larger for the upper graph. The larger effect of silt concentration is also visible when comparing the fractions of both sediment types to the total deposition. In the right graphs, it can be seen that the silt is adding for significantly larger fraction to the total deposition. It is also seen that the fraction is decreasing towards the shoreline, with the peak as an exception. This is in line with the discussion in Appendix E.1.

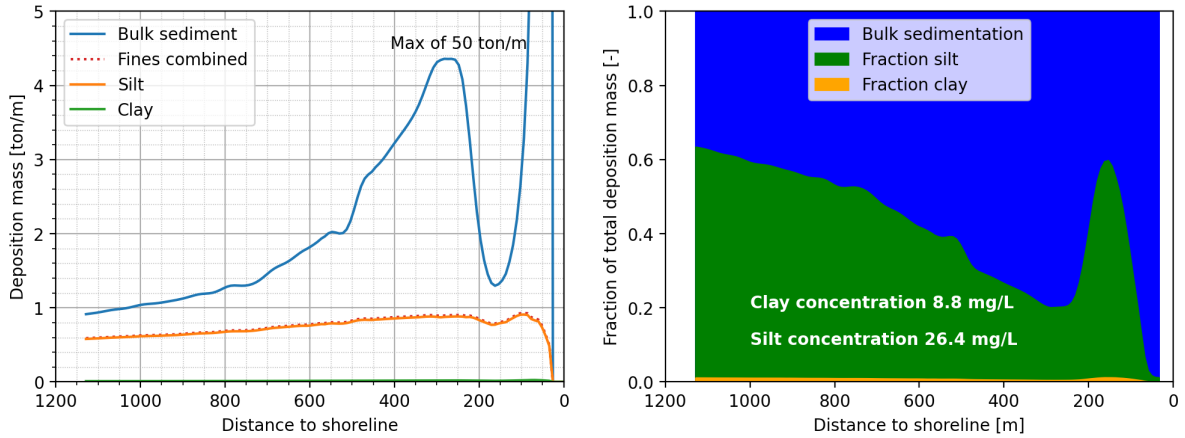

(a) optimal variables set based on weighted average

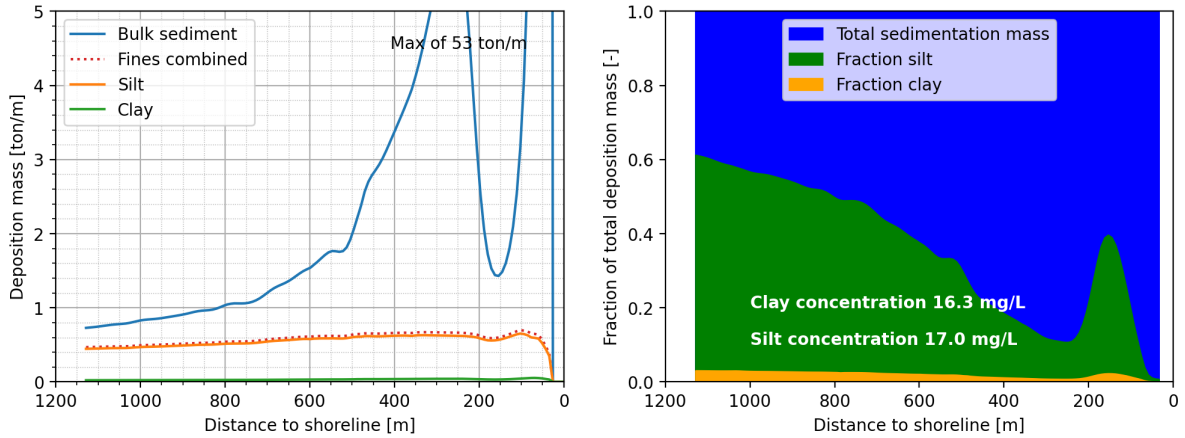

(b) Optimal variables set based on spatial distribution

Figure E.2: Contribution of silt and clay to the total deposition of sediment, in deposited mass as well as in terms of fraction. The total sediment represents sand, silt, and clay. The peaks of the total sedimentation mass are excluded grom this graph to increase the readability of the graph. The peak value of the most onshore peak is stated in the figures.

F

Time-dependence trench siltation

The siltation rates of the trench are strongly dependent on the hydrodynamics and their variability. As a result, the siltation rates show strong fluctuations in time. The aim of this appendix is to visualise the evolution of the siltation processes in time.

Figure F.1 shows the total siltation volume throughout time. The red line is representing the siltation volume during period 1, while the blue line represent the siltation volume during period 2. Both periods where simulated in two separate runs. The third line represent the siltation of the total period, simulated in one run. In theory, one would expect that line of the total period is identical to the lines of the two periods separate. However, the small mismatch of 2 % between those lines is due to the effect of the bed level change in the trench. As mentioned in Section 4.7, the bed level change is the only process in the model that affects future timesteps. When running the two periods separate, the siltation layer at the end of the first period is not considered as starting point for the second period. This leads to a slight overestimation of the trench depth, which gives the trench a larger trapping efficiency. However, as the siltation rates in the first period are not enormous, the effect of neglecting the bed level change after the first period is only 2%.

It is an easy fix to include the siltation rates after period 1 as an initial siltation thickness to the simulation of the second period. However, by excluding the initial siltation thickness, the two periods can be seen as independent simulations.

Figure F.1 also shows the effect of the wave height and the wave direction on the increase in siltation volume. Three situations with a clear increase in siltation rate are identified in Figure F.1a, indicated by the vertical dashed lines. These three moments clearly coincide with the three moments of significant wave height increase in Figure F.1b. The three moments do not coincide with the largest angles of incidence, which are plotted in Figure F.1c. Based on this graphical information, it can be concluded that the wave height is having a larger probability of causing high siltation rates than the wave angle. This is exactly in line with was concluded in Section 5.2.2.

Figure F.2 shows the siltation thickness on three different locations on the transect. The three dashed lines represent again the moments of increased wave height and siltation rates. It can be seen that the siltation thickness is responding especially strong in the lower depths (location 1). In general, it can be concluded that a large fraction of the siltation is occurring in a relative short span of the whole period of exposure to waves and current.

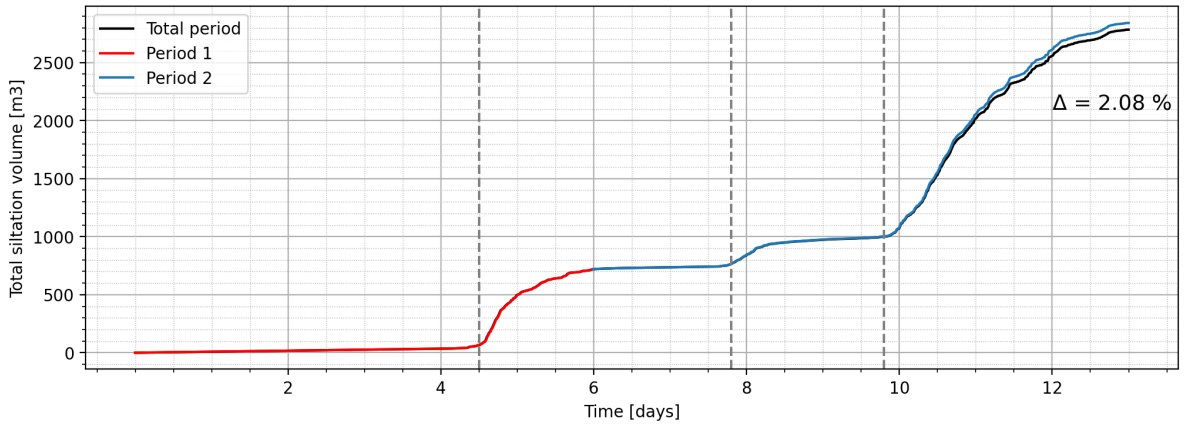

(a) Total siltation volume in time (Between 12.9 m depth and the shoreline)

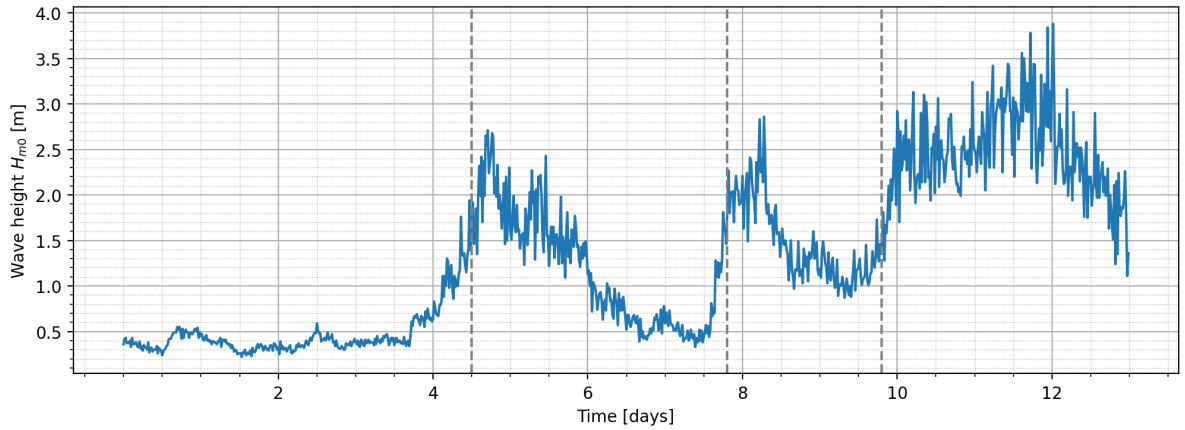

(b) Offshore wave heights

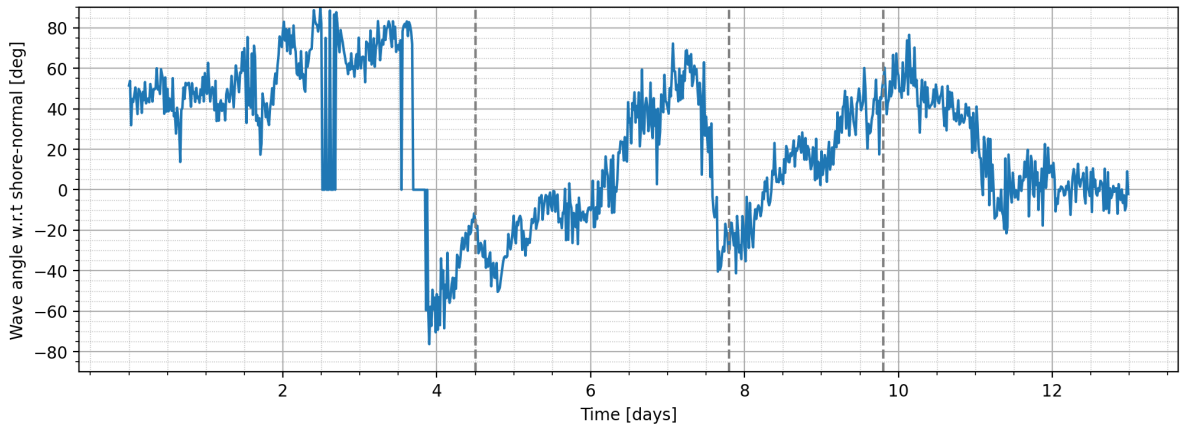

(c) Wave angle with respect to the shore-normal

Figure F.1: Evolution of the total siltation volume through time, along with the offshore wave height and wave angle. The vertical dashed lines indicate three moments of significant increase in wave height.

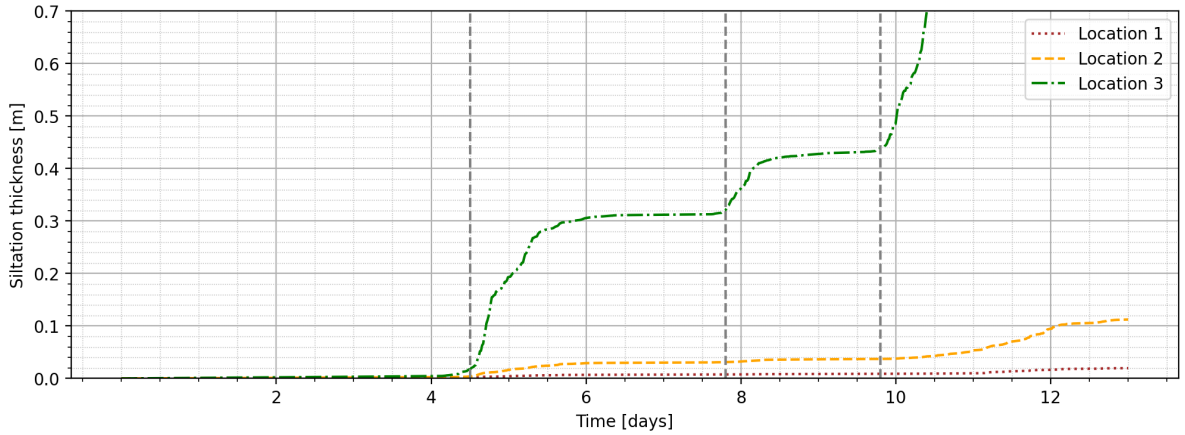

(a) Evolution in time of the siltation thickness on three locations no the transect.

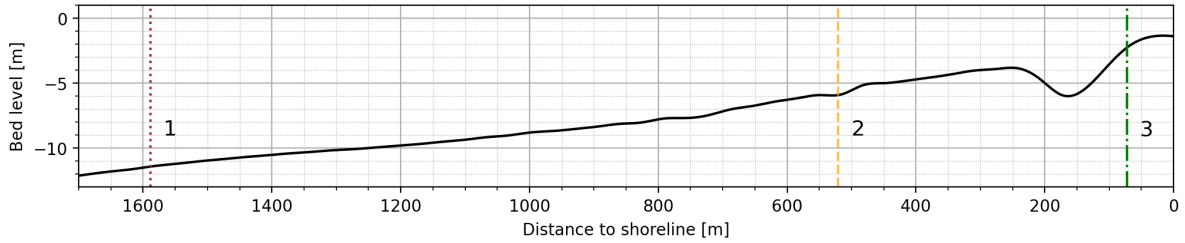

(b) Bed profile

Figure F.2: Evolution in time of the siltation thickness on three locations no the transect. The vertical dashed lines indicate three moments of significant increase in wave height.

G

Metocean conditions in reduced timeseries - GLUE

This appendix presents the approach of creating the reduced timseries. First the steps that were taken to obtain a reduced timeseries are presented. The applied model is a simplified approach, which is sensible to loss of information. Therefore, an extensive check on the resulting accuracy is presented in this appendix. A more robust and physically correct approach would be to condense and average the timeseries based on the wave energy. However, due to the limited available time for this research, a faster and simpler approach is used, which will be presented below.

A larger sample size N of variable sets gives a more accurate representation of the probability distribution of the selected variables. As the available computation power is a limiting factor in this research, certain methods to reduce the needed computation time were explored. The most promising way to reduce the computation time is the reduction of the timeseries. By increasing the original timestep of 20 minutes to a larger step, the needed computation time can be reduced significantly. However, an increase in timestep leads to an increased loss of information regarding the intermediate timesteps. As the GLUE-method includes a comparison of the modelled data to field data, it is important to minimise the loss of information. This leads to the trade-off between computation time reduction, and loss of information. To find the optimal choice in this trade-off, different timesteps have been evaluated.

First of all, as the available dataset contains metocean data, the dataset is very spiky, which is referred to as ”noise”. To reduce the noise of a dataset, several methods exist, including the moving-average method. However, when using the method of a moving-average, most of the peaks in the timeseries will be excluded. This can be counteracted by choosing a small ”window size” for the moving-average method, which minimises the loss of information of peaks. However, there are more efficient methods to describe spiky random timeseries. One of these method is the Savitzky-Golay (SG) smoothing, which was first presented by Savitzky and Golay (1964). In SG-smoothing, smoothing is added to a signal by varying the order of the local polynomial which approximates the signal (de Rooi et al., 2014). The SG-smoothing adds more attention to peak values than the moving-average method does, which makes it possible to remain some of the characteristics of the peaky timeseries of the metocean data. For more background on the SG-smoothing, the reader is referred to Savitzky and Golay (1964).

In applying the SG-smoothing, two parameters have to be defined by the user. First of all the ”window size”. This indicates the region in the timeseries that will be used to find an approximated new value. Secondly, the polynomial order has to be defined.

The goal while selecting the window size is to find a window size that yields a new dataset that is as close as possible to the original dataset (Vivó-Truyols & Schoenmakers, 2006). A window size equal to 1 yields the exact same dataset as the original, while a too large window size reduces the variability in the dataset too much, with loss of information as result. In the end, the choice of the window size was based on trial-and-error and the optimal choice has been determined graphically. In this judgement,

the goal was to find a value that results in a new dataset that has some peaks, while not showing too large outliers compared to the estimated mean.

The polynomial order is less important in the context of smoothing. The polynomial order affects the resulting dataset similar to the effect of the window size. A large polynomial order leads to a more noisy dataset, while a low polynomial order over-simplifies the dataset. It is also important to note that the polynomial order has to be lower than the window size (Vivó-Truyols & Schoenmakers, 2006).

A window size of 10 was chosen, in combination with a polynomial order of 4.

The next step is to actually reduce the timeseries. While the smoothing process has reduced the noise, it hasn't yet condensed the timeseries itself. In order to keep the process of reducing the time-series uncomplicated, it has been chosen to reduce the timeseries by simply skipping certain timesteps, and remaining the value constant in between the skipped timesteps. This makes it easy to select the right timesteps from all relevant variables of the metocean data, without the risk of combining different timesteps for different variables. Besides that, there is no need to work with any interpolation between the available timesteps when staying on the "grid" of the existing dataset.

Consequently, the level of reduction can be described by a factor (which as to be an integer to stay on the existing "grid"), that defines how many timesteps are skipped. The value that will be used during the newly created timestep is based on the value at the start of that period in the original dataset, instead of taking the average value in the new period. When taking the average value during the period of the new timestep, instead of the value from the original dataset at the start of the new timestep, one would basically mimic the moving-average method. By taking the value from the original dataset at the start of the new timestep, peak values are included in a random manner in the reduced timeseries. The downside of this random aspects in inclusion of values is that the accuracy of the reduced timeseries does not show a clear correlation with the increase in timesteps. Due to this randomness, a smaller timestep might be a less good representation of the original dataset. This creates the need to analyse a range of possible reduction factors manually, and test them on their accuracy compared to the original dataset. In Table G.1, the results of 12 different reduction factors are shown. It is important to state that this reduction is done after the initial SG-smoothing. That is the reason that the timeseries with a reduction factor of 1 does also show a mismatch compared to the original dataset. The error is based on the comparison of the total siltation volume, as it was defined in Section 4.7, where the result of the reduced timeseries is compared to the result of the (pre-smoothing) original dataset.

Table G.1: Comparison between different factors of time reduction. The computation time is the time that is needed to compute the siltation during the whole duration of period 2.

Factor	Timestep (minutes)	Error [m³]	% Error	Computation time [s]
12	240	95	4.2	4
11	220	266	11.7	4
10	200	155	6.8	7
9	180	202	8.9	6
8	160	95	4.2	7
7	**140**	**53**	**2.3**	**7**
6	120	144	6.3	9
5	100	236	10.4	10
4	80	190	8.3	13
3	60	217	9.5	18
2	40	205	9.0	28
1	20	205	9.0	60

The resulting reduced timeseries are shown in Figure G.1, which includes the wave height H_{m0}, wave peak period T_p, wave angle w.r.t. the shore-normal θ, the tidal current U_{tide} and the tidal water level.

The dark blue line represents the dataset that has been obtained after performing the SG-smoothing. It can be seen that the SG-smoothing remains the peaky character of the metocean conditions, but significantly reduces the magnitude of the outliers. One important thing to mention is the data on the water level (see Figure G.1e). As this data was not retrieved from a buoy, but from the DelftDashboard (Van Ormondt et al., 2020), it is based on numerical predictions and therefore do not include any noise. In this case, it is more accurate to use the average value during the duration of the new timestep, than taking the first value. As the original water level data already does not include any peaks, no peaky characteristics of the water level data are lost.

Some important additional remarks on this method: first of all, it is important to state that the SG-smoothing already leads to a loss of information. As a result, the timestep reduction of factor 1 in Table G.1 does show an error compared to the original dataset. Secondly, the error that is stated in Table G.1 in Appendix G is based on the total siltation volume as it was defined in Section 4.7.

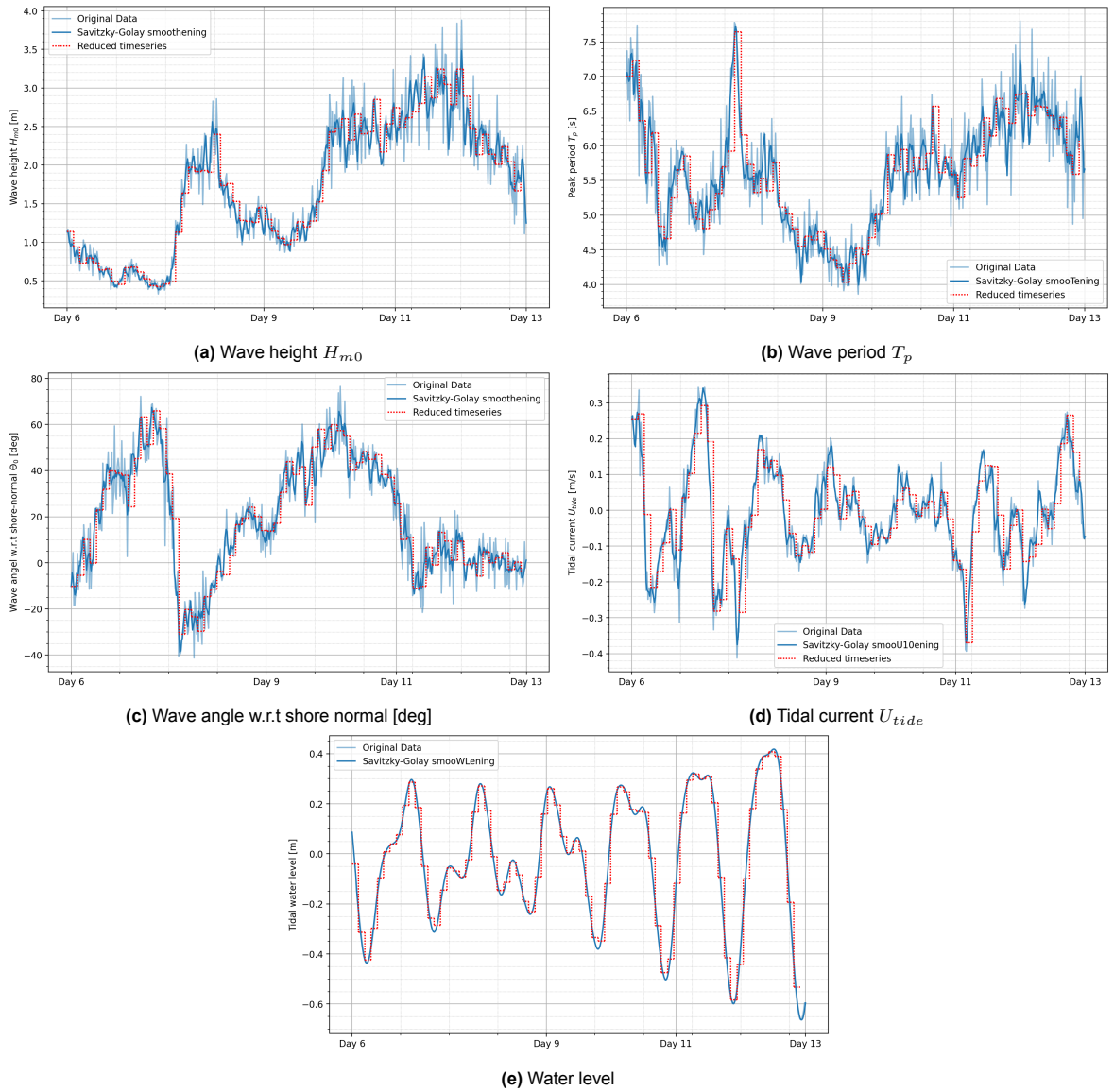

(a) Wave height H_{m0}

(b) Wave period T_p

(c) Wave angle w.r.t shore normal [deg]

(d) Tidal current U_{tide}

(e) Water level

Figure G.1: Reduced timeseries to reduce computation time in the GLUE-analysis. The light blue line represents the original data, the dark blue line represents the result of the Savitzky-Golay smoothening, which reduces the noise of the data. The red line shows the reduced timeseries, with a timestep that has been reduced by a factor 7 compared to the original data.

Based on the results in Table G.1 it can be concluded that the reduction with a factor 7 is the optimal

trade-off between computation time and accuracy. The timestep will be increased from 20 minutes in the original dataset, to 140 minutes in the reduced dataset. This reduces the computation time by a factor of 9, from 60 seconds to 7 seconds. In absolute sense, the accuracy of 2.3 % seems acceptable. However, as this error is related to the total siltation volume, it does not say anything on the accuracy on the shape of the resulting siltation curve. For an arbitrary set of input variables, the siltation volume along a trench is plotted in Figure G.2. The section of the trench that is plotted starts at the start of the nearshore zone, as defined in Section 4.7. It can be concluded that the shape of the siltation curve, based on the reduced timeseries, does show a good match compared to the original dataset. The two insets in Figure G.2 show two locations where the accuracy is at its worst. As expected, these are the locations where a peak in siltation is modelled. Due to small alterations in metocean conditions, the locally generated currents will have a different magnitude, leading to slightly different siltation volumes at these locations.

To conclude, the error of 2.3% on the total siltation volume, and the good match of the shapes of the siltation curves show that the significant decrease of computation time by reducing the timeseries by a factor of 7, does not lead to significant loss of information. An important remark on this approach is, that this approach is tailored on this specific case. Due to the above-mentioned randomness in the accuracy of the reduced timeseries, the optimal reduction factor will be different for different metocean conditions.

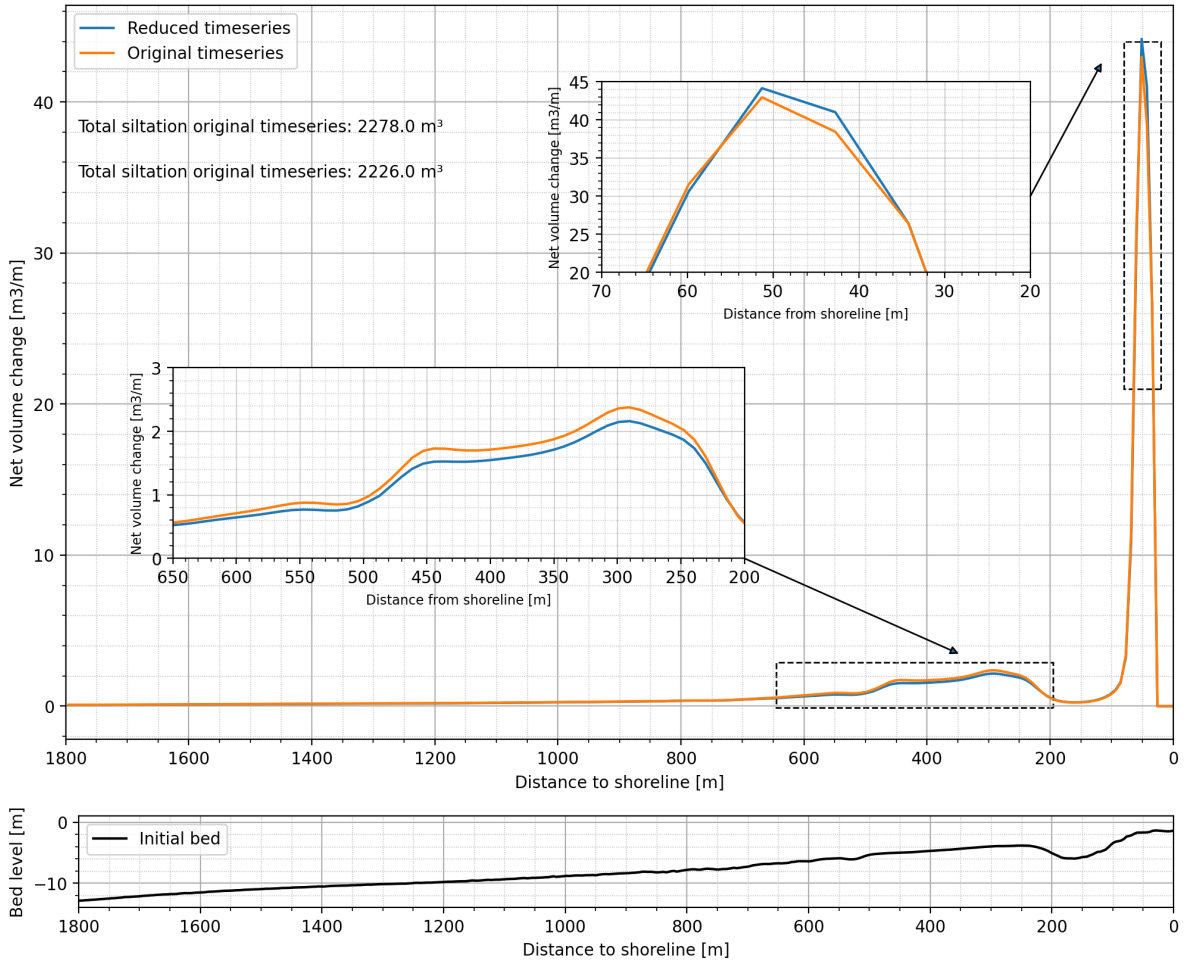

Figure G.2: Accuracy of the reduced timeseries, compared to the original timeseries. The two insets show the regions with the largest offset.

H

Effects of subjective choices in GLUE-analysis

The GLUE-analysis is known as a powerful calibration method, and method to approximate independent variables and quantify model uncertainty (Beven & Binley, 1992). However, the GLUE-analysis is known as a method that strongly relies on some subjective choices throughout the process. This appendix aims to visualise and further discuss the effects of some of the subjective choices in the GLUE-analysis in this research.

The definition of performance measures is the first choice that a user of the method has to define. This step is not characteristic for the GLUE-analysis specifically, as it is the first step in any method to evaluate a model's performance. In this research, two performance measures are defined: BSS_s which addresses the spatial distribution of siltation volumes, and BSS_{tot} which addresses the total siltation volume. While the definition of BSS_{tot} is relatively straightforward, is the definition of BSS_s a bit more complicated. Section 4.8.2 discusses the presence and the effect of the "double penalty" in more detail (Bosboom, 2020). Figure H.1 shows the effect of the correction that is applied to avoid the "double penalty". The orange line shows the optimal fit, if no correction for the peak location would be included. The blue line shows the optimal fit, if the correction is included. It can be clearly seen that including the correction leads to a fit which is a better representation of the observed values. This also comes back in the BSS_s score of both fits.

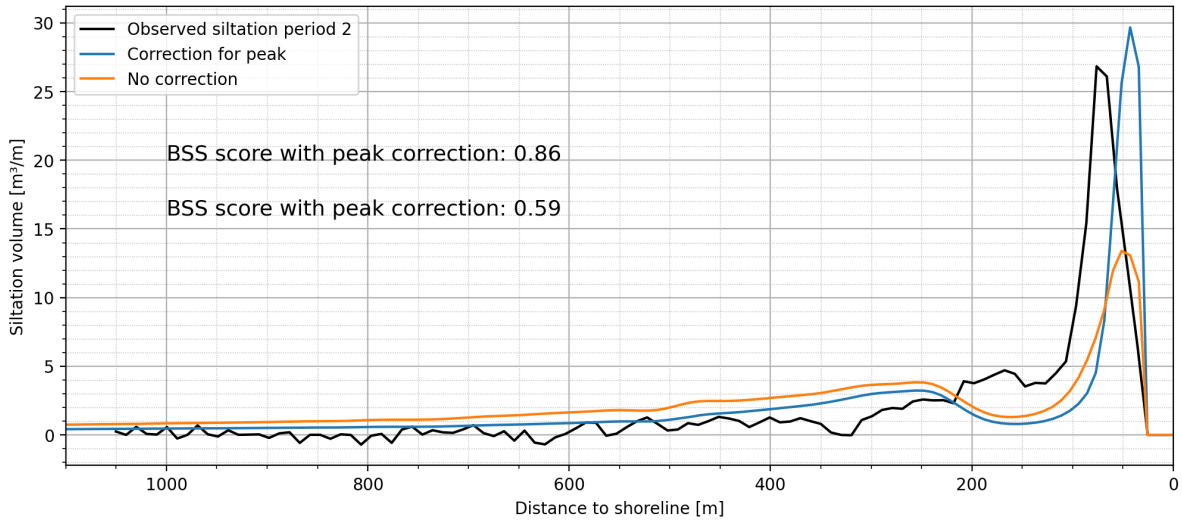

Figure H.1: The effect of applying the correction for the peak location on the optimal fit for the shape. The orange line represents the optimal fit if no correction for the peak location is applied, resulting in the inclusion of the "double penalty".

The decision on which performance thresholds are used has major implications on the results of the GLUE-analysis. To illustrate this, the values that are used throughout the research are compared to values that represent lower thresholds. Instead of values for BSS_s and BSS_{tot} of 0.6 and 0.8 respectively, the comparison case uses values of 0.4 and 0.5 for BSS_s and BSS_{tot} respectively. A direct consequence of this is the larger amount of behavioural runs, indicated by N_{bhv} in Figure H.2. The wider range of behavioural runs has its effects on the posterior optimised parameter distribution in Figure H.3

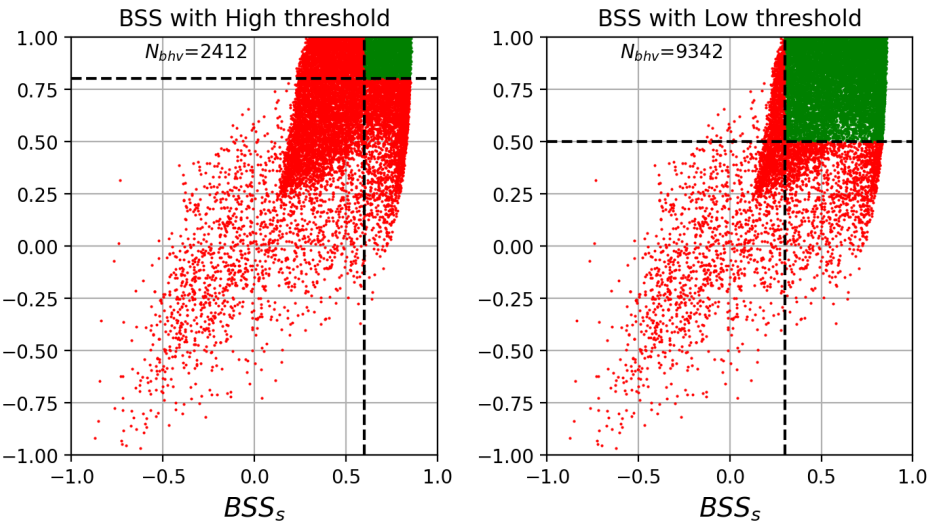

Figure H.2: The effect of lower thresholds on the selection of behavioural sets of variables. N_{bhv} indicates the number of accepted runs.

As the lower thresholds allows the method to include more sets of variables as behavioural runs, the relative importance of each set is smaller. This leads to a less pronounced variation of the posterior distribution, compared to the prior distribution.

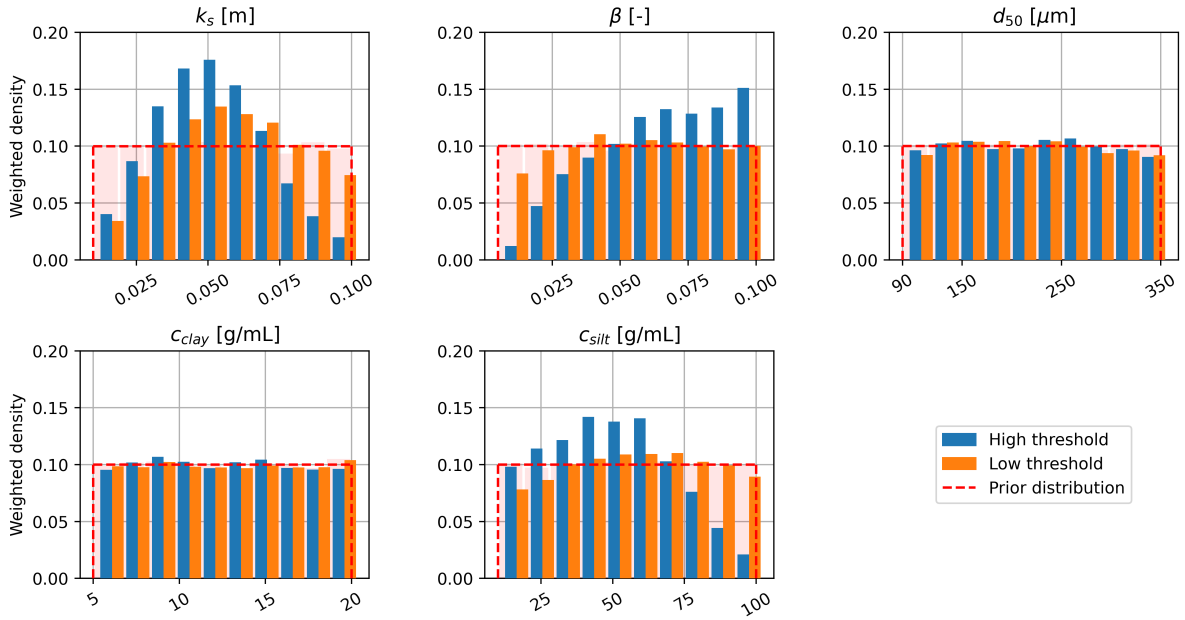

Figure H.3: The effect of lower thresholds on the posterior parameter optimisation. The blue bins are the results of the original thresholds. The orange bins indicate the distribution for lower thresholds. Red is indicating the prior distribution.

Next, the wider range of behavioural independent variables affects the 95% confidence interval of the

model's outcomes. The confidence interval corresponding to the lower thresholds is depicted by the light blue band. It can be seen that it is indeed exceeding the confidence interval of the higher threshold, albeit not being significantly at most of the locations.

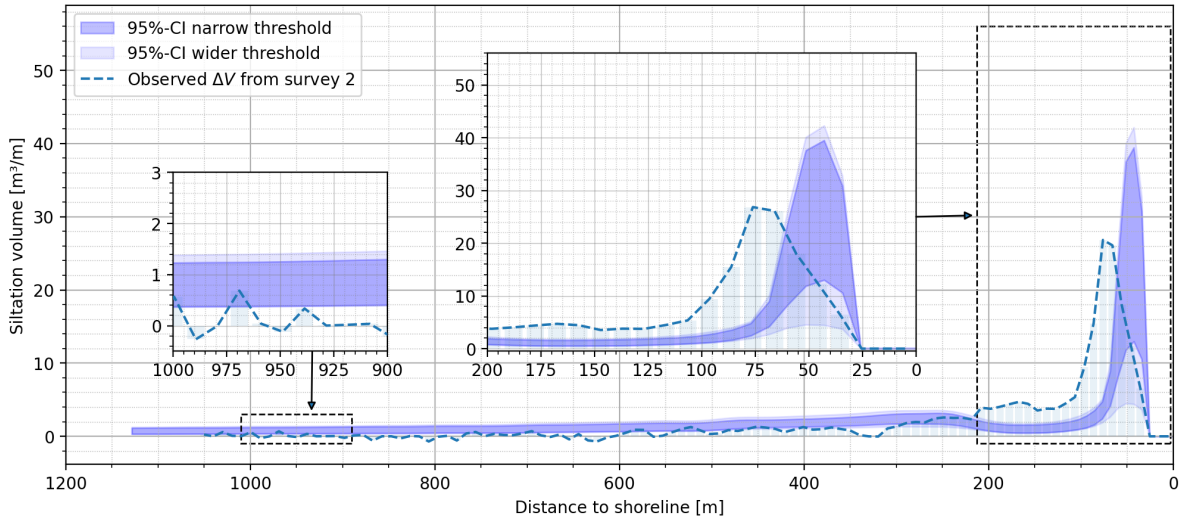

Figure H.4: The effect of lower thresholds on the resulting 95% confidence interval. The lighter blue is indicating the interval for the lower thresholds.

Finally, the choice of performance thresholds is clearly seen in the distribution of the remaining predicted siltation volumes. When comparing to to the distribution of the higher thresholds, it can be seen that a wider range reveals that the modelled siltation volumes shows some characteristics of a normal distribution. As the larger thresholds compromises the modelled data to a narrow range of behavioural results, these characteristics were not yet observed.

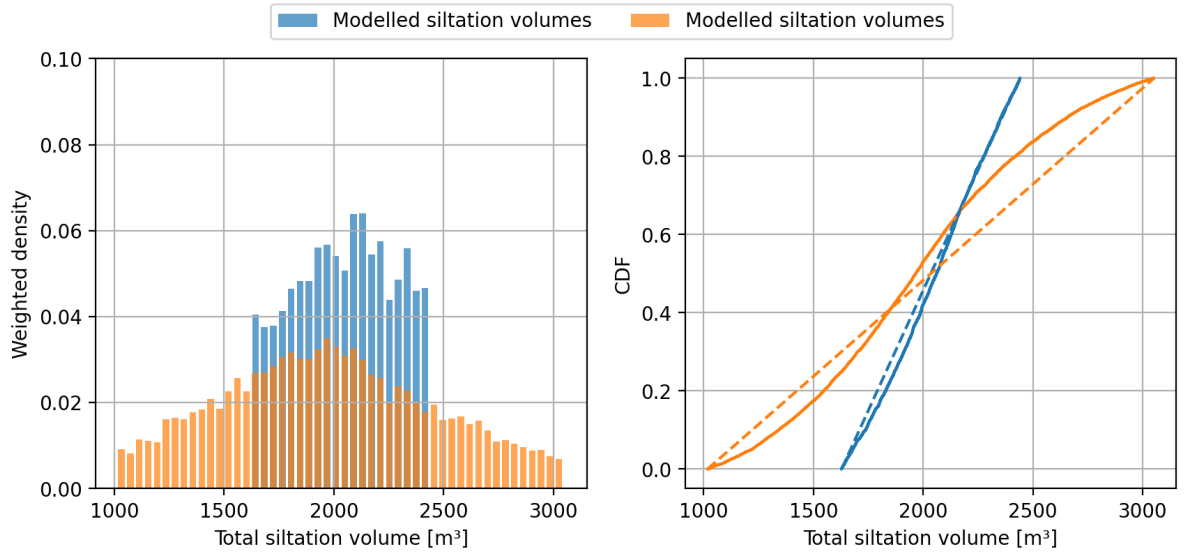

Figure H.5: Probability distribution of total siltation volumes in period 2 for original and lower thresholds. The right graph shows the CDF for both selections of modelled values.